THE ROLE OF MTO2 IN TEMPORAL AND SPATIAL REGULATION OF CYTOPLASMIC MICROTUBULE NUCLEATION IN *Schizosaccharomyces pombe*

Lynda M. Groocock, MBChem (Hons)

Thesis presented for the degree of Doctor of Philosophy

The University of Edinburgh

January 2010

ACKNOWLEDGMENTS

The first and foremost person that I would like to acknowledge for his unbridled support during my PhD research is my supervisor Dr Kenneth E. Sawin. Ken's endless enthusiasm and willingness to share his seemingly limitless knowledge has been invaluable to my research experience. I would also like to thank both past and present Sawin lab members: Hilary Snaith, Claudia Bicho, Eric Lynch, Vicky Miller, Itaru Samejima and Andreas Anders for all their extremely helpful discussions and advice.

During my project I have been privileged to be joined by students Struan Murray [University of Oxford] and Adokiye Berepiki [University of Edinburgh], whose projects have contributed either directly to this thesis or provided extra support for my research.

At the Wellcome Trust Centre for Cell Biology we are lucky enough to be surrounded by a number of excellent research groups, in addition to having access to high quality instruments and equipment. As well as providing a rich learning environment, this has given me the opportunity to seek the best advice from many experienced people and allowed me to perform my research to be best of my ability. I would particularly like to acknowledge the groups of Kevin Hardwick, Hiro Okura, Adele Marston and Peter Fantes. I would also like to thank my graduate committee of Prof. Robin Allshire [second supervisor], Prof. Paul Taylor, and Dr. Juri Rappsilber. For their technical support within the microscope facility and general wellbeing of the centre, I am grateful to Dr David Kelly and Greg Anderson.

I would like to thank Dr Flavia de Lima Alves and Dr Juri Rappsilber for their expertise with the Mass Spectrometry analyses, and Dr. Akihisa Matsuyama and Dr. Didier Busso for providing plasmids.

Importantly, I am grateful to the BBSRC for their financial support over three years.

On a personal level, there are many people that have provided me with the support and encouragement without which I would not be here today. My parents, Sue and Martin, who have been my rock throughout my whole education, my grandparents, Peter and Wynne, who, although, are no longer with us, I know will be very proud. A special thanks goes to Air Cdre. Alan Waldron and Mrs Celia Waldron who, at the point when I had to make a decision on whether to take this path, pushed me in the right direction. Also my dear friend Nadia Korfali, who was an ear to listen whenever it was needed. Last but not least, I would like to thank my partner Stephen, who in the final stages gave me everything I needed to see the light at the end of the tunnel.

DECLARATION

I hereby declare that this thesis has been composed by myself and the work presented herein is my own. Where the research has been performed with the aid of another, this has been clearly stated within the text.

Lynda M. Groocock

ABSTRACT

The microtubule [MT] cytoskeleton of *S. pombe* is a highly dynamic network of filaments that facilitates intracellular transport, determines cell polarity and plays an essential role in chromosome separation during mitosis. In fission yeast, MTs are nucleated in a temporally and spatially regulated manner from sites called Microtubule Organising Centres [MTOCs], through the activity of both the γ-tubulin complex [γ-TuC] and the Mto1/2 complex. The Mto1/2 complex determines the localisation of the γ-TuC at MTOCs, which change throughout the cell cycle. As cells enter mitosis the cytoplasmic array of MT bundles depolymerise. They are replaced by the intranuclear mitotic spindle and cytoplasmic spindle pole body-derived astral MTs that in turn give way to the formation of the post-anaphase array. Although much is known about the properties of each type of MT array, the mechanism by which the timing of MT nucleation at different MTOCs is regulated over the cell cycle remains unclear.

In the Mto1/2 complex, Mto1 is thought to provide the primary interaction with the γ-TuC, and Mto2 functions by reinforcing this interaction. Due to the lack of structural information for the Mto1/2 complex, the molecular mechanism of Mto1/2-mediated assembly of the γ-TuC at MTOCs is unknown. The aim of my study is to investigate the possibility that the Mto1/2 complex is able to promote γ-TuC assembly by forming a direct template. In addition, I will attempt to determine the molecular role of Mto2 within the Mto1/2 complex and examine ways in which regulation of Mto2 may influence the function the Mto1/2 complex at specific MTOCs.

As part of the investigation into the mechanism of Mto2 function, an *in vitro* analysis of recombinant protein demonstrated that in the absence of Mto1, purified Mto2 is able to self-interact as a tetramer. I have confirmed this interaction *in vivo* and have also shown that Mto2 forms a dimer as cells enter mitosis. However, in the context of an Mto1/2 complex the significance of the change in Mto2 oligomeric state remains unknown. Hydrodynamic analysis of a truncated form of the Mto1/2 complex suggests that it may form a heterotetramer, a hypothesis which is consistent with the equimolar levels of Mto2 and Mto1 protein within the cell. This information provides some structural insight as to how the Mto1/2 complex may interact with the γ-TuC at MTOCs. Further analysis of the Mto1/2 complex revealed that *in vivo*, the Mto1-Mto2 interaction is disrupted during mitosis. This was found to correlate with the hyperphosphorylation of Mto2, which occurs as cells enter mitosis. Subsequently, an *in vitro* kinase assay demonstrated that phosphorylation of the Mto1/2 complex reduces the stability of the complex. Mass spectrometry techniques and sequence conservation were used to identify several phosphorylated residues within Mto2 and the ability of these mutants to bind to Mto1 was analysed *in vivo* and *in vitro*. In summary, in this study I have uncovered a mechanism which allows fission yeast cells to regulate the nucleation of cytoplasmic MT nucleation in a cell-cycle dependent manner, through a phosphorylation-dependent remodelling of the Mto1/2 complex.

TABLE OF CONTENTS

LIST OF ABBREVIATIONS

aa	Amino acid
AMP	Ampicillin
BME	β-mercapto-ethanol
BSA	Bovine serum albumin
CA	Chloroamphenicol
CLAAPE	AEBSF 4-[2-Aminoethyl] benzenesulfonyl fluoride hydrochloride
CAPS	3-[cyclohexlamino]-1-propanesulfonic acid
CHAPS	3-[[3-Cholamidopropyl]dimethylammonio]-1-propanesulfonate
DTT	Dithiothreitol
DMSO	Dimethylsulfoxide
EDTA	Ethylenediaminetetraacetic acid
EGTA	Ethylene glycol tetraacetic acid
eMTOC	Equatorial Microtubule Organising Centre
EtBr	Ethidium bromide
FL	Full length
γ-TuRC	Gamma tubulin ring complex
γ-TuSC	Gamma tubulin small complex
γ-TuC	Gamma tubulin ring/small complex
GFH	GFP FLAG His_6
GFP	Green fluorescent protein
HEPES	N-[2-hydroxethyl]piperazine-N'-[2-ethanesulfonic acid]
HFG	His_6 FLAG GFP
HTB	His6 TEV biotinylation signal
iMTOC	Interphase Microtubule Organising Centre
IP	Immunoprecipitation
IPTG	Isopropylthio-β-D-galactosidase
MBP	Maltose binding protein
MOPS	3-[N-morpholino]propanesulfonic acid

MT	Microtubule
NusA	N-utilising substance A
ORF	Open reading frame
PAA	Post-Anaphase Array
PEG	Polyethylene glycol
PMSF	Phenylmethanesulphonylfluoride
PNPP	p-Nitrophenyl phosphate
SPB	Spindle Pole Body
SDS	Sodium dodecyl sulfate
TAPS	Tandem affinity purification – S-peptide
TCA	Trichloroacetic acid
TEMED	N,N,N',N'-Tetramethylethylenediamine
TEV	Tobacco etch virus protease
WT	Wild-type
g	x gravity
Sec	Second
Min	Minute
Hr	Hour
Rpm	Revolutions per minute
RT	Room temperature
O/N	Overnight
L	Litre
ml	Millilitre
µl	Microlitre
M	Molar
mM	Millimolar
µM	Micromolar
nM	Nanomolar
Da	Daltons
kDa	Kilodaltons

LIST OF FIGURES

LIST OF TABLES

LIST OF MOVIES

CHAPTER ONE

INTRODUCTION

1.1 Microtubule function

Microtubules [MTs] are found in all eukaryotic cells and form a filamentous network between central peri-nuclear regions and the outer domains of the cell interior. MTs have important functions in regulating cell shape, growth and cell polarity. This is achieved by delivery of numerous polarity factors to sites of cell growth (Drubin *et al.* 1996; Ahringer 2003; Small *et al.* 2003; Snaith *et al.* 2005b). In addition, MTs also support processes such as endocytosis and exocytosis through the formation of an efficient transport and communication network that allows motor-driven movement of membrane vesicles around the cell [reviewed in (Caviston *et al.* 2006; Soldati *et al.* 2006). MTs also provide information that helps to regulate the positioning of several types of intracellular organelles such as the nucleus, Golgi apparatus and mitochondria (Ayscough *et al.* 1993; Yaffe *et al.* 1996; Hagan *et al.* 1997; Tran *et al.* 2000). In specialised motile cells such as epithelial or neuronal cells, MTs co-ordinate with the actin cytoskeleton to promote cell protrusion and migration (Ballestrem *et al.* 2000; Gibney *et al.* 2003). MTs are essential during mitosis and meiosis, as they form the spindle, which connects the chromosomal DNA to centrosomes and facilitates separation of the genomes into two daughter cells. For the purpose of this report, the mitotic spindle will not be discussed, however, for reviews of the regulation and behaviour of MTs of the mitotic spindle see (Mishima *et al.* 2004; Glotzer 2009).

Microtubules were first observed by electron microscopy studies on epithelial cilia and spermatozoid flagella. Later studies confirmed the existence of similar tubular-like structures within the cytoplasm of many cell types. These structures were given the term ‘microtubules’ (Gibbons 1961; Ledbetter *et al.* 1963; Slautterback 1963).

In the proliferating cells of higher eukaryotes, MTs are arranged into radial arrays that emanate from a peri-nuclear structure called the centrosome. The centrosome is composed of a pair of centrioles that are encased in amorphous peri-centriolar material [PCM]. The protein complexes found within the PCM nucleate MTs that form the cytoplasmic radial array (Gould, R. R. *et al.* 1977; Dictenberg *et al.* 1998). Centrioles are short barrel-like structures that are approximately 0.5 µm long and 0.23 µm wide and usually contain nine triplet MT seeds composed of glutamylated αβ-tubulin. These structures are essential for cell division in most but not all cell types [e.g. female gametes]. However, centrioles are not present in higher plants or fungi (Marshall 2009). During non-proliferative growth, centrioles can migrate to the cell cortex where they form basal bodies and nucleate axonemal MTs that are required to generate cilia and flagella. These structures have multiple functions depending on cell type. Non-motile primary cilia are found in the majority of cells and function as a hub for chemical sensation and signal transduction [reviewed in (Singla *et al.* 2006)]. Motile cilia exist on the apical surface of epithelial cells of the respiratory and reproductive tracts where a harmonious beating of cilia generates flow to move extracellular particles and/or clear debris. A specialised version of motile cilia called flagella have been developed in certain eukaryotic cells e.g. spermatozoa. The movement of the flagella is powered by MT motors, which unlike the beating movement of cilia, causes a screw-like or wave-like motion that allows the cells to efficiently propel themselves through the surrounding media (Berg *et al.* 1973).

The cytoskeletal structure of prokaryotes is less well defined. However, it has been shown that they have cytoskeletal structures that are constructed from polymers of the FtsZ protein which is an evolutionary ancestor of the MT constituent protein, tubulin (Lutkenhaus, J. F. *et al.* 1980). The structure of the FtsZ protein prevents it from forming the same MT structure as observed in higher eukaryotes and instead FtsZ is thought to form single protofilaments, sheets and tubule-like conformations (Erickson *et al.* 1996b). Unlike eukaryotes, where MTs have important roles throughout the cell cycle, FtsZ polymers appear to function primarily during cytokinesis, where FtsZ forms Z-rings at the cell division site (Addinall *et al.* 1996). Many of the proteins that are required for cell division are targeted to the Z-ring

during cytokinesis; consequently deletion of FtsZ protein leads to long aseptated cells (Lutkenhaus, J. *et al.* 1997).

In addition to centrosomal and basal body-derived radial MT arrays there are a number of non-centrosomal linear MT arrays. Comparatively, our current understanding of the function and regulation of non-centrosomal MTs is significantly less clear than what has been established for centrosomal arrays. It appears that there is a certain level of redundancy between the two, as cells which have had their centrosome removed can re-establish a relatively normal interphase cellular array from centrosome independent sites (Karsenti *et al.* 1984). Cells that have had their centrosomes removed can also nucleate a bipolar spindle. The majority of these MTs are nucleated from sites on the chromosomes themselves; however, these cells often fail to complete cytokinesis due to spindle alignment defects (Khodjakov *et al.* 2000; Khodjakov *et al.* 2001).

Non-centrosomal linear MT arrays run parallel to the cell axis and are primarily found in differentiated cells such as in neurons, epithelial and muscle cells (Keating *et al.* 1999; Bartolini *et al.* 2006). These MTs are thought to be generated from a mixture of sources including release from the centrosome, MT breakage events and nucleation from non-centrosomal sites at the nuclear envelope or from pre-existing MTs (Bugnard *et al.* 2005).

Cells of higher plants do not have centrosomes. Therefore all MT arrays are non-centrosomal and, depending on the cell type and stage of the cell cycle, adopt a variety of different architectures. In epidermal cells, a cortical array is formed in G_1 and S phase where MTs are nucleated at the cell cortex from pre-existing MTs or at *de novo* sites, and then are quickly arranged to form an organised array (Ehrhardt 2008). During interphase and G_1, MTs are nucleated from the nuclear envelope to form the peri-nuclear array which is believed to regulate the shape of the nucleus (Stoppin *et al.* 1994). The pre-prophase band is formed at the cell division site in late G_2 and is required for proper organisation of the mitotic spindle (Ambrose *et al.* 2008). The phragmoplast MTs are formed in telophase and align perpendicular to the cell division plate. These MTs are required to guide vesicles and cell wall material to the growing plate [reviewed in (Jurgens 2005)].

In *Saccharomyces cerevisiae*, all MTs are nucleated from the centrosome equivalent, the spindle pole body [SPB]. However, like higher eukaryotes, MT nucleation in the closely related fission yeast *Schizosaccharomyces pombe* occurs from a mixture of both centrosomal and non-centrosomal sources. In addition to centrosomal MTs that are nucleated from the SPB, non-SPB MT arrays such as the post-anaphase array and a number of interphase MTs are nucleated from a several different sites throughout the cell cycle (Hagan 1998). These arrays are important for maintenance of cell shape and positioning of the organelles such as the nucleus which in turn determines the site of cell division. These linear arrays also insure that polarity factors such as Tea1 are delivered to the cell tips, so that a bipolar growth pattern is preserved (Radcliffe *et al.* 1998; Sawin *et al.* 1998; Snaith *et al.* 2005a).

1.2 Structure of the Microtubule

MTs are protein polymers composed of dimers of α- and β-tubulin. A MT filament is composed from several polymers or protofilaments to form a hollow cylinder that is approximately 25 nm in diameter. The first in depth structural analysis of tubulin came in 1998 where electron crystallography was used to determine the structure of tubulin α/β dimers isolated from bovine brain tissue (Nogales *et al.* 1998). This analysis described the same basic structure for both α and β variants of tubulin. These proteins can be divided into two functional domains, the amino-terminal domain containing the nucleotide binding region and the carboxyl terminal domain which is thought to be the target of MT associated proteins [MAPs] and motor proteins. The tubulin dimers are arranged so that the nucleotide binding pocket of α-tubulin is hidden between the dimer interface. As a result, only β-tubulin bound GTP is able to hydrolyse, and α-tubulin remains GTP-associated.

MTs are held together by both longitudinal and lateral associations between α- and β- tubulin monomers. The lateral line of like subunits is orientated with a 10° pitch from the horizontal, resulting in a 3-start helix, where upon full rotation the last monomer is three units above the first [8 nm apart]. Consequently at the seam of the MT there are lateral associations between α and β tubulin monomers (Mitchison, T. J. 1993; Fan *et al.* 1996). Longitudinal associations of the α/β dimer give the

protofilament an intrinsic polarity, where the β-subunit is exposed at the plus end of the MT and α-tubulin is exposed at the minus end.

There was much debate over the exact structure of MTs, with early work proposing protofilament numbers ranging from 8-15 (Burton 1966; Bertolini *et al.* 1970). Some of the first evidence for the composition of MTs based on a 13-protofilament structure came from the laboratory of Daniel Snyder (Tilney *et al.* 1973). They used electron microscopy to show clear images of 13 subunit rings of equally spaced tubulin monomers from both cytoplasmic and cilia derived centrosomes. Subsequent work has shown that this number is subject to particular polymerisation conditions. For example, when polymerisation is induced *in vitro*, a mixture of 13,14, and 15 protofilaments have been observed (Langford 1980; McEwen *et al.* 1980; Evans *et al.* 1985). This number may also be species specific, for example in *Caenorhabditis elegans* the majority of MTs are 11-protofilament structures, however specific neuronal cells have been found to contain 15-protofilament fibres, both of which respond differently to MT depolymerising drugs (Chalfie *et al.* 1982).

1.3 Microtubule nucleation and polymerisation

Following purification of tubulin, the presence of molecules of GTP nucleotide within the MT was discovered (Weisenberg *et al.* 1968; Lee *et al.* 1975; Weisenberg *et al.* 1975). Some of the first efforts to analyse the properties of GTP hydrolysis derived kinetic data from turbidity experiments that measured polymer concentration and the release of radiolabelled inorganic phosphate [^{32}Pi]. In these experiments it was demonstrated that one GTP was hydrolysed per tubulin dimer incorporated. First order kinetic equations showed that there was a delay between incorporation and GTP hydrolysis, indicating that these two events were not strictly linked. At the same time, experiments using non-hydrolysable analogs of GTP [GMPPNP and GMPPCP] demonstrated that GTP hydrolysis is not required for tubulin polymerisation (Penningroth *et al.* 1978). This suggested that there may be a small region of newly polymerised MT that contains GTP tubulin, called the GTP cap. The GTP cap has never been directly observed, but experimental data has

predicted that the minimum number of molecules of GTP-tubulin required to support MT polymerisation is 22 ± 11, but some estimates have shown that the cap can be up to 100 subunits deep [reviewed in (Desai *et al.* 1997)].

Margolis and Wilson used the presence of the GTP cap to design experiments to measure MT dynamics (Margolis *et al.* 1978). They used pulse chase of ^{3}H-GTP to measure incorporation rates and loss rates at steady state tubulin concentration. This showed that incorporation of the label is linear with time, but when performed under steady-state where there is no net growth, there was no net increase in label incorporation, suggesting that label must be incorporated and released at equal rates. From this data they proposed a mechanism of 'MT treadmilling'. This describes the process by which addition of tubulin dimers occurs from one end and removal of tubulin occurs from the opposite end. These early experiments were misleading because the MTs were contaminated with other MAPs which altered the MT polymerisation dynamics that would otherwise have been observed for purified tubulin.

Subsequent experiments by Mitchison and Kirscher who, instead of considering the behaviour of the population as a whole, used electron microscopy to study the length of individual MTs over time and came to very different conclusion (Mitchison, T. *et al.* 1984a; Mitchison, T. *et al.* 1984b). They developed a technique which allowed them to isolate centrosomes and analyse their polymerisation properties *in vitro*. They found that the critical concentration for MT polymerisation was 14 µM in the absence of centrosome derived MT seeds and 3-4 µM in the presence of centrosomes. Using a population of pre-formed MTs, on dilution of tubulin they showed that there was a proportional depolymerisation of MTs. However, the remaining MTs are capable of polymerisation. At a 'steady-state' tubulin concentration there are two phases of MTs, the majority are growing at a steady rate and the minority are rapidly shrinking to counteract the difference in tubulin concentration. The net increase in MT length suggests that transitions between phases are relatively rare events. This behaviour was described by Mitchison as 'dynamic instability' and is now widely accepted in current literature. By comparing the mean MT length over time as a function of tubulin concentration they then used this data to calculate rates of polymerisation. These experiments

demonstrated that during polymerisation, the on-rate of tubulin dimers is higher and the off-rate is lower at the plus end than at the minus end, indicating that the plus end is more stable. However, during depolymerisation the off-rate is a lot higher for the plus end, indicating that monomers are lost quicker from this end. As Margolis and Wilson performed their experiments at steady state where there is no net growth, the polymerisation on-rate at the plus end dominated the resulting kinetic data, and the off-rates at plus ends were never observed.

The off-rate during depolymerisation was found to be three orders of magnitude higher that the off-rate during polymerisation. Mitchison and Kirschner believed that this represented the off-rates of GDP-tubulin and GTP-tubulin respectively. They also showed that shearing of MTs at steady state induced depolymerisation events, which supported the idea that the GTP cap stabilises the MT ends and that GDP-tubulin is more likely to depolymerise. This information provided one of the first experimental based theories to explain the function of GTP hydrolysis. Advances in technology have allowed analysis of MT structure at a molecular level, and it was subsequently shown that GTP bound β-tubulin forms a more stable lattice than GDP bound β-tubulin, confirming Mitchison's results (Nogales *et al.* 1998). Non-hydrolysable nucleotide analogue-bound MTs are more structurally stable than the filaments containing the hydrolysed nucleotide, which have more weakly associated lateral contacts (Mejillano *et al.* 1990). Docking of the refined structure of purified αβ-tubulin dimers onto the protofilament lattice demonstrated that the αβ-tubulin dimers have a straight conformation when present in the MT lattice (Nogales *et al.* 1999; Lowe *et al.* 2001). This straight conformation is thought to be promoted by lateral association of tubulin dimers, as the structure of αβ-tubulin dimers isolated from preformed protofilaments that do not have lateral contacts followed a curved conformation (Ravelli *et al.* 2004). This difference in conformation was subsequently shown to correlate with the hydrolysis of β-tubulin bound GTP into GDP (Wang *et al.* 2005). This observation provided the rationale for MT depolymerisation. When the straight GTP-bound tubulin dimers that stabilise the protofilament are lost from the plus end of the MT, this exposes the GDP-bound tubulin. The weakened lateral association of the curved GDP-bound tubulin causes

the individual protofilaments to peel away from the lattice. This phenomena was observed using electron microscopy of shortening MTs (Tran *et al.* 1997).

1.4 The gamma-tubulin complex

The MT nucleating activity of the centrosome depends on a tubulin variant called gamma tubulin [γ-tubulin]. γ-tubulin was first identified the product of the *mipA* gene, a suppressor of a β-tubulin mutation in *Aspergillus nidulans*. γ-tubulin was found to be an essential gene, in which mutations inhibit nuclear division as well as a reduction in the length and number of cytoplasmic MTs (Oakley, C. E. *et al.* 1989; Oakley, B. R. *et al.* 1990). Cloning of the homologous genes in higher eukaryotes showed that γ-tubulin localised to the PCM (Stearns *et al.* 1991; Zheng *et al.* 1991). Microinjection of an antibody raised against a γ-tubulin peptide into mammalian tissue culture cells prevented MT re-growth following depolymerisation induced by nocodazole or cold shock (Joshi *et al.* 1992). This suggested that γ-tubulin was a critical component of the MT nucleation machinery. The first biochemical experiments on γ-tubulin revealed that unlike α/β-tubulin, it is present as a monomer, and the protein was localised to the minus ends of MTs (Melki *et al.* 1993).

Initially there were two models to describe MT nucleation [reviewed in (Moritz *et al.* 2001)]. These are schematically represented in Figure 1.1. The Protofilament Model was proposed by Harold Erickson (Erickson *et al.* 1996a). It describes the polymerisation of α/β-tubulin dimers through lateral association with a γ-tubulin seed protofilament up to 14 subunits long, which extends into the α/β-tubulin protofilament. Recent evidence to support this model includes the discovery that γ-tubulin interacts more strongly with β-tubulin than α-tubulin despite the fact that α-tubulin is found at the minus ends of MTs (Leguy *et al.* 2000). It is known that lateral interactions between α/β dimers are very weak. It was proposed that lateral binding of γ-tubulin with β-tubulin may act to support the α/β-tubulin lateral interactions. It has also been shown that single γ-tubulin monomers are sufficient to nucleate and cap MTs, indicating that complex structures are not required for MT nucleation *in vitro* (Leguy *et al.* 2000).

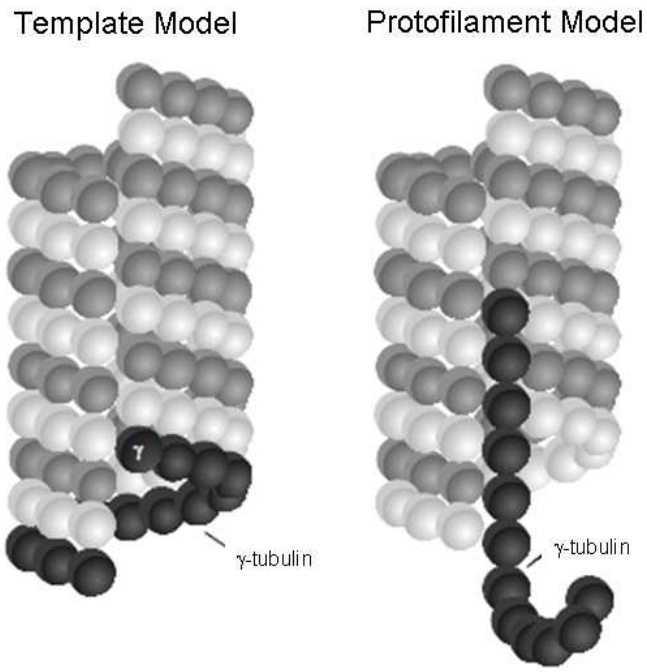

Figure 1.1 Models of γ-tubulin induced MT nucleation. In the Template model [left] the γ-tubulin interacts laterally to form a ring like structure which associates longitudinally with α-tubulin. The Protofilament model [right] describes the unwinding of the γ-tubulin ring into a short protofilament, which laterally associates with αβ-tubulin dimers. Figure modified from (Moritz *et al.* 2001).

A second model, the Template model, was proposed by Yixian Zheng (Zheng *et al.* 1995). The Template Model describes the polymerisation of α/β dimers through longitudinal associations with a ring-like template of γ-tubulin. The proposed γ-tubulin structure is a 3-start helix which can extend up to 12 nm into the protofilament to assimilate the pitch of the α/β-tubulin MT. This model was supported by negative stain electron-microscopy of MTs extracted from *Xenopus laevis* egg extracts, where incubation with gold particle-conjugated secondary antibody showed that γ-tubulin is not found more that 15 nm away from the minus end of the MT. This contradicted the Protofilament model which predicted that when fully extended the 14-subunit γ-tubulin protofilament would extend up to 50 nm into the fibre (Keating *et al.* 2000). The position of γ-tubulin was confirmed when measurements taken from reconstituted nucleation events showed that 90% of gold-labelled γ-tubulin was within 40 nm of the end of the MT (Wiese *et al.* 2000).

Purification of γ-tubulin revealed that it is part of a large complex with several other proteins and has a nucleation efficiency similar to that of the *Drosophila melanogaster* centrosome (Kellogg *et al.* 1992; Raff *et al.* 1993; Stearns *et al.* 1994; Zheng *et al.* 1995). Some of the most elegant experiments were performed by Zheng and colleagues, who used electron microscopy of γ-tubulin complexes purified from *X. laevis* to show that the complexes adopted a ring-like structure, 25-28 nm in diameter that was found to associate with the minus ends of MTs (Zheng *et al.* 1995). This was confirmed through additional imaging of both isolated centrosomes and purified γ-tubulin complexes from *D. melanogaster* (Moritz *et al.* 1995a; Moritz *et al.* 1995b; Moritz *et al.* 2000). Supporters of the Protofilament model would argue that MT-free helix structures represent arched protofilaments of γ-tubulin, similar to the structures formed from single α/β-tubulin protofilaments at depolymerising ends of MTs. It has also been predicted that single γ-tubulin molecules would be sufficient to cap minus ends of MTs, as they would form a 3-turn helix that would prevent closing of the filament sheet (Erickson 2000; Leguy *et al.* 2000). However, evidence of a domed structure at the ends of MTs and the absence of γ-TuC spirals that extend out from the main protofilament, means the Template Model of MT nucleation is now widely accepted in the microtubule community.

Subsequent research went on to characterise the purified γ-tubulin containing complexes. Extracts from *D. melanogaster* were analysed by sucrose gradient centrifugation and it was shown that γ-tubulin exists in two complexes of different size. Hydrodynamic analysis of the large complex demonstrated that it had an S-value of 35.5 S, Stokes' radius of 15 nm and a molecular mass of approximately 2.2 MDa. Analysis of the small complex demonstrated that it had an S-value of 9.8 S, Stokes' radius of 7 nm and a molecular mass of 280 KDa (Oegema *et al.* 1999). Upon treatment with 0.5 M salt the large complex is converted to small complex suggesting that the former is made up of subunits of the latter. Both of these complexes when isolated from sucrose gradient or gel-filtration can complement the salt stripped centrosome, which suggests that the interaction between the γ-tubulin containing complex and the centrosome scaffold is direct (Moritz *et al.* 1998; Oegema *et al.* 1999).

Purification of the γ-tubulin containing complex in several organisms allowed identification of the protein components. Many of these proteins contained so-called 'grip motifs', however, the function of these domains remain unknown (Gunawardane *et al.* 2000a). γ-tubulin complex components include: Dgrip84/Xgrip110/SpAlp4/GCP2 and Dgrip91/Xgrip109/SpAlp6/GCP3, Dgrip128/Xgrip133/SpMod21/GCP5, Dgrip75/Xgrip75/SpGfth1/GCP4, Dgrip163/Xgrip210/SpAlp16/GCP6 and more recently Dgrip71WD/GCP-WD/NEDD1. The entire complex was named the γ-tubulin ring complex [γ-TuRC] (Martin *et al.* 1998; Murphy *et al.* 1998; Zheng *et al.* 1998; Oegema *et al.* 1999; Gunawardane *et al.* 2000b; Murphy *et al.* 2001; Fujita *et al.* 2002; Gunawardane *et al.* 2003; Anders *et al.* 2006; Haren *et al.* 2006; Luders *et al.* 2006; Verollet *et al.* 2006). The smaller complex isolated from salt-stripped centrosomes was found to consist of two copies of γ-tubulin and one copy of Dgrip84/Xgrip110/SpAlp4/GCP2 and Dgrip91/Xgrip109/SpAlp6/GCP3, and was designated the gamma tubulin small complex [γ-TuSC] (Oegema *et al.* 1999; Gunawardane *et al.* 2000b). A coverslip nucleation assay was developed to measure the nucleation activity of both complexes. It was found that the γ-TuRC has a 150 fold higher nucleation activity per mole of complex than the γ-TuSC (Oegema *et al.* 1999). However, RNAi knockdown of

GCP-4/5/6 in *D. melanogaster* has shown that the γ-TuSC is sufficient to nucleate a basic centrosomal array (Verollet *et al.* 2006).

S. cerevisiae do not have homologs of GCP4-6, suggesting that the primary source of MT nucleation is via the γ-TuSC [known in budding yeast as the Tub4 complex]. This indicates that other regulatory mechanisms may exist in budding yeast that promote the activity of this complex either though post-translational modifications or structural rearrangements. Research performed in the laboratory of David Agard attempted to address this problem by using electron microscopy to study the structure of the Tub4 complex (Kollman *et al.* 2008). They found that Tub4 [γ-tubulin], Spc97p [GCP2] and Spc98p [GCP3] assemble to form a 'Y-shaped' complex, where immuno-gold-labelling was used to determine the position of Tub4 at the arms and FRET was used to demonstrate that the N-terminal tails of both Spc98 and Spc97 form the body of the 'Y'. Interestingly, several classes of Tub4 complex structure were observed, where the distance between the Tub4 subunits on the arms varied between 85 Å and 70 Å, suggesting a degree of flexibility in that part of the molecule. This supports the idea that Tub4/γ-TuSC undergoes a structural change that favours MT nucleation. However, as the authors argue, it is unlikely that the level of variation seen in purified complex is sufficient to facilitate the formation of lateral interactions between α/β-tubulin monomers, suggesting additional factors exist that enhance any structural rearrangement.

GCP1-6 are conserved in *S. pombe*. As in higher eukaryotes, the *S. pombe* γ-TuSC homologues, Gtb1, Alp4 and Alp6 are all essential for viability (Horio *et al.* 1991; Stearns *et al.* 1991; Vardy *et al.* 2000). Strains containing temperature-sensitive alleles show large cytoplasmic MT bundles which curve around the cell tips (Paluh *et al.* 2000; Vardy *et al.* 2000). Nucleation assays in *alp4-ts* mutants show that the nucleation of cytoplasmic MTs is reduced (Zimmerman, S. *et al.* 2005). Additional members of the γ-TuRC, Gfh1, Alp16, and Mod21 [designated non-core γ-TuRC components] are not essential for viability, but the deletion mutants display moderate interphase MT defects. The number of interphase MTs is reduced to 1-3 in non-core mutants, compared with 3-5 for wild-type cells, and nucleation from non-SPB sites is reduced by 30%. As the γ-TuSCs localise and nucleate from non-SPB

sites in non-core deletion mutants, this suggests that these proteins are able to compensate for the loss of γ-TuRC formation (Fujita *et al.* 2002; Venkatram *et al.* 2004; Anders *et al.* 2006).

The relative contribution of both the γ-TuRC and the γ-TuSC, collectively known as the γ-tubulin complex [γ-TuC], to nucleation of the different MT arrays in fission yeast is unclear. When γ-TuC components are analysed by sucrose gradient sedimentation, γ-tubulin is mostly present in a low S-value complex [~8-9S], unlike γ-tubulin from both *Xenopus* and *Drosophila* extracts, which are mostly present in a large S-value complex [30-35 S] (Oegema *et al.* 1999). However, recent data suggest that members of the γ-TuRC co-localise with γ-TuSC at the minus ends of MTs, indicating that the large complex may be assembled.

1.5 γ-tubulin associated proteins

There are a number of additional γ-TuC associated proteins that are required for the γ-TuC to function as an efficient MT nucleator. Several proteins have been shown to play a role in the recruitment and/or anchoring of the γ-TuRC within the PCM, many of which are influenced by levels of cell cycle-dependant regulation.
Pericentrin is a large scaffold protein that exists in a number of different isoforms. Zimmerman and colleagues (Zimmerman, W. C. *et al.* 2004b) showed that Pericentrin A is required for anchoring of the γ-TuC at the PCM specifically during mitosis, through an interaction with GCP2/3 via its C-terminal domain, and this recruitment is required for proper spindle formation.
Ninein is another protein that is required to localise the γ-TuRC to the PCM (Mogensen *et al.* 2000; Ou *et al.* 2002). However, Ninein has also been found at non-centrosomal nucleation sites in specialised epithelial cells (Mogensen 1999). The similar Ninein-like protein [Nlp] plays a structural role in centrosome organisation where it is required to localise the γ-TuC to the centrosome during interphase. Nlp is phosphorylated by Plk-1 early in mitosis, causing it to dissociate from the centrosome. This is thought to allow the association of mitotic specific scaffold proteins the PCM (Casenghi *et al.* 2003).

GCP-WD/NEDD1 is another protein that is required for γ-TuRC localisation to the centrosome. GCP-WD interacts with many of the γ-TuC components, and functions as a targeting factor (Gunawardane *et al.* 2003; Luders *et al.* 2006). During mitosis, GCP-WD also becomes phosphorylated by both Plk1 and Cdk1, which is required to localise the γ-TuRC to the spindle poles (Zhang, X. *et al.* 2009).

Although homologs of many of these proteins have yet to be identified fission yeast, there are a number of proteins that are able to carry out the same recruitment and anchoring functions. For example *S. pombe* Mto1 has been shown to have structural resemblance to Ninein, and is also required to localise the γ-TuC to the SPB (Sawin *et al.* 2004; Venkatram *et al.* 2004).

1.6 Microtubule Organisation in *S. pombe*

Fission yeast is a unicellular haploid organism that is popular among scientists due to its short generation time, high recombination rates and genetic tractability. *S. pombe* are rod-like cells that are between 12 – 15 nm long and 3 – 4 nm wide. They grow in a bipolar manner until they reach the required length at which point they divide by medial fission. Fission yeast is a preferred organism to study MTs as the low number and size of MT bundles allows tracking and measurement of MT dynamics. Fluorescent markers can easily be introduced into the cell and used to label the plus and minus ends of the MTs, as well as follow the behaviour of many other MT associated proteins. Additionally, as fission yeast is more closely related to higher eukaryotes than budding yeast, many of the factors involved in MT regulation are conserved and so give a better comparison than other unicellular species.

MTs are nucleated at specific sites within the cell called Microtubule Organising Centres [MTOCs]. Different MTOCs are schematically depicted in Figure 1.2. In fission yeast, in addition to the centrosome equivalent, an extensive non-centrosomal array is nucleated from other sites within the cell. For example, MTs are nucleated from the equatorial MTOC [eMTOC], and from interphase MTOCs [iMTOCs] (Hagan 1998). MTs nucleated from these different sites have a number of different functions within the cell and are required at different points

during the cell cycle. These properties make fission yeast a good model for studying the nature of MT nucleation from non-centrosomal MTOCs.

Unlike the centrosome, the structure of the SPB is relatively undefined. Electron microscopy has shown that it is composed of a cytoplasmic layer and nucleoplasmic layer that are connected by striations through the nuclear envelope (Ding *et al.* 1997). As *S. pombe* undergoes a closed mitosis, the SPB embeds itself into the nuclear envelope at the start of mitosis (Uzawa *et al.* 2004). Once in the membrane, in addition to nucleating MTs, the SPB is known to act as a signalling hub for many regulatory proteins including those involved in cell cycle progression e.g. the Plo1/PLK1 kinase (Doxsey *et al.* 2005; Hagan 2008).

In anaphase, astral MTs are nucleated from the both the nucleoplasmic and cytoplasmic face of the duplicated SPBs. The proposed function of *S. pombe* cytoplasmic astral MTs are to assist in the alignment of the spindle along the cell axis so that equal segregation of genetic material between both daughter cells is ensured (Tolic-Norrelykke *et al.* 2004). However, cells which lack these structures do not display any major spindle elongation or alignment defects (Zimmerman, S. *et al.* 2005). Astral MTs are essential for spindle orientation in budding yeast, as they guide the spindle MTs into the bud neck between mother and daughter cells [reviewed in (Bloom 2003)]. A similar process occurs in tissue cells of higher eukaryotes, where astral MTs are directed by extracellular cues, such as the substrate plane, to establish spindle polarity (Toyoshima *et al.* 2007). Additionally, unlike yeast, which determine their cell division plane prior to mitosis, it is thought that astral MTs of higher eukaryotes also contribute to localisation of the cleavage furrow by distributing proteins involved in actin polymerisation at the central cortex (Inoue *et al.* 2004; Bringmann *et al.* 2005).

Following completion of anaphase and initiation of spindle disassembly, a post-anaphase array [PAA] is nucleated in the division plane between the separated nuclei. Nucleation of the PAA is dependent on the formation of the cortical actin ring [CAR] (Pardo *et al.* 2003). This is an actin structure that is formed early in mitosis. It is assembled following release of Mid1 from the nucleus, which is required to establish the CAR at the cell cortex proximal to the nucleus (Chang *et al.* 1996;

Sohrmann *et al.* 1996). Mid1 functions by recruiting myosin II heavy and light chain proteins and several regulators of actin dynamics, including Rng2, the Cdc12 formin, and Cdc15 (Fankhauser *et al.* 1995; Chang *et al.* 1997; Kitayama *et al.* 1997; Eng *et al.* 1998). Together these proteins induce actin polymerisation, which is further organised by the recruitment of tropomyosin, α-actinin and Myp2 (Balasubramanian *et al.* 1992; Bezanilla *et al.* 1997; Wu *et al.* 2001).

Regulation of the PAA is influenced by two major signalling pathways. The Septation Initiation Network [SIN] is activated in late anaphase and causes the ring to constrict and induces formation of the septum [reviewed in (Krapp *et al.* 2004; Krapp *et al.* 2008)]. However, activation of the SIN alone is not sufficient to induce PAA formation, as the PAA does not form when SIN is induced during interphase using *cdc16.116ts* allele (Heitz *et al.* 2001).

The Anaphase Promoting Complex [APC] is a ubiquitin ligase which among other things is required to activate separase, an enzyme that proteolytically degrades cohesin, and allows sister-chromatid separation as cells enter anaphase (Ciosk *et al.* 1998; Uhlmann *et al.* 1999). The activity of the APC is also required for the formation of the PAA as temperature sensitive alleles of Cut4 and Cut9 [APC components] and Cut8 [required to localise the APC to the nuclear periphery] do not form a PAA at restrictive temperature. However, these mutants all form an actin ring, and progress through cytokinesis as normal, indicating that the SIN occurs independently of the APC (Heitz *et al.* 2001).

The mitotic Polo kinase has regulatory roles in both the APC and the SIN, and is therefore considered to be the missing link between the two pathways that connects them to the formation of the PAA [reviewed in (Archambault *et al.* 2009)]. When Polo kinase Plo1 was expressed in G_2 arrested fission yeast cells, PAA and primary septum formation was induced (Heitz *et al.* 2001). So far the intricate complexity of both the APC and the SIN pathways mean that the mechanism that directly link them to the PAA through the Plk1 kinase remains unclear.

The exact function of the PAA is uncertain, as cells that lack the PAA are viable (Sawin *et al.* 2004; Venkatram *et al.* 2005). Evidence suggests that the PAA may act to stabilise the position of the CAR during anaphase, as cells that are arrested in late anaphase with a stable actin ring, show a displaced non-centralised

ring position when treated with MT-depolymerising drug carbendazim [MBC] (Pardo *et al.* 2003). Other research has suggested that the PAA may also help to separate dividing nuclei (Hagan *et al.* 1988; Hagan *et al.* 1997). Homologous structures have been observed in higher plants, for example, the pre-prophase band that is required to organise the MT spindle (Ambrose *et al.* 2008), however, PAA-like structures have yet to be confirmed in other yeasts.

Interphase MT organising centre [iMTOCs] is a descriptive term that encompasses any MTOC that nucleates MTs during interphase. During interphase, *S. pombe* contain 3-5 MT bundles, each containing 2-5 MTs that extend across the longitudinal axis of the cell (Hagan 1998; Drummond *et al.* 2000; Carazo-Salas *et al.* 2007). The majority of these MTs are oriented with their minus ends anchored at the centre of the cell and their plus end facing towards the cell tip. There is also a region of overlap proximal to the nucleus where the MTs are bundled in an anti-parallel fashion (Drummond *et al.* 2000; Tran *et al.* 2001; Sagolla *et al.* 2003).

Traditionally, iMTOCs were defined as locations of MT nucleation following cold-shock or treatment with MT depolymerising drugs [e.g. MBC]. This description was later shown to be misleading, as upon cold-shock the majority of MTs were nucleated from sites on the nuclear surface as a result from a redistribution of the MT nucleation machinery (Sawin *et al.* 2004). In addition, following MBC treatment, there can be ambiguity to whether MT growth occurs from true *de novo* nucleation sites or from MT 'stubs' found at regions of MT overlap that are resistant to MBC (Busch *et al.* 2004). Defined more broadly from *in vivo* imaging of GFP-tubulin, iMTOCs are found in a number of locations. These include the iSPB, the surface of the nuclear envelope, sites along the length of pre-existing MTs and very rarely from sites in the cytoplasm free from other MT polymers (Mata *et al.* 1997; Janson *et al.* 2005).

It is difficult to say how much each iMTOC contributes to the total cytoplasmic array. Observation of MT nucleation along pre-existing MTs is particularly difficult as polymerised seeds are quickly bundled into parent MTs. However, the high concentration of γ-TuC proteins along the length of the MT indicates that this may occur with a relatively high frequency. MT nucleation

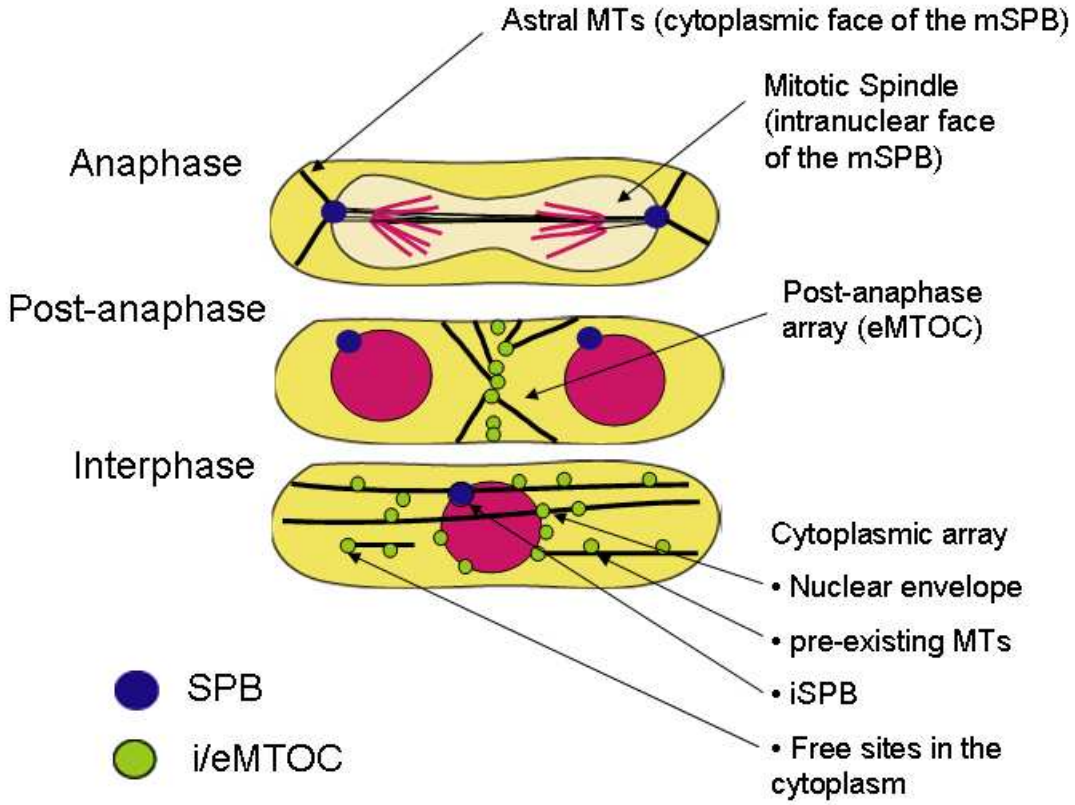

Figure 1.2 Microtubule organising centres of *S. pombe*. mSPB [mitotic spindle pole body]; iSPB [interphase spindle pole body]; eMTOC [equatorial MT organising complex]; iMTOC [interphase MT organising complex]. MT bundles are represented here as uniform structures, however, *in vivo* bundles are composed of several MTs which are distributed unevenly along the length of the bundle with multiple regions of overlap.

from the nuclear envelope is thought to facilitate a large number of *de novo* nucleation events. However, the mechanism by which the γ-TuC proteins are localised and anchored to the surface is unclear.

1.7 Mto1 and Mto2

Regulation of γ-TuC localisation and function in *S. pombe* has been shown to be dependent on a number of auxiliary proteins, the most prominent of which are *m*icro*t*ubule *o*rganiser *1* and *2* [Mto1/Mto2]. Both proteins localise to all cytoplasmic MTOCs and are essential for nucleation of all non-SPB derived MTs (Sawin *et al.* 2004; Venkatram *et al.* 2004; Samejima *et al.* 2005; Venkatram *et al.* 2005). Mto1 and Mto2 were initially identified in the Sawin lab due to the curved cell phenotypes observed in the mutants isolated from a mutagenesis screen (Sawin *et al.* 2004; Samejima *et al.* 2005). Distant homologues for Mto1 have been identified in other metazoa e.g. *S. cerevisiae* Spc72, *D. melanogaster* centrosomin [*Cnn*], and human proteins CDK5RAP2 and myomegalin (Sawin *et al.* 2004). Recent release of the genomic sequence of closely related fission yeast *Schizosaccharomyces japonicus* has lead to the identification of the only known Mto2 homologue, SJAG_03264.2.

Deletion of Mto1 results in a complete loss of MT nucleation from cytoplasmic iMTOCs and both astral MTs and the PAA are absent. Interphase MTs are fewer and form large bundles (Sawin *et al.* 2004; Venkatram *et al.* 2004). It was shown that the cytoplasmic MTs present in the *mto1Δ* background are derived from nucleation events that occur on the nucleoplasmic face of the SPB, initiated by a functional homolog of Mto1 called Pcp1 (Flory *et al.* 2002; Zimmerman, S. *et al.* 2004a). Once nucleated inside the nucleus, these MTs break through the nuclear envelope and escape into the cytoplasm. As a result there is a negligible MT regeneration following MT depolymerisation in *mto1Δ* cells (Sawin *et al.* 2004; Zimmerman, S. *et al.* 2005).

In *mto2Δ* cells, MT nucleation from the cytoplasmic face of the SPB is preserved, therefore the *mto2Δ* phenotype is overall less severe. Astral MTs are present, and there are more cytoplasmic MTs than in *mto1Δ*. However, there are

fewer MTs than wild-type, and they are present in large bundles. Nucleation from the eMTOCs is also occasionally observed in *mto2Δ* cells, but at a highly reduced level.

Staining for tubulin in *mto1Δ* and *mto2*Δ cells revealed that the regulation of MT growth at the cell tip appears to be defective, resulting in the extension of MTs around the tip which gives the curved cell phenotype (Venkatram *et al.* 2004; Samejima *et al.* 2005). Some evidence has suggested that this mis-regulation may occur as a result of defective loading of plus-tip proteins e.g. EB1, in the early stages of MT polymerisation (Cuschieri *et al.* 2006; Fong, K. W. *et al.* 2009b).

Mto2 is a smaller protein of 397 aa. It does not have any distinctive structural domains except for a small region of coiled-coil in the N-terminus. Unlike Mto2, Mto1 is a large protein of 1115 aa and is composed of several structurally significant domains. It has extensive regions of coiled-coil in its C-terminus in addition to a large globular domain at its N-terminus. Mutagenesis of Mto1 has revealed a stretch of conserved sequence within the globular region called the Centrosomin Motif 1 [CM1] domain, which has been shown to be essential for the interaction with the γ-TuC (Samejima *et al.* 2008). The function of the CM1 domain is conserved in Mto1 homologs, Cnn and CDK5RAP2 (Zhang, J. *et al.* 2007; Fong, K. W. *et al.* 2008).

Co-immunoprecipitation experiments show that Mto1 and Mto2 strongly interact to form a complex [the Mto1/2 complex] (Samejima *et al.* 2005; Venkatram *et al.* 2005). The Mto2 interaction domain has been localised to a central region within the coiled-coil of Mto1. Both the Mto2 interaction domain and the CM1 domain are required for the interaction of Mto1 with the γ-TuSC (Samejima *et al.* 2005; Samejima *et al.* 2008). Further mutagenesis of the Mto1 C-terminal tail has identified regions of sequence that act as a localisation modules which target Mto1 to specific sites within the cell. For example, region 1049-1095 is required to localise Mto1 to the SPB during mitosis, 1049-1075 is required for SPB localisation during interphase, and 1028-1065 is required to localise Mto1 to the eMTOC. A separate region between 500-1065 is required for the localisation of Mto1 to pre-existing MTs.

Mto1 is required for Mto2 localisation to MTOCs, however, Mto1 is able to localise normally in *mto2Δ* cells, indicating that Mto2 does not function as a localisation or targeting factor for Mto1. As both proteins are required to efficiently interact with and localise the γ-TuC at cytoplasmic MTOCs, this suggests that Mto2

may have a structural role in the assembly of the Mto1/2 complex (Sawin *et al.* 2004; Samejima *et al.* 2008). However, exactly how Mto2 is able to influence the structure of Mto1 is currently unknown.

The targeting modules of Mto1 allow it to specify the location of the Mto1/2 complex within the cell and therefore spatially regulate the nucleation of MTs. How the timing of this localisation is regulated is less clear. As described above, MT nucleation occurs from different MTOCs at different stages of the cell cycle. It is predicted that regulation of assembly and/or disassembly of the γ-TuC by the Mto1/2 complex may be one way in which the cell is able to achieve this.

1.8 Protein phosphorylation

From the first description of protein phosphorylation by Eugene Kennedy in 1954 (Burnett *et al.* 1954), phosphorylation continues to function at the heart of molecular biology, contributing to the regulation of a multitude of cellular processes, from signal transduction, differentiation, and development to cell cycle and metabolism. Protein phosphorylation involves the transfer of the gamma phosphate group PO_4^{2-}, from a nucleoside tri-phosphate to a hydroxyl group of an amino acid, i.e. serine, threonine, or tyrosine. This reaction is performed by protein kinases, and the reverse dephosphorylation reaction is carried out by protein phosphatases.

The primary functions of protein phosphorylation can be to turn ‘off’ or ‘on’ protein activity, change cellular localisation, or association with other proteins in a reversibly acute manner (Hunter 1995). The most common method by which phosphorylation acts to regulate protein activity is via a change in surface charge and/or protein conformation. Recent sequencing of various key genomes has highlighted the importance of phosphorylation, where it has been demonstrated that proteins directly involved in phosphorylation make up 2% of the human genome (Lander *et al.* 2001; Venter *et al.* 2001). It is estimated that one in three proteins are phosphorylated (Zolnierowicz *et al.* 2000).

1.9 Phosphorylation over the cell cycle

Phosphorylation is a key regulatory component of the cell-cycle control system. Transition between cell-cycle stages is regulated by several kinases including CDK1, PLK1 and the Aurora kinases, and all of which have been shown to phosphorylate targets related to MT nucleation.

In fission yeast, there is one CDK1 [Cdc2] which controls entry into different stages of the cell cycle through an association with different cyclins. Cyclin binding induces a conformational change which partially activates the CDK. However, Cdc2 must also be phosphorylated in its active site to be fully active [reviewed in (Pavletich 1999)]. Phosphorylation also plays a role in CDK inhibition. During the G_2-M transition, if various checkpoints have not been satisfied, Cdc2 is inhibited by the Wee1 kinase (Russell *et al.* 1987). When the requirements for mitosis have been fulfilled, this inhibitory phosphorylation is relieved by Cdc25 phosphatase (Russell *et al.* 1986). CDK1-Cyclin phosphorylates many proteins throughout the cell cycle, many of which contain a S/T-P-X-R consensus sequence (Endicott *et al.* 1999).

As has already been mentioned, PLK-1/Polo/Plo1 kinase plays a major role in many of the processes linked to MT nucleation. It is a conserved S/T kinase that also plays a key regulatory role in mitosis (Carmena *et al.* 1998; Barr *et al.* 2004). In human cells, PLK1 is required for centrosome maturation and bipolar spindle formation in early mitosis as well exit from mitosis and cytokinesis (Sumara *et al.* 2004; Brennan *et al.* 2007; Santamaria *et al.* 2007). The yeast homologue of Polo kinase, ScCdc5/SpPlo1 has a less important role in early mitosis, but is essential for mitotic exit pathway and cytokinesis (Yoshida *et al.* 2006). Polo kinase localisation changes during mitosis, reflecting its function at different subcellular structures [reviewed in (Petronczki *et al.* 2008)]. In prophase, Polo kinase is found at the centrosome where it is involved in the recruitment of γ-tubulin that is required for nucleation of the mitotic spindle (Casenghi *et al.* 2003; Zhang, X. *et al.* 2009). During metaphase, Polo kinase is enriched at the kinetochore, where it is thought to play a role in the spindle assembly checkpoint through phosphorylation of BubR1, a member of the APC (Matsumura *et al.* 2007). At anaphase it accumulates at the spindle mid-body where it interacts with centralspindlin and Ect5, which have a

pivotal role in the assembly of the cortical actin ring at the future cleavage furrow site (Brennan *et al.* 2007; Santamaria *et al.* 2007; Petronczki *et al.* 2008). In all roles Polo kinase acts via well characterised mechanisms which involves interaction with its targets via a C-terminal polo-box domain [PBD]. The PBD binds to phospho-peptides that are present within a S-S^P/T^P-P-X/R consensus site (Elia *et al.* 2003a; Elia *et al.* 2003b). The inclusion of S/T^P-P within this binding site means that substrates must be primed before they interact with the PBD e.g. NEDD1 is phosphorylated be CDK1 prior to phosphorylation by PLK-1, and event that is required to target the γ-TuRC to the centrosome in mitosis (Zhang, X. *et al.* 2009). The optimal PLK-1 phosphorylation sequence was identified as [D/E]-X-[pS/pT]-Φ-[D/E]-[D/E] (Nakajima *et al.* 2003), where the presence of acidic residues at either +2 or -2/-3 positions constitute the minimum requirement for PLK-1 phosphorylation (Dephoure *et al.* 2008). Dobbelaere and colleagues performed an RNAi screen to identify proteins required for centrosome maturation and duplication in *D. melanogaster*, and identified Cnn as a key component of this process (Dobbelaere *et al.* 2008). They later went on to show that phosphorylation of Cnn by Polo kinase is essential for centrosome maturation, a process that describes the recruitment of MT nucleation machinery to the centrosome. More recently it has been shown that Pcp1 is also phosphorylated by Plo1 (Fong, C. S. *et al.* 2009a).

This data supports the idea that temporal regulation of MT nucleation may be achieved through phosphorylation of the Mto1/2 complex. Phosphorylation of Mto1 has yet to be observed, however, when analysed by a western blot Mto2 is present in several isoforms that are likely to represent different phosphorylation states of Mto2 (Samejima *et al.* 2005; Venkatram *et al.* 2005).

1.10 Human disorders associated with the γ-TuC associated proteins

A number of human genetic disorders have been found to be associated with factors related to targeting of the γ-TuC and efficient MT nucleation, including CDK5RAP2, the human homolog of Mto1. CDK5RAP2/Cep215 was initially identified in a yeast-2-hybrid screen to identify interactors of the CDK5-regulatory protein 1 in rat cerebral cortex (Ching *et al.* 2000). Mutations found within this

protein lead to a condition called primary microcephaly. This is an autosomal recessive disorder physiologically characterised by a reduction in the size of the cerebral cortex and an associated mental retardation. In addition to CDK5RAP2/MCPH3, genetic mutations have been mapped to several other recessive loci, which result in a number of indistinguishable disorders. All encoded proteins have found to localise to the centrosome, where they are involved in nucleation and/or organisation of the mitotic spindle. The MCPH phenotype is thought to arise during division of the neuronal progenitor cells in the ventricular zone of the embryonic brain. When cell division is compromised this leads to a reduction in cell number and consequently brain size. Despite this, other aspects of cerebral development remain unaffected.

MCPH1 [microcephalin] is linked to other syndromes where DNA checkpoint dependent processes have been perturbed such as Seckel syndrome, which is characterised by defective ATR signalling (Jackson *et al.* 2002; Alderton *et al.* 2006). Studies have shown that cells derived from MCPH-1 patient lines display premature chromosome condensation (Trimborn *et al.* 2004). In wild-type cells, microcephalin prevents premature entry into mitosis by targeting Chk-1 to the centrosome during interphase (Tibelius *et al.* 2009). Chk-1 is a G_2-M checkpoint kinase which inhibits Cdc25B, preventing Cdc25B from activating centrosomal CDK1-Cyclin B. Upon entry into prophase, Aurora A phosphorylates Cdc25B, activating CDK1-Cyclin B which then commits the cell to mitosis resulting in chromosome condensation and centrosome separation (Kramer *et al.* 2004).

MOPD II [microcephalic osteodysplastic primordial dwarfism type Majewski II] is another primary microcephalic disease and is also characterised by the inability to recruit CDK1-Cyclin B to the centrosome. MOPD II is caused by mutations in pericentrin [PCNT], a binding partner of microcephalin (Rauch *et al.* 2008; Tibelius *et al.* 2009; Willems *et al.* 2009).

Other MCPH-associated genes include MCPH5/abnormal spindle-like, microcephaly associated [ASPM], MCPH6/centromere protein J [CENPJ], and the recently identified MCPH7/STIL. The *D. melanogaster* homolog of ASPM, *asp*, has been shown to be required for organisation of MTs at the spindle poles and central spindle during mitosis (Wakefield *et al.* 2001), and it is predicted that ASPM has a

similar role. The STIL protein mutated in MCHP7, has been found to have a related function, where it localised to the spindle-poles during metaphase in HeLa cells, and is required for mitotic spindle organisation in *Danio rerio* (Pfaff *et al.* 2007). MCPH6/CENPJ is a centrosomal protein that is associated with the γ-TuRC. Analysis of the *C. elegans* homolog suggests that CENPJ may have a role in centrosome duplication in early mitosis.

1.11 Project aims and objectives

Many of the proteins involved in MT nucleation have been identified. This has allowed researchers to begin to determine how these factors may function together to form an active nucleation complex. Studies on purified γ-tubulin containing-complexes in higher eukaryotes have identified two complexes that are able to nucleate MTs. The γ-TuRC appears to be the main active complex in these organisms and has a nucleation activity that is significantly higher than its composite γ-TuSC. The situation is very different in *S. cerevisiae*, where the γ-TuSC/Tub4 complex is the main nucleation complex. The nature of the nucleation complex formed in *S. pombe* is less clear, as there is evidence to suggest that both complexes may be active.

The Sawin lab among others, have identified Mto1 and Mto2, which are proteins required to recruit the γ-TuC to the MTOC. In this project I want to examine the properties of the complex formed by Mto1 and Mto2. It was proposed that Mto2 may promote co-operative binding of the γ-TuSC components to Mto1/2 (Samejima *et al.* 2008). I predict that this may result in the assembly of a large complex containing many molecules of Mto1/2 that may act in a γ-TuRC-like fashion. Deletion of the non-core γ-TuRC components results in a 30% reduction in MT nucleation from non-SPB iMTOCs, this is compared with 100% reduction in nucleation in either *mto2Δ* or *mto1Δ*. This suggests that the Mto1/2 complex may be able to compensate for the loss of non-core components by promoting higher-order assembly of the γ-TuSC. Examination of the size of the Mto1/2 complex may offer evidence to reinforce an Mto1/2 directed γ-TuSC multimerisation, and provide a better understanding of the nature of the nucleation complexes formed in *S. pombe*.

Additionally, I aim to investigate the role of Mto2 in Mto1/2 complex multimerisation. It has been demonstrated that Mto2 is not required to localise Mto1 to the MTOCs, therefore it does not act simply as a targeting factor. Instead, it is proposed that Mto2 may promote Mto1/2 complex assembly. I plan to investigate the effect of Mto2 on the multimerisation state of Mto1, and whether this is instigated by its own multimerisation.

The Mto1/2 complex is responsible for nucleation from MTOCs that are active at different points in the cell cycle. Ensuring that certain types of MT arrays are restricted to specific stages of the cell cycle is essential, as ectopic nucleation events may have drastic effects. For example, nucleation of a cytoplasmic array during mitosis may titrate αβ-tubulin dimers away from the nucleus and compromise the formation of the spindle. The changing pattern of active MTOCs suggests that the Mto1/2 complex may be subject to levels of cell cycle-dependent regulation. Several mechanisms of regulation have been suggested, including phosphorylation of both Mto1 and Mto2. In this thesis I am going to concentration on Mto2 phosphorylation, and investigate the consequence of this on the Mto1-Mto2 interaction as well as the proposed Mto2 multimerisation.

CHAPTER TWO

MATERIALS AND METHODS

2.1 MATERIALS

2.1.1 General materials used

Unless otherwise stated all analytical and reagent grade chemicals were purchased from Sigma-Aldrich. General labware and disposables including plastic and glassware were supplied by Fisher Scientific, U.S.A. Nitrocellulose membrane and broad range molecular weight markers, in addition to western blotting apparatus for 8.3 x 7.3 cm and 16 x 20 cm gels were supplied by BioRad [U.S.A.], larger 20.5 x 10 cm, low-wide gels were cast and run in apparatus supplied by Helena Biosciences, U.K. Oligonucleotide primers were produced by Eurofins MWG Operon, supplied as lyophilised material, which was then re-suspended in 1 X TE to 100 µM and stored at -20°C. All DNA was amplified using the PCR performed on a DNA Engine Dyad Peltier Thermal Cycler [MJ Research]. Centrifugation of microfuge tubes was performed at RT in a Biofuge Pico [Heraeus, Germany], and at 4°C using a Biofuge Fresco [Heraeus, Germany]. Centrifugation of 15 ml and 50 ml tubes was performed in a 5810 R Centrifuge [Eppindorf, Germany].

2.1.2 Grades of water used

All pure water was generated by the Purite Bio unit [Pur1te, U.K.]. Common buffers [Section 2.1.4] were made up using Grade II quality water [1-15 MΩ.cm]. Ultrapure deionised water with a resistivity of 18.2 MΩ.cm was used for molecular biology methods and addition to other sterile solutions.

2.1.3 Solution sterilisation

All standard buffers [used for molecular biology/cell culture], media and plastic/glassware were sterilised prior to use. This was done by autoclaving at 120°C for 30 min at 15 psi [BMM Western, U.K.]. Specialised buffers were sterilized by filtration through 0.22 µm filter [VWR international].

2.1.4 Common Buffers

TE [Tris EDTA pH 8.0]	10 mM Tris-HCl pH 8.0, 1 mM EDTA pH 8.0
Tris-buffered saline [TBS]	50 mM Tris base, 150 mM NaCl. pH is adjusted to 7.6 with 10 N HCl
TAE	40 mM Tris base, glacial acetic acid, 1 mM EDTA.
Laemmli Sample Buffer	2% [w/v] SDS, 10% [v/v] glycerol, 100 mM DTT, 60 mM Tris-HCl pH 6.8, 0.01% [w/v] bromophenol blue
Laemmli Running Buffer	25 mM Tris-base, 192 mM glycine, 0.1% [w/v] SDS. pH is adjusted to 8.3 with 10 N HCl.
CAPS transfer Buffer	10 mM CAPS pH 11.0 [pH adjusted with 10 N NaOH], 10% [v/v] MeOH
Coomassie Stain	50% [v/v] methanol, 10% [v/v] acetic acid, 0.25% [w/v] Brilliant Blue R-250]
Coomassie Destain	25% [v/v] methanol, 10% [v/v] acetic acid
Ponceau S Stain	0.2% [w/v] Ponceau S, 3% [w/v] trichloroacetic acid, 3% [w/v] sulfosalicylic acid]
Ponceau S Destain	5% [v/v] acetic acid

2.1.5 Antibodies used in this study

Primary antibodies	Dilution
anti-Myc 9E10 mouse monoclonal	1:1000
anti-GFP sheep polyclonal (Sawin et al., data unpublished]	1:500

anti-Mto1 sheep polyclonal (Sawin *et al.* 2004)	1:1000
anti-Mto2 sheep polyclonal (Samejima *et al.* 2005)	1:1000
anti-Alp4 sheep affinity purified polyclonal (Samejima *et al.* 2008)	1:300
anti-Alp6 sheep affinity purified polyclonal (Samejima *et al.* 2008)	1:300
anti-γ-tubulin GTU-88 mouse monoclonal [Sigma, U.S.A.]	1:1000
anti-Nop1 mouse polyclonal [Gift from D. Tollervey]	1:1000
anti-phospho-tyrosine mouse monoclonal [Upstate, U.S.A]	1:1000

Secondary/tertiary antibodies [Sigma, U.S.A.]	
GT-34 mouse anti-sheep/goat IgG monoclonal	1:10,000
GT-34-HRP mouse anti-sheep/goat IgG monoclonal HRP linked	1:10,000
Sheep anti-mouse IgG	1:10,000
anti-mouse IRDye800 [Licor Bioscience, U.S.A.]	1:5000
anti-mouse IRDye600 [Licor Bioscience, U.S.A.]	1:5000

2.1.6 Yeast media

Media used for fission yeast growth and manipulation are as described in Moreno *et al* (Moreno *et al.* 1991).

YE5S/4XYE5S — 0.5% [w/v] Difco Yeast Extract, 3.0% [w/v] glucose, 250 mg/l adenine/leucine/histidine/lysine hydrochloride, and uracil. Where 4 X applies to all ingredients. 5 mg/l phloxin B, 150 mg/l G418 [Geneticin], 100 µg/ml hygromycin/neomycin were added where required.

EMM-N [Edinburgh Minimal Media]

NH_4Cl [2.2 g/l] or L-glutamic acid monosodium salt [3.75 g/l]. 14.7 mM potassium hydrogen phthallate, 15.5 mM Na_2HPO_4, 2% glucose, 1 X salts [50 X stock solution: 52.5 g/l $MgCl_2 \cdot 6H_2O$, 0.735 mg/l $CaCl_2 \cdot 2H_2O$, 50 g/l KCl, 2 g/l Na_2SO_4], 1 X vitamins [1000 X stock: 1 g/l

pantothenic acid, 10 g/l nicotinic acid, 10 mg/l biotin] and 1 X minerals [10,000 X stock:5 g/l boric acid, 4 g/l $MnSO_4$, 4 g/l $ZnSO_4 \cdot 7H_2O$, 2 g/l $FeCl_2 \cdot 6H_2O$, 0.4 g/l molybdic acid, 1 g/l KI, 0.4 g/l $CuSO_4 \cdot 5H_2O$ and 10 g/l citric acid].

SILAC media — EMM + 6 mM NH_4Cl, 40 mg/ml $^{13}C6^{15}N4$-arginine, 30 mg/ml $^{13}C6^{15}N2$-lysine

SPA agar — 1% glucose, 1 g/l KH_2PO_4, 1 X vitamins [as above], 45 mg/l amino acid supplements [as above], 2% [w/v] Difco Bacto agar.

2.1.7 Bacteria Media

SOC (Sambrook *et al.,* 2001)

Difco Bacto tryptone [20 g/l], Difco Bacto yeast extract [5 g/l], NaCl [10 mM], KCl [2.5 mM]. After autoclaving and cooling to 50°C, sterile $MgCl_2$ and $MgSO_4$ were added to a final concentration of 10 mM. Sterile glucose was added to a final concentration of 20 mM.

Luria-Bertani Medium [LB] [Miller, 1972]

Difco Bacto tryptone [10 g/l], Difco Bacto yeast extract [5 g/l], NaCl [5 g/l]. Before autoclaving the pH was adjusted to 7.2 using 10 M NaOH. Solid LB agar plates are made by adding 2% [w/v] Difco Bacto agar to the media.

2.1.8 Antibiotics used this study

Antibiotics were supplied by Melford, U.K. Antibiotics used for bacterial selection were Ampicillin [100 µg/ml], Chloroamphenicol [25 µg/ml] and Kanamycin [50 µg/ml].

2.1.9 *Escherichia coli* strains and genotypes

One Shot® TOP10 Chemically competent *E. coli* [Invitrogen]

F- mcrA Δφ80lacZΔM15 ΔlacX74 recA1 araD139 Δ[ara-leu] 7697 galU galK rpsL [StrR] endA1 nupG λ-

XL10-Gold Ultracompetent *E. coli* [Stratagene]

TetrD[*mcrA*]*183* D[*mcrCB-hsdSMR-mrr*]*173 endA1 supE44 thi-1 recA1 gyrA96 relA1 lac* Hte [F´ *proAB lacI*qZD*M15* Tn*10* [Tetr] Amy Camr].

BL21-CodonPlus[DE3]-RIL *E. coli* [Stratagene]

B F– *ompT hsdS*[rB– mB–] *dcm*+ Tetr *gal endA* Hte [*argU ileY leuW*Camr]

2.2 MOLECULAR BIOLOGY METHODS

2.2.1 Manipulation of bacteria

2.2.1.1 Growth of *E. coli* strains

All bacterial strains were grown at 37°C unless otherwise stated. *E. coli* grown on LB-Agar was incubated for 1 - 2 days then stored at 4°C. Liquid cultures were grown in LB on a shaker at 200 rpm. Cells intended for plasmid purification were grown until stationary phase.

2.2.1.2 Preparation of transformation-competent cells

Single colonies were used to inoculate 5 ml of LB culture. The resultant stationary phase culture was used to inoculate 500 ml of LB which was grown to OD_{650nm} = 0.5. Culture was transferred into 450 ml centrifuge bottles and incubated on ice for 10 min. Culture was then spun at 24000 rpm at 4°C for 15 min [Beckmann Avanti J-25 centrifuge using a JLA 10-500 rotor]. Supernatant was removed and pellet re-suspended in 165 ml Buffer A. Cells were incubated on ice for 45 min.

Culture was then spun at 24000 rpm at 4°C for 15 min [Beckmann Avanti J-25 centrifuge using a JLA 10-500 rotor] and cells were re-suspended in 40 ml Buffer B, and incubated on ice for a further 15 min. Aliquots of 200 µl were transferred to a screw-cap tube, then frozen in liquid nitrogen and stored at -80°C. Buffer A: 100 mM RbCl, 50 mM $MnCl_2$, 30 mM potassium Acetate, 10 mM $CaCl_2$, 15% [v/v] glycerol. Buffer B: 10 mM MOPS, 10 mM $RbCl_2$, 75 mM $CaCl_2$, 15% [v/v] glycerol. Buffers were pH adjusted to 5.8 and 6.8 respectively.

2.2.1.3 Transformation of *E. coli*

200 µl aliquots of frozen competent cells were thawed on ice. 50 – 200 ng of DNA was added to the cells, mixed by inversion and incubated on ice for 30 min. Cells were then transferred to 42°C heat-block for 45 sec then incubated on ice for a further 2 min. 0.8 ml of SOC medium was added to the cells and incubated at 37°C for 1 hr on an incubation shaker. Cells were then centrifuged [13,000 **g**, 15 sec, RT] and pellet was re-suspended in 200 µl of SOC. The suspension was spit 1:9 between two LB-agar plates containing an appropriate antibiotic. Acid-washed glass beads were used to spread the cells on to the plates and were incubated O/N.

2.2.1.4 Isolation of plasmid DNA from *E. coli*

Plasmid DNA was isolated from bacteria using the Nucleospin Plasmid Kit [Machery-Nagel, Germany]. Cells from 1 - 2 ml of culture were centrifuged [11,000 **g**, 1 min, RT], and re-suspended in 250 µl P1 containing RNAse. 250 µl of buffer P2 was added and the cells were mixed by inversion. The debris was removed by centrifugation [11,000 **g**, 10 min, RT], and the clear supernatant was applied to a QIAprep spin column. The plasmid DNA was bound to the column by centrifugation [11,000 **g**, 1 min, RT], and the eluate was discarded. 750 µl of buffer PE was applied to the column and the column was washed twice by centrifugation [11,000 **g**, 30 sec RT then 11,000 **g**, 1 min, RT]. The column was transferred to a sterile microfuge tube. 30 µl of buffer EB was applied to the centre of the column matrix and left to

stand at RT for 1 min. The plasmid DNA was eluted into the microfuge tube by centrifugation [11,000 **g**, 1 min, RT] and stored at -20°C.

2.2.2 Manipulation of DNA

2.2.2.1 Calculation of oligonucleotide primer concentration

To calculate the amount of each oligonucleotide primer to be added to each PCR reaction [in pmoles] the following equation was used to normalise the amount of oligonucleotide primer present in each PCR reaction where the length in oligonucleotide was different by > 20%. 330 Da is the average Mw of a nucleotide base.

$$\text{X pmoles of oligo} = \frac{\text{ng of oligo}}{\text{330 x No. of bases in the oligo}} \text{ X } 1000$$

2.2.2.2 PCR amplification from plasmid DNA

PCR from plasmid DNA was used to add HTB/TAPS tags following the protocol described by Bahler and colleagues (Bahler *et al.* 1998). DNA containing HTB/TAPS tag flanked by pFA6 multiple cloning site and the kanamycin resistance gene [KanMX6] were amplified from pKS466 (Tagwerker *et al.* 2006) and pKS422 (Cheeseman *et al.* 2001), respectively. Oligonucleotide primers OKS257 and OKS258 were used for the amplification form both plasmids. OKS257 contained in 5'-3' direction, 80bp of the SPBC902.06 exon, excluding the TAG STOP codon, and 20bp of the pFA6a module. OKS258 contained in 3'-5' direction, 80bp of the SPBC902.06 3'UTR and 20bp of the KanMX6 module. This allowed amplification of TAG-KanMX6 from each plasmid flanked by homologous Mto2 sequence. The polymerase reaction contained 400 ng of plasmid template DNA, 0.2 µM of each oligonucleotide, 500 µM of each dNTP, 3.5 mM $MgCl_2$, 75 mM Tris-HCl pH8.8, 20

mM $[NH_4]_2SO_4$, 0.01% [v/v] Tween® 20, 200 units of Taq DNA Polymerase, 250 U of Pwo diluted 1:60 in Pwo buffer [200 mM Tris-HCl pH 8.8, 100 mM KCl, 100 mM $[NH_4]_2SO_4$, 20 mM $MgSO_4$, 1.0% [v/v] Triton X-100 and 1 mg/ml nuclease-free BSA] in a total volume of 1 ml. Cycling parameters were as follows: 1] 2 min at 95°C, 2] 15 sec at 95°C. 3] 30 sec at 60°C, 4] 2 min extension at 72°C, which was repeated 25 times from step 2, then final extension for 5 min at 72°C.

2.2.2.3 PCR amplification from cell lysate (Chen *et al.* 1995)

A match-head sized patch of cells from a colony were suspended in 30 µl of 0.25% [w/v] SDS, 1 X TE pH 8.0. Solution was then incubated at 100°C for 5 min. Boiled cells were then spun in a centrifuge [13,000 **g**, 1 min, RT] and 20 µl of the supernatant was transferred to a fresh tube. The reaction mix contained 1 µl of genomic template DNA, 75 mM Tris-HCl pH8.8, 20 mM $[NH_4]_2SO_4$, 0.01% [v/v] Tween® 20, 0.5 µM of each oligonucleotide primer, 200 µM dNTPs, 1.5 mM $MgCl_2$, 1% [v/v] Triton X-100, 5 U Taq polymerase, 0.075 U of the proof-reading polymerase from *Pyrococcus furiosus* Pfu [Promega, USA] diluted 1:60 in Pfu buffer [200 mM Tris-HCl pH 8.8, 100 mM KCl, 100 mM $[NH_4]_2SO_4$, 20 mM $MgSO_4$, 1.0% [v/v] Triton X-100 and 1 mg/ml nuclease-free BSA]. Cycling parameters used for amplification were as follows: 1] 94°C for 2 min, 2] 94°C for 15 sec, 3] 50°C for 30 sec, 4] 68°C for 3 min, which was repeated 35 times from step 2 followed by a final extension at 68°C for 10 min.

2.2.2.4 Site Directed Mutagenesis

Site Directed Mutagenesis was performed using kits provided by Stratagene, USA. Amplification was performed using the following parameters: 1] 95°C for 30 sec, 2] 95°C for 30 sec, 3] 55°C for 1 min, 4] 68°C for 5 min, this was repeated 12 times from step 2 with a final 5 min extension at 68°C. 10 U of Dpn1 restriction enzyme was added to the mix and incubated at 37°C for 1 hr to digest un-mutagenised, methylated dsDNA template. The nicked mutagenised dsDNA was then transformed into XL1-Blue super-competent cells. Single-site directed

mutagenesis reactions contained 50 ng of dsDNA template, 125 ng of each oligonucleotide primer. 1 µl of the dNTP mix provided in the kit was used per reaction in addition to 1 X Reaction Buffer [10 mM KCl, 10 mM $[NH_4]_2SO_4$, 20 mM Tris-HCl pH 8.8, 2 mM $MgSO_4$, 0.1% [v/v] Triton X-100, 0.1 mg/ml nuclease-free BSA]. Multi-site directed mutagenesis was performed in a final volume of 25 µl and contained 100 ng of dsDNA template, 100 ng of each oligonucleotide primer. 1 µl of the dNTP mix provided in the kit was used per reaction in addition to 2.5µl of 10 X Reaction Buffer, 0.5 µl of QuickSolution [components unknown] and the 1µl of the QuickChange® Multi enzyme mix [other than the presence of *Pfu Turbo* DNA polymerase, the exact components are unknown]. Table 2.1 lists the oligonucleotide combinations used for the generation of all mutants analysed in this study.

2.2.2.5 Sequencing of plasmids

DNA sequencing was carried out on in house ABI 3730 capillary sequencing instruments [Applied Biosystems, USA]. The sequencing reaction contained 250 ng plasmid DNA, 3.2 pmol of primer, 1 X BigDye Terminator v3.1 [Applied Biosystems] 10 mM Tris-HCl pH 8.5, 2.5 mM $MgCl_2$ in a final volume of 10 µl. The sequencing reaction was carried out using the following parameter: 24 cycles of 1] 96°C for 30 sec, 2] 50°C for 15 sec and 3] 60°C for 4 min. Digital output file of the DNA sequence was then further analysed using Seqman sequence analysis software [DNASTAR Inc.]

2.2.2.6 Extraction of amplified DNA fragments from agarose gel

PCR products that had been separation by electrophoresis were purified using the QIAquick PCR Purification Kit [Qiagen, USA]. The band of DNA was cut from the agarose gel, placed in a sterile microfuge tube and weighed. 3 volumes of buffer QC were added, where 1 g of DNA / gel = 1 ml buffer QC. The mixture was incubated at 50°C for 10 min, until the agarose had fully dissolved, and 1 X volume of 100% [v/v] isopropanol was added. The DNA was bound to the column by centrifugation [11,000 **g**, 10 min, RT] and the eluate was discarded. 750 µl buffer PE

Mutant	Oligonucleotide primers	Template Plasmid	Construct Plasmid
T35A	OKS1251, OKS1252 *[sdm]*	pKS535	pKS1059
S179A	OKS1253, OKS1254 *[sdm]*	pKS535	pKS1060
S220A	OKS1255, OKS1256 *[sdm]*	pKS535	pKS1061
S366A	OKS1257, OKS1258 *[sdm]*	pKS535	pKS1062
T396A	OKS1259, OKS1260 *[sdm]*	pKS535	pKS1063
5A: T35A, S179A, S220A, S366A ,T396A	OKS1252, OK1254, OKS1256, OKS1260 *[msdm]*	pKS1062	pKS1064
Y168F	OKS1408, OKS1409 *[sdm]*	pKS535	pKS1084
Y269F	OKS1410, OKS1411 *[sdm]*	pKS535	pKS1085
Block 1 : S159A, S169A, T174A, S176A, S179A, T185A	OKS1780 *[msdm]*	pKS535	pKS1071
Block 2: S275A, S276A, S282A, S284A	OKS1781 *[msdm]*	pKS535	pKS1072
Block 3: S361A, S362A, S366A, S369A	OKS1782 *[msdm]*	pKS535	pKS1073
Block 1: S169D, T174D, S176D, S179D	OKS1783, OKS1831, OKS1832 *[msdm]*	pKS535	pKS1074
Block 2: S282D, S284D	OKS1784 *[msdm]*	pKS535	pKS1075
Block 3: S366D, S369D	OKS1785 *[msdm]*	pKS535	pKS1076

Table 2.1 Oligonucleotide primer combinations used for site-directed mutagenesis [sdm] and multi-site directed mutagensis [msdm] reactions performed in this study.

was applied to the column twice [11,000 **g**, 30 sec, RT then 11,000 **g**, 2mins, RT]. The column [bound with plasmid DNA] was transferred to a sterile microfuge tube. 30 µl of buffer EB was applied to the centre of the column and left to stand at RT for 1 min. The DNA was eluted into the microfuge tube by centrifugation [11,000 **g**, 1 min, RT] and stored at -20°C.

2.2.2.7 Phenol chloroform extraction

This technique was used to isolate 5-20 µg of DNA amplified by PCR. An equal volume of phenol/chloroform/isoamyl alcohol [25:24:1] was added to the PCR

reaction in a microfuge tube, mixed and spun in a table-top centrifuge [13,000 **g**, 5 min, RT]. The upper aqueous layer was recovered leaving the phenol, chloroform and isoamyl alcohol in the tube. This was repeated. Chloroform alone was then added to the supernatant, mixed, spun [13,000 **g**, 5 min, RT] and new supernatant was recovered. NaOAc was added to a final concentration of 0.3 M, solution mixed and then 2 X volumes of ethanol was added. This was agitated at RT for 5 min. Precipitated DNA was then spun in a centrifuge [13,000 **g**, 1 min, 4°C]. The DNA pellet was washed with 1 ml 70% ethanol, and supernatant removed leaving the pellet to air dry. DNA was then re-suspended in 50 µl 1 X TE, and stored at -20°C.

2.2.2.8 Determination of DNA concentration

Absorbance at 260nm was measured using a Nanodrop™ 1000 Spectrophotometer [Thermo Scientific, USA]. Concentration was calculated using the Beer-Lambert Law:

$$c = [A \times \varepsilon] / l$$

Where **c** is the nucleic acid concentration in $ng\mu l^{-1}$, **A** is the absorbance in AU, **ε** is the wavelength-dependent extinction coefficient in $ng^{-1}cm\mu l^{-1}$ and **l** is the length of the light path in cm. The extinction co-efficient for dsDNA is 50 $ng^{-1}cm\mu l^{-1}$. Nanodrop™ 1000 Spectrophotometer is washed with 2 µl dH_2O, then blanked with 1 µl buffer EB [or dH_2O]. 1 – 2 µl of DNA solution is then used per measurement, which is taken 3 times, and the instrument is blanked with buffer EB or 1 X TE between each measurement.

2.2.2.9 Electrophoresis of DNA on agarose gels

1% [w/v] agarose gels were prepared using agarose I [Amresco, USA]. Agarose was dissolved in 1 X TAE buffer by heating in a microwave then cooled to approximately 60°C. 0.4 µg/ml EtBr was added to the solution and it was poured into a gel tray and left to solidify at RT. DNA was diluted in 6 X DNA loading buffer [0.05% [w/v] Orange G, 5% [w/v] glycerol] and loaded into the gel which was run at 100 V. DNA was examined under UV illumination at 360nm. 1 kb ladder was used

for all applications containing; 10.0 kb, 8.0 kb, 6.0 kb, 5.0 kb, 4.0 kb, 3.0 kb, 2.0 kb, 1.5 kb, 1.0 kb and 0.5 kb fragments. 0.5 µg of marker was loaded per gel.

2.2.2.10 Restriction enzyme digestion

Reactions were set up that contained 5 µg of plasmid DNA, 2 µl of 10 X NE Buffer 3 [100 mM NaCl, 50 mM Tris-HCl, 10 mM $MgCl_2$, 1 mM DTT pH 7.9] and 10 U of restriction enzyme [typically Not I] in a final volume of 20 µl. This was incubated at 37°C for 1 hr. Digestion efficiency was analysed on a 1% [w/v] agarose gel.

2.2.3 Gateway® cloning

The Gateway® cloning Technology developed by Invitrogen is based on site-specific recombination system used by Phage I to integrate DNA into *E. coli* chromosomes. Both Phage and *E. coli* DNA contain specific recombination sites, *attP* and *att*B, respectively. Additionally, they each encode lysogenic enzymes: the phage I Int [Integrase] and the *E. coli* protein IHF [Integration Host Factor]. Following integration into the bacteria, recombination occurs between *attB* and *attP* sites to generate *attL* and *attR* sites that flank the integrated piece of Phage DNA on the *E. coli* chromosome (Landy 1989). This reaction has been used to develop an *in vitro* system which allows efficient transfer of DNA between plasmids containing modified versions of the recombination sites (Hartley *et al.* 2000). The Gateway recombination system is schematically represented in Figure 2.1.

2.2.3.1 Construction of Entry vectors

2.2.3.1.1 Generation of Mto2 containing *attB1/2* flanking sites

Primer design and amplification procedure were based on guidelines from accompanying literature from BP Clonase™ II mix [Invitrogen, USA] and Phusion® Hot Start High-Fidelity DNA Polymerase [Finnzymes, Finland]. Amplification of

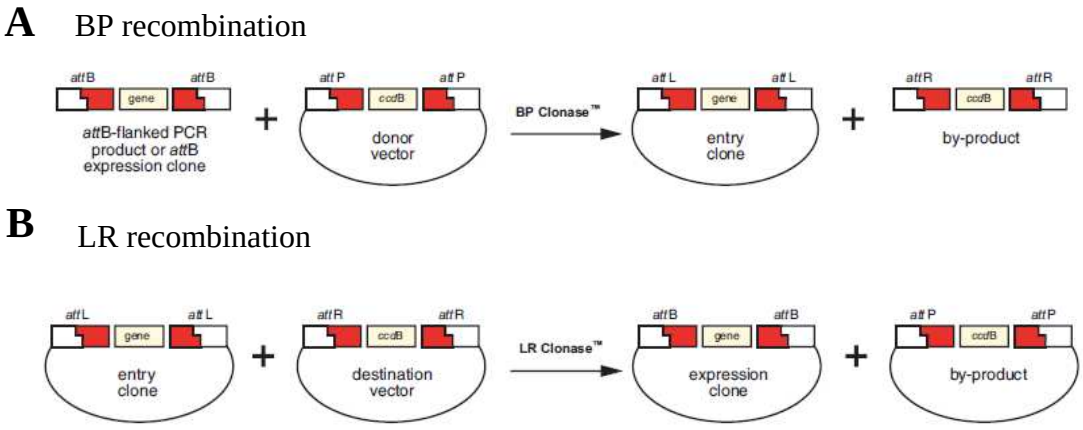

Figure 2.1 The Gateway® Recombination system. Figure modified from Invitrogen. [A] Schematic representation of the BP recombination reaction to create entry clone from DNA amplified with *attB1* and *attB2* flanking sequence. [B] LR recombination where genes within entry clones can be transferred to expression clones using *attL1* and *attL2* sequences.

DNA containing flanking *attB*1/2 sites, required oligonucleotides incorporating sequence covering 31bp of *attB1/2* sequence and ~20 bp of template specific sequence. In order to avoid the use of long [> 50bp] oligonucleotide primers a two-step amplification strategy was used. Reaction mix for step 1 contained 10 ng of template DNA, 1 X Phusion HF Buffer [containing 1.5 mM $MgCl_2$], 10 pmoles of primers, 200 µM dNTPs, and 1 U of Phusion® Hot Start High-Fidelity DNA Polymerase [Finnzymes, Finland] in a final volume of 50µl. Thermal cycling parameters for step 1 were set as follows: 1] 98°C for 30 sec, then 20 cycles of a 2] 98°C for 10 sec, 3] 50°C for 30 sec, 4] 72°C for 20 sec, then a final extension at 72°C for 5 min. In step 2 of the amplification reaction, 10 µl of the reaction mix from the first step was transferred to 15 µl of the above reaction mix, containing 40 pmoles of each adaptor primer [OKS1204 and OKS1205]. Cycling parameters for the second step were set as follows: 1] 98°C for 30 sec, then 5 cycles of 2] 98°C for 10 sec, 3] 45°C for 30 sec, 4] 72°C for 20 sec, then a further 20 cycles at an annealing temperature of 55°C before a final extension for 10 min at 72°C. *AttB1/2*

flanked DNA was then run on 1% [w/v] agarose gel and DNA band was excised from the gel and purified. Using primers OKS1201 and OKS1202, this method was used to create DNA encoding for *att*B1/2 flanked Mto2 that contained 2 X TAG STOP codons. This DNA was then used to generate plasmids containing N-terminal tagged and un-tagged Mto2.

2.2.3.1.2 Generation of Mto2 truncations containing *attB1/2* flanking sites

Mto2 truncations were constructed using PCR amplification of Mto2 ORF sequence flanked by *attB1/2* sites. Positions of oligonucleotide primers used for the amplification are described in Figure 2.2.

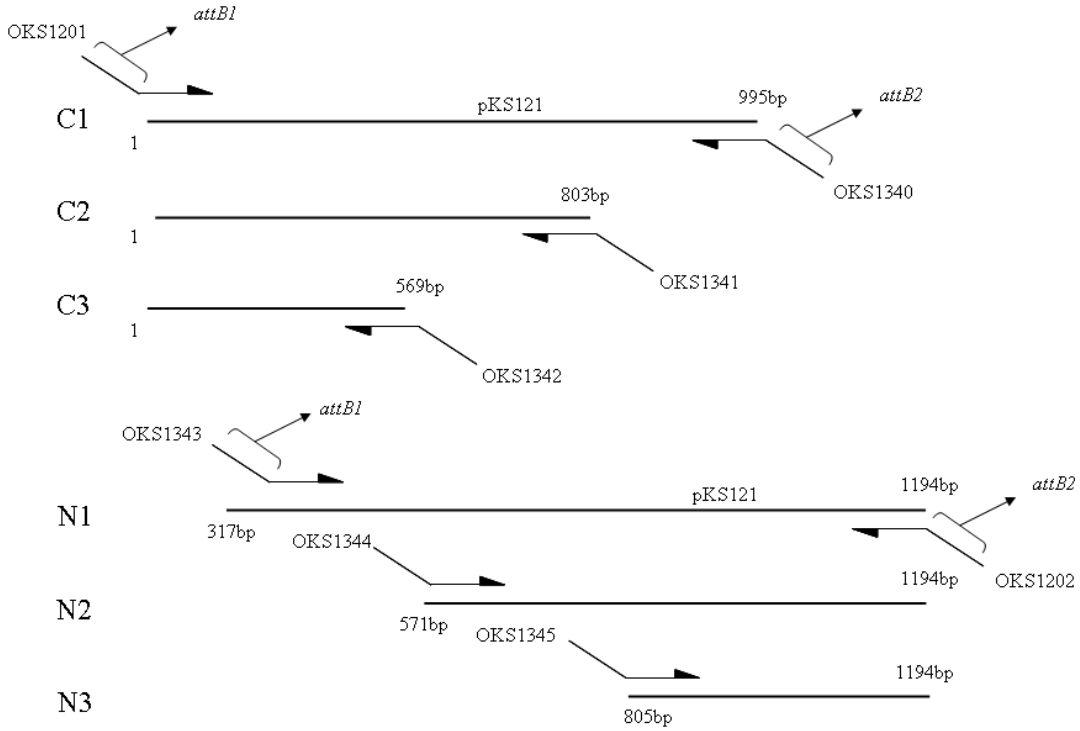

Figure 2.2 Construction of Mto2 truncations. Schematic diagram representing PCR amplification of C1-3 / N1-3 truncations from pKS121 using oligonucleotide primers OKS1201, OKS1202 and OKS1340-45. Primers were designed to include 18 bp of *att*B1/2 sequence which is extended to the full 36 bp upon a second round of PCR using adapter primers OKS1203 and OKS1204.

2.2.3.1.3 Generation of TEV-Mto2 containing *attB1/2* flanking sites

AttB1/2 flanked DNA was synthesised using oligonucleotide primers OKS1684/OKS1202 and adaptor primers OKS1203/OKS1204. This placed the TEV site 5' of the start methionine of the *mto2* ORF.

2.2.3.2 BP recombination reaction

The reaction mix contained 50 fmoles of *attB1/2* flanked PCR product and 50 fmoles of pDONR™221 donor vector, 1 X TE Buffer pH 7.0 and 2 µl BP Clonase™ II enzyme mix in a final reaction volume of 10 µl. The recombination mix was incubated at 25°C O/N. The reaction was stopped by adding 2 µg of Proteinase K and incubating the mix at 37°C for 1 hr. 5 µl of the reaction was then transformed into TOP10 *E. coli*, where the *ccdB* gene from the pDONR211 plasmid provided negative selection against empty vector.

2.2.3.3 Construction of Destination vectors

2.2.3.3.1 LR recombination reaction

The reaction mix was prepared in a microfuge as follows: 150 ng of pDONR™221 containing Mto2 template flanked by *attL1/2* sites, 150 ng of Destination vector containing *attR1/2* sites, 1 X TE pH 8.0 and 2 µl of LR Clonase™ II enzyme mix in a final volume of 10µl. Microfuge tube was gently agitated and then incubated O/N at 25°C. 2 µg of Proteinase K was added to the mixture and incubated for 1 hr at 37°C. 10 µl of the reaction mix was then transformed into One Shot® TOP10 *E. coli* which were plated onto LB agar plus the appropriate antibiotic. The *ccdB* gene from the pDONR211 plasmid and destination vectors provided negative selection against empty vector.

2.2.3.2.2 LR recombination using pDUAL tagging vectors (Matsuyama *et al.* 2004)

pDUAL vectors allow addition of a number of different tags under different strengths of thiamine inducible promoters [*nmt81/nmt41/nmt1*] on both the N- and C-termini. These plasmids can then be integrated in the *S. pombe* genome by homologous recombination at the *leu1* locus. Integrants are maintained due to the presence of 5'region of *leu1* ORF, which when integrated into strains containing the *leu1-32* autotrophic allele, results in leucine prototrophy. Table 2.1 lists the LR recombination reactions that were performed with pDUAL plasmids.

pDUAL vector	pDONR vector	Construct
pDUAL-HFG81c	pKS1032	nmt81:HFG-Mto2
pDUAL-HFG81c	pKS1036	nmt81:HFG-Mto2 N1
pDUAL-HFG81c	pKS1037	nmt81:HFG-Mto2 N2
pDUAL-HFG81c	pKS1039	nmt81:HFG-Mto2 C1
pDUAL-HFG81c	pKS1048	nmt81:HFG-Mto2 L133DL137D
pDUAL-HFG41c	pKS1048	nmt41:HFG-Mto2 L133DL137D
pDUAL-HFG81c	pKS1071	nmt81:HFG-Mto2 1A
pDUAL-HFG81c	pKS1072	nmt81:HFG-Mto2 2A
pDUAL-HFG81c	pKS1073	nmt81:HFG-Mto2 3A
pDUAL-HFG81c	pKS1074	nmt81:HFG-Mto2 1D
pDUAL-HFG81c	pKS1075	nmt81:HFG-Mto2 2D
pDUAL-HFG81c	pKS1076	nmt81:HFG-Mto2 3D
pDUAL-HFG81c	pKS1059	nmt81:HFG-Mto2 T35A
pDUAL-HFG81c	pKS1060	nmt81:HFG-Mto2 S179A
pDUAL-HFG81c	pKS1061	nmt81:HFG-Mto2 S220A
pDUAL-HFG81c	pKS1062	nmt81:HFG-Mto2 S366A
pDUAL-HFG81c	pKS1063	nmt81:HFG-Mto2 T394A
pDUAL-HFG81c	pKS1064	nmt81:HFG-Mto2 5A
pDUAL-HFG81c	pKS1084	nmt81:HFG-Mto2 Y168F
pDUAL-HFG81c	pKS1085	nmt81:HFG-Mto2 Y269F

Table 2.2 LR recombination reactions between pDONR entry vector and pDUAL plasmids and their resulting constructs.

2.2.3.2.3 LR recombination into pHGWA bacterial expression vectors (Busso *et al.* 2005)

Plasmids pKS1034 and pKS1035 encoding N-terminal tagged versions of Mto2 were created by an LR recombination reaction between pKS1032 and

pHNGWA / pHMGWA. 2 – 3 single colonies from each reaction were isolated and the protein expression was tested by SDS-PAGE analysis of total protein from 1 ml of cells induced using 1 mM IPTG. MBP-TEV-Mto2 was created through the LR recombination reaction with pKS1057 containing *attL1/2* flanked *mto2* with amino terminal TEV cleavage and pHMGWA.

2.2.4 Gene synthesis

Mto2 mutants were supplied by GENEART [Germany]. Lyophilised plasmid DNA was re-suspended in 1 X TE to 100 ng/µl. Sequences contained the mutagenised Mto2 ORF, within a pMK [KanR] derived vector. This was used as a template for PCR amplification to generate *attB*1/2 flanking sequence [section 2.2.3.1.1]. Linear DNA was purified by agarose gel extraction and used in a BP recombination reaction with pKS535.

2.3 FISSION YEAST METHODS

2.3.1 Growth on Agar

Non-*ts* strains were grown at 30°C. Once woken up from -80°C storage, yeast cells were grown on YE5S-agar until colonies were visible. For strains containing selective markers, these were replica-plated onto non-selective plates then back onto selective media and YE5S plus phloxin B to test for stability, where dark pink phloxin B staining indicated dead cells. Once stable strains were acquired, these were incubated at RT for a maximum of 1 week, after which plates were stored at 4°C for up to 1 month.

2.3.2 Growth in media

When proteins were expressed under *nmt41/nmt81* thiamine repressible promoters, following initial inoculation of 5 ml of EMM plus appropriate nitrogen source and amino acid supplements, cultures were grown O/N at 32°C. To ensure

expression culture was diluted 1:50 and cells were grown O/N or for at least 16 hrs at 32°C (Maundrell 1990).

2.3.3 Growth of SILAC strains

Pre-cultures of KS5477 and KS5479 were diluted into the required amount of media, and were grown for at least six generations to an OD_{595nm} 0.4. KS5477, which did contain the *nda3-KM311* allele was grown in unlabelled SILAC media and KS5477, which did not contain *nda3-KM311* was grown in heavy labelled SILAC media. Cultures were agitated in a temperature controlled incubator at 18°C for 9 hr. After 9 hr cultures had reached mid-log phase [$OD_{595\ nm}$ = 0.8]. Normalised cells cultures were combined and then harvested.

2.3.4 Strain construction

2.3.4.1 Transformation of yeast by lithium acetate (Bahler *et al.* 1998)

Yeast strains were cultured in YE5S medium at 32°C to an OD_{595nm} of 0.8. 20 ml [~ 10^7 cells] were used per transformation. Cells harvested by centrifugation [4,000 **g**, 3 min, RT]. Cell pellet was re-suspended in 20 ml dH_2O and spun again [4,000 **g**, 3 min, RT]. Pellet was re-suspended in 1 ml dH_2O and transferred to a microfuge tube. Cells were spun again [5,000 **g**, 1 min, RT] then re-suspended in 1 ml 100 mM LiOAc, 1 X TE pH 7.5. Cells were spun again [5,000 **g**, 1 min, RT] and re-suspended in 100 mM LiOAc, 1 X TE pH 7.5, up to a volume of 100 µl. 20 µg of DNA was then added to the cells and incubated at RT for 10 min. 260 µl of 40% [w/v] $PEG_{MW}4000$, 100 mM LiOAc, 1 X TE pH 7.5, was then added to the cells, mixed then incubated at 30°C. After 45 min, 43 µl of DMSO was added and cells were heat-shocked at 42°C for 5 min in a heat block. Transformed cells were then spun in a microfuge [5,000 **g**, 1 min, RT] and washed in 1 ml dH_2O, cells are then spun again and re-suspended in 0.5 ml. 2 X 250 µl of cell suspension are then plated out onto YE5S agar using acid washed glass beads to spread the cells, and the plates are incubated overnight at 32°C.

2.3.4.2 Transformation of linearised Mto2 from pDUAL vectors

5µg of pDUAL plasmid containing Mto2 was subject to Not I restriction enzyme digestion, then linear DNA was transformed into *mto2Δ* strains. Following transformation, yeast were spread onto EMM agar + 10 mM glutamate + ade/ura/his/lys [250 µg/ml]. Integrants were selected for leucine prototrophy.

2.3.4.3 Mating of yeast

h^+ and h^- fission yeast mating type strains are spotted onto a SPA agar plate and mixed together with 5 µl of dH_2O. Plates are incubated at 30°C for 48 hr. For mating determination, mated cells are examined under a light microscope or are exposed to iodine vapour from iodine pellets spread on the lid of a petri-dish, whereby the iodine strongly stains spore walls found in cells that have undergone meiosis.

2.3.4.4 Tetrad dissection

Mated cell populations are streaked down the middle of a YE5S agar plate and incubated for 1 hr at 37°C. Spores are then separated using a Singer MSM 300 dissection microscope [Singer Instruments, U.K.]. Spores from non-*ts* mutants are incubated at 30°C for 3-4 days, or until colonies are visible.

2.4 PROTEIN BIOCHEMISTRY

2.4.1 Preparation of protein extracts

2.4.1.1 Preparation of soluble native extracts from yeast

Typically 50 ml of yeast were grown to an OD_{595nm} of 0.8 [mid-log phase ~ 10^7 cells ml^{-1}]. Cells were then harvested using centrifugation [4,000 **g**, 4 min, RT]. Cell pellet was transferred to a 2 ml conical screw cap tube and washed with 1 ml of

lysis buffer by centrifugation [5,000 **g**, 4 min, RT]. Pellet was then re-suspended in equal volume of lysis buffer. 0.5 mm Zirconia/Silica beads [BioSpec Products, U.S.A.] were added to the meniscus and cells were disrupted in a Ribolyser [Hybaid, U.K.] for 30 sec at a speed of 6.5 at 4°C. The bottom of the tube was then pierced with a hot sterile needle and the tube was placed in a 5 ml polyethylene tube and extract was collected by centrifugation [1,500 **g**, 2 min, RT]. Isolated cell extract was transferred to a fresh microfuge tube and cleared by centrifugation [13,000 **g**, 15 min, 4°C]. Supernatant was transferred and lysates were stored at -20°C.

2.4.1.2 Preparation of total protein extracts from yeast

Typically 20 ml of yeast were grown to an OD_{595nm} of 0.8 [mid-log phase ~ 10^7 cells ml^{-1}]. Cells were then harvested using centrifugation [4,000 **g**, 4 min, RT]. Cell pellet was transferred to a 2 ml conical screw cap tube and washed with 1 ml of dH_2O by centrifugation [5,000 g, 4 min, RT]. Pellet was then re-suspended in equal volume of dH_2O and incubated at 100°C for 7 min. 0.5 mm Zirconia/Silica beads [BioSpec Products, U.S.A.] were added to the boiled extract up to the meniscus and cells were disrupted in a Ribolyser [Hybaid, U.K.] for 30 sec at a speed of 6.5. The bottom of the tube was then pierced with a hot needle and the tube was placed in a 5 ml polyethylene tube and extract was collected by centrifugation [1,500 **g**, 2 min, RT]. Isolated cell extract was the diluted with 1 X volume of 2 X Sample buffer [- DTT and bromophenol blue] and transferred to a fresh microfuge tube and boiled for 5 min. Extract was then cleared by centrifugation [13,000 **g**, 15 min, RT]. Supernatant was transferred to a fresh tube and stored at -20°C.

2.4.1.3 Preparation of large scale fission yeast extracts

Culture was grown to an OD_{595nm} = 0.8 [1 X YE5S] or OD_{595nm} = 12 [4 X YE5S]. For cultures [< 6 L] cells were harvested using Beckmann Avanti J-25 centrifuge using a JLA 10-500 rotor [10,000 rpm, 10 min, 4°C], for culture > 6 L, cells are harvested using a Beckmann Avanti J-25 centrifuge using a JLA 8.1000 rotor [5,000 rpm, 15 min, 4°C]. Pellet was re-suspended in 0.1 X culture volumes of

20 mM HEPES pH 7.6, and cells were collected as before. Cell pellet was then re-suspended in 0.3 X cell volumes of 20 mM HEPES pH 7.6. Cell solution was then frozen, drop-wise into a sieve immersed in liquid nitrogen. Balls of cells were then stored in 15 / 50 ml tubes at -80°C. 5 – 40 g of frozen cells were ground in a Retsch RM100 electric mortar-grinder [Retsch, Germany]. The balls of cells were poured into the Retsch Grinder, which had been pre-cooled to -80°C with liquid nitrogen. Cells were ground until > 70% disruption had been achieved as assessed by examination under light microscope. Cell powder was then stored at -80°C. The required amount of disrupted cell powder was acquired by weighing aliquots into a cooled tube. Powder was then thawed on ice for 5 min, and re-suspended in 2 X lysis buffer [50 mM HEPES pH 7.6, 75 mM KCl, 1 mM $MgCl_2$, 1mM EGTA, 0.1% [v/v] Triton X-100, 0.5 mM DTT, 1 mM PMSF, 1 mM benzamidine, 10 µg/ml CLAAPE]. Cell suspension was cleared in a table-top centrifuge [13,000 **g**, 5 min, 4°C], extract supernatant was transferred to a fresh tube and spun again [13,000 **g**, 10 min, 4°C]. The cleared supernatant was recovered and transferred to a fresh microfuge tube.

2.4.1.4 Induction of protein expression in *E. coli*

BL21- CodonPlus® competent *E. coli* [Stratagene, USA] were chosen as an expression strain as they express from a pACYC based plasmid containing *argU*, *ileY*, *leuW* tRNA genes to provide extra copies of rare tRNAs which frequently limit translation during high-level expression. The *E. coli* strain also contains the T7 promoter where expression of the T7 phage RNA polymerase is driven by the lacUV5 promoter in response to IPTG. Stationary culture was diluted 1:50 and grown for 2 hr at 37°C. Protein expression was then induced using 0.05 mM IPTG [Melford, U.K.] and shifted to 18°C and incubated O/N. For small cultures [< 200 ml] cells pellets from 1-5 ml aliquots are collected by centrifugation [13,000 **g**, 2 min, RT] and stored in microfuge tube. For large cultures [> 200 ml] cells were harvested using Beckmann Avanti J-25 centrifuge and JLA 10-500 rotor [10,000 rpm, 10 min, 4°C], for culture > 6 L, cells are harvested using a Beckmann Avanti J-25 centrifuge using a JLA 8.1000 rotor [5,000 rpm, 15 min, 4°C]. Cell pellet was then collected

with a spatula and spread onto a polythene sheet. Cell pellet was sealed within the sheet using an Impulse heat sealer. Bags were stored at -80°C.

2.4.1.4.1 Preparation of native extracts from bacteria

Aliquots of frozen cells were thawed on ice and cell pellet was re-suspended in a Tris-based binding buffer [see section 2.4.4.1]. 400 µl of buffer was added to the cell pellet for every 1 ml of culture. Suspension was then sonicated using a Branson Sonifer at 4 X 10 sec cycles at 30% output, duty cycle of 3. Lysate was cleared by centrifugation [13,000 **g**, 15 min, 4°C].

2.4.1.4.2 Preparation of total protein extracts from bacteria

Total protein extracts were made to test protein expression levels. Cell pellets from induced BL21-RIL strains were re-suspended in 1 X TBS [200 µl per ml of cultured cells]. Re-suspended cells were boiled at 100°C for 5 min. Lysate was cooled to RT then sonicated using a Branson Sonifer at 4 X 10 sec cycles at 30% output, duty cycle of 3. Equal volume of 2 X SB was then added to the lysate, and boiled at 100°C for 5 min.

2.4.2 Measurement of protein concentration

2.4.2.1 Bradford Assay (Bradford 1976)

The Bradford Assay was used to determine protein concentration for soluble native extracts. Protein solution was diluted 1:5 with dH_2O and 2 µl was added to 1 ml of the Bradford reagent [diluted 1:5 with dH_2O] [BioRad, U.S.A.]. $OD_{595\ nm}$ was measured using a spectrophotometer. Concentration was calculated based on calibration with BSA [data not shown] where 30 µg/µl of BSA gave an OD_{595nm} = 0.8.

2.4.2.2 Bicinchoninic acid protein assay (Smith *et al.* 1985)

The BCA assay was used to measure protein concentration for total protein extracts. 20 µl of 4% [w/v] copper [II] sulphate solution was added to 1 ml Bicinchoninic acid, 1 µl of protein solution was added to the assay and incubated at 65°C for 15 min. $OD_{562\ nm}$ was then measured using a spectrophotometer. Protein concentration was based on calibration with BSA [data not shown] where 1 µg/µl of BSA gave an $OD_{562\ nm} = 0.04$.

2.4.2.3 Determination of protein concentration by comparison with BSA calibration curve

10 mg/ml BSA [NEB, U.S.A.] was used to create a dilution series from 0.01 µg/µl to 1 µg/µl. 10 µl of each BSA solution was loaded onto a 10% SDS-PAGE gel. Gel was stained with Coomassie, and the signal was quantified using Odyssey V3.0 software. Gels were placed in the Odyssey flatbed scanner and were kept moist with 1 X TBS during the analysis. Scans were performed using the 700 channel under medium quality resolution [192 µm]. The integrated intensity for each band was measured and used to create a standard curve against protein concentration.

2.4.3 Western blot analysis

2.4.3.1 SDS-PAGE

2.4.3.1.1 Preparation of polyacrylamide gel

Separating gel was poured and over-layed with 0.5 – 5 ml dH_2O saturated n-butanol, and gel was incubated until polymerised. Separating gel was then rinsed with dH_2O, and the stacking gel poured on top. Appropriate comb was inserted into the stacking gel and assembly was incubated at RT until gel had polymerised. Comb was removed and wells were washed out with 1 X Laemmli running buffer (Laemmli 1970).

8%	5ml	10ml	20ml
H_2O	2.3	4.6	9.3
30% Acrylamide Mix	1.3	2.7	5.3
1.5M Tris pH 8.8	1.3	2.5	5.0
10% SDS	0.05	0.1	0.2
10% APS	0.05	0.1	0.2
TEMED	0.003	0.006	0.012
10%	5ml	10ml	20ml
H_2O	2.0	4.0	7.9
30% Acrylamide Mix	1.7	3.3	6.7
1.5M Tris pH 8.8	1.3	2.5	5.0
10% SDS	0.05	0.1	0.2
10% APS	0.05	0.1	0.2
TEMED	0.002	0.004	0.008
12%	5ml	10ml	20ml
H_2O	1.6	3.3	6.6
30% Acrylamide Mix	2.0	4.0	8.0
1.5M Tris pH 8.8	1.3	2.5	5.0
10% SDS	0.05	0.1	0.2
10% APS	0.05	0.1	0.2
TEMED	0.002	0.004	0.008

STACKING	1ml	2ml	5ml
H_2O	0.68	1.4	3.4
30% Acrylamide Mix	0.17	0.33	0.83
1.0 M Tris pH 6.8	0.13	0.25	0.63
10% SDS	0.01	0.02	0.05
10% APS	0.01	0.02	0.05
TEMED	0.001	0.002	0.005

Table 2.3. Recipe for polyacrylamide gel solutions. Modified from Harlow, E and Lane, D. 1988.

2.4.3.1.2 Loading of samples and electrophoresis

All protein samples were diluted in SB and boiled for 5 min at 100°C before loading onto the acrylamide gel. 60 µg of total protein was loaded for all input samples. 1 X SB was used to fill empty lanes. Mini-PROTEAN gels were run at 35 mA per gel, low-wide gels were run at 60 mA per gel and PROTEAN II XL gels were run at 300 V, or until the loading buffer dye front had run off the gel.

2.4.3.1.3 Staining with Coomassie

Coomassie brilliant blue stain was used to detect proteins at levels > 0.1 µg. SDS-PAGE gel was incubated in a tray containing 100 ml of Coomassie stain then placed in a microwave [900 W] for 30 sec on high power. The tray was then incubated on a gyro-rocker at RT for 10 min. Staining solution was replaced with 100 ml Coomassie destain, absorbent paper towel was placed in the tray and gel was

then microwaved for 30 sec at high power. Gel was incubated in destain on a gyro-rocker at RT for 10 min. The destain wash was repeated until adequate contrast was achieved between gel and protein bands.

2.4.3.1.4 Staining with silver nitrate

Silver staining was used to detect protein in SDS-PAGE gels at levels > 0.5 ng. Gel was washed on a gyro-rocker for 10 min at RT in 100 ml of successive solutions: 1] 50% [v/v] methanol, 2] 5% [v/v] methanol, 3] 3.2 µl of 1 M DTT in 100 ml of dH_2O, and 4] 0.2% [w/v] $AgNO_3$. The gel was then washed 3 X 5 sec in 100 ml dH_2O. Following a brief wash in developer solution [3% [w/v] Na_2CO_3, 50 µl 37% [v/v] formaldehyde in 100 ml], the gel was re-incubated in dH_2O. Gel was then transferred to developer solution and incubated at RT for up to 10 min or until adequate contrast is observed between gel and protein bands. Reaction was quenched by incubating the gel in 5% [v/v] acetic acid for 10 min.

2.4.3.2 Immuno-blotting

2.4.3.2.1 Transfer onto Nitrocellulose Membrane

A wet-transfer system was used to transfer SDS-PAGE gels onto nitrocellulose membrane. A transfer sandwich soaked in CAPS transfer buffer was set up inside a gel holder cassette to be aligned from negative electrode to positive electrode as follows: 1 X 10 cm x 9 cm fibre pads, 2 X 10 cm x 9 cm 3MM paper [Whatmann, USA], polyacrylamide gel, 10 cm x 9 cm nitrocellulose membrane, 2 X 10 cm x 9 cm 3MM paper, 2 X 10 cm x 9 cm fibre pads. Sandwich was then placed in buffer tank and immersed in CAPS transfer buffer. When using the Mini Trans-Blot Cell [BioRad] a Bio-Ice cooling unit is placed in the tank during transfer. Voltage and transfer times were tailored for each experiment. When immunoblotting against Mto2 [45 kDa], proteins were transferred for 60 min at 60 V, when immunoblotting against Mto1 [120 kDa] the gel was transferred at 90 V for 90 min.

Other proteins analysed had a molecular weight between 45 kDa and 120 kDa and their transfer parameters were adjusted accordingly.

2.4.3.2.2 Ponceau S Staining

Membrane was incubated in 1 X Ponceau S stain for 10 min at RT on shaker. Stain was then replaced with destain and incubated for a further 10 min or until there is adequate contrast between the membrane and protein bands. To remove the protein staining completely, the membrane was washed in dH_2O and then incubated in 1 X TBS.

2.4.3.2.3 Antibody incubation

All short [1-2 hr] incubations were carried out at RT and longer incubations were carried out at 4°C. Membranes were first incubated in blocking solution [2% [w/v] milk, 0.2% [v/v] Tween-20, 1 X TBS]. Membranes were then incubated with primary antibody diluted in buffer [2% milk, 0.02% [v/v] Tween-20, 1 X TBS]. Following incubation, membranes were washed 3 X 100 ml wash buffer [1 X TBS, 0.02% [v/v] Tween-20]. Membranes were then transferred to secondary antibody diluted in buffer [2% [w/v] milk, 0.02% [v/v] Tween-20, 1 X TBS]. Following incubation, membranes were washed 3 X 100 ml wash buffer [1 X TBS, 0.02% [v/v] Tween-20]. For membranes incubated with IRDye conjugated IgG, the final wash was without Tween-20.

2.4.3.2.4 Enhanced Chemiluminescence [ECL] detection

Excess wash buffer was blotted off the membrane and then the membrane was incubated in 10 ml ECL [100 mM Tris-HCl pH 8.5, 2.5 mM luminol, 0.4 mM p-coumaric acid, 0.02% [v/v] H_2O_2] for 5 min. Excess ECL was removed and membrane was placed between a Saran wrap sandwich, and secured into an exposure cassette with tape. Blue sensitive X-ray film [A. Somerville Ltd. U.K.] was then

placed on top of the membrane before being processed by the SRX-101A tabletop film processor [Konica, U.S.A.].

2.4.3.2.5. Protein quantification by fluorescence

Donkey anti-mouse IRDye800 were used for fluorescence quantification by the Odyssey Scanner and software [Odyssey V2.0]. GT-34 secondary was used [mouse anti-sheep IgG] for immunoblots probed with anti-sheep polyclonal antibodies. IRDye800 was directly incubated with membrane probed with mouse monoclonal antibodies [GTU-88, 9E10]. Membranes were placed in the flatbed scanner and were kept moist with 1 X TBS during the analysis. Scans were performed using the 800 channel under medium quality resolution [192 µm] Images were adjusted using only linear contract enhancement with Odyssey V2.0 or Photoshop [Adobe] software.

2.4.4 Protein-Protein Interaction Assays

2.4.4.1 MBP pulldown assay

Soluble extracts are made from 1 – 2 ml of induced BL21- CodonPlus® Competent cells [Stratagene, U.S.A] containing MBP- or NusA-tagged protein. Concentration of the tagged protein was estimated by comparison with a BSA calibration curve. 50 µl of packed amylose resin was used per pulldown. Beads are washed with 3 X 1 ml dH_2O by centrifugation [4,000 **g**, 1 min, RT] and pre-equilibrated by centrifugation [4,000 **g**, 1 min, 4°C] in 1 X 1 ml binding buffer containing 50 mM Tris-HCl pH 8.0, 150 mM NaCl, 5% [v/v] glycerol, 1 mM BME, 0.2% [v/v] Triton X-100, 1 mM PMSF, 1 mM aprotinin. Normalised levels of cleared cell lysate [~400 µl] were added to the resin and incubated for 1 hr at 4°C on a rotating wheel. Following incubation, amylose resin was washed 5 X 1 ml binding buffer by centrifugation [4,000 **g**, 1 min, 4°C]. Protein was eluted by adding 20 µl of binding buffer plus 10 mM maltose to the resin and incubating on a rotator for 10 min at 4°C. Eluate was collected boiled at 100°C for 5 min in 50 µl 2 X SB.

2.4.4.2 Antibody immunoprecipitation

Soluble extracts were made from 0.5 g of ground yeast strains. Approximately 3 x 10^7 of Protein G-Dynabeads [Invitrogen, U.S.A.] were used per IP. Beads were washed 3 X 1 ml dH_2O by performing a brief centrifugation [< 4,000 **g**] to remove solution from the lid of the tube then incubated on a Magnetic Particle Concentrator [Invitrogen, U.S.A.]. Dynabeads were then equilibrated with 2 X 1 ml IP buffer using the same method. 1.2 µg of sheep anti-GFP 3.0 antibody or affinity purified anti-Mto2 were used per IP. Antibody was added to the beads in 500 µl of IP buffer and incubated for 30 min on a rotator at RT. Following incubation with antibody, beads were washed with 2 X 1 ml IP buffer using the same method as described above. Normalised amounts of cleared cell extract [typically 20 – 40 mg total protein] were added to the Protein G-Dynabeads and incubated on a rotator at 4°C for 1 hr. After incubation, the supernatant was removed, and each IP was washed 3 X 1 ml IP buffer, using the method described above. Beads were transferred into a fresh screw-cap tube and then washed a further 3 X 1 ml IP buffer. Beads were then re-suspended in 30 µl of 1 X SB [- DTT and bromophenol blue] and incubated at 50°C for 10 min. Eluate was transferred to a fresh tube and DTT and bromophenol blue was added to a final concentration of 100 mM and 0.01% [w/v] respectively. Samples were then incubated at 100°C for 5 min and stored at -20°C.

2.4.4.3 TAPS affinity tag pulldown

Soluble extracts were made from 0.5 g of cell powder from a strain containing TAPS tagged protein. Resultant protein concentration of extract was typically 20 – 50 µg/µl. ~3 x 10^7 of IgG-linked-Dynabeads [Invitrogen, U.S.A.] were used per pulldown. Dynabeads were washed with 3 X 1 ml dH_2O by performing a brief centrifugation [< 4,000 **g**] to remove solution from the lid of the tube then incubation on a Magnetic Particle Concentrator [Invitrogen, U.S.A.]. Dynabeads were then equilibrated with 2 X 1 ml IP buffer using the same method. Normalised extract [typically 20 – 40 mg] was added to the beads and agitated at 4°C for 1 hr.

After incubation, the supernatant was removed and each IP was washed 3 X 1 ml IP buffer using the method described above. Beads were transferred into a fresh screw-cap tube and then washed a further 3 X 1 ml IP buffer. Beads were then re-suspended in 30 µl of 1 X SB [- DTT and bromophenol blue] and incubated at 50°C for 10 min. Eluate was transferred to a fresh tube and DTT and bromophenol blue was added to a final concentration of 100 mM and 0.01% [w/v] respectively. Samples were then incubated at 100°C for 5 min.

2.4.5 Large scale protein purification

2.4.5.1 Large scale purification of Mto2 from bacteria

4 X pellet volumes of lysis buffer [50 mM Tris-HCl pH 8.0, 150 mM NaCl, 0.2% [v/v] Triton X-100, 1 mM EDTA, 1 mM DTT, 1 mM PMSF, 1 mM benzamidine, 10 µg/ml CLAAPE] were added to fragmented bacterial pellet at 4°C. Once cells were re-suspended, they were passed through a glass homogeniser [VWR International, U.S.A] 30 X loose pestle, 30 X tight pestle. Cells were disrupted using a cooled French Pressure Cell Press [ThermoSpectronic, U.S.A.]. 30 ml of cell suspension were passed through the press in each batch at 15,000 psi between 3 – 5 times, until the viscosity of the solution was sufficiently reduced that it passed drop-wise in to the collecting vessel. 3 U of benzonase nuclease [Novagen, Germany] were added per ml of culture, in addition to 6 mM of $MgCl_2$ and incubated at 4°C for 1 hr. Cell lysate was then cleared by centrifugation using a Beckmann Avanti J-25 centrifuge with a JA-20 rotor [Beckmann] [20,000 rpm, 20 min, 4°C]. Supernatant then underwent a second clearing step in a Beckmann XL-100 Ultracentrifuge with a Type 45Ti rotor, [40,000 rpm, 1 hr, 4°C]. Amylose resin was added to a 20 ml general purpose chromatography column to a 2 ml bead volume [one column per 20 ml lysate] which was washed with 50 ml of lysis buffer. 20 ml of cleared extract was added to each column which was then sealed and incubated on a rotator O/N at 4°C. Column was secured and stopper was released to allow the lysate to drain through. Resin was then washed with 100 ml TEV cleavage buffer [50 mM Tris-HCl pH 8.0, 150 mM NaCl, 0.2% [v/v] Triton X-100, 1 mM EDTA, 1 mM DTT] or until OD_{280}

$_{nm}$ = 0.00 for three consecutive readings following 10 ml washes measured using a NanoDrop Spectrophotometer. Resin from each column was combined into a single 10 ml column and re-suspended in 5 ml TEV Cleavage Buffer. 500 U of AcTEV protease [Invitrogen, U.S.A.] was added to the suspension. Cleavage reaction was incubated for 72 hr at 4°C. Column was placed in a 15 ml falcon tube and supernatant was recovered by centrifugation [1,500 **g**, 2 min, 4°C]. Isolated cleavage product [~5 ml] was then transferred to an Amicon Ultra-4 Centrifugal Filter Device 30,000 NMWL [Millipore, U.S.A.], and centrifuged for [4,000 g, 20 min, 4°C] after which the final volume of cleavage product had been reduced to 250 µl. 250 µl of 100% [v/v] glycerol was added to the purified protein and this was stored at -80°C.

2.4.5.2 Large Scale purification of Mto2 from yeast

2.4.5.2.1 Two-step denaturing purification of Mto2

Denaturing purification was performed using 35 g of ground cell powder. Powder was re-suspended in 70 ml denaturation buffer [6 M GuHCl, 25 mM Tris-HCl pH 7.5, 300 mM NaCl, 20 mM imidazole]. Extract was cleared in a Beckmann Avanti J-25 centrifuge using a JA25.50 rotor [8000 rpm, 20 min, 4°C], then supernatant was transferred to a fresh tube and centrifugation step was repeated at [20,000 g, 30 min, 4°C]. 1 ml bead volume HisBind Fractogel [Novagen, Germany] was washed with 3 X 10 ml dH_2O by centrifugation [4,000 **g**, 3 min, RT] and activated with 1 ml 0.5 M $NiSO_4$ and incubated for 10 min at RT. Resin was then washed 6 X 5 ml dH_2O [4,000 **g**, 3 min, RT], and 2 X 5 ml denaturation buffer [4,000 **g**, 3 min, RT]. Beads were split between two 50 ml tubes and 35 ml of cell extract was added to both, and tubes were agitated for 3 hr at 4°C. Resin was then batch washed with consecutively weaker concentration of GuHCl. 2 X 10 ml Buffer 1 [6 M GuHCl, 25 mM Tris-HCl pH 7.5, 300 mM NaCl, 20 mM imidazole], 2 X 10 ml Buffer 2 [3 M GuHCl, 25 mM Tris-HCl pH 7.5, 300 mM NaCl, 20 mM imidazole], 2 X 10 ml Buffer 3 [1 M GuHCl, 25 mM Tris-HCl pH 7.5, 300 mM NaCl, 20 mM imidazole], then 3 X 10 ml Buffer 4 [25 mM Tris-HCl pH 7.5, 300 mM NaCl, 20 mM imidazole]. Protein was eluted from the Fractogel in 5 ml elution

buffer [25 mM Tris-HCl pH 7.5, 300 mM NaCl, 300 mM imidazole. 1 mM DTT, 1 mM PMSF, 1 mM benzamidine, 10 µg/ml CLAAPE, 60 mM β-glycerol phosphate, 15 mM PNPP, 10 mM sodium orthovanadate]. ~4.5 x 10^8 beads of MyOne Streptavidin C1 Dynabeads [Invitrogen, U.S.A.] were used in the second purification step. Dynabeads were washed with 3 X 1 ml dH_2O by performing a brief centrifugation [< 4,000 **g**] to remove solution from the lid of the tube then incubation on a Magnetic Particle Concentrator [Invitrogen, U.S.A.]. Dynabeads were then equilibrated with 2 X 1 ml IP buffer using the same method. 5 ml Fractogel elution was added to the beads and incubated on a rotator for 2 hr at 4°C. Dynabeads were washed as described above with 3 X 2 ml Tris binding buffer [- protease inhibitors], then 3 X 2 ml of TEV cleavage buffer [25 mM Tris-HCl pH 8.0, 150 mM NaCl, 0.1% [v/v] Triton X-100, 0.5 mM EDTA, 1 mm DTT]. Beads were re-suspended in 500 µl of TEV cleavage buffer and 500 U of AcTEV protease [Invitrogen, U.S.A.] was added. The cleavage reaction was left O/N at 4°C. TEV cleavage product was recovered from the beads and concentrated using TCA precipitation. Protein pellet was re-suspended in 30 µl 1 X SB.

2.4.5.2.1.1 Trichloroacetic acid precipitation [TCA]

100% [w/v] TCA was added to the protein solution to a final concentration of 10% and incubated for 30 min on ice. If solution contained urea or guanidine, it was diluted to < 0.2 M before addition of TCA. Precipitated protein was collected by centrifugation [13,000 **g**, 15 min, 4°C]. Protein pellets were then washed with 2 X 1 ml ice-cold wash buffer [70% [v/v] acetone, 20% [v/v] ethanol, 10 mM Tris-HCl pH 7.5, 0.0025% [w/v] bromophenol blue] using centrifugation [13,000 **g**, 10 min, 4°C]. Pellets were then left to air dry. Acidic pellets were neutralised with ammonium hydroxide vapours then re-suspended in 1 X SB and boiled for 5 min.

2.4.5.2.2 Large Scale Mto2-TAPS affinity purification from SILAC strains

15 g of cell powder containing cells from both mitotic non-labelled and isotope labelled asynchronous culture were used for the purification. Cell powder

was re-suspended in 20 ml of phosphate buffer [15 mM Na_2HPO_4, 10 mM NaH_2PO_4, 150 mM NaCl, 2 mM EDTA, 1% [v/v] NP-40, 2 mM benzamidine, 2 mM PMSF, 1 mM DTT, 60 mM β-glycerol phosphate, 5 mM sodium azide, 10 mM sodium fluoride, 1 mM sodium orthovanadate, 50 nM calyculin, 50 nM okadaic acid, 10 µM cyclosporin, 10 µg/ml CLAAPE]. Cell lysate was then clarified by centrifugation using a JA 25-50 rotor in a Beckmann Avanti J-25 centrifuge [20,000 rpm, 10 min, 4°C]. 1.5 $x10^9$ IgG-linked Dynabeads [Invitrogen, U.S.A.] were washed with 3 X 1 ml dH_2O by performing a brief centrifugation [< 4,000 **g**] to remove solution from the lid of the tube then incubation on a Magnetic Particle Concentrator [Invitrogen, U.S.A.]. Dynabeads were then equilibrated with 2 X 1 ml lysis buffer using the same method. Beads were added to cleared cell lysate and incubated on a roller for 1.5 hr at 4°C. Supernatant was removed and Dynabeads were washed with 5 X 10 ml lysis buffer [without protease inhibitors], using the Magnabot large volume separation device [Promega, U.K.]. TAPS-tagged protein was eluted by re-suspension in 1 X SB and incubated at 50°C for 15 min. Eluate was recovered into a fresh microfuge tube and stored at -20°C.

2.4.6 Hydrodynamic analysis

2.4.6.1 Sucrose Density Gradient Analysis

2 ml gradients were made in Ultra-Clear Tubes [11 x 34 mm] [Beckman, U.S.A.]. 0.5 ml of 20%, 15%, 10%, 5% [w/w] sucrose solutions were carefully layered into the tube with a blunt P1000 pipette tip. Sucrose solutions were made up with the same buffer as the sample to be analysed. Each gradient was incubated at RT for 1 hr, then prior to centrifugation incubated in an ice-water bath for 10 min. A gradient containing molecular weight markers [Sigma, U.S.A.] accompanied each analysis [see Appendix I and II]. 2 ml gradients were spun in an OptimaMax Ultracentrifuge [Beckman Coulter, U.S.A.] using a TLS-55 swinging bucket rotor assembly. 2 mg of total soluble protein was analysed in each gradient. Analyses of complexes > 20 S gradients were spun at 55,000 rpm for 30 min. Analyses of complexes < 20 S gradients were spun at 55,000 rpm for 3.5 hr. Following

sedimentation, 100 µl gradient fractions were manually removed with a blunt P200 pipette tip and were stored at 4°C. For immediate analysis fractions were added to 100 µl 2 X SB and boiled for 5 min. Pellet fraction was obtained by re-suspending pellet in 200 µl 1 X SB.

2.4.6.1.1 Preparative sucrose gradients

14 ml gradients were made in polyallomer centrifuge tubes [14 x 95 mm] [Beckman, U.S.A.]. 7 ml of 20% and 5% sucrose solutions, made with TEV cleavage buffer, were poured into the tube. Solutions were sealed inside the tube and the gradient was established using a Gradient Master 107 [Biocomp, U.S.A.]. Gradients were incubated in an ice-bath for 10 min prior to use. 500 ml of sucrose solution was removed from the top of the gradient to allow space for sample. Centrifugation was carried out in a Beckmann XL-100 Ultracentrifuge using SW-40 Ti swinging bucket rotor [Beckman, U.S.A]. This was spun for at 35,000 rpm for 16 hr at 4°C. Following sedimentation 0.5 ml fractions were collected, these were stored at 4°C. For immediate analysis fractions were added to 0.5 ml 2 X SB and boiled for 5 min.

2.4.6.2 Size-exclusion gel chromatography

Size-exclusion gel chromatography was performed on using a BioLogic Duoflow chromatography system [BioRad, U.S.A], where protein samples were analysed on a Superose 6 10/300GL high performance column [GE healthcare, U.S.A]. The HPLC system and column were stored in 20% [v/v] ethanol at 4°C. All water and buffers were filter sterilised using a 0.2µm filter unit [Nalgene, U.S.A.] and de-gassed using a vacuum pump. Prior to use, the HPLC system and column were washed with 70 ml dH_2O. System and column were then equilibrated with 48 ml lysis buffer. Yeast lysates were run on KS1 Superose 6, and purified protein was run on KS2 Superose 6. Soluble native extracts were subject to a pre-clearing centrifugation step [13,000 g, 15 min, 4°C]. Then a second clearing step was performed using the OptimaMax Ultracentrifuge in a TLA-100.3 fixed angle rotor [50,000 rpm, 20 min, 4°C]. Supernatant was collected and filtered through a 0.22µm

cellulose acetate membrane by centrifugation [13,000 g, 5 min, 4°C]. Protein concentration of the flow through was measured by Bradford assay, and solution was diluted to 0.2 mg/ml. 100 µl [2 mg] of protein extract was loaded onto the column using an AVR7-3 sample injection valve. For KS1, flow rate was established at 0.3 ml/min [136 psi], for KS2 for fractionation of purified protein, column was run at 0.4 ml/min [107 psi]. 30 ml of lysis buffer was passed through the column. 1 ml fractions were collected using an automated fraction collector. Collection started at 6 ml where void volume eluted at 7 ml [KS1] and 8 ml [KS2]. 30 X 1 ml fractions were collected in total. 25 µl of 5 X SB [- DTT] are added to the fractions and stored at -80°C. Molecular weight standards [GE Healthcare/Sigma] were run on both columns to determine a calibration curve [see Appendix III and IV]. Loading of cell lysate to the Superose-6 column [GE Healthcare] and subsequent fractionation was performed by A. Anders. All samples from sucrose gradient analysis and gel-filtration chromatography were analysed by western blot on the low-wide system.

2.4.7 Protein Phosphorylation Analysis

2.4.7.1 λPPase treatment

Total protein extracts were prepared from KS516. Extract buffer contained 20 mM Tris-HCl pH7.5, 150 mM NaCl, 0.1 mM EGTA, 2 mM DTT, 0.01% TX-100, 2 mM $MgCl_2$, 1 mM PMSF, 1 mM benzamidine, 10 µg/ml CLAAPE. In buffer that contained phosphatase inhibitors the following was also added: 10 mM Na_3VO_4, 10 mM EDTA, 60 mM β-glycerol-phosphate, 5 mM NaN_3, 10 mM NaF, 50 nM calyculin, 50 nM, okadaic acid. For extract to be treated with phosphatase 2 mM $MnCl_2$ was also added. The protein concentration of extracts was measured by Bradford Assay. 400 U of λ-PPase [N.E.B., U.S.A] was heat inactivated by incubation with 10 mM EDTA at 65°C for 1 hr. 400 U of λ-PPase or HI enzyme was then added to normalised protein extracts in 50 µl final volume and incubated at 30°C for 30 min. The reaction was stopped by the addition of 50 µl 2 X SB and boiled for 5 min.

2.4.7.2 CDK1-Cyclin B kinase assay of purified Mto1/2 complex

0.5 g of cell powder from KS3476 [Mto1 [1-800]-TAPS] and KS516 were re-suspended in lysis buffer [20 mM Tris-HCl pH 7.5, 6 mM $MgCl_2$, 150 mM NaCl, 0.05% [v/v] Triton X-100, 2 mM DTT, 10% [v/v] glycerol, 1 mM PMSF, 1 mM benzamidine, 10 µg/ml CLAAPE]. A TAPS affinity purification was performed using IgG-linked-Dynabeads [Invitrogen, U.S.A.] After incubation, the beads were transferred into a fresh screw-cap tube re-suspended in 50 µl of extract buffer and 200 µM final concentration of dATP was added to each sample. 5µl of beads were then taken and protein eluted for input. 100 ng of CDK1-Cyclin B [Invitrogen, U.S.A.] was added to the beads, and agitated for 30 mins in a 30°C water bath. CDK kinase supernatant was recovered into a fresh microfuge tube. 50 µl of 2 X SB was added and incubated at 100°C for 5 min. The remaining beads were washed in 3 X 1 ml extract buffer by centrifugation using the method described above. Dynabeads were re-suspended in 100 µl of 1 X SB and incubated at 50°C for 10 min. Supernatant was recovered using a brief centrifugation [13,000 **g**] and incubation on the Magnetic Particle Concentrator. Eluate was then incubated at 100°C for 5 min.

2.4.7.3 *cdc25-22^{ts}* G_2 block and release

cdc25-22^{ts} strains were grown at 25°C O/N to an $OD_{595\ nm}$ = 0.2. Temperature was shifted to 35.5°C and culture was grown for 4 hr. Culture was then returned to permissive temperature by brief incubation in an ice slurry, then into a water bath at 25°C. T_0 time point was taken on temperature shift, successive time point were taken every 20 min for 180 min. At each time point 40 ml of culture was collected and washed with 10 ml STOP buffer [150 mM NaCl, 50 mM NaF, 10 mM EDTA, 1 mM NaN_3] and 5 ml HB salts buffer [25 mM MOPS pH 7.2, 15 mM $MgCl_2$, 15 mM EGTA, 1 mM DTT] using a Büchner funnel and 0.45 µm Durapore membrane filters [MILLIPORE, U.S.A.]. Cells are transferred to a screw-cap microfuge tube in 1 ml HB salts, and cell pellet was snap frozen in liquid nitrogen.

2.4.7.3.1 Determination of septation index

500 µl aliquots were taken from each cell cycle block and release time point. 0.1% [w/w] glyceraldehyde final concentration was added to the cells and they were incubated on a rotator at RT for 20 min. Fixed cells were washed with 1 ml 1 M sorbitol using a tabletop centrifuge, re-suspended in 30 µl of 1 M sorbitol and stored at 4°C. 5µl of cell solution were incubated with 5µl fluorescent brightener [0.1% fluorescent brightener, 10 mM Tris HCl pH 7.5] for 10 min at RT. 5 µl of cells were placed on a microscope slide and examined under the wide-field microscope using a DAPI filter set. ~ 200 cells were counted where the percentage of cells which had a septum was calculated for each time point. Those cells which had formed a septum, but had started to separate or had been released from sister cells were not counted.

2.4.7.4 *nda3-KM311* metaphase arrest

nda3-KM311 cold-sensitive allele was used to arrest cells in metaphase. Cultures were grown at 32°C to an $OD_{595\ nm}$ = 0.2. Cultures were then quickly cooled to 18°C using an ice bath and incubated at 18°C for 9 hr. The extent of the arrest was assessed by light-microscopy, where arrested cells were longer than wild-type and had a low septation index.

2.5 MASS SPECTROMETRY ANALYSIS

All mass spectrometry analyses were performed by Flavia Alves and Juri Rappsilber.

2.5.1 Sample Preparation

Protocol as described in (Pidoux *et al.* 2009). Coomassie strained band corresponding to the expected molecular weight was excised from the gel cut into small pieces. Proteins were then reduced in 20 mM DTT for 30 min at 37°C, alkylated in 50 mM iodoacetamide for 30 min at RT in the dark, and incubated with 12.5 ng/µl trypsin O/N at 37°C (Shevchenko *et al.* 1996). The digestion medium was

then acidified to 0.1 [v/v] % of trifluoroacetic acid and spun onto StageTips (Rappsilber *et al.* 2003). Peptides were eluted in 20 µl 80% [v/v] acetonitrile, 0.5% [v/v] acetic acid and were concentrated to 2 µl [concentrator 5301; Eppendorf AG, Hamburg, Germany]. They were then diluted to 5 µl with 0.1% [v/v] trifluoroacetic acid for liquid chromatography-tandem mass spectroscopy [LC-MS-MS] analysis.

2.5.2 Mass spectrometry analysis

LC MS/MS was performed on an LTQ-Orbitrap mass spectrometer [ThermoElectron] that was coupled online to an Agilent 1100 binary nanopump [Palo Alto, CA] and an HTC PAL autosampler [CTC, Zwingen, Switzerland]. A C18 material LC column [3-µm ReproSil-Pur C18-AQ; Maisch GmbH, Ammerbuch-Entringen, Germany] was used to separate peptides prior to ESI. Raw files were processed using DTAsupercharge 0.62 [a kind gift from M. Mann]. The generated peak lists were searched against protein databases using Mascot 2.0. The results were parsed through MSQuant [http://msquant.sourceforge.net/]. A significance score was given to each phosphorylated residue based on comparison with a target-decoy database (Elias *et al.* 2007). Peptides with scores 25 and higher were reported and individual cases manually validated.

2.6 MICROSCOPY

2.6.1 Equipment and image analysis

Prior to imaging, cells were placed on a 2% [w/v] agarose/EMM pad. Coverslips were secured onto the slide using liquid VALAP [33% [w/w] Vaseline, 33% [w/w] lanolin, 33% [w/w] paraffin] which had been melted at 70°C. Wide-field images were acquired used a Nikon 100x/1.40 NA Plan Apo objective on a Nikon TE300 inverted microscope. This was connected to a Coolsnap HQ CCD camera [Photometrics]. Confocal images were acquired using a Nikon 100x/1.45 NA Plan Apo objective on a Nikon TE2000 inverted microscope, connected to a Yokogawa CSU-10 spinning disc confocal head [Visitech] and a Coolsnap HQ CCD

camera. Image acquisition, processing and analysis were carried out using Metamorph software [Molecular Devices]. Microscope images were adjusted using only linear contract enhancement with Metamorph [Molecular Devices] or Photoshop [Adobe] software. Time-lapse images to compare samples were imaged under identical illumination conditions; the brightness and contrast was later scaled using consistent values to allow accurate comparisons to be made.

2.6.2 Image parameters

All wide-field images in this study are maximal projections of Z-sections. 8 Z-sections were taken over a range of 4.2 µm, with a 0.6 µm step size. 800 ms exposure time was used for illumination at 488 nm. Images were subject to 2X2 pixel binning.

All images taken on the spinning disk confocal are maximal projections of Z-sections. 11 Z-sections were taken over a range of 4 µm, with a 0.4 µm step size. 200 ms exposure time was used for illumination at 488 nm. 500 ms exposure time was used for illumination at 561 nm. EM Gain was 300 ms. These images were subject to 1X1 pixel binning.

2.7 BIOINFORMATIC ANALYSIS

2.7.1 Mto2 homolog identification using BLASTP

The *S. japonicus* homologues of *S. pombe* Mto2 was identified as SJAG_03264.2 by performing a BLASTP search (Altschul *et al.* 1997) with SPBC902.06 against the *S. japonicus* genome available online from the Broad Institute Sequencing database at: http://www.broadinstitute.org/annotation/genome/schizosaccharomyces_group/MultiHome.html. The e - score for the High Scoring segment pairs [HSPs] alignment was $1e^{-24}$. An E - score describes the number of sequence Pairs in the database which would align as good as or better by chance, therefore the lower the e - score the higher the significance of the hit. SJAG_03264.2 and Mto2 amino acid sequences were entered into the CLUSTALW2 alignment

program (Larkin *et al.* 2007) available from the European Bioinformatics Institute [http://www.ebi.ac.uk/]. The *Schizosaccharomyces octosporus* homolog SOCG_01774.2 was identified from the BLASTP server at the Broad Institute as described above. Other fungal homologs of Mto2 were identified using a BLASTP search using SPBC902.06 as bait against all non-redundant sequence databases available from the NCBI [available online at http://blast.ncbi.nlm.nih.gov/Blast.cgi].

2.7.2 Coiled-coil prediction by PAIRCOIL2

The PAIRCOIL2 coiled-coil prediction software was developed at the Massachusetts Institute of Technology to predict the presence of coiled-coils in amino acid sequences (McDonnell *et al.* 2006). The program algorithm is based on pairwise residue correlations from a coiled-coil database (Berger *et al.* 1995). PAIRCOIL2 is available at http://groups.csail.mit.edu/cb/paircoil2/.
Helical wheel projections were generated using online software available at http://cti.itc.virginia.edu/~cmg/Demo/wheel/wheel App.html. Sequential 18aa regions of the coiled-coil sequence identified by PAIRCOIL2 were entered into the applet generating a series of wheel projections.

2.7.3 Mto2 secondary structure prediction by Jpred3

Secondary structure was predicted using online software Jpred3 (Cole *et al.* 2008). Jpred3 is available at http://www.compbio.dundee.ac.uk/www-jpred/.

2.7.4 Phosphorylation site scoring using NetPhos 2.0

The NetPhos 2.0 software is available at http://www.cbs.dtu.dk/services/NetPhos/ (Blom *et al.* 1999). The NetPhos program is a neural network that uses sequence and structural data from a database of known phosphorylated sites to NetPhos was used to generate a score for each S/T/Y amino acid that describes the probability that that residue is phosphorylated.

Table 2.4 List of plasmids used in this study. Database name, genotype, source and are listed.

Plasmid	Description/ Markers	Source
pKS422	pFA6-TAPS:KanMX6	(Brune *et al.* 2005)
pKS466	pFA6-HTB:KanMX6	(Tagwerker *et al.* 2006)
pKS121	c902 cosmid	Sanger Institute, U.K
pKS535	pDONR221 Kan^R	Invitrogen, U.S.A.
pKS1032	pDONR221 Mto2-STOP Kan^R	This study
pKS537	p0GWA N-terminal His6 Amp^R	(Busso *et al.* 2005)
pKS545	pHNGWA His6-NusA Amp^R	(Busso *et al.* 2005)
pKS544	pHMGWA His6-MBP Amp^R	(Busso *et al.* 2005)
pKS1034	His6-MBP-Mto2 Amp^R	This study
pKS1035	His6-NusA-Mto2 Amp^R	This study
pDUAL29	pDUAL-HFG41c Amp^R	(Matsuyama *et al.* 2004)
pDUAL31	pDUAL-HFG81c Amp^R	(Matsuyama *et al.* 2004)
pDUAL40	pDUAL-GFH81c Amp^R	(Matsuyama *et al.* 2004)
pKS1036	pDONR221 Mto2 N1 Kan^R	This study
pKS1037	pDONR221 Mto2 N2 Kan^R	This study
pKS1038	pDONR221 Mto2 N3 Kan^R	This study
pKS1039	pDONR221 Mto2 C1 Kan^R	This study
pKS1040	pDONR221 Mto2 C2 Kan^R	This study
pKS1041	pDONR221 Mto2 C3 Kan^R	This study
pKS1042	His6-MBP-Mto2 N1 Amp^R	This study
pKS1043	His6-MBP-Mto2 N2Amp^R	This study
pKS1044	His6-MBP-Mto2 N3 Amp^R	This study
pKS1045	His6-MBP-Mto2 C1 Amp^R	This study
pKS1046	His6-MBP-Mto2 C2 Amp^R	This study
pKS1047	His6-MBP-Mto2 C3Amp^R	This study
pKS1048	pDONR211 Mto2-L133DL137D Kan^R	This study
pKS1049	His6-MBP-Mto2 L133DL137D Amp^R	This study
pKS1050	nmt81:HFG-Mto2 Amp^R	This study
pKS1051	nmt81: HFG-Mto2 L133DL137D Amp^R	This study
pKS1052	nmt41: HFG-Mto2 L133DL137D Amp^R	This study
pKS1053	nmt81: HFG-Mto2 N1 Amp^R	This study
pKS1054	nmt81: HFG-Mto2 N2 Amp^R	This study
pKS1055	nmt81: HFG-Mto2 C1 Amp^R	This study
pKS1056	His6-MBP-TEV-Mto2 Amp^R	This study
pKS1057	pDONR221 TEV-Mto2 Kan^R	This study
pKS1059	pDONR221 Mto2 T35A Kan^R	This study
pKS1060	pDONR221 Mto2 S179A Kan^R	This study
pKS1061	pDONR221 Mto2 S220A Kan^R	This study
pKS1062	pDONR221 Mto2 S366A Kan^R	This study
pKS1063	pDONR221 Mto2 T395A Kan^R	This study
pKS1064	pDONR221 Mto2 5A Kan^R	This study
pKS1065	nmt81: HFG-Mto2 T35A Amp^R	This study
pKS1066	nmt81: HFG-Mto2 S179A Amp^R	This study
pKS1067	nmt81: HFG-Mto2 S220A Amp^R	This study
pKS1068	nmt81: HFG-Mto2 S366A Amp^R	This study
pKS1069	nmt81: HFG-Mto2 T395A Amp^R	This study
pKS1079	nmt81: HFG-Mto2 5A Amp^R	This study

pKS1071	pDONR221 Mto2 1A Kan^R	This study
pKS1072	pDONR221 Mto2 2A Kan^R	This study
pKS1073	pDONR221 Mto2 3A Kan^R	This study
pKS1074	pDONR221 Mto2 1D Kan^R	This study
pKS1075	pDONR221 Mto2 2D Kan^R	This study
pKS1076	pDONR221 Mto2 3D Kan^R	This study
pKS1077	nmt81: HFG-Mto2 1A Amp^R	This study
pKS1078	nmt81: HFG-Mto2 2A Amp^R	This study
pKS1079	nmt81: HFG-Mto2 3A Amp^R	This study
pKS1080	nmt81: HFG-Mto2 1D Amp^R	This study
pKS1081	nmt81: HFG-Mto2 2D Amp^R	This study
pKS1082	nmt81: HFG-Mto2 3D Amp^R	This study
pKS1083	His6-MBP-Mto2 1D Amp^R	This study
pKS1084	pDONR221 Mto2 Y168F Kan^R	This study
pKS1085	pDONR221 Mto2 Y269F Kan^R	This study
pKS1086	nmt81: HFG-Mto2 Y168F Amp^R	This study
pKS1087	nmt81: HFG-Mto2 Y269F Amp^R	This study
pKS1088	pDONR221 Mto2 V1 STOP Kan^R	This study
pKS1089	pDONR221 Mto2 V2 STOP Kan^R	This study
pKS1090	pDONR221 Mto2 V3 STOP Kan^R	This study
pKS1091	pDONR221 Mto2 V4-STOP Kan^R	This study
pKS1092	pDONR221 Mto2 V5-STOP Kan^R	This study
pKS1093	pDONR221 Mto2 V6-STOP Kan^R	This study
pKS1094	pDONR221 Mto2 V7-STOP Kan^R	This study
pKS1095	nmt41:Mto2-V1-STOP Amp^R	This study
pKS1096	nmt41:Mto2-V2-STOP Amp^R	This study
pKS1097	nmt41:Mto2-V3-STOP Amp^R	This study
pKS1098	nmt41:Mto2-V4-STOP Amp^R	This study
pKS1099	nmt41:Mto2-V5-STOP Amp^R	This study
pKS1100	nmt41:Mto2-V6-STOP Amp^R	This study
pKS1101	nmt41:Mto2-V7-STOP Amp^R	This study

Table 2.5 List of fission yeast strains used in this study. Database name, genotype, and source are listed.

Strain Number	Genotype	Source
515	ade6-M216 ura4-D18 leu1-32 h+	Laboratory Stock
516	ade6-M210 ura4-D18 leu1-32 h-	Laboratory Stock
976	h- mto2Δ::kanMX6 ade6-M216 leu1-32 ura4-D18	Laboratory Stock
977	h+ mto2Δ::kanMX6 ade6-M216 leu1-32 ura4-D18	Laboratory Stock
1017	h+ mto1Δ::kanM X6 ade6-M216 leu1-32 ura4-D18	Laboratory Stock
1235	h+ kanMX::nmt81::GFP-atb2 ade6-M210 leu1-32 ura4-D18	Laboratory Stock
1238	h- nda3-km311 ade6-M210 leu1-32 ura4-D18	Laboratory Stock
1239	h- mto1Δ::kanMX nda3-km311 ade6-M210 leu1-32 ura4-D18	Laboratory Stock
1280	h- cdc25-22 ade6-M216 leu1-32 ura4-D18	Laboratory Stock
1409	h- mto2Δ::kanMX6 kanMX:nmt81:GFP-atb2 ade6-M210 leu1-32 ura4-D18	Laboratory Stock
1457	h- mto2:GFP:KanMX mto1Δ::kanM X6 ade6-M216 ura4-D18	Laboratory Stock
1460	h- mto2:GFP:KanMX6	Laboratory Stock

1504	h– mto2:myc:kanMX ade6-M210 leu1-32 ura4-D18 m	Laboratory Stock
1507	h+ mto1-13myc:kanMX ade6-M216 leu1-32 ura4-D18	Laboratory Stock
1567	h- alp16Δ::kanMX ade6-M210 leu1-32 ura4-D18	Laboratory Stock
1956	h+ mto1 [1-800]:ura4+ ade6-210 leu1-32	Laboratory Stock
1999	h- mto1 [1-800]-GFP:kanMX6 ade6-M210 leu1-32 ura4-D18	Laboratory Stock
2007	h+ mto1[9A1] ade6-M216 leu1-32 ura4-D18	Laboratory Stock
2739	h- tea1-TAPS:kanMX6 ade6-M210 leu1-32 ura4-D18	Laboratory Stock
3475	h+ mto1 [1-1051]-TAPS:kanMX6 ade6-M216 leu1-32 ura4-D18	Laboratory Stock
3476	h+ mto1 [1-800]-TAPS:kanMX6 ade6-M216 leu1-32 ura4-D18	Laboratory Stock
3524	h+ mto1-TAPS:kanMX6 ade6-M216 leu1-32 ura4-D18	Laboratory Stock
3575	h+ mto1-TAPS:kanMX6 nda3-km311 ade6-M216 leu1-32 ura4-D18	Laboratory Stock
3577	h+ mto1[1-1051]-TAPS:kanMX6 nda3-km311 ade6-M216 leu1-32 ura4-D18	Laboratory Stock
3915	h- nmt81:His6FLAG:GFP-mto2 mto2Δ::kanMX6 ade6-M216 leu1-32 ura4-D18	This study
3920	h- nmt81:His6FLAG:GFP-mto2 mto2-myc:kanMX6 ade6-M210 leu1-32 ura4-D18	This study
3923	h- nmt81:His6FLAG:GFP-mto2-T35A mto2Δ::kanMX6 ade6-M216 leu1-32 ura4-D18	This study
3925	h- nmt81:His6FLAG:GFP-mto2-S179A mto2Δ::kanMX6 ade6-M216 leu1-32 ura4-D18	This study
3927	h- nmt81:His6FLAG:GFP-mto2-S220A mto2Δ::kanMX6 ade6-M216 leu1-32 ura4-D18	This study
3929	h- nmt81:His6FLAG:GFP-mto2-S366A mto2Δ::kanMX6 ade6-M216 leu1-32 ura4-D18	This study
3931	h- nmt81:His6FLAG:GFP-mto2-T394A mto2Δ::kanMX6 ade6-M216 leu1-32 ura4-D18	This study
3933	h- nmt81:His6FLAG:GFP-mto2-5A mto2Δ::kanMX6 ade6-M216 leu1-32 ura4-D18	This study
3943	h+ cdc25-22 mto2Δ::kanMX6 ade6-M216 leu1-32 ura4-D18	Laboratory Stock
3953	h- mto2-HTB:kanMX6 ade6-M210 leu1-32 ura4-D18	This study
3956	h- mto2-TAPS:kanMX6 kanMX6 ade6-M210 leu1-32 ura4-D18	This study
4185	h- nmt81:His6FLAG:GFP-mto2-Y168F mto2Δ::KanMX6 ade6-M216 leu1-32 ura4-D18	This study
4186	h- nmt81:His6FLAG:GFP-mto2-Y269F mto2Δ::KanMX6 ade6-M216 leu1-32 ura4-D18	This study
4230	h- nmt41:mto1-GFP-FLAG-His ade6-M216 leu1-32 ura4-D18	This study
4323	h- mto1-TAPS:kanMX6 mto2Δ::kanMX6 ade6-M216 leu1-32 ura4-D18	This study
4373	h- nmt41:mto1-GFP-FLAG-His; mto1-13myc:KanMX6; mto2Δ:KanMX6 ade6-M216 leu1-32 ura4-D18	This study
4450	h- nmt81:His6FLAG:GFP-mto2 mto2Δ::kanMX6 mto1Δ::kanMX6 ade6-M216 leu1-32 ura4-D18	This study
4461	h- nmt81:His6FLAG:GFP-mto2L133DL137D mto2Δ::KanMX6 ade6-M216 leu1-32 ura4-D18	This study

4463	h- nmt81:His6FLAG:GFP-mto2L133DL137D mto2Δ::KanMX6 nmt81:atb2-GFP ade6-M216 leu1-32 ura4-D18	This study
4466	h- nmt81:His6FLAG:GFP-mto2-1A mto2Δ::KanMX6 nmt81:atb2-GFP ade6-M216 leu1-32 ura4-D18	This study
4469	h- nmt81:His6FLAG:GFP-mto2-2A mto2Δ::KanMX6 nmt81:atb2-GFP ade6-M216 leu1-32 ura4-D18	This study
4472	h- nmt81:His6FLAG:GFP-mto2-3A mto2Δ::KanMX6 nmt81:atb2-GFP ade6-M216 leu1-32 ura4-D18	This study
4475	h- nmt81:His6FLAG:GFP-mto2-1D mto2Δ::KanMX6 nmt81:atb2-GFP ade6-M216 leu1-32 ura4-D18	This study
4478	h- nmt81:His6FLAG:GFP-mto2-2D mto2Δ::KanMX6 nmt81:atb2-GFP ade6-M216 leu1-32 ura4-D18	This study
4481	h- nmt81:His6FLAG:GFP-mto2-3D mto2Δ::KanMX6 nmt81:atb2-GFP ade6-M216 leu1-32 ura4-D18	This study
4596	h+ mto2Δ::kanMX6 mto1-13myc:kanMX ade6-M216 leu1-32 ura4-D18	Laboratory Stock
4600	h- nmt81:His6FLAG:GFP-mto2-1D+2 mto2Δ::KanMX6 nmt81:atb2-GFP ade6-M216 leu1-32 ura4-D18	This study
4603	h- nmt81:His6FLAG:GFP-mto2-1-320 [T1] mto2Δ::KanMX6 ade6-M216 leu1-32 ura4-D18	This study
4606	h- nmt81:His6FLAG:GFP-mto2-89-397 [T4] mto2Δ:;KanMX6 ade6-M216 leu1-32 ura4-D18	This study
4609	h- nmt81:His6FLAG:GFP-mto2-180-397 [T5] mto2Δ::KanMX6 ade6-M216 leu1-32 ura4-D18	This study
4612	h- nmt81:His6FLAG:GFP-mto2-1-320 [T1] mto2Δ::kanMX6 nmt81:GFP-atb2 ade6-M216 leu1-32 ura4-D18	This study
4615	h- nmt81:His6FLAG:GFP-mto2-89-394 [T4] mto2Δ::kanMX6 nmt81:GFP-atb2 ade6-M216 leu1-32 ura4-D18	This study
4618	h- nmt81:His6FLAG:GFP-mto2-180-394 [T5] mto2Δ::kanMX6 nmt81:GFP-atb2 ade6-M216 leu1-32 ura4-D18	This study
4621	h- nmt41:His6FLAG:GFP-mto2L133DL137D mto2Δ::KanMX6 ade6-M216 leu1-32 ura4-D18	This study
4627	h- nmt41:mto1-GFP-FLAG-His; mto1-13myc:KanMX6 ade6-M216 leu1-32 ura4-D18	This study
4973	h- mto1-TAPS:kanMX6 nmt81:His6FLAG:GFP-mto2 mto2Δ::kanMX6 ade6-M216 leu1-32 ura4-D18	This study
4976	h- mto1-TAPS:kanMX6 nmt81:His6FLAG:GFP-mto2-L133DL137D mto2Δ::KanMX6 ade6-M216 leu1-32 ura4-D18	This study
5050	h+ arg1-230 car2Δ::KanMX4 lys3-37 nda3-km311	Laboratory Stock
5349	h+ mto1 [1-549]-GFP:kanMX6 mto2Δ::kanMX6 ade6-M216 leu1-32 ura4-D18	Laboratory Stock
5354	h- mto1 [1-800]:ura4+ mto2Δ::kanMX6 ade6-M210 leu1-32 ura4-D18	Laboratory Stock
5470	h+ mto1-TagRFP-T:natMX6 hphMX6:nmt81-GFPabt2 ura4-D18 leu1-32 ade6-M210	Laboratory Stock
5477	h- car2Δ::KanMX4 mto2-TAPS:KanMX6 lys3-37 arg1-230 nda3-KM311	This study
5479	h- car2Δ::KanMX4 mto2-TAPS:kanMX6 arg1-230 lys3-37	This study

5572	h- nmt81:His6FLAG:GFP-mto2 L133DL137D mto2Δ::kanMX6 mto1Δ::kanMX6 ade6-M216 leu1-32 ura4-D18	This study
5573	h+ mto1Δ::kanMX6 mto2-13myc:kanMX ade6-M216 leu1-32 ura4-D18	This study
5574	h- nmt81:His6FLAG:GFP-mto2 mto2-13myc:kanMX mto1Δ::kanMX6 ade6-M216 leu1-32 ura4-D18	This study
5575	h- nmt81:His6FLAG:GFP-mto2 L133DL1337 mto2-13myc:kanMX6 mto1Δ::kanMX6 ade6-M216 leu1-32 ura4-D18	This study
5576	h- mto1-TagRFP-T:natMX6 hphMX6:nmt81-GFP-abt2 mto2Δ::kanMX6 ura4-D18 leu1-32 ade6-M210	This study
5578	h- mto1[1-1051]-TAPS:kanMX6 mto2Δ::kanMX6 ade6-M216 leu1-32 ura4-D18	Laboratory Stock
5579	h- mto1-TAPS:kanMX6 nda3-km311 mto2Δ::kanMX6 ade6-M216 leu1-32 ura4-D18	Laboratory Stock
5580	h- mto1[1-1051]-TAPS:kanMX6 nda3-km311 mto2Δ::kanMX6 ade6-M216 leu1-32 ura4-D18	Laboratory Stock
5609	h+ mto1[1-549]-GFP:kanMX6 ade6-M210 leu1-32 ura4-D18	Laboratory Stock
5647	h- natMX6:nmt81:mto1[1-549]-GFP:kanMX6 ade6-M210 leu1-32 ura4-D18	Laboratory Stock
5712	h- nmt81:His6FLAG:GFP-mto2 mto2Δ::kanMX6 kanMX::nmt81::GFP-atb2 ade6-M210 leu1-32 ura4-D18	This study
5784	h- nmt81:mto2-L133DL137D mto2Δ::KanMX6 ade6-M216 ura4-D18	This study
5785	h- nmt81:mto2-L133DL137D mto2Δ::KanMX6 mto1Δ::KanMX6 nda3-km311 ade6-M216 ura4-D18	This study
5787	h- nmt81:mto2-L133DL137D mto2Δ::KanMX6 mto1Δ::KanMX6 ade6-M216 ura4-D18	This study
5795	h- mto1-TAPS:kanMX6 cdc25-22 ade6-M216 ura4-D18	This study
5801	h- natMX6:nmt81:mto1[1-549]-GFP:kanMX6 kanMX6:nmt41:mto2 ade6-M210 leu1-32 ura4-D18	This study
5802	h- natMX6:nmt81:mto1[1-549]-GFP:kanMX6 mto2Δ::KanMX6 ade6-M210 leu1-32 ura4-D18	This study
5803	h- mto1[1-549]-GFP:kanMX6 kanMX6:nmt41:mto2 ade6-M210 leu1-32 ura4-D18	This study
5920	h- mto2Δ::KanMX6 cut-12tdT:KanMX6 natMX6:nmt81:mto1[1-549]-GFP:KanMX6 ade6-M210 leu1-32 ura4-D18	Lynch *et al*., data unpublished
5972	h- nmt81:mto2-varient 1 mto2Δ::KanMX6 mto1Δ::KanMX6 nda3-km311 ade6-M216 ura4-D18	This study
5973	h- nmt81:mto2-varient 2 mto2Δ::KanMX6 mto1Δ::KanMX6 nda3-km311 ade6-M216 ura4-D18	This study
5974	h- nmt81:mto2-varient 3 mto2Δ::KanMX6 mto1Δ::KanMX6 nda3-km311 ade6-M216 ura4-D18	This study
5975	h- nmt81:mto2-varient 4 mto2Δ::KanMX6 mto1Δ::KanMX6 nda3-km311 ade6-M216 ura4-D18	This study

Table 2.6 Oligonucleotides used in this study. Allocated number, sequence and section reference for all of the oligonucleotides used in this study.

Oligonucleotide Primer	5'-3' Sequence
M13 sequencing primer fwd	GTAAAACGACGGCCAGT
M13 sequencing primer rev	AACAGCTATGACCATG
OKS248	CGTCCTAGTAGGATTAGCAACTTCTT
OKS257	GAGTTGCTCATCCTATTATCCCCCAGAGGGCGTCTCCAGCATCAC AGTCTTTTCCTTCTCTTCAAGACACTCCTTCCCCCCGGATCCCCG GGTTAATTAA
OKS258	TCCTCAATCAATGTTTGTATGAACTTACATGTATGAGAAGAACCTG ATTTACTTGATAAACACAAAGAAAAATTGATTCAGAATTCGAGCTC GTTTAAAC
OKS505	CCTCTTCCGACCATCAAGCATTTTATCC
OKS1199	AAAAAGCAGGCTTCGAAGGAGATATTCGCATGTCTGAACATAATT ACCAG
OKS1200	AGAAAGCTGGGTCGGGGGAAGGAGTGTCTTGAAG
OKS1201	AAAAAGCAGGCTTCATGTCTGAACATAATTACCAG
OKS1202	AGAAAGCTGGGTCTACTAGGGGGAAGGAGTGTCTTGAAG
OKS1203	GGGGACAAGTTTGTACAAAAAAGCAGGCT
OKS1204	GGGGACCACTTTGTACAAGAAAGCTGGGT
OKS1340	AGAAAGCTGGGTCTACTAGGAATCATCAGAAAAGAGAGT
OKS1341	AGAAAGCTGGGTCTACTATAAAGAGTTTGAGCTTTCCTG
OKS1342	AGAAAGCTGGGTCTACTACGGTGAGTGAGGTGAATGAGT
OKS1343	AAAAAGCAGGCTTCATGGCAAACGTGAATTCAATGAAG
OKS1344	AAAAAGCAGGCTTCATGGCGCCGCTAAGCACGATGCAA
OKS1345	AAAAAGCAGGCTTCATGGATCTTGTCCGTCATACACCA
OKS1251	CAAATTCGCGAATCTGCTCCAAGAGGTTCACCA
OKS1252	TGGTGAACCTCTTGGAGCAGATTCGCGCGAATTTG
OKS1253	CATTCACCTCACGCACCGGCGCCGC
OKS1254	GCGGCGCCGGTGCGTGAGGTGAATG
OKS1255	CACCTTGGTAAACACCGCTCCATCGAGTGTGGT
OKS1256	ACCACACTCGATGGAGCGGTGTTTACCAAGGTG
OKS1257	ATCGAGCTTGCATCCAGCACCAACGTCTTTGCG
OKS1258	CGCAAAGACGTTGGTGCTGGATGCAAGCTCGAT

OKS1259	TTCCTTCTCTTCAAGACGCTCCTTCCCCCTAG
OKS1260	CTAGGGGGAAGGAGCGTCTTGAAGAGAAGGAA
OKS1408	CATATCGTTCTCCTAACAGTTTCCCTTCTCTTTTACCCT
OKS1409	AGGGTAAAAGAGAAGGGAAACTGTTAGGAGAACGATATG
OKS1410	TGTCCGTCATACACCACCATTGAATTTTACCAGTTCTGTTG
OKS1411	CAACAGAACTGGTAAAATTCAATGGTGGTGTATGACGGACA
OKS1683	AAAAAGCAGGCTTCGAAAATCTTTACTTTAATGGTATGTCTGAACA TAATTACCAG
OKS1780	TATCATAACAATCTTGCTCCATATCGTTCTCCTAACAGTGCCCCTG CTCTTTTACCCTCTGCTCATGCACCTCACGCACCGGCGCCGCTAA GCGCGATGCAAACGGCTC
OKS1781	ATCTTGTCCGTCATGCACCACCATTGAATGCTACCGCTGCTGTTG ATGCTGCACCACAACGTATGGCCGCTGATGCTTATGGTAGGCCTT C
OKS1782	AATTCTACAAACAAAGCGGCCTTGCATCCAGCACCAACGGCTTTG CGAGTTGCTC
OKS1783	TATCATAACAATCTTGATCCATATCGTTCTCCTAACAGTTACCCTG ATCTTTTACCCTCTGATCATGACCCTCACGATCCGGCGCCGCTAA GCGATATGCAAACGGCTCTT
OKS1784	GATCTTGTCCGTCATGATCCACCATTGAATTATACCGATGATGTTG ATGACGATCCACAACGTATGGCCGACGATGACTATGGTAGGCCTT CT
OKS1785	AATTCTACAAACAAAGATGACTTGCATCCAGACCCAACGGATTTG CGAGTTGCTCA
OKS1786	CAGGAGCTTGAAAATAAGCGAGAACGCAAGAATCAAGTAGAGCTT
OKS1787	CAGGAGCTTGAAAATGATCGAGAACGCGATAATCAAGTAGAGCTT
OKS1831	GAGCGACCCTCTGACTACTTAGGC
OKS1832	CATAACAATCTTGATCCATATCGTTC

CHAPTER THREE

BIOCHEMICAL ANALYSIS OF MTO1/2 COMPLEX

3.1 INTRODUCTION

In higher eukaryotes several copies of the γ-TuSC in addition to a number of non-core components [e.g. GCP4/5/6 and GCP-WD] are assembled into a large complex called the γ-TuRC (Oegema *et al.* 1999; Gunawardane *et al.* 2000b). Electron microscopy studies have shown that the γ-TuRC forms a 3-start helix or ring structure that can associate with the minus ends of MTs (Moritz *et al.* 1995a; Oegema *et al.* 1999; Moritz *et al.* 2000). Two models have been proposed that describe the mechanism by which the γ-TuRC is able to facilitate the nucleation of MTs, and both of these models involve some level of γ-TuSC multimerisation (Zheng *et al.* 1995; Erickson *et al.* 1996a). In budding yeast, the γ-TuSC/Tub4 complex is the only source of MT nucleation as the proteins required for γ-TuRC assembly are not conserved (Geissler *et al.* 1996; Spang *et al.* 1996). The nature of the nucleation complex formed by the γ-TuSC components in *S. pombe* has yet to be determined. Conservation of many of the γ-TuRC components suggests that, like higher eukaryotes, a ring structure is formed. However, deletion of non-core γ-TuRC components has only minor effects on MT nucleation from non-SPB iMTOCs, and nucleation from other MTOCs remains unaffected (Fujita *et al.* 2002; Venkatram *et al.* 2004; Anders *et al.* 2006). This indicates that either formation of the γ-TuRC is not required for MT nucleation in *S. pombe*, or that the cell is able to compensate for

the loss of non-core component- mediated assembly of γ-TuRC by promoting γ-TuSC multimerisation via other mechanisms.

I predict that multimerisation of the complex formed by Mto1 and Mto2 [the Mto1/2 complex], due to the presence of the γ-TuSC interaction domain in the N-terminus of Mto1, could potentially interact with many γ-TuSCs and promote γ-TuSC multimerisation. Unlike the non-core components, the deletion phenotype of both Mto1 and Mto2 suggest that the Mto1/2 complex is absolutely required for MT nucleation at non-SPB iMTOCs. This could indicate that the Mto1/2 complex may form the primary template structure, and the efficiency of the subsequent assembly and/or stabilisation of γ-TuSCs is increased by the presence of the non-core components.

Alternative to acting as a direct template, the Mto1/2 complex may instead function as a targeting factor and, by increasing the local concentration of the γ-TuSC at the MTOC, may promote self-assembly of the γ-TuRC [in the presence or absence of non-core components].

A structural analysis of the Tub4 complex has demonstrated that the lateral distance between γ-tubulin molecules is too large to facilitate the lateral association of αβ-dimers (Kollman *et al.* 2008). This has suggested that an additional change in conformation in the γ-TuSC may be required for MT nucleation. I hypothesise that the interaction with the Mto1/2 complex, as well as promoting γ-TuSC assembly, may also induce the structural rearrangement of the γ-TuSC required to form an active MT nucleation complex.

3.1.1 Aims and Objectives

In this chapter I aim to investigate the nature of the Mto1/2 complex, concentrating on the copy number of each protein required to form an active nucleation complex, with the hope of providing insight into the structure of the complex and how it might relate to the assembly of the γ-TuSC. For example, if the Mto1/2 complex is comprised of several copies of Mto1, this might support a template model for γ-TuRC assembly via the Mto1/2 complex.

I will use the following approaches to address this problem:

- Hydrodynamic analysis of the Mto1/2 complex to investigate the size of the complex, and whether it is altered by the presence of the γ-TuSC.
- Hydrodynamic analysis of an Mto1/2 complex whose localisation is restricted to non-SPB iMTOCs and is predicted to be unable to form large multimeric associations.

3.2 RESULTS

3.2.1. Mto1 and Mto2 co-fractionate within a 60 – 80 S complex

In order to investigate the size and stoichiometry of Mto1 and Mto2 proteins within the Mto1/2 complex, a fission yeast extract was subject to sucrose density gradient centrifugation. Figure 3.1, Panel A shows that the majority of signal from Mto1 and Mto2 did not co-fractionate, indicating that the proteins are present in independent complexes. The peak fractions were compared with a calibration curve based on markers of known S-value [Appendix II]. Mto2 sedimented at ~5.6 S, while Mto1 sedimented at between 10 – 14 S. In both cases the distribution of protein was spread across multiple fractions, indicating that the calculated S-values are likely to represent the average size of a mix of heterogeneous protein complexes. Despite a pre-clearing spin to remove large particles [> 100 S], there was a large proportion of both Mto1 and Mto2 in the pellet fraction. The nature of the pellet material was investigated by subjecting the sucrose gradients to a short spin that allowed resolution of complexes larger than 20 S. Commercially available molecular weight markers are limited to 19 S, therefore the 90 S pre-ribosomal component Nop1 (Schimmang *et al.* 1989) was used to resolve the gradient within this range. Figure 3.1, Panel B shows that in wild-type extract, the majority of both Mto1 and Mto2 were found in fractions corresponding to 60 – 80 S. The sedimentation pattern of Mto1 was not altered in *mto2Δ*, indicating that Mto2 is not required for Mto1 to be present in this large complex. However, Mto1 was required for the inclusion of Mto2 in the 60 – 80 S complex, as in *mto1Δ* extracts Mto2 peaked in a fraction

representing protein complexes smaller than 19 S. The presence of an Mto2-independent Mto1 60 - 80 S complex was unexpected as previous observations have suggested that Mto2 may act to promote assembly of the Mto1/2 complex (Samejima *et al.* 2005; Samejima *et al.* 2008). For the purpose of this study the 60 – 80 S complex formed by Mto1 will be called the Mto1/2 60 – 80 S complex.

Mto1 and Mto2 were distributed over several fractions of the gradient, suggesting that the 60 – 80 S complex is unlikely to contain proteins in a defined stoichiometry. The unusually large size of the Mto1/2 60 – 80 S complex indicates that it is likely to contain multiple copies of Mto1 in addition to several other protein complexes. Alternatively, it is possible that the 60 – 80 S may arise from the association of Mto1 with large fragments of cellular debris such as the SPB.

3.2.2 Mto2 and Mto1 interact within the 60 – 80 S complex

Mto1 is required for Mto2 to be present within the 60 - 80 S complex. To confirm that Mto1 and Mto2 interact within this range an Mto1-TAPS pulldown was performed on an extract pre-fractionated by sucrose gradient centrifugation. Figure 3.2 shows that the inputs of Mto1-TAPS and Mto2 were present in fractions 6 - 12, corresponding to 60 – 80 S, as previously observed in Figure 3.1. The distribution of Mto1 in the eluates reflected the distribution of material in the input, however, only Mto2 present within the 60 – 80 S range was found to co-precipitate with Mto1. This result confirms that the inclusion of Mto2 within the 60 – 80 S is likely to occur as a result of an interaction with Mto1.

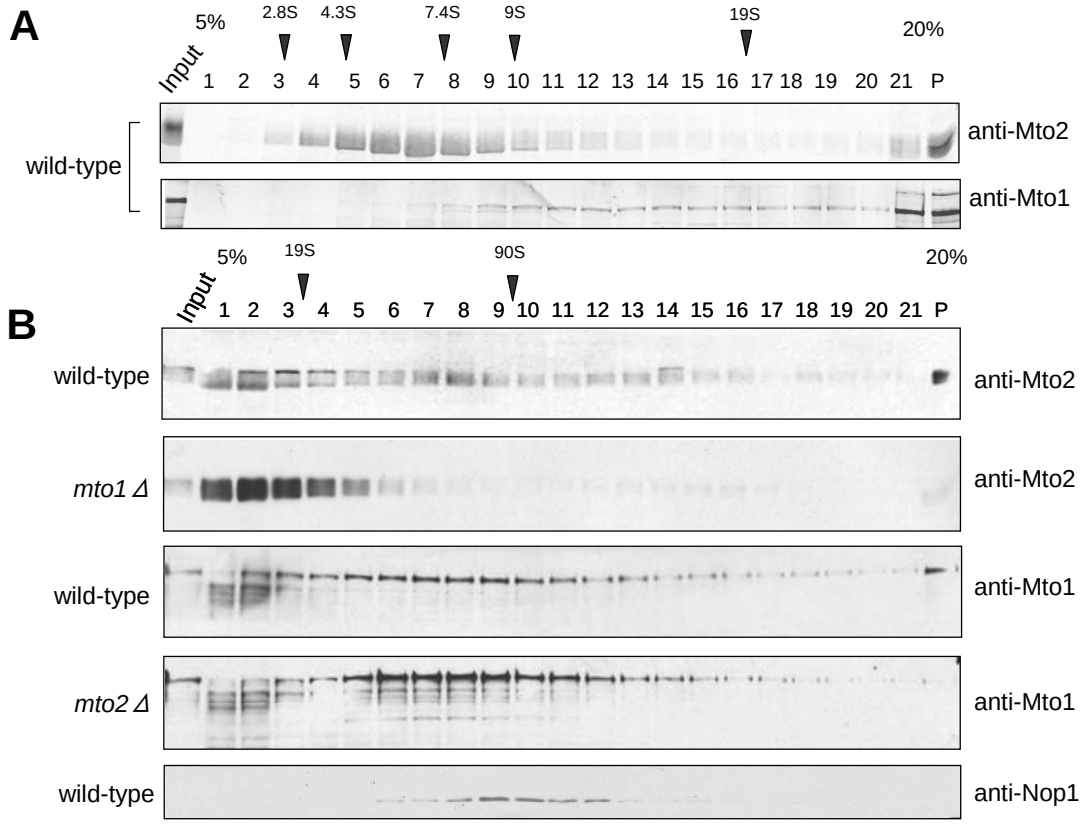

Figure 3.1 Sucrose gradient centrifugation analyses of endogenous Mto1 and Mto2. An extract was subject to centrifugation at 55,000 rpm for [A] 3.5 hr or [B] 30 min in a Beckman TLS-55 rotor [Strains KS516, KS976 and KS1017]. The fractions including the pellet [P] were analysed by 10% SDS-PAGE and the western blot was probed with anti-Mto1 and anti-Mto2 antibodies. The signal intensities were detected using the Odyssey V3.0 software. The peak locations for molecular weight standards run on parallel gradients are indicated [black arrows]. The western blot was also probed with anti-Nop1 antibody. Nop1 peak intensity is also indicated [90S]. Images represent typical results obtained from two experiments.

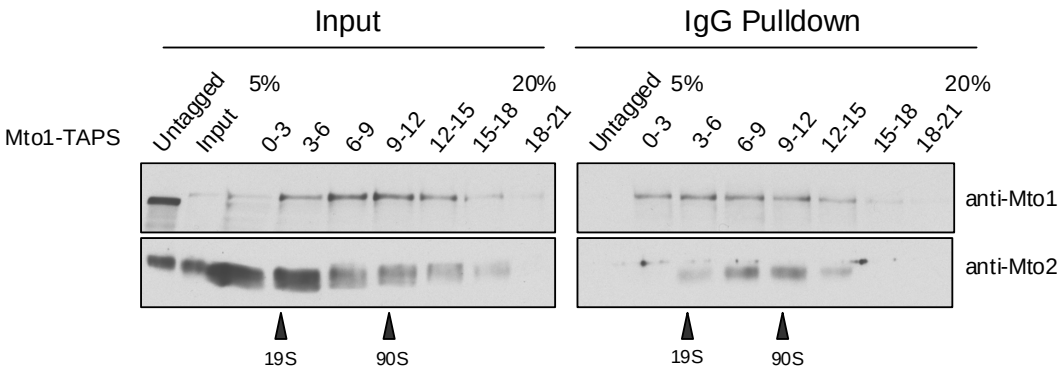

Figure 3.2 Analysis of the Mto1-Mto2 interaction within the 60 – 80 S complex. The extract [KS3524] was fractionated by sucrose gradient centrifugation at 55,000 rpm for 30 min in a Beckman TLS-55 rotor. Every third fraction was pooled and incubated with IgG-linked Dynabeads. Non-fractionated extract from untagged Mto1 was used as a negative control [KS516]. The input sample was taken from non-fractionated extract prior to centrifugation. The samples were analysed by 10% SDS-PAGE and the western blot was probed with anti-Mto1 and anti-Mto2 antibodies. The signal from GT-34-HRP was detected by ECL. The peak locations for Thyroglobulin [19S] and Nop1 [90S] are indicated [black arrows]. Images represent typical results obtained from two experiments.

3.2.3 The Mto1/2 60 – 80 S complex is formed independently of the γ-TuC

The Mto1/2 60 – 80 S complex potentially could include several copies of the γ-TuSC, and therefore represent a γ-TuRC-like complex. This would support my proposed template model for Mto1/2 induced γ-TuRC assembly. To test this idea, the fractionation patterns of members of the γ-TuSC were compared in wild-type, *mto1Δ* and *alp16Δ* backgrounds. Alp16 is required for the interaction of the other non-core components with the γ-TuC (Anders *et al.* 2006). Therefore, as the non-core components of the γ-TuRC are not able to associate in the absence of Alp16, the size of the resulting Mto1/2 60 – 80 S complex may be reduced. This does not exclude the possibility that several copies of the γ-TuSC may be able to associate with Mto1 independently of non-core γ-TuRC components.

Figure 3.3 shows that in the wild-type extract both γ-tubulin and Alp6 proteins were distributed along a number of fractions within the same 60 – 80 S range as Mto1, indicating that the γ-TuSC proteins are present in a complex of similar size. The distribution of γ-tubulin and Alp6 was not significantly altered in *mto1Δ*, implying that Mto1 is not required for the inclusion of the γ-TuSC proteins in the 60 – 80 S complex. This observation is supported by the analysis of Mto1-9A1, a variant of Mto1 that contains mutations in the CM1 domain that prevent Mto1 from interacting with the γ-TuSC (Samejima *et al.* 2008). Mto1-9A1 was also found within the 60 – 80 S range, which suggests that the γ-TuSC components are not required for the inclusion of Mto1 in the Mto1/2 60 – 80 S complex. The sedimentation pattern of Mto1 in *alp16Δ* was similar to wild-type, indicating that the

non-core components also do not contribute significantly to the presence of Mto1 within the Mto1/2 60 – 80 S complex.

Interestingly in *alp16Δ,* Alp6 and γ-tubulin peaked in a fraction representing a smaller molecular weight complex than observed in wild-type extracts. This suggests that assembly of the 60 – 80 S complex containing the γ-TuSC is partly due to the inclusion of non-core components. Previous estimates have indicated that the γ-TuRC from *D. melanogaster* has an S-value of approximately 35 S (Oegema *et al.* 1999). Therefore the unusually large size of the *S. pombe* 60 – 80 S γ-TuC is unlikely to reflect the equivalent γ-TuRC of higher eukaryotes. It is possible that the 60 – 80 S γ-TuC complex includes other protein complexes and cellular debris. Alternatively, the substantial distribution of material along the gradient suggests that the 60 – 80 S complex may represent several unstable copies of the γ-TuC that may have associated during the cell lysis procedure.

Unfortunately the poor resolution of the gradients in Figure 3.3 has prevented any conclusive statements from being made regarding the behaviour of the γ-TuSC and the Mto1/2 complex within the 60 – 80 S range. Additionally, without knowing the copy number of proteins present within the complex it is not possible to distinguish between Mto1 60 – 80 S complex formation as a result of protein aggregation or association with large fragments of cellular debris. This is important as removal of proteins present in low copy number would not significantly alter the size of the 60 – 80 S complex and correlate with the results described above. In order to determine the true nature of both the Mto1/2 and γ-TuSC complexes this analysis needs to be performed with reconstituted complex constructed from purified protein.

3.2.4. The Mto1/2 60 – 80 S complex formation is promoted by Mto1 localisation to the SPB

In addition to potential protein aggregation, it is postulated that the Mto1/2 60 – 80 S complex may result from association with soluble fragments of the SPB and/or other soluble cellular debris. This association may be physiologically relevant to Mto1/2 function, e.g. it may provide a way to consolidate excess Mto1 protein, in order to restrict the number of cytoplasmic MTs. Alternatively localisation to the SPB may promote Mto1 aggregation due to an increase in local concentration. To test SPB-dependent Mto1/2 60 – 80 S formation, a truncated version of Mto1 [1-1051] was analysed that lacks the C-terminal domain required for Mto1 localisation to the eMTOC and SPB (Samejima *et al.*, manuscript in preparation). If the Mto1/2 60 – 80 S complex is formed as a consequence of association with the SPB, then it should not be present in Mto1 [1-1051].

Figure 3.4 shows that compared with full length protein, the amount of Mto1 [1-1051]-TAPS found within fractions 1-3 [< 20 S] was increased. This result suggests that formation of the Mto1/2 60 – 80 S complex is partially due to localisation of the Mto1 to the SPB. This indicates that either Mto1 aggregation is promoted by SPB association, or the Mto1/2 60 – 80 S complex may represent Mto1 association with fragments of the SPB. To test this one could examine the sedimentation pattern of other SPB-associated proteins such as Sad1 (Hagan *et al.* 1995). The presence of residual 60 – 80 S complex indicates that Mto1 can also form large associations in the absence of SPB localisation.

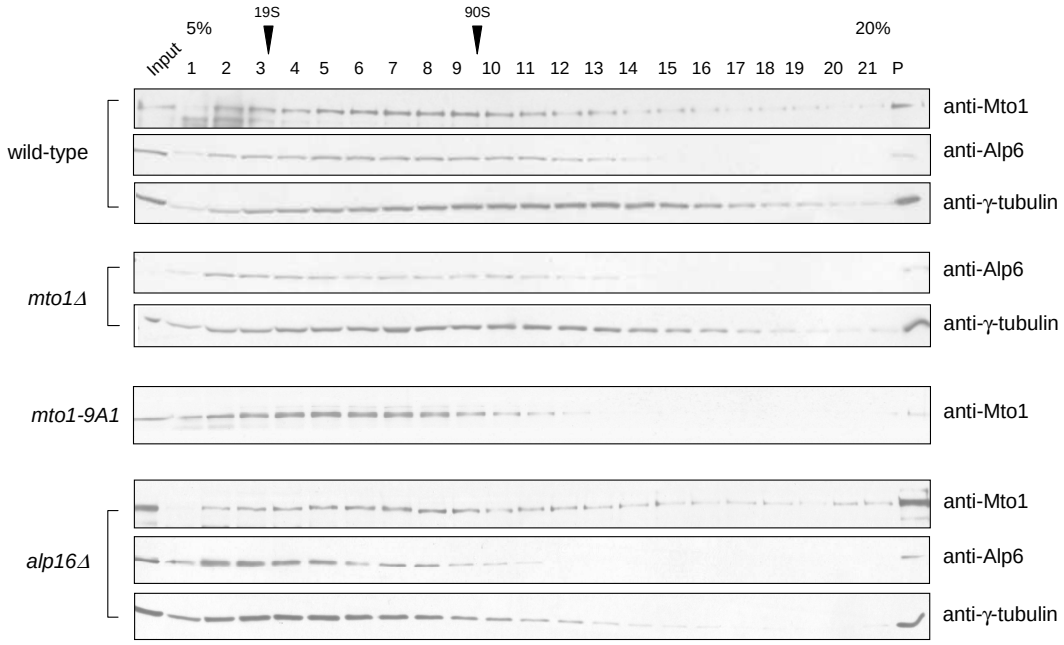

Figure 3.3 60 – 80 S complex formation in γ-TuC mutants. The extracts were subject to sucrose gradient centrifugation at 55,000 rpm for 30 min in a Beckman TLS-55 rotor. [Strains KS516, KS1017, KS2007 and KS1567]. The fractions including the pellet [P] were analysed by 10% SDS-PAGE and the western blot was probed with anti-Mto1, anti-Alp6, and anti-γ-tubulin [GTU-88] antibodies. The signals from GT-34-HRP and anti-mouse IgG-HRP antibodies were detected using ECL. The peak locations for Thyroglobulin [19S] and Nop1 [90S] are indicated [black arrows]. Image represents result obtained from a single experiment.

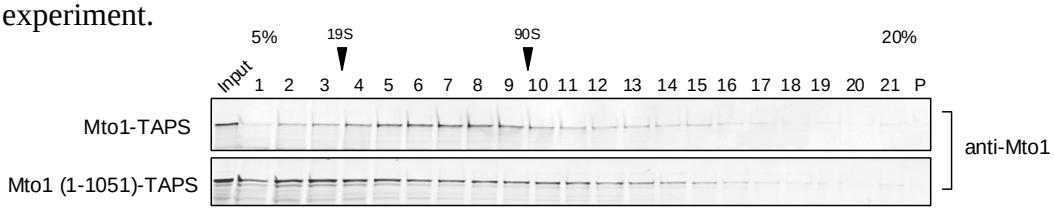

Figure 3.4 60-80 S formation in Mto1 [1-1051]-TAPS. The extracts were subject to sucrose gradient centrifugation at 55,000 rpm for 30 min in a Beckman TLS-55 rotor. [Strains KSKS3475 and KS5578]. The fractions including the pellet [P] were analysed by 10% SDS-PAGE and the western blot was probed with anti-Mto1 antibody. Integrated intensity of the signals from IRDye800 were measured using Odyssey V3.0. The peak locations for Thyroglobulin [19S] and Nop1 [90S] are indicated [black arrows]. Image represents result obtained from a single experiment.

3.2.5 Foci formed by Mto1-tdRFP at non-SPB iMTOC are weakened in the absence of Mto2

To investigate the function of the Mto1/2 60 - 80 S complex *in vivo*, the properties of fluorescently tagged Mto1 were examined in *mto2*$^{+}$ and *mto2Δ* backgrounds. As biochemical analysis has shown that the Mto1 60 - 80 S complex is assembled in both *mto2*$^{+}$ and *mto2Δ*, only Mto1 structures present in both backgrounds [apart from SPB/eMTOC associated protein] can be considered as Mto1/2 60 – 80 S candidates.

Figure 3.5, Panel A, demonstrates that wild-type strains contained the canonical 3 – 4 bundles of MTs per cell and Mto1-tdRFP satellite foci decorated the whole length of each MT bundle in addition to bright signals at the SPB and eMTOC [fig 3.5, Panel B]. As previously documented, *mto2Δ* cells contained 1 – 2 hyperstable MT bundles, which curved around the cell tip (Samejima *et al.* 2005). Only a small proportion of MT bundles were decorated with Mto1-tdRFP satellite foci, and the signal from these foci was significantly less intense than wild-type. The presence of bright Mto1-tdRFP signals from the SPB and eMTOCs in *mto2Δ* supports the conclusion that a proportion of the Mto1/2 60 – 80 S complex may result from Mto1 association with the SPB and eMTOC [fig 3.5, Panel B]. The only non-SPB/eMTOC associated Mto1-tdRFP foci present in both backgrounds were faint satellites found along pre-existing MTs. It is possible that these structures may represent the 60 – 80 S complexes. The intensity of these foci suggest that they represent a relatively small number of Mto1 molecules that are stably associated with other large cellular debris or protein complexes that are yet to be identified.

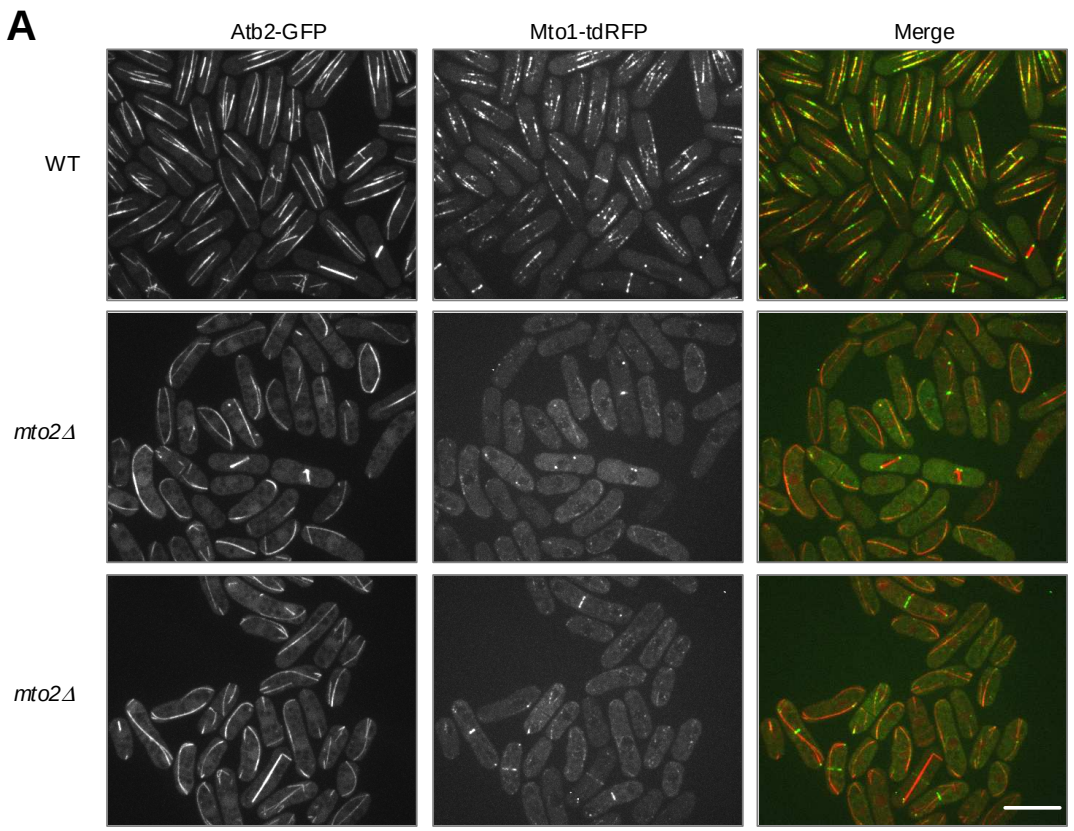
A
Atb2-GFP
Mto1-tdRFP
Merge
WT
mto2Δ
mto2Δ

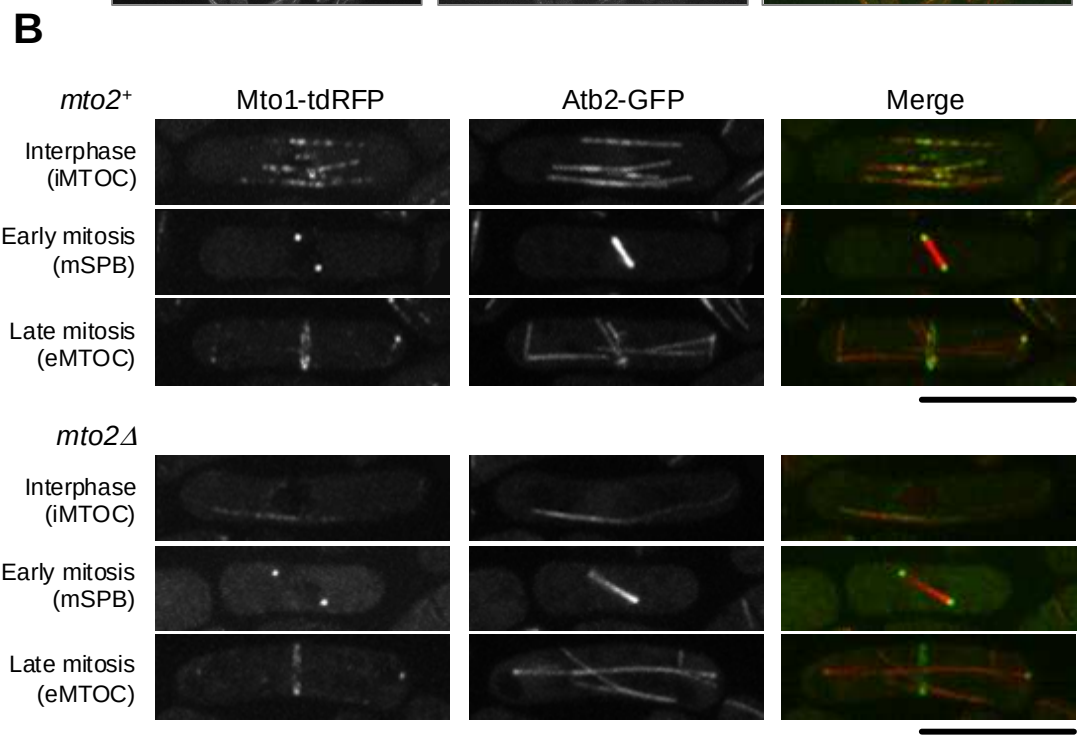
B
mto2+
Mto1-tdRFP
Atb2-GFP
Merge
Interphase (iMTOC)
Early mitosis (mSPB)
Late mitosis (eMTOC)
mto2Δ
Interphase (iMTOC)
Early mitosis (mSPB)
Late mitosis (eMTOC)

Figure 3.5 Microscopic analysis of Mto1-tdRFP demonstrates that Mto2 is required for the assembly of bright foci at non-SPB iMTOCs. Images were taken on a spinning disk confocal microscope. Maximum projections of [A] whole field or [B] single cells expressing *nmt81:mto1-tdRFP* and *nmt81:atb2-GFP* in either *mto2*$^{+}$ or *mto2Δ* background [Strains KS3470 and KS5576]. Single cell projections are representative of three different cell cycle stages as indicated. Scale bars = 10µm.

Due to the size of the complex, I believe that the 60 – 80 S complex most likely represents an aggregated form of Mto1 formed during the cell lysis procedure. Mto1 may be prone to aggregation due to the presence of extensive regions of coiled-coil along the length of the protein. Aggregation may be promoted when Mto1 is present at high concentrations, [for example, at the SPB and eMTOC], which is consistent with the observation that Mto1 60 – 80 S formation is reduced in Mto1 [1-1051]. To test this prediction, one needs to examine 60 - 80 S formation in a version of Mto1 that lacks its coiled-coil domains.

In addition, this *in vivo* analysis has demonstrated that Mto2 functions as an Mto1/2 complex assembly factor, as in the presence of Mto2 the Mto1-tdRFP satellite foci observed at non-SPB iMTOCs were significantly brighter. The function of Mto2 within the Mto1/2 complex will be discussed further in chapter four.

3.2.6 Mto1 [1-800] interacts with Mto2 to form a complex smaller than 60 – 80 S

Evidence collected so far suggests that the Mto1/2 60 – 80 S complex may not be assembled *in vivo* and instead may result from aggregation of proteins during cell lysis. To test this, an extract containing a truncation mutant of Mto1, Mto1 [1-800], that lacked a large portion of the C-terminal coiled-coil domains predicted to promote Mto1 aggregation [fig 3.6, Panel A], was analysed by sucrose gradient centrifugation. Figure 3.6, Panel B shows that in comparison to full length GFP-Mto1, the majority of GFP-Mto1 [1-800] was found within fractions 1-6, which correspond to protein complexes < 20 S. This indicates that removal of sections of

coiled-coil from Mto1 prevent it from forming the large 60 - 80 S complex. To confirm that Mto1 [1-800] and Mto2 form a complex that is smaller than 60 - 80 S, an interaction assay was performed with an extract from Mto1 [1-800]-TAPS that had been pre-fractionated by sucrose density centrifugation. Figure 3.6, Panel C shows that only Mto2 present in fractions 1-6 were found in the co-precipitate, and confirms that the complex formed by Mto1 [1-800] and Mto2 is smaller than 60 - 80 S.

These results support the prediction that the coiled-coil domains in the Mto1 C-terminus lead to the formation of the Mto1 60 – 80 S complex. Analysis of Mto1 [1-800] phenotype has demonstrated that Mto1 [1-800] is sufficient to induce MT nucleation (K. Sawin, personal communication). This indicates that Mto1 and Mto2 do not need to be present within a 60 – 80 S complex to form an active complex, and further demonstrates that the 60 - 80 S complex may not be a physiological phenomenon.

3.2.7 Hydrodynamic analysis of the Mto1 [1-800] / Mto2 complex indicates that it is a heterotetramer

Analysis of the MTs behaviour in an Mto1 [1-800] background indicate that the truncated protein is able to promote MT nucleation. Biochemical analysis has shown that when in complex with Mto2, Mto1 [1-800] forms a complex that is smaller than 20 S. This smaller complex lies within the resolution range of the sucrose gradient centrifugation and gel filtration analyses, therefore one can accurately measure its molecular weight. This information can then be used to

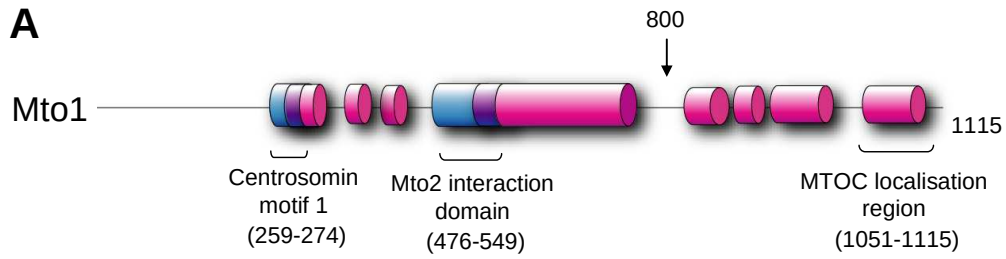
A
800
Mto1
1115
Centrosomin
motif 1
(259-274)
Mto2 interaction
domain
(476-549)
MTOC localisation
region
(1051-1115)

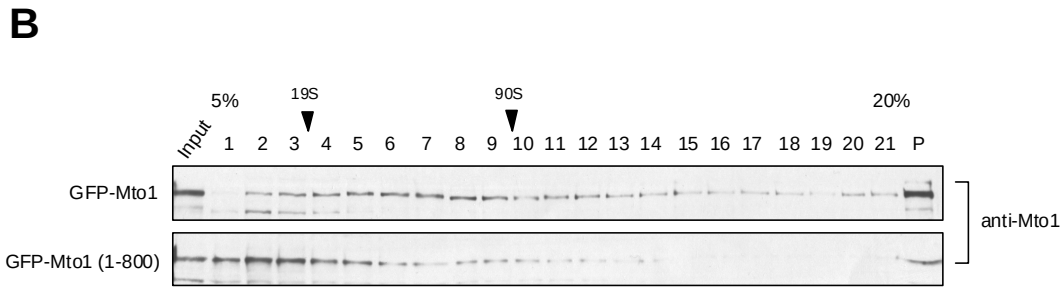
B
5%
19S
90S
20%
Input
1 2 3 4 5 6 7 8 9 10 11 12 13 14 15 16 17 18 19 20 21 P
GFP-Mto1
GFP-Mto1 (1-800)
anti-Mto1

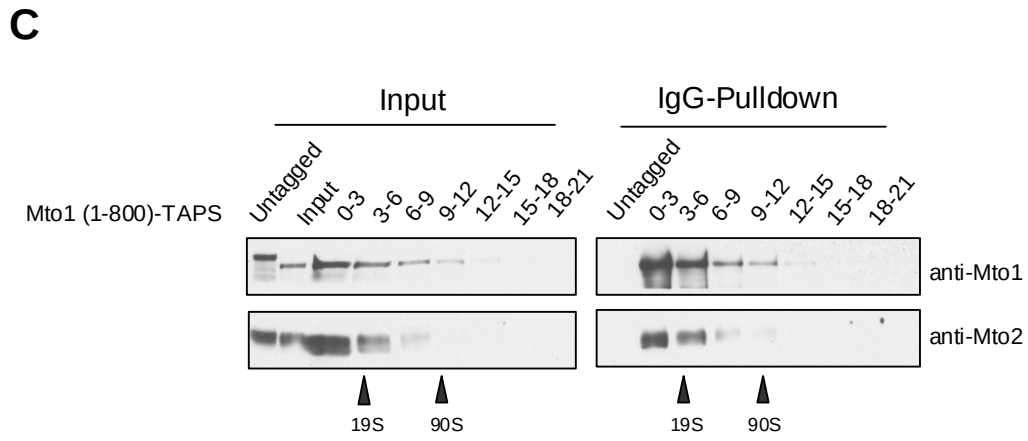
C
Input
IgG-Pulldown
Mto1 (1-800)-TAPS
Untagged
Input
0-3
3-6
6-9
9-12
12-15
15-18
18-21
anti-Mto1
anti-Mto2
19S
90S

Figure 3.6 Removal of Mto1 coiled coil prevents Mto1/2 60 – 80 S formation. [A] Schematic map of Mto1 depicting PAIRCOIL2 predicted coiled-coil domains [pink] and regions of overlap [purple] with protein interaction domains [blue]. Amino acid residue numbers are indicated including the 1-800 truncation [black arrow]. [B] The extract was analysed by sucrose gradient centrifugation at 55,000 rpm for 30 min in a Beckman TLS-55 rotor. [Strains KS4230 and KS1999]. Fractions including the pellet [P] were analysed by 10% SDS-PAGE and the western blot was probed with anti-Mto1 antibody. The signal from GT-34-HRP secondary antibody was detected by ECL. Image represents result obtained from a single experiment. [C] The extract from KS3476 was fractionated by sucrose gradient centrifugation at 55,000 rpm for 30 min in a Beckman TLS-55. Every third fraction was pooled and incubated with IgG-linked Dynabeads. Non-fractionated extract from untagged Mto1 [KS516] was used as a negative control. The input sample was taken from a non-fractionated extract prior to centrifugation. The samples were analysed by 10% SDS-PAGE and the western blot was probed with anti-Mto1 and anti-Mto2 antibodies. Signal from GT-34-HRP was detected by ECL. Peak locations for Thyroglobulin [19S] and Nop1 [90S] are indicated [black arrows]. Image represents typical result obtained from two experiments.

calculate the number of molecules present within the complex. Figure 3.7, Panels A and C show the sucrose gradient centrifugation analyses where in *mto2*$^{+}$ background Mto1 [1- 800] peaked in fraction 8.2 whereas Mto2 peaked in fraction 7. When compared with a calibration curve in Appendix II, this corresponded to a sedimentation co-efficient for Mto1 [1-800] of 8 S. In *mto2Δ,* Mto1 [1-800] peaked in fraction 6.2 which corresponded to an S-value of 5.9 S. The incomplete co-fractionation of Mto2 is likely to represent a mixture of complexed Mto2 [8 S] and un-complexed Mto2 [5.6 S] [fig 3.1, Panel A]. Extracts from Mto1 [1-800] were also analysed by gel filtration. Figure 3.7, Panels B and D show that in both the presence and absence of Mto2, Mto1 [1-800] peaked in fraction 5.6, which, when compared to a calibration curve generated from molecules weight markers of known Stokes' radius [Appendix III], corresponded to a Stokes' Radius of 10.1 nm.

A theory developed by Seigel and Monty allows one to calculate the molecular weight of proteins based on their Sedimentation coefficient and Stokes' Radius using the equation below (Siegel *et al.* 1966):

$$M = 6\pi\eta N \bullet a \bullet s / [1-\nu_2\rho]$$

Where M is molecular mass, η is viscosity [0.01g $cm^{-1}s^{-1}$ for weak aqueous solutions], N is Avogadro's constant [$6.02x10^{23}$], a is the Stokes radius [cm], s is the sedimentation co-efficient [sec], ρ is the density of the solvent [1.0 g/cm^3 for dH_20], and ν is the partial specific volume [$\nu_2\rho = 0.73\ cm^3g^{-1}$].

Given the constants of known value the equation can be summarised as:

$M = 3909 \cdot a \cdot s$

Mto1 [1-800] / Mto2:

$M = 3909 \cdot a \cdot s$

$M = 3909 \cdot 10.1\ nm \cdot 8.0\ S$

$M = 315.9\ kDa$

Mto1 [1-800]:

$M = 3909 \cdot a \cdot s$

$M = 3909 \cdot 10.1\ nm \cdot 5.9\ S$

$M = 232.9\ kDa$

The presence of Mto2, which has a theoretical molecule weight of 44kDa, increases the molecular weight of the Mto1 [1-800] complex by 83 kDa, indicating that there are approximately 1.88 molecules of Mto2 present.
Therefore, given that the theoretical molecular weight of Mto1 [1-800] is 92.27 kDa, this indicates that there are approximately 2.52 molecules of Mto1 [1-800] per complex.

These calculations assume that Mto1 and Mto2 are the only proteins that contribute to the molecular weight of the complex. Based on this result it is likely that the complex formed by Mto1 [1-800] and Mto2 contain two molecules of Mto2 and two molecules of Mto1. This result suggests that Mto1 [1-800] is able to form dimers in the absence of Mto2, therefore there are regions of the protein outside of the coiled-coil domain [800-1115 aa] that contribute to the Mto1-Mto1 interaction.

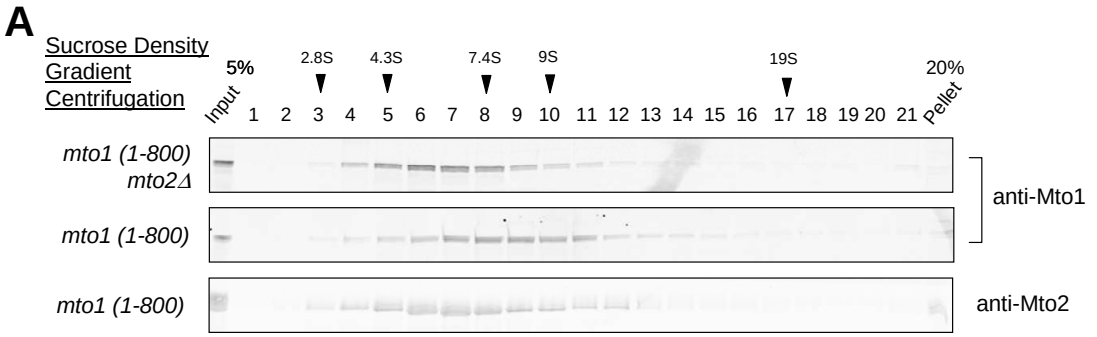
A
Sucrose Density Gradient Centrifugation
5%
2.8S
4.3S
7.4S
9S
19S
20%
Input
1 2 3 4 5 6 7 8 9 10 11 12 13 14 15 16 17 18 19 20 21
Pellet
mto1 (1-800) mto2Δ
mto1 (1-800)
anti-Mto1
mto1 (1-800)
anti-Mto2

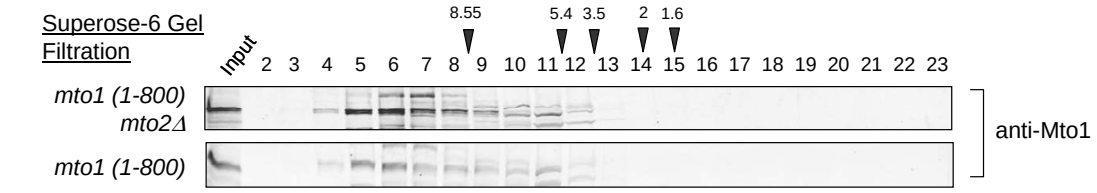
B
Superose-6 Gel Filtration
8.55
5.4
3.5
2
1.6
Input
2 3 4 5 6 7 8 9 10 11 12 13 14 15 16 17 18 19 20 21 22 23
mto1 (1-800) mto2Δ
mto1 (1-800)
anti-Mto1

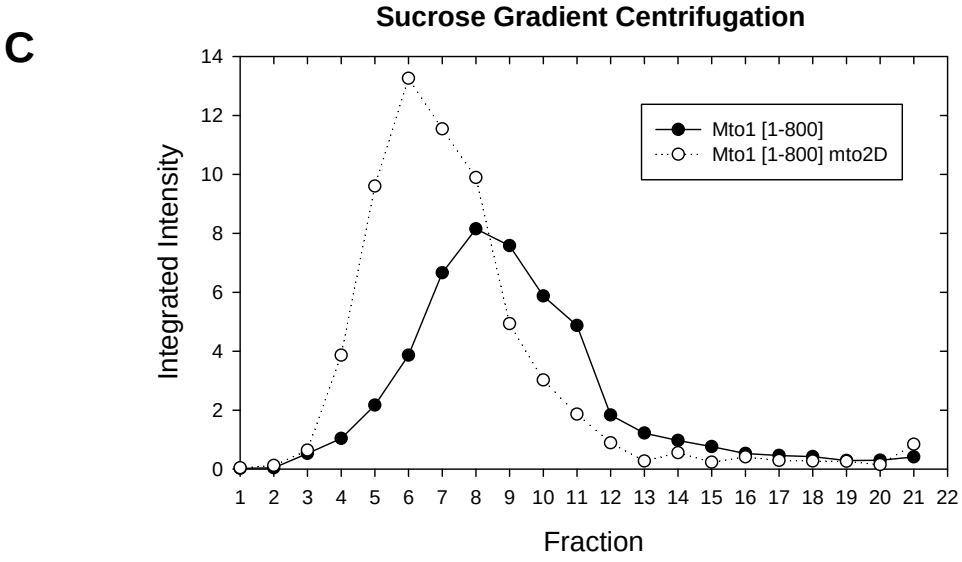
C
Sucrose Gradient Centrifugation
Integrated Intensity
Fraction
Mto1 [1-800]
Mto1 [1-800] mto2D

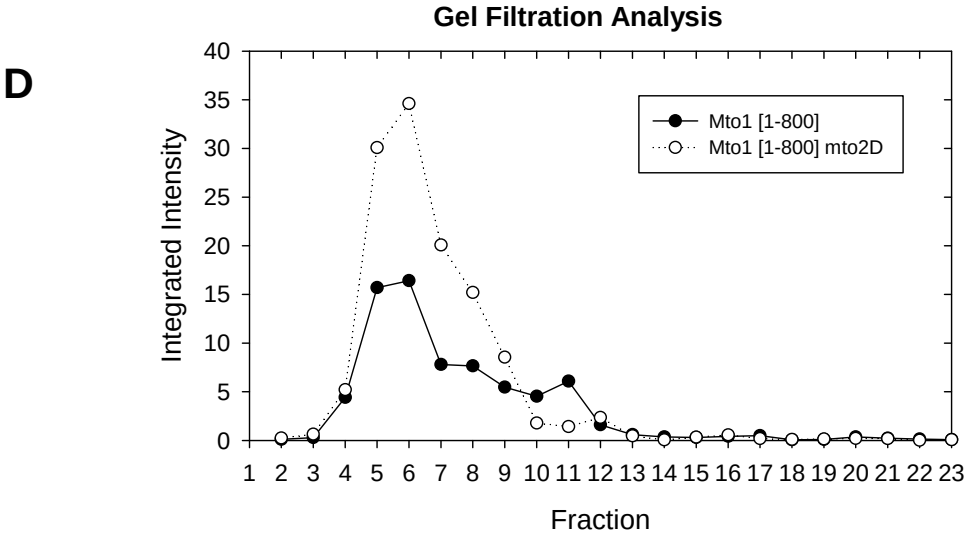
D
Gel Filtration Analysis
Integrated Intensity
Fraction
Mto1 [1-800]
Mto1 [1-800] mto2D

Figure 3.7 Hydrodynamic analysis of the Mto1 [1-800] / Mto2 complex indicates that it is a heterotetramer. [A] Extracts were subject to sucrose gradient centrifugation at 55,000 rpm for 30 min in a Beckman TLS-55 rotor. [B] Extracts were analysed by gel filtration on a Superose-6 column [KS1] [Strains KS1956 and KS5354]. Fractions including the pellet [P] were analysed by 10% SDS-PAGE and the western blot was probed with anti-Mto1 and anti-Mto2 antibodies. [C and D] The integrated intensity of signal from IRDye800 was measured using Odyssey V3.0. The peak locations for molecular weight standards run on parallel gradients are indicated [black arrows]. Standards in [B] are indicated in nm. Mto2D = *mto2Δ*. Images represent typical results obtained from two experiments.

The small size of the Mto1 [1-800] / Mto2 heterotetramer indicates that it may represent a ‘sub-complex’ or minimal function unit. It is likely that the C- terminal coiled-coil domains of full length Mto1, in addition to association of Mto2 with Mto1, facilitate the multimerisation of the Mto1/2 heterotetramers into larger assemblies that may resemble a template structure for γ-TuSC association.

3.2.8 Mto2 interaction efficiency with Mto1 [1-800] is comparable to full length protein

Hydrodynamic analysis of the Mto1 [1-800] / Mto2 complex has demonstrated that it is smaller than the Mto1/2 complex containing full length Mto1. To test whether the efficiency of the Mto1-Mto2 interaction has been altered in the Mto1 [1-800] / Mto2 complex, the levels of Mto2 co-precipitated by Mto1-TAPS were compared between full length Mto1 and Mto1 [1-800]. Figure 3.8 Panel A and B show the integrated intensity of the Mto2 signal in the pulldown, which has been normalised relative to the levels of Mto1-TAPS. The levels of Mto2 pulled down by full length Mto1-TAPS and Mto1 [1-800]-TAPS were comparable, indicating that truncation of Mto1 does not affect the stability of the interaction with Mto2. This data also suggests that the ratio of Mto1 to Mto2 molecules within the Mto1 [1-800] / Mto2 complex is comparable to full length Mto1/2. This supports the prediction that the full length Mto1/2 complex is composed of several copies of the Mto1/2 heterotetramer.

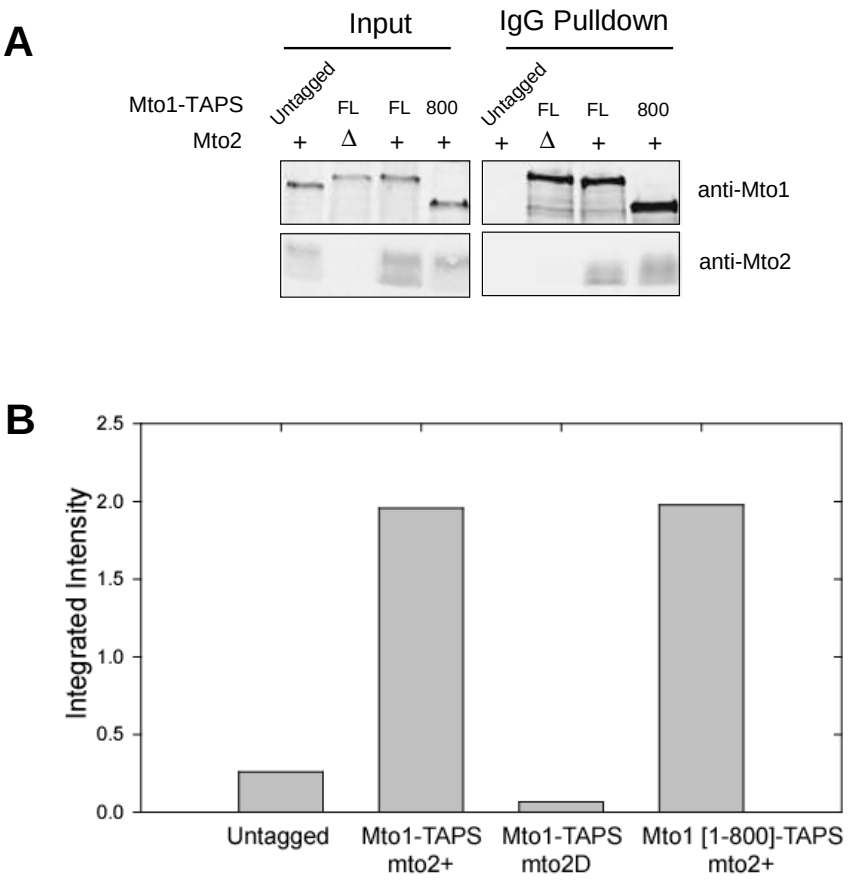

Figure 3.8 The efficiency of the Mto1-Mto2 interaction is not affected by heterotetramer formation. Extracts were incubated with IgG-Dynabeads [Strains KS516, KS3524, KS4323 and KS34760]. [A] Eluates were analysed by 10% SDS-PAGE and the western blot was probed with anti-Mto2 and anti-Mto2 antibodies. [B] Integrated intensities of IRDye800 signal were measured using Odyssey V3.0. Mto2 signal was normalised relative to the signal from Mto1. Mto2D = *mto2Δ*. Image represents result obtained from a single experiment.

3.2.9 The Mto1-Mto1 interaction is independent from Mto2

Hydrodynamic analysis of the Mto1 [1-800] / Mto2 complex has suggested that Mto1 [1-800] exists as a dimer and that this interaction is independent from Mto2. The Mto1-Mto1 interaction was confirmed by performing an anti-GFP immunoprecipitation in a strain that contained Mto1-GFH expressed from an *nmt41* thiamine repressible promoter at the *leu1* locus and Mto1-13myc expressed from the endogenous *mto1* promoter. Figure 3.9 shows that in the absence of Mto1-GFH, Mto1-13myc was not co-precipitated, however, in the presence of Mto1-GFH, Mto1-13myc was present in the eluate. The levels of Mto1-13myc that interacted with Mto1-GFH did not change in *mto2Δ*. This result confirms that Mto1 can self-interact.

3.2.10 Mto2 can self-interact *in vitro*

The presence of dimeric Mto2 within the Mto1 [1-800] / Mto2 heterotetramer suggests that Mto2 can also self-interact, however, it is not known whether Mto1 is required for this interaction. To investigate this, an interaction assay was performed *in vitro*. Mto2 was tagged with N-terminal MBP by Gateway recombination (Busso *et al.* 2005), to allow expression of soluble protein that could be purified on amylose resin. Mto2 was also tagged with NusA to allow expression of soluble protein with a larger molecular weight that could be distinguished from MBP-Mto2 upon SDS-PAGE analysis. Figure 3.10 shows the Coomassie stained SDS-PAGE gel of the MBP-pulldown assay. When NusA-Mto2 was incubated with the MBP-Mto2 bound amylose resin, significantly more NusA-Mto2 was present compared with amylose

resin alone. This result indicates that recombinant MBP-Mto2 can interact with NusA-Mto2, although it does not discount the possibility that the NusA tag may be binding to MBP-Mto2 and not Mto2. This discrepancy can be clarified in future experiments by using a NusA only control. This *in vitro* experiment indicates that the Mto2-Mto2 interaction is direct.

3.2.11 The Mto2-Mto2 interaction is independent from Mto1

To confirm the Mto2-Mto2 interaction *in vivo*, an anti-GFP immunoprecipitation was performed on a strain that contained two copies of Mto2, either endogenously tagged with 13myc or tagged with a HFG-tag. HFG-tagged protein was constructed by Gateway recombination of Mto2 into *nmt81:HFG tagging* vector. This sequence was transformed into an *mto2Δ* strain at the *leu1* locus and was then crossed with Mto2-13myc. Figure 3.11 shows that Mto2-13myc did not bind to the anti-GFP linked Dynabeads in the absence of HFG-Mto2. However, Mto2-13myc was found in the co-precipitate of HFG-Mto2 both in $mto1^{+}$ and *mto1Δ*. This indicates that Mto2 is able to self-interact *in vivo*, and confirms that this interaction is independent from Mto1. This Mto2-Mto2 interaction may be required for multiple aspects of Mto2 function within the Mto1/2 complex. This interaction will be investigated further in chapter four.

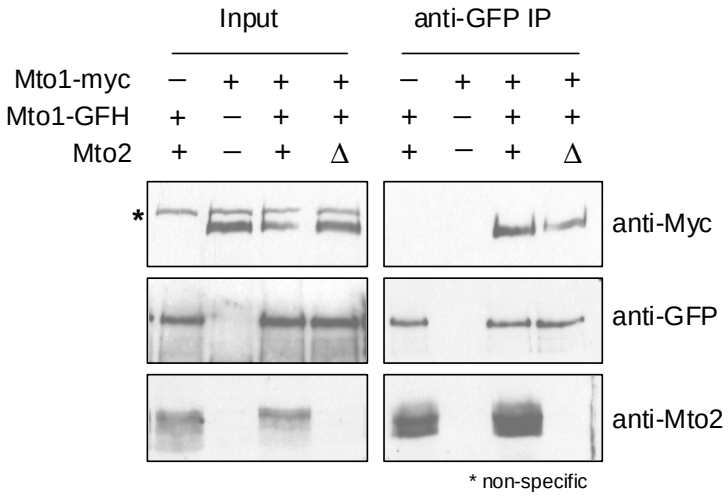

Figure 3.9 Mto1 can self-interact independently from Mto2. Yeast extracts were incubated with anti-GFP linked Protein G Dynabeads [Strains KS4230, KS1507, KS4627 and KS4373]. The eluates were analysed by 8% and 10% SDS-PAGE and the western blot was probed with anti-Myc [9E10], anti-GFP and anti-Mto2 antibodies. The signal from GT-34-HRP and anti sheep-IgG-HRP secondary antibodies were detected by ECL. * = non-specific band. Image represents a typical result obtained from three experiments.

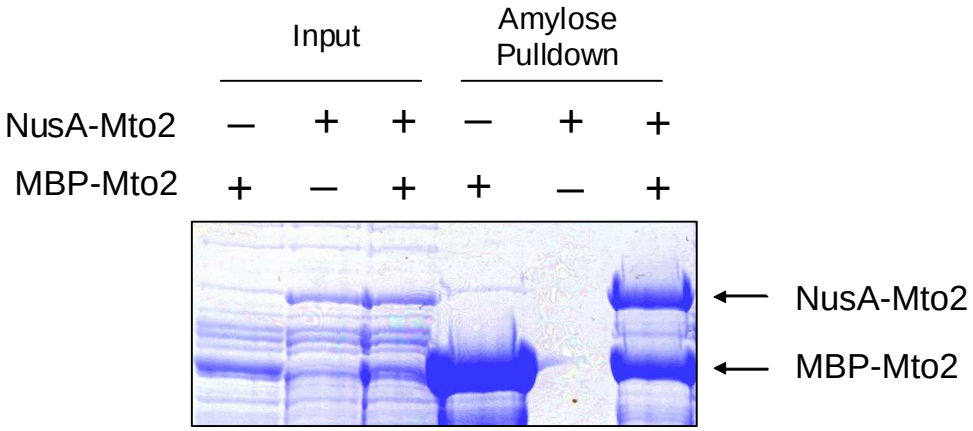

Figure 3.10 Mto2 can self-interact *in vitro*. Bacterial extracts expressing MBP-Mto2, NusA-Mto2 or a combination of both tagged proteins were incubated with amylose resin. Eluates were analysed by 10% SDS-PAGE and gel was stained with Coomassie. Image represents a typical result obtained from three experiments.

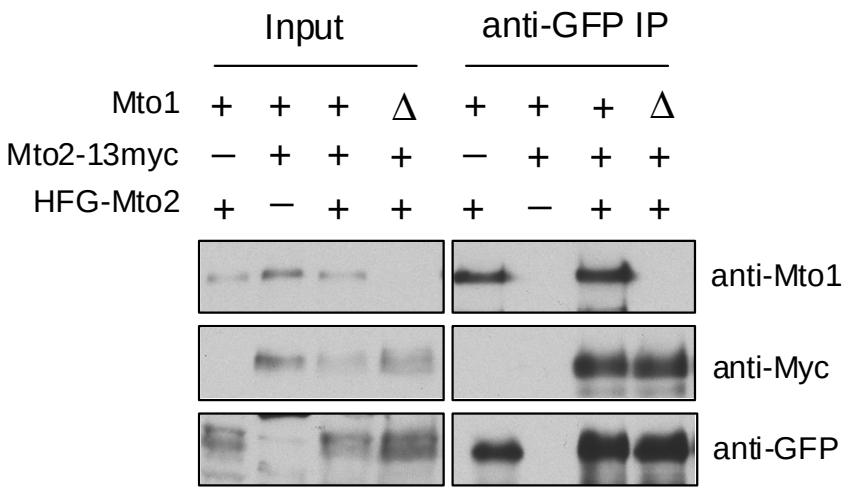

Figure 3.11 Mto2 can self-interact *in vivo* independently of Mto1. Yeast extracts were incubated with anti-GFP linked Protein G Dynabeads [Strains KS1504, KS3915, KS3920, and KS5574]. The eluates were analysed by 10% SDS-PAGE and the western blot was probed with anti-Myc [9E10], anti-GFP and anti-Mto1 antibodies. The signal from GT-34-HRP and anti sheep-IgG-HRP secondary antibodies were detected by ECL. Image represents a typical result obtained from three experiments.

3.3 SUMMARY OF RESULTS

In this chapter I have investigated the properties of the Mto1/2 complex. When analysed by sucrose density gradient centrifugation I demonstrated that both Mto1 and Mto2 are present within a very large assembly of approximately 60 – 80 S. Inclusion of Mto2 in the 60 – 80 S complex required Mto1 but not vice versa. The size of the complex was not affected by the failure of Mto1 to interact with the γ-TuSC or by the absence of γ-TuRC non-core components, indicating that this large complex does not represent the Mto1/2-γ-TuRC complex that I predict may be present at the minus ends of MTs.

There are two reasons why the Mto1/2 complex and the γ-TuSC might be found within separate 60 – 80 S complexes. Firstly, these complexes may arise from protein aggregation. Analysis of purified γ-TuSC in other systems has shown that it is prone to aggregation (Oegema *et al.* 1999). The presence of extensive regions of coiled-coil in Mto1 is likely to encourage protein association as demonstrated for other structural elements of the cytoskeleton that contain coiled-coils e.g. myosin and intermediate filament proteins (Alberts *et al.*, 2002). Secondly, the Mto1/2 complex and the γ-TuSC may associate with large cellular particles/debris that sediment within an S-value of 60 – 80 S. The presence of Mto1 within the 60 – 80 S complex was partially disrupted when Mto1 was unable to localise to the SPB and eMTOC, indicating that the 60 – 80 S complex is partially due to association with the SPB. As the γ-TuSC localises to the SPB in *mto1Δ*, this suggests that γ-TuSC 60 - 80 S complex formation may also be promoted by its association with the SPB.

Attempts to visualise the 60 – 80 S complex *in vivo* revealed that weak Mto1-tdRFP foci were visible in *mto2Δ* at non-SPB/eMTOC sites. It is possible that these weak foci represent the 60 – 80 S particles, particularly as they are highly variable in signal intensity. This correlates with the heterogeneous nature of the complex analysed by sucrose density gradient centrifugation. Without knowing how many molecules of Mto1-tdFRP are present within these foci, and what other protein complexes they may be associating with, it is difficult to say whether these particles correspond to the 60 – 80 S complex and whether they are physiologically relevant to MT nucleation. However, phenotypic analysis of another Mto1 truncation mutant, Mto1 [1-800], which was not present with a 60 – 80 S complex but was able to nucleate MTs (Sawin *et al.,* data unpublished), has shown that the presence of the Mto1/2 60 – 80 S complex is not required for Mto1/2 complex activity.

Alternatively, it is possible that the Mto1/2 60 – 80 S may be a result of protein aggregation. During cell harvesting cells are cooled to 4°C and at this temperature the MT bundles depolymerise which causes a re-distribution of Mto1 to the surface of the nucleus (Sawin *et al.* 2004). By concentrating Mto1 at the nuclear envelope, this may exacerbate the aggregation. Analyses of the *D. melanogaster* Mto1 homolog, Centrosomin [Cnn], have shown that when over-expressed it forms large aggregates within the cell, which supports the idea that aggregation of these proteins may be promoted by increases in concentration (Kofron *et al.* 1998; Terada *et al.* 2003).

In summary, attempts to determine the copy number of molecules within Mto1/2 complex containing full length Mto1 have been unsuccessful due to the

formation of the Mto1/2 60 – 80 S complex. Additionally, due to its size and heterogeneity, it has not been possible to determine whether the Mto1/2 60 – 80 S complex has a physiological role *in vivo*.

In the second part of this chapter, I performed a hydrodynamic analysis of the Mto1 [1-800] / Mto2 complex and demonstrated that it is likely to be composed of two molecules of Mto1 and two molecules of Mto2. I demonstrated that both Mto1 and Mto2 are able to self-interact, independently of each other. This suggests that the heterotetramer is composed of independent dimers of both Mto1 and Mto2. I predict that this heterotetramer represents the major subunit of the Mto1/2 complex, which may then multimerise to provide a template-like structure that can promote γ-TuRC assembly. Comparison of the purified Mto1 [1-800] / Mto2 complex with the full length Mto1/2 complex indicates that the stable complexes from both contain similar levels of Mto1 and Mto2. This further supports the idea that the Mto1/2 complex containing full length Mto1 is composed of several copies of the heterotetramer.

Examination of the Mto1-GFP foci *in vivo* has demonstrated that the intensity of non-SPB iMTOC foci are comparable between full length Mto1-GFP and Mto1 [1-800]-GFP (Sawin *et al.*, data unpublished). The bright signals in both backgrounds indicate that many molecules are likely to be present at each iMTOC, and that the quantitative levels of the Mto1/2 complex at the MTOCs are the same. However, as only single heterotetramers were observed in the biochemical analysis [most likely as a result of dissociation following the reduction in temperature during the cell harvesting and lysis procedure] it has not been possible to determine the copy number of each protein within the active nucleation complex.

However, it is also possible that Mto1 [1-800] / Mto2 heterotetramers could support γ-TuRC assembly without multimerising e.g. by individually targeting small numbers of γ-TuSC to the non-SPB iMTOC to a concentration sufficient to promote γ-TuRC self-assembly. Alternatively, as observed *in vitro*, a complex containing one or two γ-TuSC may be sufficient to nucleate MTs (Oegema *et al.* 1999). This would support the Protofilament Model of MT nucleation (Erickson *et al.* 1996a).

In vitro reconstitution from purified γ-TuSC and the Mto1 [1-800] / Mto2 heterotetramer would be one way to determine the nature of the complex formed by Mto1/2 and γ-TuSC. This would allow examination of the hydrodynamic properties of Mto1 [1-800] / Mto2 complex in association with the γ-TuSC. If complexes > 35 S were observed, this would favour Mto1/2-directed γ-TuRC assembly, if complexes < 35 S were observed this would indicate that complexes containing a small number of γ-TuSC are sufficient for MT nucleation.

The model in Figure 3.12 describes possible arrangements of the Mto1/2 complex. Panel A depicts the arrangement of Mto1 and Mto2 in the Mto1 [1-800] heterotetramer. This assumes that the Mto1 dimer is configured in a parallel arrangement, with the N-terminal γ-TuC interaction domains facing in the same direction. Panel B describes a potential explanation for what happens to Mto1 when the 60 – 80 S complex is formed. Multimeric association of Mto1 via its C-terminal coiled-coil domains facilitates protein aggregation. This process is promoted by localisation to the SPB due to the increase in local concentration of Mto1. Panels C and D suggest potential arrangements of the multimeric Mto1/2 heterotetramer containing full length Mto1.

There are a number of key points that need to be investigated in order to conclusively demonstrate the Mto1/2 complex configuration. The analysis of the Mto1 60 – 80 S complex described in this chapter indicates that the oligomerisation state of Mto1 is going to be very difficult to determine biochemically. Alternatively, by using *in vivo* methods such as Fluorescence Correlation Spectroscopy (FCS) to measure the fluorescence of single molecules, it may be possible to estimate the numbers of Mto1-GFP at iMTOCs. The orientation of the Mto1 dimers is most likely to be parallel, as this would consolidate both the N-terminal γ-TuC interaction domain and the C-terminal localisation signal. Experiments that involve cross-linking regions of the protein as described in (Gruber *et al.* 2006) would be one way of addressing this problem.

One also needs to address the oligomeric state of Mto2. In Figure 3.5, I demonstrated that Mto2 facilitates the multimerisation of Mto1 *in vivo*, based on the increase in Mto1-tdRFP signal in the presence of Mto2. Mto2-induced Mto1 multimerisation could occur by two mechanisms, either Mto2 binding induces a structural change in Mto1 that promotes its multimerisation e.g. exposure of coiled-coil, or Mto2 itself multimerises and brings multiple molecules of Mto1 together. The role of Mto2 oligomerisation in Mto1/2 complex formation will be investigated further in chapter four.

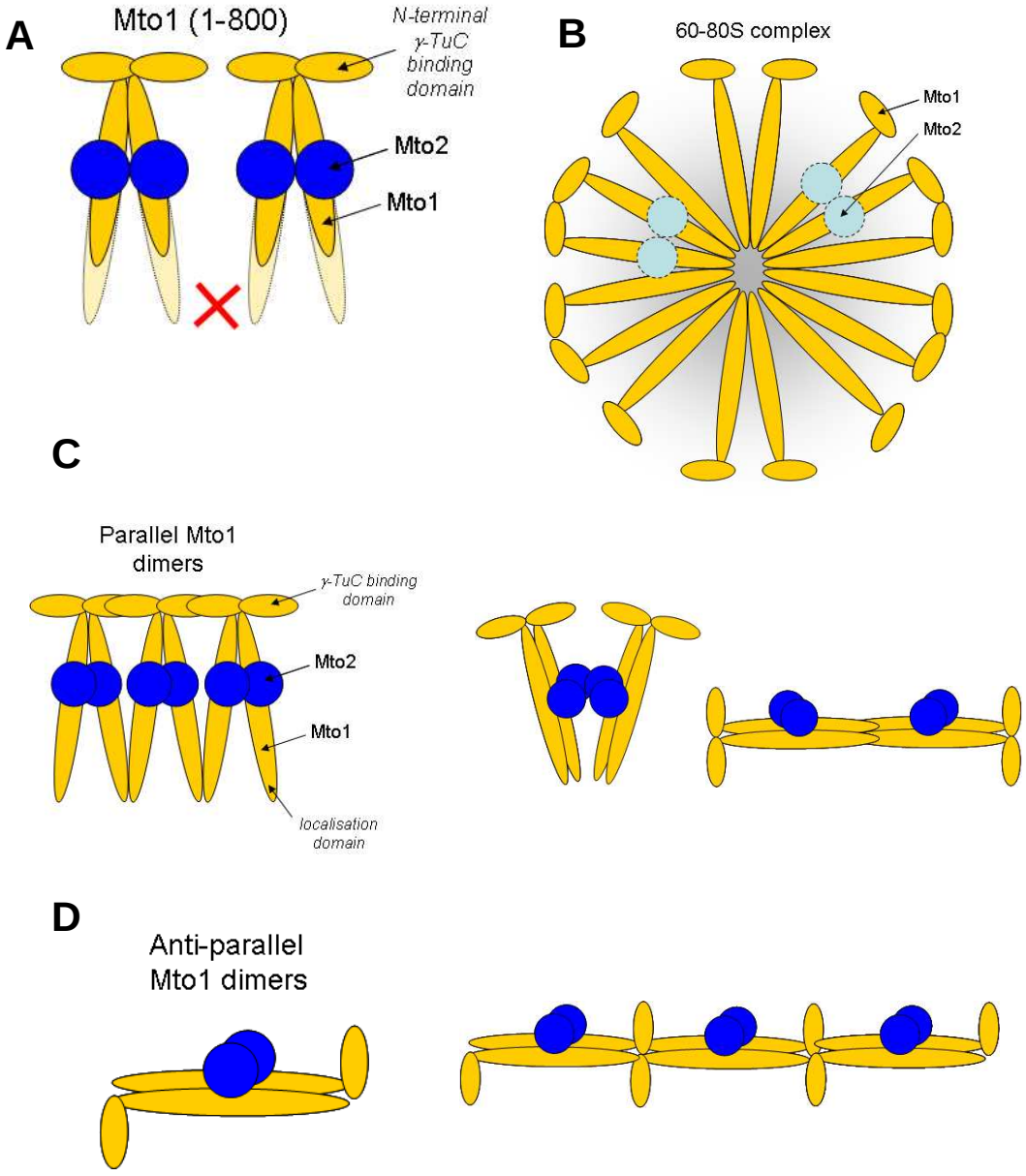

Figure 3.12 Model of Mto1/2 complex conformation. [A] Heterotetramer formation in Mto1 [1-800], where lack of the C-terminal coiled-coil prevents multimerisation. [B] Possible configuration of the 60-80S complex which is likely to assemble during cell lysis. [C-D] Potential conformations of the Mto1/2 complex *in vivo*.

CHAPTER FOUR

ANALYSIS OF THE MTO2 SELF INTERACTION

4.1 INTRODUCTION

The research presented in the previous chapter attempted to address whether the Mto1/2 complex is able to assemble into a large a template structure that can direct γ-TuSC multimerisation. I found that the Mto1 [1-800] / Mto2 complex is likely to be composed of two molecules of Mto1 and two molecules of Mto2. Mto1 is dimeric and, as Mto2 can self-interact independently of Mto1, it is likely that Mto2 is also present within the complex as a dimer. Although not shown biochemically, I predict that *in vivo*, several copies of the Mto1/2 heterotetramer associate into a large complex. Evidence from chapter three suggests that higher-order multimerisation of Mto1 is most likely to be facilitated via its C-terminal coiled-coil domain. However, analysis of the signal of Mto1-tdRFP at non-SPB iMTOCs *in vivo*, show that Mto2 also contributes to the multimerisation of Mto1.

Mto2 may promote Mto1 multimerisation in one of two ways. Firstly, it is possible that Mto2 may induce multimerisation through interaction-induced structural changes that expose domains on Mto1 that are required for multimerisation. Secondly, Mto2 may promote Mto1 multimerisation through its own multimerisation, e.g. Mto2 tetramerisation may cause the association of two Mto1/2 heterotetramers.

Biochemical evidence has shown that Mto2 is required for Mto1 to efficiently interact with the γ-TuSC (Samejima *et al.* 2008). However, the mechanism by which this occurs, and whether it requires the Mto2-Mto2 interaction is unknown. It is possible that Mto2-mediated multimerisation of Mto1 is sufficient to induce a co-operative increase in the efficiency of Mto1 / γ-TuSC interaction. Alternatively, Mto2 may have a more direct role in the γ-TuSC interaction, e.g. by inducing a conformation change in Mto1 that may increase the affinity of Mto1 for the γ-TuSC or Mto2 itself may contribute to the γ-TuSC interaction interface.

4.1.2 Aims and Objectives

In this chapter I aim to investigate the stoichiometry of the oligomeric form of Mto2 and examine whether disruption of the Mto2-Mto2 interaction has adverse effects on the function of the Mto1/2 complex either through loss of Mto1 multimerisation or loss of interaction efficiency with the γ-TuSC.

I will take the following approaches to investigate this problem:

- Hydrodynamic analysis of Mto2 to determine the multimerisation state of purified recombinant protein and endogenous yeast protein
- Mapping of the Mto2-Mto2 interaction
- Construction and analysis of Mto2-Mto2 interaction mutants

4.2 RESULTS

4.2.1 Hydrodynamic analysis of recombinant Mto2 purified from *E. coli*

Hydrodynamic analysis of the active Mto1 [1-800] / Mto2 complex has revealed that there are two copies of Mto2 present within the complex. I have shown that Mto2 is able to self-interact independently of Mto1, which suggests that Mto2 is able to form some higher-order structure. I predict that further multimerisation of Mto2 may contribute to the association of Mto1/2 heterotetramers.

To examine stoichiometry of the Mto2 oligomer, recombinant Mto2 was purified and subject to hydrodynamic analysis. Figure 4.1, Panel A and B show that Mto2 peaked in fraction 17. When compared to the calibration curve generated from molecular weight standards of known S-value [Appendix I] corresponded to 7.25 S. Purified Mto2 was also subject to gel filtration chromatography. Figure 4.1, Panel C and D show that the integrated intensity of the Mto2 signal peaked in fraction 9.2. This was compared with a calibration curve created from markers of known Stokes' radii [Appendix IV] and was found to correlate to a Stokes' radius of 7.7 nm.

4.2.2 Recombinant Mto2 is tetrameric

Using the values calculated in section 3.2.7, the molecular weight of endogenous Mto2 was calculated as described below:

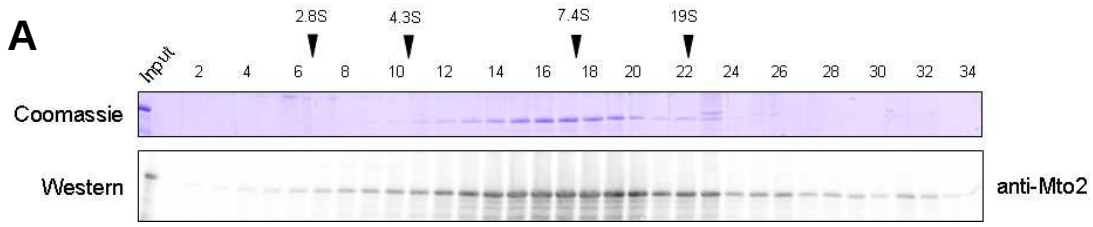
A
2.8S
4.3S
7.4S
19S
Input
2 4 6 8 10 12 14 16 18 20 22 24 26 28 30 32 34
Coomassie
Western
anti-Mto2

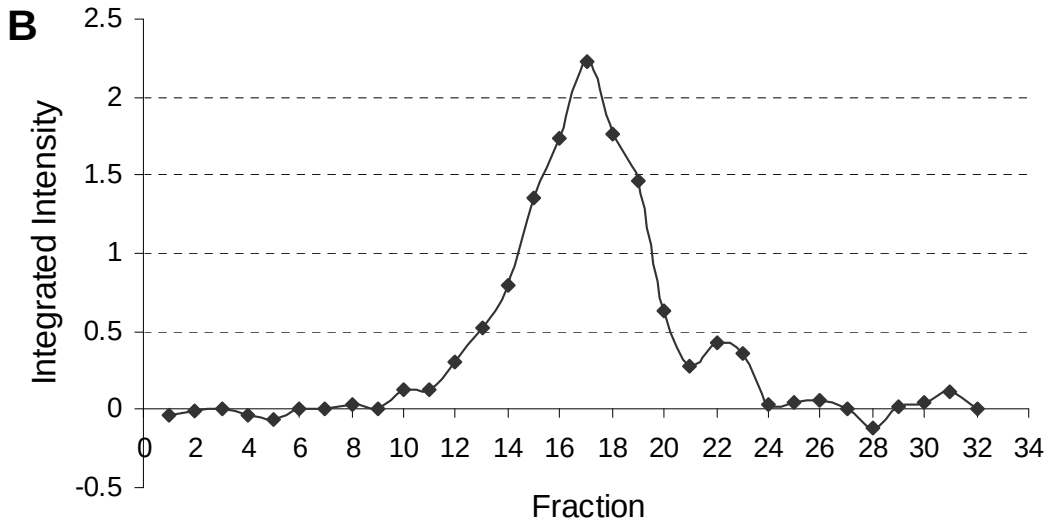
B
Integrated Intensity
2.5
2
1.5
1
0.5
0
-0.5
0 2 4 6 8 10 12 14 16 18 20 22 24 26 28 30 32 34
Fraction

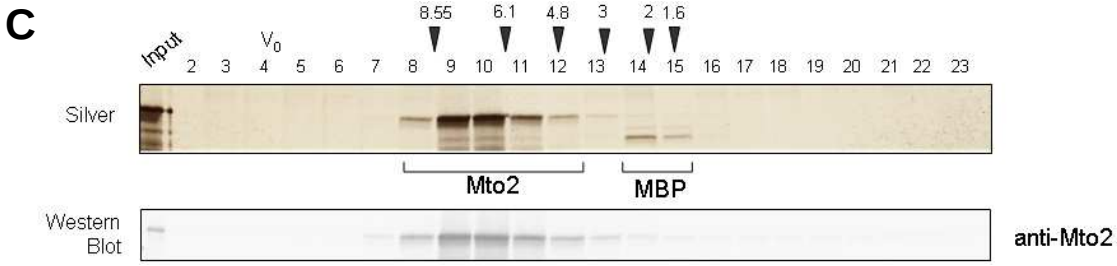
C
8.55
6.1
4.8
3
2
1.6
Input
V0
2 3 4 5 6 7 8 9 10 11 12 13 14 15 16 17 18 19 20 21 22 23
Silver
Mto2
MBP
Western Blot
anti-Mto2

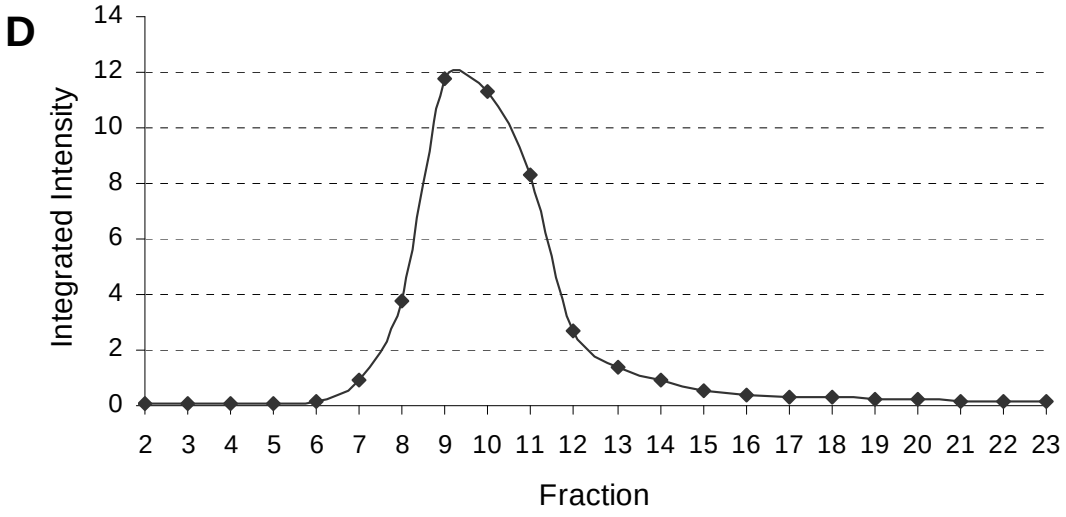
D
Integrated Intensity
14
12
10
8
6
4
2
0
2 3 4 5 6 7 8 9 10 11 12 13 14 15 16 17 18 19 20 21 22 23
Fraction

Figure 4.1 Hydrodynamic analysis demonstrates that purified recombinant Mto2 is a tetramer. [A] 2.5 µg of purified Mto2 was subject to 5 – 20% sucrose density gradient centrifugation at 55,000 rpm for 3.5 hr in a Beckman TLS-55 rotor. The fractions were analysed by 10% SDS-PAGE and the gel was stained with Coomassie stain. A western blot was probed with anti-Mto2 antibody. [B] The integrated intensity from IRDye800 signal was measured using Odyssey V3.0 and plotted against gradient fraction. [C] 2.5 µg of purified recombinant Mto2 was fractionated by gel filtration using a Superose-6 column [KS2]. The fractions were analysed by SDS-PAGE. Silver staining of the gel revealed a protein that was confirmed as Mto2 by western blot probed with anti-Mto2 antibody. [D] The integrated intensity of signal from IRDye800 was measured using Odyssey V3.0 and plotted against gradient fraction. The peak locations for molecular weight standards run on parallel fractionations are indicated [black arrows]. Standards in [C] indicated in nm. V_0 = void volume. Images represent typcial results obtained from two experiments.

Recombinant Mto2:

$M = 6\pi\eta N \bullet a \bullet s / [1-\nu\rho]$

$M = 3909 \bullet a \bullet s$

$M = 3909 \bullet 7.7\ nm \bullet 7.25\ S$

$M = 218.2\ kDa$

The theoretical molecular weight of Mto2 is 44 kDa, this would correspond to 4.96 molecules of Mto2 per oligomer. This large Mto2 complex lies at the high end of the resolution range of the Superose-6 column, therefore it is difficult to assign an exact number of molecules to the complex. Subsequently, it is only possible to say that purified Mto2 exists as a complex containing 4-6 molecules. Evidence from chapter three has demonstrated that the Mto1/2 heterotetramer contains two copies of Mto2, therefore it is likely that purified Mto2 is tetrameric.

4.2.3 Hydrodynamic analysis of endogenous Mto2

Purified recombinant Mto2 forms a homomeric complex that most likely contains 4 molecules of Mto2. To confirm this observation *in vivo*, endogenous Mto2 from yeast extract was also subject to hydrodynamic analysis. Figure 4.2, Panel A shows that following fractionation by sucrose gradient centrifugation, Mto2 peaked in fraction 8.5 [obtained by visual estimation]. Using the calibration curve generated from molecular weight markers of known S-value [Appendix II], the sedimentation co-efficient for Mto2 was calculated as 7.6 S. The Mto2 signal from extract fractionated by gel filtration peaked in fraction 8 [fig 4.2, Panel B and C]. When

compared to a calibration curve [Appendix III], this corresponded to a Stokes radius of 7.5 nm.

4.2.4 Endogenous Mto2 is the same size as recombinant Mto2

Using the values calculated in section 4.2.3, the molecular weight of endogenous Mto2 was calculated as described below:

Native Mto2:

$M = 6\pi\eta N \bullet a \bullet s / [1-\nu\rho]$

$M = 3909 \bullet a \bullet s$

$M = 3909 \bullet 7.5\ nm \bullet 7.6\ S$

$M = 222.8\ kDa$

The theoretical molecular weight of Mto2 is 44 kDa, this would correspond to 5.06 molecules of Mto2 per oligomer. Assuming that no other proteins co-precipitate with Mto2, this figure is consistent with the size of complex calculated for purified recombinant Mto2 [section 4.2.2].

Both *in vitro* and *in vivo* analyses have demonstrated that Mto2 oligomerises to form a complex that contains 4-6 molecules of Mto2. This supports the prediction that multimerisation of Mto2 may promote the association of the Mto1/2 heterotetramers.

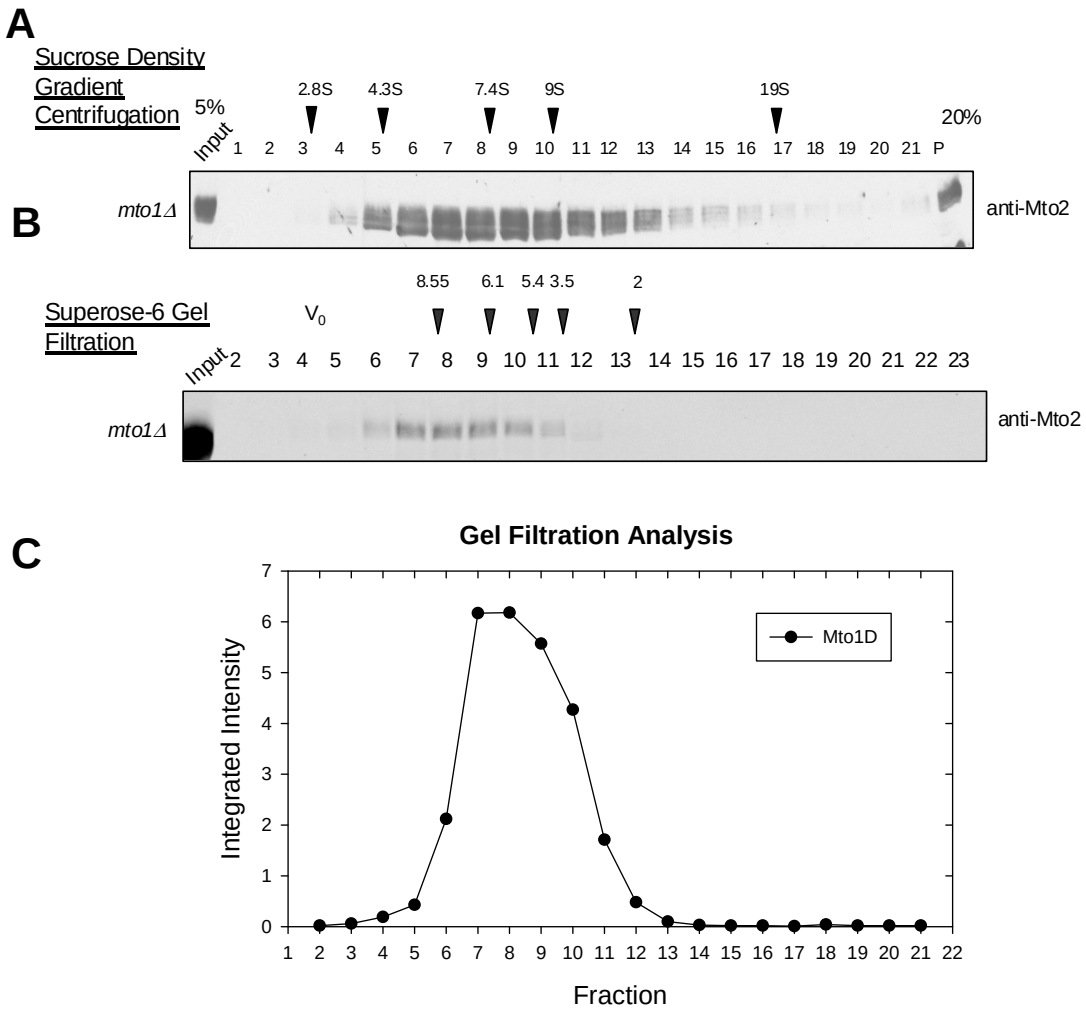

Figure 4.2 Hydrodynamic analyses of endogenous Mto2 demonstrates that it is tetrameric. [A] An extract from KS1017 was subject to sucrose density gradient centrifugation at 55,000 rpm for 3.5 hr in a Beckman TLS-55 rotor. Fractions including the pellet [P] were analysed by 10% SDS-PAGE and the western blot was probed with anti-Mto2 antibody. The signal from GT-34-HRP secondary antibody was detected by ECL. Image represents a typical result obtained from two experiments. [B] Extract was fractionated by gel filtration using a Superose-6 column [KS1]. Fractions were analysed by 10% SDS-PAGE and the western blot was probed with anti-Mto2 antibody. [C] The integrated intensity from the IRDye800 signal was detected using Odyssey V3.0. Image represents result obtained from a single experiment. The peak locations for molecular weight standards run on parallel fractionations are indicated [black arrows]. Standards in [C] indicated in nm. V_0 = void volume. Mto1D = *mto1Δ*.

4.2.5 Mto2 forms a dimer in mitosis

In addition to investigating the contribution of Mto2 to the nucleation activity of the Mto1/2 complex, how this activity is regulated is also of key interest. Disruption of the Mto1/2 interaction is the most likely mechanism of Mto1/2 complex regulation; however, the oligomerisation state of Mto2 may also be regulated. Given that non-SPB MTs are not present in mitosis, it is likely that the activity of the Mto1/2 complex is down-regulated at this point during the cell cycle. To investigate whether the stoichiometry of Mto2 is altered in mitosis, an extract from an asynchronous culture was compared with an extract from cells arrested in metaphase using the *nda3-M311* cold sensitive tubulin allele (Hiraoka *et al.* 1984). Both sucrose gradient centrifugation and gel filtration chromatography demonstrated that the mitotic Mto2 oligomer is smaller than Mto2 from an asynchronous extract. Sucrose gradient analysis showed that the reduction in complex size was independent of Mto1 [fig 4.3, Panel A and C]. Mitotic Mto2 peaked in fraction 5.2, which corresponded to a sedimentation co-efficient of 4.3 S [Appendix II]. By gel filtration, Mto2 peaked in fraction 9, which corresponded to a Stokes' radius of 6.4 nm [Appendix III] [fig 4.3, Panel B and D]. This was compared to Mto2 from asynchronous extract that had an S-value of 7.6 and a Stokes' radius of 7.5 nm.

Using these values the molecular weight of mitotic Mto2 was calculated as described below:

Mitotic native Mto2:

$M = 6\pi\eta N \bullet a \bullet s / [1-\nu\rho]$

$M = 3909 \bullet a \bullet s$

$M = 3909 \bullet 6.4\ nm \bullet 4.3\ S$

$M = 107.5\ kDa$

The theoretical molecular weight of Mto2 is 44 kDa, this would correspond to 2.44 molecules of Mto2 per oligomer. This is exactly half of the value obtained for Mto2 from asynchronous cultures, indicating that mitotic Mto2 is likely to be dimeric.

This result confirms the prediction that the oligomerisation state of Mto2 is altered during mitosis. The properties of mitotic Mto2 will be investigated further in chapter five.

4.2.6 HFG-Mto2 is dimeric

In addition to endogenous protein, the oligomerisation state of tagged Mto2 was also analysed. An extract from HFG-Mto2 was subject to sucrose density gradient centrifugation [fig 4.4, Panel A]. The signal from the anti-Mto2 antibody peaked in fraction 7.75 [as determined by visual estimation], which, when compared to a calibration curve [Appendix II] corresponded to a sedimentation coefficient of 6.8 S. Extract containing HFG-Mto2 and extract from a strain that contained Mto2-GFP were analysed by gel filtration [fig 4.4, Panel B]. Signals from HFG-Mto2 and Mto2-GFP peaked in fraction 10 [determind by visual estimation], which corresponded to a Stokes' Radius of 5.4 nm [Appendix III].

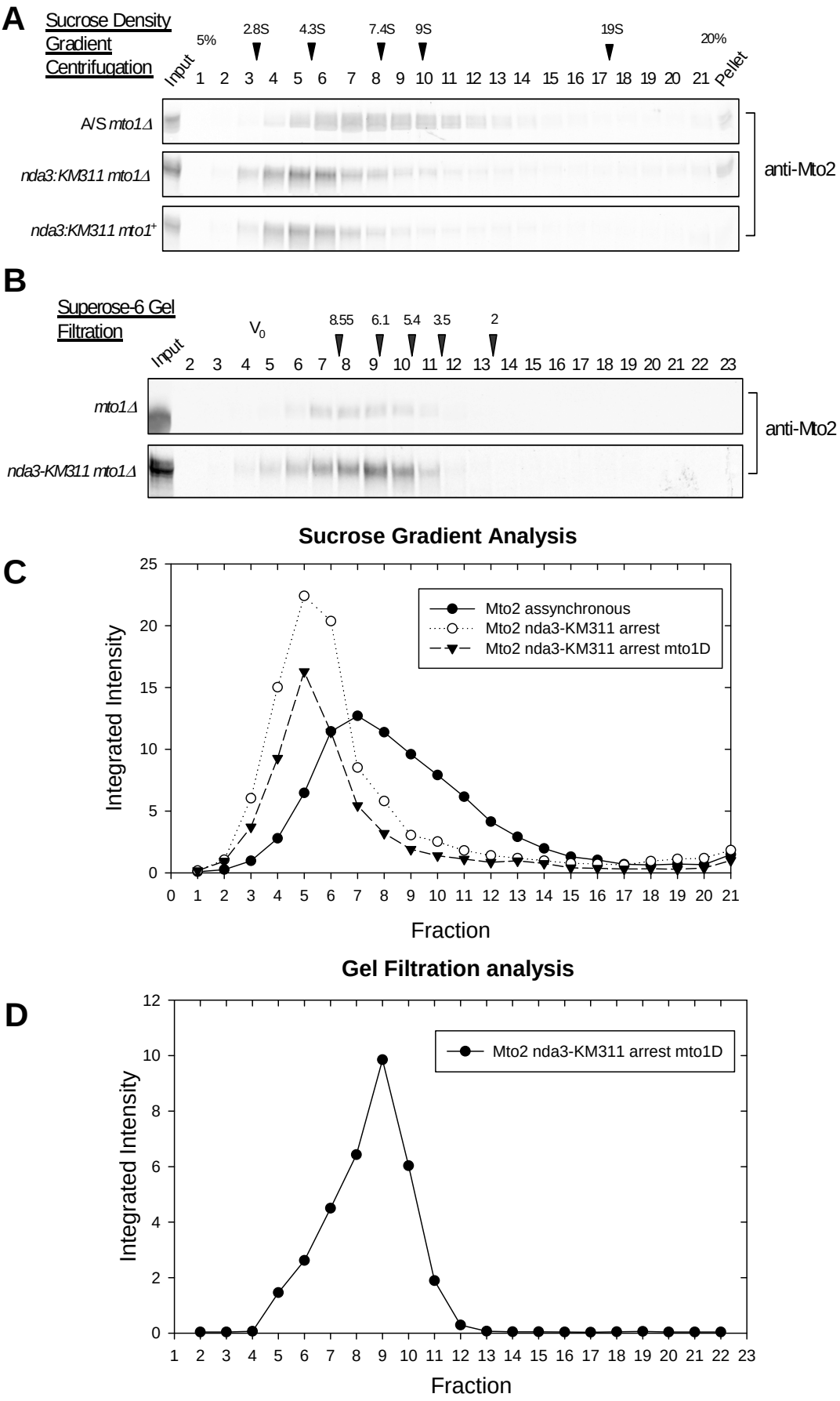
A
Sucrose Density Gradient Centrifugation
5%
2.8S
4.3S
7.4S
9S
19S
20%
Input
1 2 3 4 5 6 7 8 9 10 11 12 13 14 15 16 17 18 19 20 21
Pellet
A/S mto1Δ
nda3:KM311 mto1Δ
nda3:KM311 mto1+
anti-Mto2
B
Superose-6 Gel Filtration
V0
8.55
6.1
5.4
3.5
2
Input
2 3 4 5 6 7 8 9 10 11 12 13 14 15 16 17 18 19 20 21 22 23
mto1Δ
nda3-KM311 mto1Δ
anti-Mto2
Sucrose Gradient Analysis
C
Integrated Intensity
Fraction
Mto2 assynchronous
Mto2 nda3-KM311 arrest
Mto2 nda3-KM311 arrest mto1D
Gel Filtration analysis
D
Integrated Intensity
Fraction
Mto2 nda3-KM311 arrest mto1D

Figure 4.3 Comparative hydrodynamic analysis of asynchronous and mitotic Mto2 demonstrates that Mto2 is dimeric during mitosis. [A] The extracts were subject to sucrose density gradient centrifugation at 55,000 rpm for 3.5 hr in a Beckman TLS-55, or [B] fractionated by gel filtration using a Superose-6 column [KS1]. [Strains KS1017, KS1238, and KS1239]. The fractions including the pellet [P] were analysed by 10% SDS-PAGE the western blot was probed with anti-Mto2 antibody. [C and D] Integrated intensity of the IRDye800 signal was measured using Odyssey V3.0. The peak locations for molecular weight standards run on parallel fractionations are indicated [black arrows]. Standards in [B] indicated in nm. V_0 = void volume. Mto1D = *mto1Δ*. Image represents result obtained from a single experiment.

The molecular weight of HFG-Mto2 was calculated as described below:

HFG-Mto2:

$M = 6\pi\eta N \bullet a \bullet s / [1-\nu\rho]$

$M = 3909 \bullet a \bullet s$

$M = 3909 \bullet 5.4\ nm \bullet 6.8\ S$

$M = 138.22\ kDa$

The theoretical molecular weight of HFG-Mto2 is 74 kDa, this corresponds to 1.94 molecules of HFG-Mto2 per oligomer. Therefore, in the absence of Mto1, HFG-Mto2 exists as a dimer. This is a significantly smaller complex than the 4-6 molecule complex formed by untagged protein both *in vivo* and *in vitro*. This data suggests that the 34 kDa GFP protein tag appears to have disrupted the tetrameric Mto2 protein complex. The similar behaviour of the C-terminally tagged protein indicates that the position of the tag does not affect the oligomeric state of Mto2. This is interesting, as previous analyses have not detected altered MT dynamics in the presence of Mto2-GFP (Samejima *et al.* 2005; Venkatram *et al.* 2005), and suggests that Mto2 tetramerisation is not required for Mto2 activity. Previous research has shown that Mto1-YFP foci in the presence and absence of Mto2-CFP are not significantly different in localisation or intensity (Samejima *et al.* 2005). This indicates that higher-order multimerisation of Mto2 dimers do not contribute to Mto1 multimerisation. Rather, tetrameric Mto2 may be the preferred oligomerisation state of un-complexed Mto2, particularly if the Mto1 interaction domain is highly hydrophobic and consequently favours a more energetically sheltered conformation.

This would suggest that tetrameric Mto2 is a storage form of protein, and may not be relevant to the stoichiometry of the Mto1/2 nucleation complex.

This hypothesis would indicate that Mto2 dimer-dimer interface overlaps with the Mto1-Mto2 interaction interface such that binding of Mto1 to Mto2 would disrupt the Mto2 tetramer. Subsequently, failure to tetramerise may result in an increase number of Mto2 dimers that more readily associate with Mto1. To test whether the prevalence of Mto2 dimers affects Mto1 activity it is necessary to compare the MT nucleation dynamics in HFG-Mto2 and *mto2*$^{+}$ background.

4.2.7 MT nucleation efficiency and the Mto1 / γ-TuC interaction is wild-type in HFG-Mto2 background

Biochemical analysis has demonstrated that HFG-Mto2 forms a dimer and native untagged protein forms a tetramer. To confirm that the constraint on the oligomeric state of Mto2 does not have adverse affects on Mto1/2 complex activity, the MT nucleation pattern of HFG-Mto2 was examined in strains that contained GFP-Atb2. Figure 4.5 and movies 3A and 3B show that in both wild-type Mto2 and HFG-Mto2, the MT arrays appeared identical. They both had 3 - 4 bundles per cell, which grew and depolymerised as expected. This indicates that the nucleation capacity of HFG-Mto2 is not affected by the disruption of the Mto2 tetramer, and confirms that tetramerisation of Mto2 is not required for Mto2 function. The presence of excess HFG-Mto2 dimers does not appear to alter MT dynamics at a detectable level.

This analysis also indicates that the nature of the Mto2 dimers formed in mitosis is different to the Mto2 dimers formed in the presence of the HFG-tag, the former being unable to support MT nucleation and the latter able to promote MT nucleation at wild-type levels. This suggests that the Mto2-Mto2 tetramerisation is not a direct target of cell cycle-dependent regulation per se and instead may be a consequence of the disruption of the Mto1-Mto2 interaction.

The biochemistry of the nucleation complex formed in the presence of dimeric Mto2 was also analysed [fig 4.5, Panel B]. Integrated intensities for each protein were normalised relative to Mto1 levels in the eluate [data not shown]. Figure 4.5, Panels C-E show that when compared to *mto2*$^{+}$, the interaction between Mto1 and both Alp4 and Gtb1 in *mto2Δ* has been reduced 4-fold. In the presence of HFG-Mto2, the interaction of Alp4 and Gtb1 with Mto1 does not appear to have been significantly compromised, however the levels of HFG-Mto2 pulled down by Mto1-TAPS have been reduced by 50% compared to untagged protein.

As the levels of HFG-Mto2 pulled down by Mto1-TAPS did not increase compared to wild-type Mto2, this indicates that the presence of Mto2 in dimeric form [compared to tetrameric protein] does not increase its propensity to interact with Mto1. This suggests that the majority of Mto2 is in complex with Mto1, which correlates with their co-localisation when analysed by fluorescence microscopy (Samejima *et al.* 2005)

The reduction of Mto2 levels in the pulldown may occur due to several reasons. For example, loss of Mto2 molecules may reflect a destabilisation of the Mto1-Mto2 interaction as a result of steric restrictions imposed by the GFP tag.

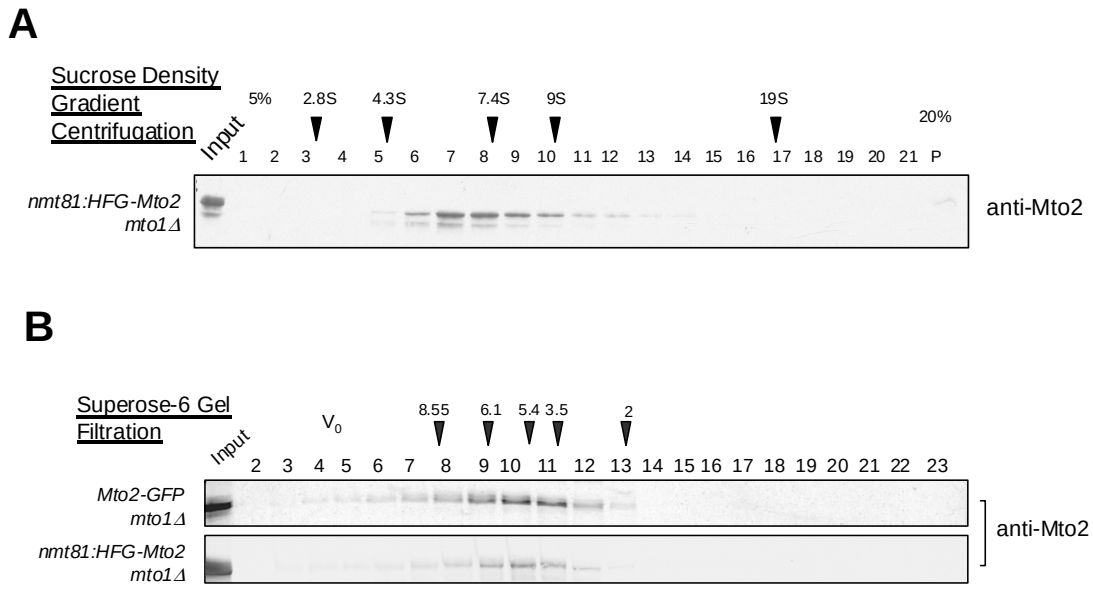

Figure 4.4 Hydrodynamic analysis of tagged Mto2 demonstrates that it is dimeric. [A] Extract from KS4450 was subject to sucrose density gradient centrifugation at 55,000 rpm for 3.5 hr in a Beckman TLS-55. The fractions including the pellet [P] were analysed by 10% SDS-PAGE the western blot was probed with anti-Mto2 antibody. Signal from GT-34-HRP was detected with ECL. Image represents typical results from two experiments. [B] The extracts were fractionated by gel filtration using a Superose-6 column [KS1] [Strains KS4450 and KS1457]. The fractions were analysed by 10% SDS-PAGE the western blot was probed with anti-Mto2 antibody. Integrated intensity of the IRDye800 signal was measured using Odyssey V3.0. Image represents result from single experiment. The peak locations for molecular weight standards run on parallel fractionations are indicated [black arrows]. Standards in [B] indicated in nm. V_0 = void volume.

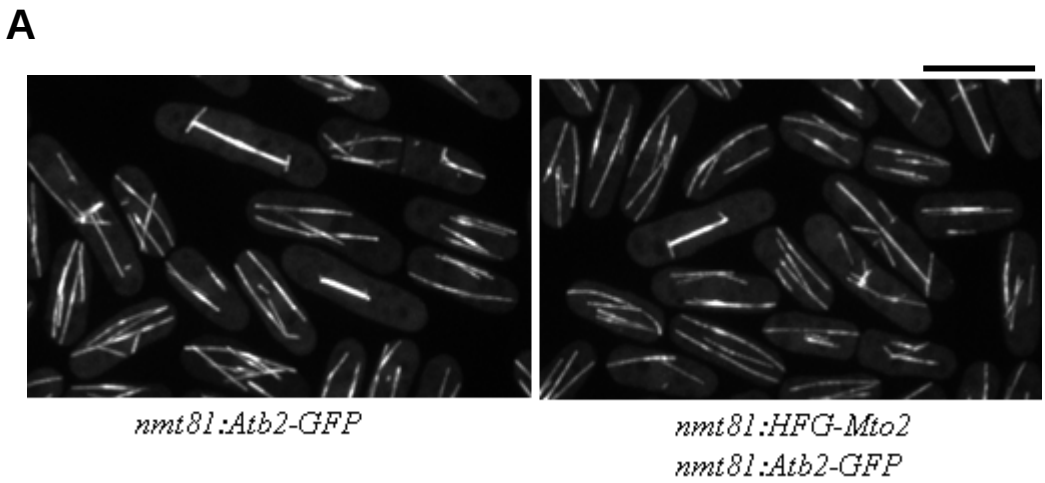
A
nmt81:Atb2-GFP
nmt81:HFG-Mto2
nmt81:Atb2-GFP
B
Input
IgG pulldown
Mto1-TAPS
Mto2
GFP
anti-Mto1
anti-Alp4
anti-Gtb1
nmt81:HFG-Mto2
mto2+
anti-Mto2
C
Mto2
Integrated Intensity
no-tag
Mto2
Mto2D
HFG-Mto2
D
Alp4
E
Gamma tubulin

Figure 4.5 Dimeric HFG-Mto2 does not affect MT nucleation efficiency or the Mto1 / γ-TuC interaction. [A] Images acquired using the spinning disk confocal microscope. Maximum projections of Atb2-GFP labelled MTs in the presence and absence of HFG-Mto2 [Movie 3B and 3C]. Scale bar = 10µm [B] Extracts were incubated with IgG-Dynabeads and the eluates were analysed by 10% SDS-PAGE [Strains KS516, KS3524, KS4323, KS4973, and KS4976]. The western blot was probed with anti-Mto1, anti-Mto2, anti-Alp4 and anti-γ-tubulin [GTU-88] antibodies. [C to E] Integrated intensities of signal from IRDye800 were measured using Odyssey V3.0. Mto2D = *mto2Δ*. Images represent result from single experiment.

Alternatively, the loss may occur through disruption of the Mto2 dimer by the HFG-tag [previous analysis has indicated that the full length Mto1/2 complex it is likely to contain two molecules of Mto2]. If dimeric Mto2 was disrupted by the HFG-tag, the Mto1/2 complex formed in the presence of HFG-Mto2 must contain two molecules of Mto1 and one molecule of HFG-Mto2. This supports the model that Mto2-induced multimerisation of Mto1 occurs as a result of a conformational change and not Mto2 multimerisation. The best way to address this question is to analyse the hydrodynamic properties of the Mto1 [1-800] / HFG-Mto2 complex to determine the number of molecules of HFG-Mto2.

Despite the reduction in Mto2 levels, the Mto1 / γ-TuC interaction remains unaffected. This correlates with the microscopy data which shows that there are no detectable changes in nucleation dynamics in the presence of dimeric HFG-Mto2.

4.2.8 Mapping of the Mto2-Mto2 interaction domain

4.2.8.1 Regions at the N- and C-terminus are required for the Mto2-Mto2 interaction *in vitro*

This work was performed with the assistance of Struan Murray [summer project student, University of Oxford].

The research described above suggests that formation of the Mto1/2 complex is unlikely to occur as a result of higher-order multimerisation of Mto2. Alternatively, it is possible that Mto2 binding may induce changes in Mto1 structure that promote Mto1 self-association. It is unknown whether binding of Mto2 in dimeric form is

required or whether individual recruitment of Mto2 would be sufficient [although energetically less efficient, given that Mto1 is dimeric] to induce a change in conformation of Mto1. To assess the contribution of the dimeric Mto2-Mto2 interaction to the function of the Mto1/2 complex, a monomeric version of Mto2 is required. Identification and mutagenesis of the interaction domains is complicated by the fact that there are two Mto2-Mto2 interaction domains, the dimer association interface and the dimerisation interface. It is unclear whether Mto2 tetramerisation occurs as a successive association of specific dimers, however, I predict that the Mto2 dimers that interact with Mto1 are preferentially formed, which then associate into tetramers upon release from Mto1. Mutagenesis of the correct Mto2-Mto2 interaction domain [or both] is essential to generate monomeric Mto2.

To identify regions that may be involved in the Mto2-Mto2 interaction, an interaction mapping was performed. The Mto2 protein sequence was divided into five sections, each section encoding peptides approximately 90 aa in length. Protein truncations were made by successive removal of sections from the N- and C- termini [fig 4.6, Panel A]. Mto2 truncations were designed around regions of predicted secondary structure in order to minimise the disruption of structural domains which may be important for protein folding and stability.

Five of the six truncations were used in subsequent experiments as N3 [283 – 397 aa] was found to be expressed at a low level [data not shown]. Mto2 truncations were tagged with MBP and used as bait in a pulldown assay with full length Mto2 tagged with NusA. Figure 4.6, Panel B shows a Coomassie stained SDS-PAGE gel of the MBP-pulldown assay. As previously demonstrated in section 3.2.11, NusA-Mto2 is pulled down by full length MBP-Mto2. Analysis of MBP-Mto2 truncations

shows that only MBP-Mto2 N1 [89-397 aa] retained the ability to pull down NusA-Mto2. Further truncation from the N-terminus and all C-terminal truncations lead to failure to interact with NusA-Mto2 above the low level of non-specific binding observed in the negative control.

This analysis indicates that there are areas in both the N- and C-termini of Mto2 that contribute to the Mto2-Mto2 interaction. Assuming that MBP-Mto2 is tetrameric, this may correspond to the Mto2 dimer association and the Mto2 dimerisation interaction. The fact that removal of either of the interacting termini disrupts the interaction with full length Mto2 indicates that either form of dimeric protein is unstable under these conditions. Alternatively, it is possible that removal of large sections of protein has induced a disruption of protein folding that prevents the assembly of an Mto2 interaction surface. In this case, one can not make any conclusions regarding the function of each 90 aa domain.

It is possible that either Mto2-N2 or C1 truncations are monomeric when in complex with Mto1, therefore these truncations were expressed in fission yeast cells, in order to analyse their impact on MT nucleation.

4.2.8.2 Mto2 truncations have an *mto2Δ*-like phenotype

To assess the phenotype of the Mto2 truncations in yeast, N-terminal *nmt81:HFG*-tagged Mto2-N1/N2/C1 were constructed using Gateway recombination and the pDUAL vector system (Matsuyama *et al.* 2004). Sequences were integrated into *mto2Δ* and GFP-Atb2; *mto2Δ* backgrounds at the *leu1* locus [KS976 and KS1409]. Figure 4.7, Panel A shows that all of the HFG-Mto2 truncations were able

to localise to the SPB, eMTOC and to iMTOCs along pre-existing MTs, although compared to full length HFG-Mto2, the signal was quantitatively reduced from all MTOCs except the SPB. The MT arrays formed in the presence of truncated HFG-Mto2 had fewer MT bundles than wild-type, particularly in HFG-Mto2 N2 and HFG-Mto2 C1 backgrounds, which typically had only 1 MT bundle per cell. The phenotype was less severe in HFG-Mto2 N1 positive control, where 2 - 3 bundles were present. This indicates that these proteins are not able to efficiently promote MT nucleation.

The localisation of the Mto2 truncations suggests that they have some capacity to interact with Mto1, as Mto2 does not localise to MTOCs in *mto1Δ* (Samejima *et al.* 2005). However, as a high level of cytoplasmic signal is observed for all truncations, including the HFG-Mto2 N1 positive control, this suggests that the majority of truncated Mto2 is unable to interact with Mto1.

Alternatively, it is possible that these proteins are subject to a high level of protein degradation. To assess the stability of the HFG-Mto2 truncations the expression level was quantified by western blot.

4.2.8.3 Mto2 truncation phenotype is due to reduced protein stability

Protein expression levels of HFG-Mto2 truncations were examined by western blot of total protein extract. Figure 4.7, Panel B and C show that the *nmt81* driven protein expression was relatively consistent between truncation strains, indicating that observed differences in the phenotype of each truncation were not due to differences in Mto2 abundance. However, there was a six-fold reduction in protein

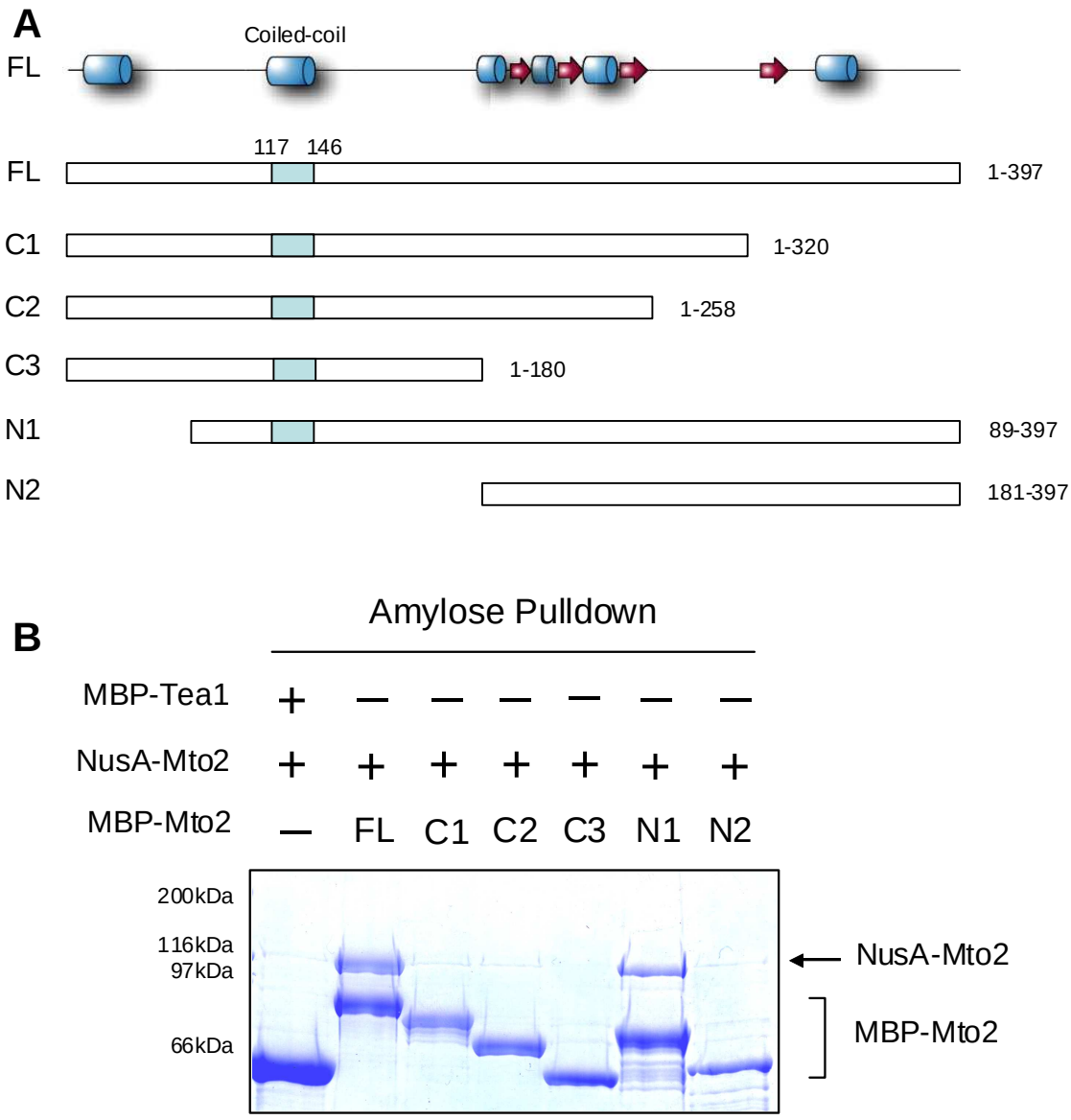

Figure 4.6 Mapping of the Mto2-Mto2 interaction demonstrates that two regions of Mto2 are involved in the Mto2-Mto2 interaction. [A] Schematic representation of Mto2 truncations. α-helices [blue cylinders] and β-sheets [red arrows]. The secondary structure of Mto2 was predicted using Jpred3. Amino acid residue numbers are indicated. Coiled-coil at 117 - 146 aa. [B] Bacterial extracts containing MBP-Mto2 truncations and NusA-Mto2 were incubated with amylose beads. MBP-Tea1 was used as a negative control. Eluates were analysed by 10% SDS-PAGE and the gel was stained with Coomassie. Images represent typical results from three experiments.

A

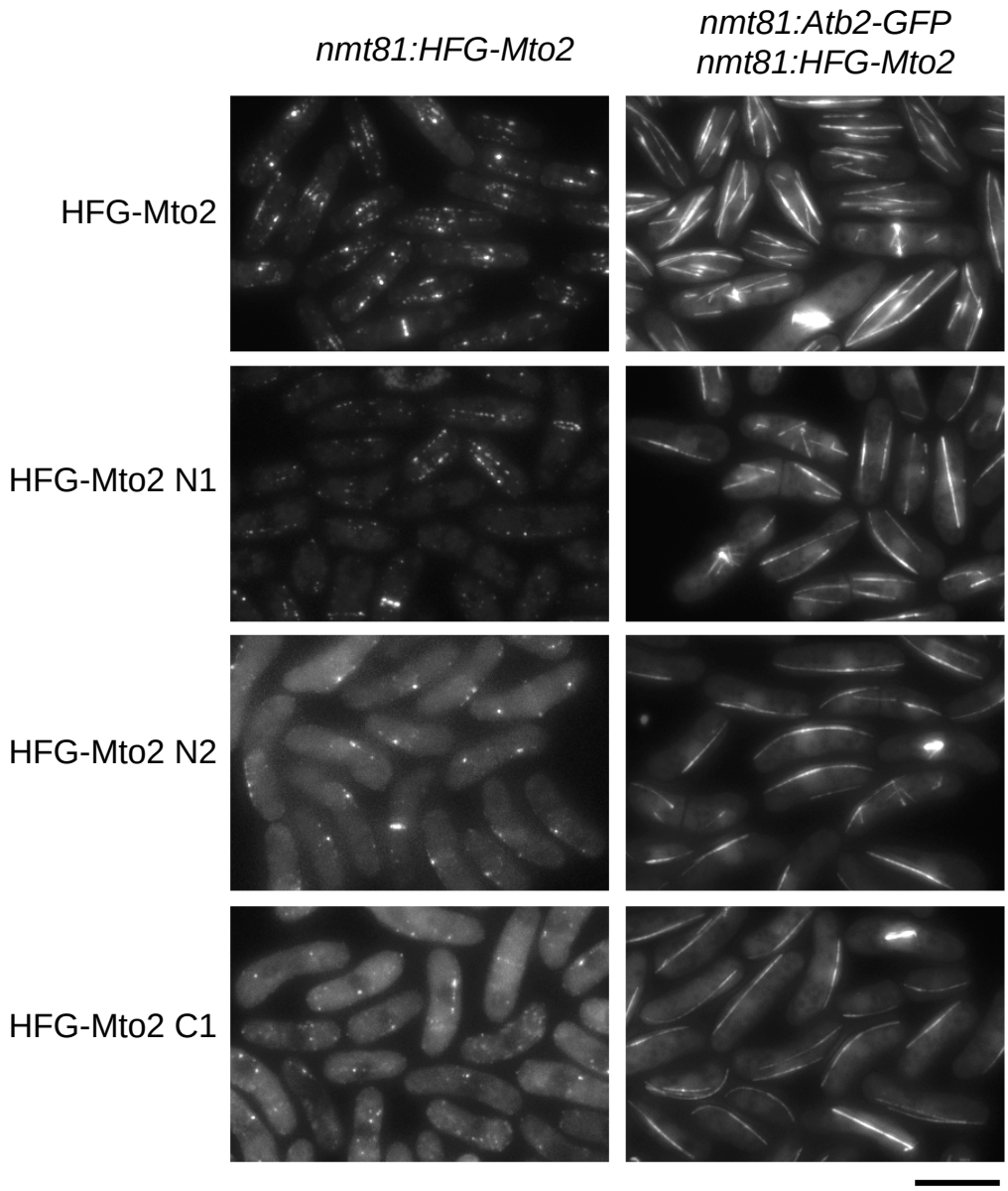
nmt81:HFG-Mto2
nmt81:Atb2-GFP
nmt81:HFG-Mto2
HFG-Mto2
HFG-Mto2 N1
HFG-Mto2 N2
HFG-Mto2 C1

B

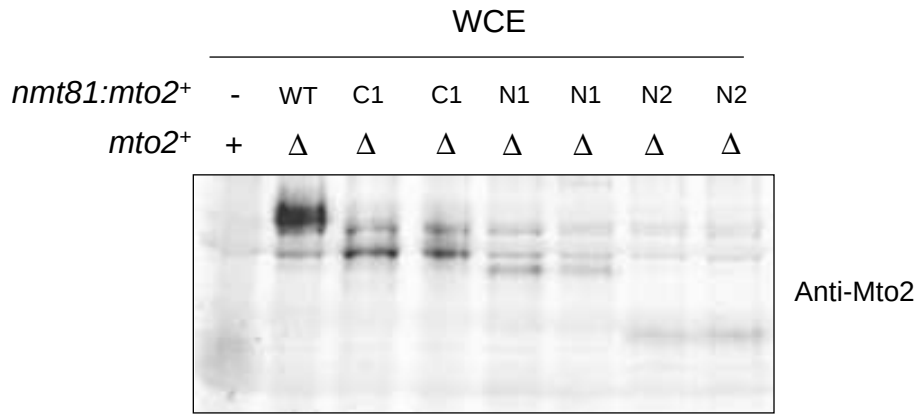
WCE
nmt81:mto2+ - WT C1 C1 N1 N1 N2 N2
mto2+ + Δ Δ Δ Δ Δ Δ Δ
Anti-Mto2

C

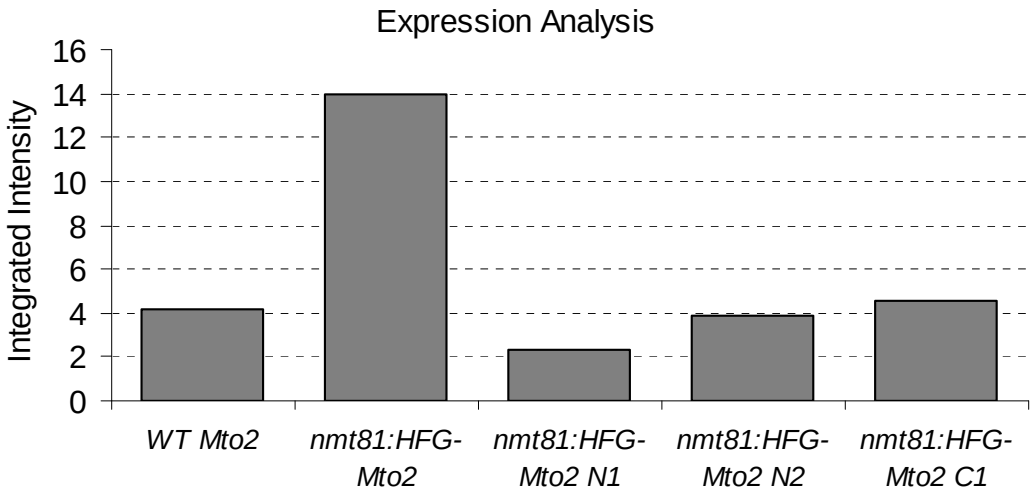

Figure 4.7 *Mto2Δ*-like phenotypes of HFG-Mto2 truncations N1, N2 and C1 were due to low protein stability levels. [Strains KS4603, KS4606, KS4609, KS4612, KS4615 and KS4618]. [A] Maximum projection wide-field images of HFG-Mto2 truncations and in the presence and absence of Atb2-GFP. Scale bar = 10µm. [B] Total extracts were analysed by 10% SDS-PAGE and the western blot was probed with anti-Mto2 antibody. Two isolates from each truncation were analysed to confirm protein stability. Left isolate was used for imaging. [C] Integrated intensity from the IRDye800 signals were measured using Odyssey V3.0. Integrated intensity for C1, N1 and N2 are the mean value of the expression from two isolates. Images represent results from single experiment. WCE = whole cell extract.

levels compared with *nmt81:HFG-Mto2*. The degradation products observed on the western blot indicates that the majority of protein loss is due to a reduction in protein stability [data not shown]. Unfortunately, the reduction of Mto2 protein levels is likely to explain the loss of nucleation efficiency in the Mto2 truncations therefore conclusive statements regarding the relationship between the Mto2-Mto2 interaction and the function of Mto2 cannot be made from this analysis.

4.2.9 Identification of the Mto2 coiled-coil domain [130 – 147aa]

The interaction mapping described in section 4.2.8 indicates that there is a region between 89-180 amino acids that is involved in the Mto2-Mto2 interaction. PAIRCOIL2 was used to identify a putative N-terminal coiled-coil domain within this region [114-147aa]. PAIRCOIL2 prediction scores for Mto2 [104 – 152aa] are listed in Appendix VI. Figure 4.8, Panel A shows the Mto2 sequence with the predicted coiled-coil highlighted in red. A helical wheel projection was generated from a section of the coiled-coil sequence [130 – 147aa]. The projection contained a non-polar face that followed a slight left handed pitch common to all coiled-coils [fig 4.8, Panel B]. The heptad repeats [*abcdefg*] within this sequence contain non-polar residues at positions *a* and *d* that are predicted to play key roles in the hydrophobic interaction interface [fig. 4.8, Panel C].

A

```
1    MSEHNYQSDR EVAEDPFLNY EASANQLSSN SRESTPRGSP WRAGMRSASL MTEPLEDSMY

61   SDNNYLDNGV SFTKDENPLY SPSWPSLADA NVNSMKSNNA IQEHKAAKFV SEKSLEKVST

121  ADNNLVLQEL ENLRERLNQV ELQLSERPSS YLGYHNNLSP YRSPNSYPSL LPSTHSPHSP

181  APLSTMQTAL MRLRTYHPSP IILKPVEQAV NHAITLVNTS PSSVVDALCR SLAELCLGLV

241  QEAIDASILS QQESSNSLDL VRHTPPLNYT SSVDSSPQRM ASDSYGRPSL HLNDPFPSVD

301  LQSNELSHHN VRTTLFSDDS RFHSKIHTHS TPPSQMYSAA SHFRYRSDPS TRHVSNSTNK
```

B

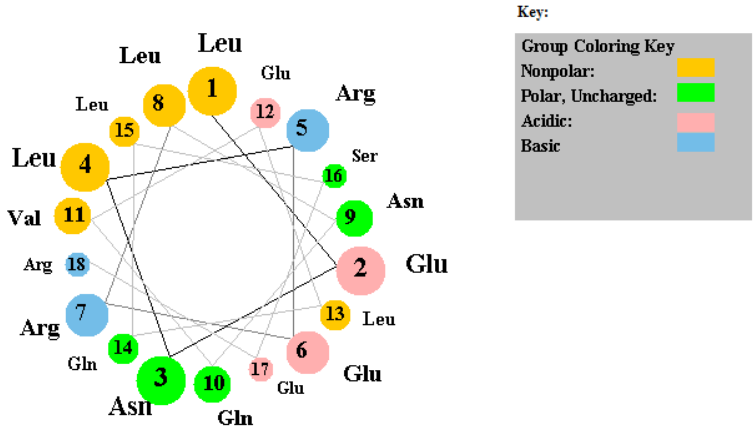

C

SLEKVSTADNNLVLGE**LENLRERLNQVELQ**LSER

a b c d e f g a b c d e f g

Figure 4.8 PAIRCOIL2 coiled-coil prediction of Mto2 protein sequence. [A] Mto2 sequence with high-scoring 34-residue domain highlighted in red. [B] Helical wheel projection of amino acids 130-147, where the hydrophobic patch is highlighted in yellow. [C] 34 aa coiled-coil domain identified by PAIRCOIL2 where amino acids used for helical wheel projection are underlined with the corresponding *abcdefg* heptad repeat.

4.2.9.1 Introduction of the L133DL137D coiled-coil mutations disrupts the Mto2-Mto2 interaction *in vitro*

Preliminary interaction mapping indicated that a region of Mto2 around the predicted coiled-coil [114 – 147 aa] may contribute to the Mto2-Mto2 interaction. To test this more rigorously a mutant was constructed that contained polar substitutions within the coiled-coil domain, that have previously been shown to disrupt coiled-coil interactions (Williams *et al.* 2008). I predicted that the introduction of polar residues into the hydrophobic interface would have a disruptive effect on the hydrophobic coiled-coil interaction. Helical wheel projections of a section of the predicted coiled-coil sequence [130 – 147 aa], indicated that there were two structurally significant hydrophobic leucine residues at positions 133 and 137, which correspond to positions *a* and *d* of the heptad repeat [fig 4.9, Panel A]. A mutant that contained negatively charged aspartic acid substitutions at these sites [Mto2-L133DL137D] was created by site-directed mutagenesis. The resultant gene was recombined into an N-terminal MBP-tagging vector (Busso *et al.* 2005), and the Mto2-Mto2 interaction was tested by amylose pulldown with full length NusA-Mto2. Figure 4.9, Panel B shows that compared to pulldown with MBP-Mto2, co-precipitation of NusA-Mto2 with MBP-Mto2-L133DL1337D did not occur above levels seen in the MBP-Tea1 negative control, indicating that the interaction between NusA-Mto2 and MBP-Mto2-L133DL137D has been disrupted. This result confirms the hypothesis that the coiled-coil domain is involved in the Mto2-Mto2 interaction and is consistent with the results of the *in vivo* mapping. However, due to the proposed instability of Mto2 dimers *in vitro* [section 4.2.8.1], this result does not distinguish between the

involvement of the coiled-coil in the Mto2 dimer association interaction or the Mto2 dimerisation interaction.

4.2.9.2 Introduction of the L133DL137D coiled-coil mutations did not disrupt the Mto2-Mto2 interaction *in vivo*

The result of the *in vitro* MBP pulldown assay in section 4.2.9.1 indicates that disruption of the hydrophobic face of the coiled-coil disrupts the Mto2 self-interaction. To verify these results *in vivo*, the interaction of Mto2-13myc with the HFG-Mto2-L133DL137D was tested using anti-GFP immunoprecipitation. Mto2-L133DL137D was N-terminally tagged with HFG by recombination into a *nmt81:HFG* tagging vector (Matsuyama *et al.* 2004). The sequence was then integrated into an *mto2Δ* strain at the *leu1* locus and was crossed with Mto2-13myc [KS1504]. All immunoprecipitations were performed in the absence of Mto1. Figure 4.10 shows that co-precipitation of Mto2-13myc was not evident in strains that did not contain HFG-Mto2. However Mto2-13myc was observed in the eluate of both wild-type HFG-Mto2 and the HFG-Mto2-L133DL137D mutant at a comparable level, which indicates that HFG-Mto2-L133DL137D is still able to interact with wild-type Mto2.

The *in vitro* interaction assay suggests that either the Mto2 dimer association or Mto2 dimerisation interaction has been disrupted by the Mto2-L133DL137D coiled-coil mutation. The presence of the HFG-tag has previously been shown to disrupt tetramerisation in section 4.2.6, therefore as HFG-Mto2-L133DL137D can still self-interact, this indicates that the same interaction is disrupted by both the

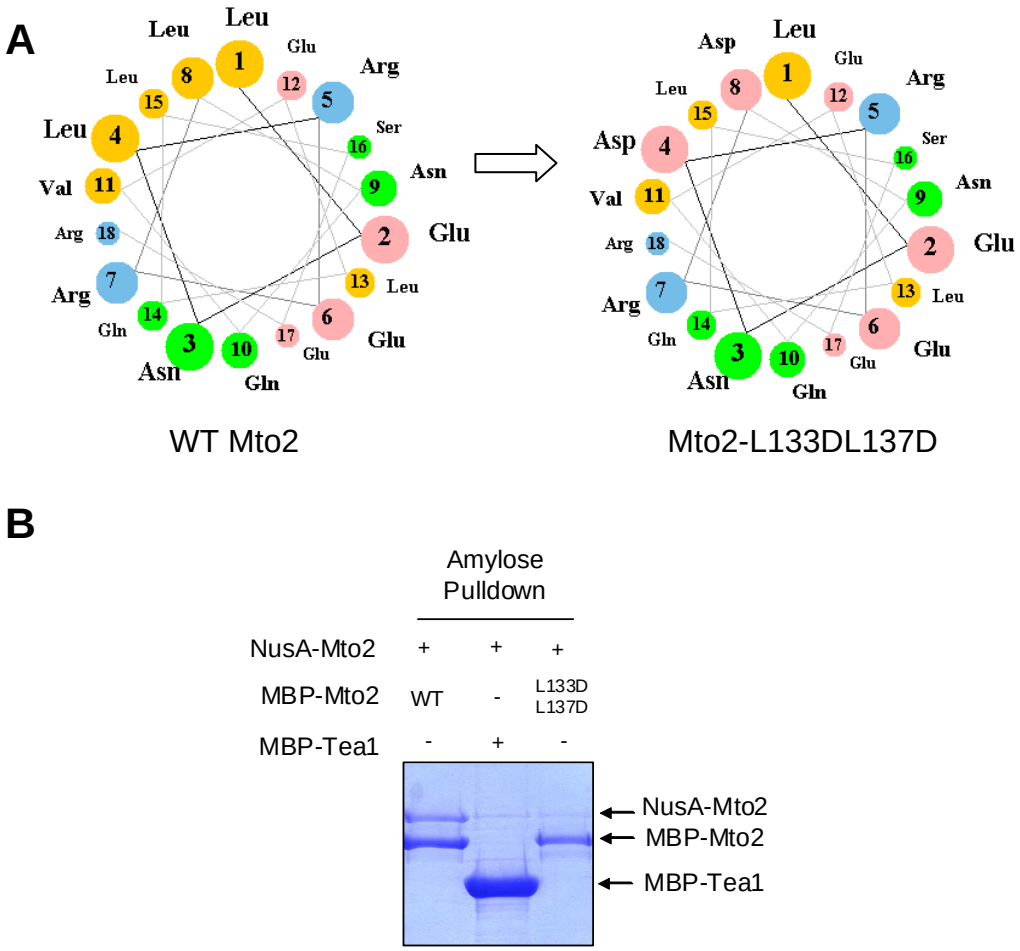

Figure 4.9 The Mto2-Mto2 interaction is disrupted by Mto2 L133DL137D *in vitro*. [A] Helical wheel projections of residues 130 - 147 in WT Mto2 and Mto2-L133DL137D showing the impact of the introduction of the polar residues into the hydrophobic face of the predicted coiled-coil. [B] Bacterial extract containing NusA-Mto2 and either MBP-Mto2 or MBP-Mto2-L133DL137D were incubated with amylose beads. MBP-Tea1 was used as a negative control. Eluates were analysed by 10% SDS-PAGE and the gel was stained with Coomassie. Image represents typical result from three experiments.

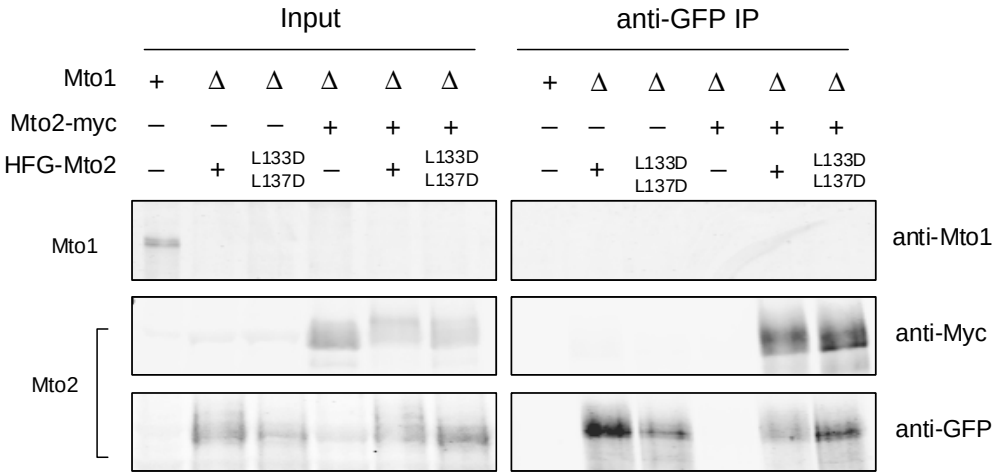

Figure 4.10 The Mto2-Mto2 interaction was not disrupted by HFG-Mto2 L133DL137D *in vivo*. Extracts were incubated with anti-GFP linked Protein G-Dynabeads [Strains KS516, KS4450, KS5572, KS5573, KS5574 and KS5575]. Eluates were analysed by 10% SDS-PAGE and the western blot was probed with anti-Mto1, anti-Myc [9E10] and anti-GFP. Signal from IRDye800 was detected by Odyssey V3.0. Image represents typical result from three experiments.

coiled-coil mutation and the HFG-tag. Based on this idea, one would predict that both HFG-Mto2-L133DL137D and Mto2-L133DL137D would be dimeric through disruption of the dimer association interaction domain.

4.2.9.3 Mto2-L133DL137D coiled-coil mutant is dimeric

To definitively examine the effect of the coiled-coil mutation on Mto2 stoichiometry, Mto2-L133DL137D was subject to hydrodynamic analysis. An untagged version of Mto2-L133DL137D was constructed by recombining the sequence containing 2 X TAG stop codons into a C-terminal *nmt81:GFH* tagging vector (Matsuyama *et al.* 2004). This sequence was then integrated at the *leu1* locus into both *mto1*$^{+}$ and *mto1Δ* backgrounds. The *mto1Δ* strain was crossed with *nda3-KM311* [KS1238] so that protein from both asynchronous culture and culture arrested in metaphase could be analysed. Figure 4.11, Panel A shows that Mto2-L133DL137D from asynchronous extract peaked in fraction 5 in both *mto1*$^{+}$ and *mto1Δ* strains, which corresponded to an S-value of 4.3 S [Appendix II]. Mto2-L133DL137D from metaphase arrested cells, peaked in fraction 5.5, which corresponded to an S-value of 4.7 S. The S-values of both asynchronous and mitotic Mto2-L133DL137D correspond to a range similar to the dimeric complex formed by wild-type Mto2 during mitosis [Section 4.2.5]. HFG-Mto2-L133DL137D was also analysed. This analysis would reveal whether the same Mto2-Mto2 interaction that is affected by the coiled-coil mutation is also disrupted by the HFG tag. Figure 4.11, Panel B shows that when tagged with HFG both the coiled-coil mutant and wild-type proteins sediment with the same pattern, resulting in an S-value of 5.2 S. Analysis of

HFG-Mto2-L133DL137D by gel filtration chromatography [fig 4.11, Panel C] showed a small difference between HFG-Mto2 and HFG-Mto2-L133DL137D, where the mutant peaked in fraction 9 and wild-type protein peaked in fraction 10. When compared to the calibration curve [Appendix III] this corresponded to Stokes' radii of 5.2 nm and 6.4 nm for wild-type and mutant protein respectively.

These measurements were used to calculate the molecular weight for HFG-Mto2-L133DL137D as described below:

HFG-Mto2-L133DL137D:

$M = 6\pi\eta N \bullet a \bullet s / [1-\nu\rho]$

$M = 3909 \bullet a \bullet s$

$M = 3909 \bullet 6.4\ nm \bullet 5.2\ S$

$M = 130.1\ kDa$

The theoretical molecular weight of HFG-Mto2 is 74 kDa, this corresponds to 1.76 molecules of HFG-Mto2-L133DL137D per oligomer. This demonstrates that, like wild-type HFG-Mto2, HFG-Mto2-L133DL137D was unable to form a tetramer and confirms that the same dimer-dimer interface is disrupted by the HFG-tag and coiled-coil mutations. Additionally, as monomeric Mto2-L133DL137D is not present in cells arrested in metaphase, this suggests that the same Mto2 dimer-dimer interface is also disrupted during mitosis.

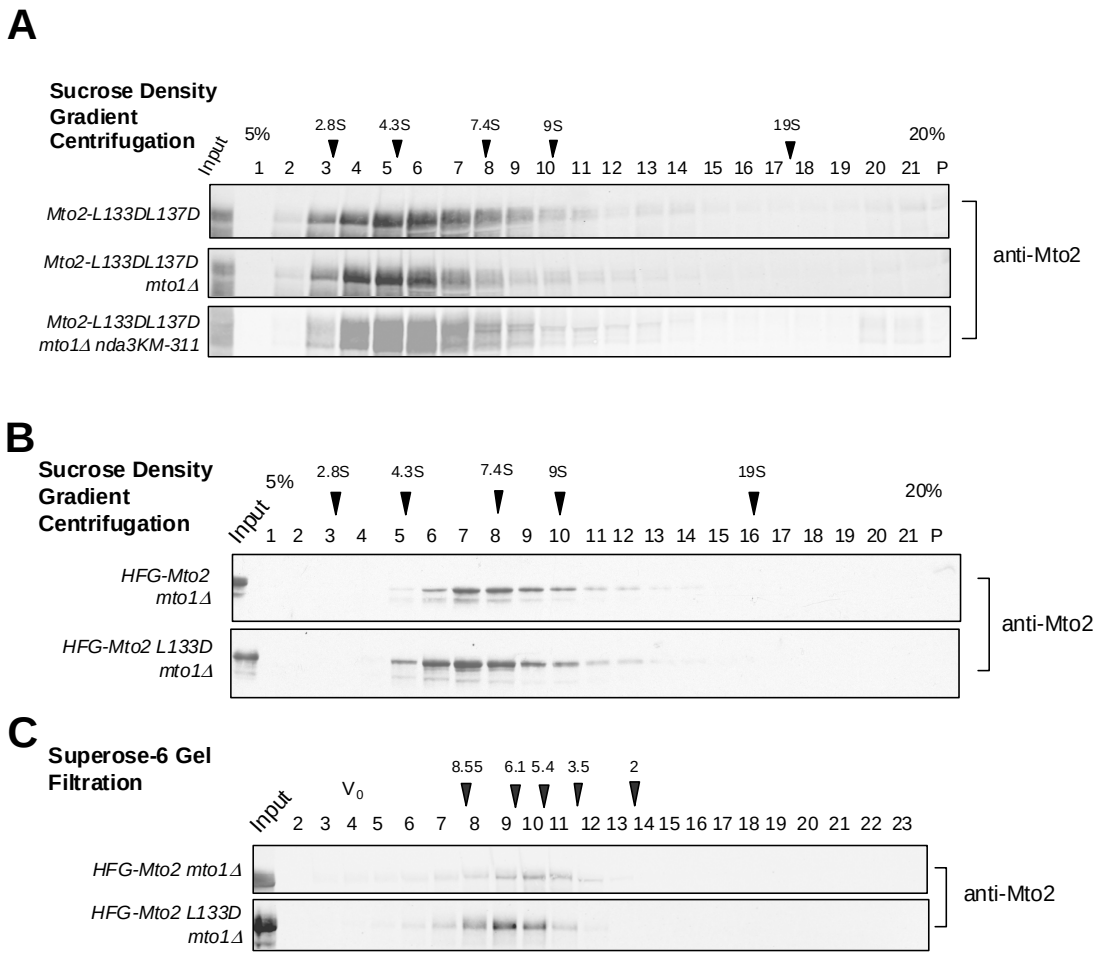

Figure 4.11 Hydrodynamic analysis of Mto2-L133DL137D coiled-coil mutant demonstrates that it is dimeric. [Strains KS4450, KS4461, KS5784, KS5785 and KS5787]. Extracts were subject to sucrose density gradient centrifugation at 55,000 rpm for 3.5 hr in a Beckman TLS-55. Fractions including the pellet [P] were analysed by 10% SDS-PAGE the western blot was probed with anti-Mto2 antibody. [A] Integrated intensity of the signal from IRDye800 was measured using Odyssey V3.0. [B] The signal from GT-34-HRP was detected by ECL. [C] The extract was fractionated by gel filtration using a Superose-6 column [KS1]. The fractions were analysed by 10% SDS-PAGE the western blot was probed with anti-Mto2 antibody. Integrated intensity of the signal from IRDye800 was measured using Odyssey V3.0. The peak locations for molecular weight standards run on parallel fractionations are indicated [black arrows]. Standards in [C] indicated in nm. V_0 = void volume. Images represent results from a single experiment.

These results confirm the observation in section 4.2.9.2 which showed that the coiled-coil mutant does not fully disrupt the Mto2-Mto2 interaction *in vivo*, as the hydrodynamic analysis demonstrates that HFG-Mto2-L133DL137D is still able to form a dimer. Although the sedimentation pattern of Mto1 was not examined in this analysis, the absence of HFG-Mto2-L133DL137D in the pellet fractions in all cases indicates that the Mto1-Mto2 interaction may have also been disrupted in this mutant [as predicted from the presence of the 60 – 80 S complex described in chapter three].

4.2.9.4 HFG-Mto2-L133DL137D phenocopies *mto2Δ*

To investigate the consequences of disrupting the Mto2 tetramer, the phenotype of the Mto2-L133DL137D mutant was analysed. In previous analysis I have demonstrated that dimeric Mto2 is sufficient to induce MT nucleation, therefore I predict that this mutant should not have any detectable changes in Mto2 function. In addition to analysis of *nmt81:HFG-Mto2-L133DL137D* this strain was crossed with a strain that contained Atb2-GFP to allow visualisation of MT dynamics [KS1409]. Figure 4.11, Panel A; movie 3C and 3D, show that HFG-Mto2-L133DL137D localised to the SPB, eMTOC and along pre-existing MTs. However, this signal was considerably weaker than HFG-Mto2. Examination of the MTs showed that the phenotype was similar to *mto2Δ* whereby only 1 - 2 MT bundles were observed per cell. Astral MTs and the PAA were present, but the cytoplasmic MT bundles were thicker and appeared to be hyperstable i.e. bending round cell tips, resulting in the curved cell phenotype reminiscent of *mto2Δ*. Cytoplasmic levels of HFG-Mto2-L133DL137D were relatively high compared to wild-type, which

suggests that a proportion of the protein was unable to localise, either through loss of the Mto1 interaction or through a reduction in protein stability/folding.

To address whether the *mto2Δ*-like phenotype is due to a reduction of Mto2 protein levels, HFG-Mto2 was placed under an *nmt41* promoter, where it is predicted that a proportional increase in Mto2 that is able to localise to MTOCs should result in a partial rescue of MT nucleation levels. Measurement of the integrated intensity of the Mto2 signal showed that the levels of *nmt81*:HFG-Mto2-L133DL137D were higher than endogenous Mto2-GFP indicating that the *mto2Δ*-like phenotype was not due to a lower amount of protein. Expression under the *nmt41* promoter gave a 4-fold higher level of protein expression than *nmt81* and 7-fold increase in expression compared to the endogenous promoter [fig 4.12, Panel B and C]. The increased expression of *nmt41:HFG-Mto2-L133DL137D* resulted in a higher signal from the SPB, eMTOC and limited number of iMTOCs, as well as increasing the cytoplasmic signal, but this did not result in a detectable increase in the number of HFG-Mto2-L133DL137D foci at non-SPB iMTOCs [fig 4.12, Panel A].

Failure of HFG-Mto2-L133DL137D to localise indicates that a large proportion of HFG-Mto2-L133DL137D may be unable to interact with Mto1 or interacts very weakly with Mto1. Those MTOCs that contained HFG-Mto2-L133DL137D are likely to have unique properties that facilitate Mto2 localisation. This is probably related to Mto1 concentration at MTOCs; if the interaction of HFG-Mto2-L133DL137D with Mto1 were significantly weakened, areas of high concentration of Mto1, such as the SPB, might be the only place where HFG-Mto2-L133DL137D could be detected.

The phenotype of Mto2-L133DL137D mutant demonstrates that the coiled-coil domain is required for Mto2 to function, where it appears to be involved in both Mto2 dimer association and the Mto1- Mto2 interaction. The analysis of HFG-Mto2 indicates that dimeric Mto2 is sufficient to promote MT nucleation. Therefore, the *mto2Δ*-like phenotype of HFG-Mto2-L133DL137D suggests that it is disruption of the Mto1-Mto2 interaction and not disruption of tetramerisation that causes the *mto2Δ* phenotype, although these events are not mutually exclusive.

4.2.9.5 The Mto1 / γ-TuC interaction is disrupted in the Mto2-L133DL137D coiled-coil mutant

To confirm biochemically whether the *mto2Δ* - like phenotype of HFG-Mto2-L133DL137D results from the disruption of the Mto2-Mto1 interaction, an Mto1-TAPS pulldown was performed. Figure 4.13 shows that the levels of HFG-Mto2-L133DL137D in the pulldown were reduced compared to the levels of wild-type HFG-Mto2. This was also true for members of the γ-TuSC. This result suggests that the Mto1-Mto2 interaction has been weakened in the coiled-coil mutant, leading to the loss of interaction between Mto1 and the γ-TuC. This observation is consistent with the reduction in the nucleation efficiency and low level of HFG-Mto2-L133DL137D localisation in the cell [fig 4.12, Panel A].

This result indicates that the coiled-coil domain of Mto2 is required for the Mto1-Mto2 interaction and that this interaction domain overlaps with a region of the protein that, based on the *in vitro* interaction assays, is also required for the interaction of Mto2 dimers.

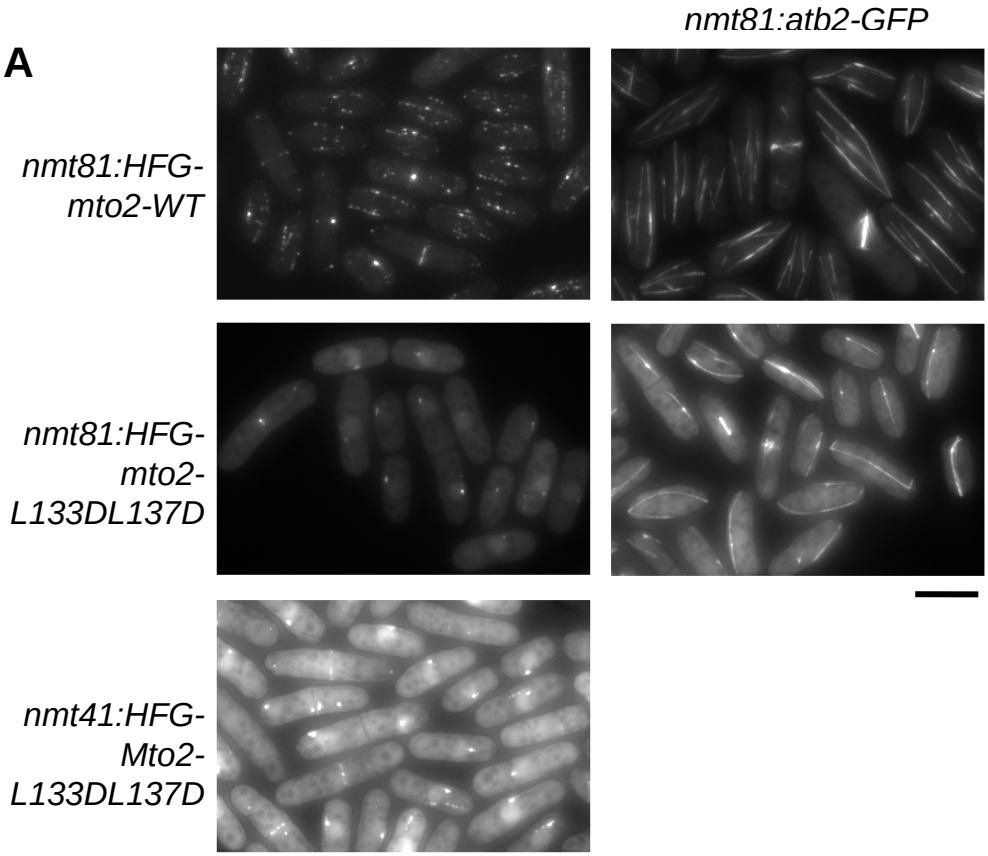
A
nmt81:atb2-GFP
nmt81:HFG-mto2-WT
nmt81:HFG-mto2-L133DL137D
nmt41:HFG-Mto2-L133DL137D

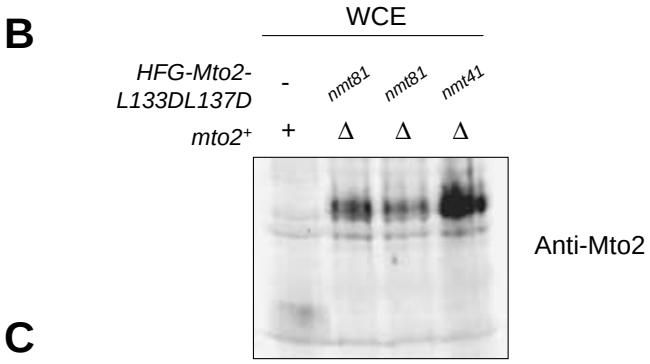
B
WCE
HFG-Mto2-L133DL137D
-
nmt81
nmt81
nmt41
mto2+
+
Δ
Δ
Δ
Anti-Mto2

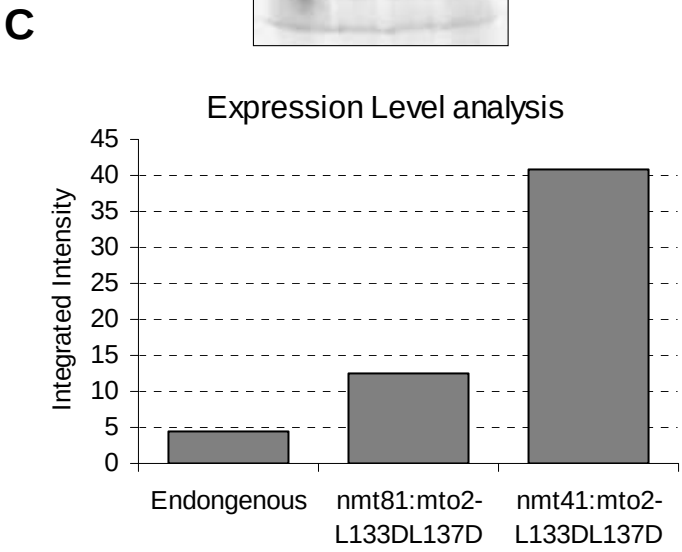
C
Expression Level analysis
Integrated Intensity
45
40
35
30
25
20
15
10
5
0
Endongenous
nmt81:mto2-L133DL137D
nmt41:mto2-L133DL137D

Figure 4.12 The phenotype of HFG-Mto2-L133DL137D is reminiscent of *mto2Δ*. [Strains KS516, KS3915, KS4461, KS4463, KS4621 and KS5712] [A] Maximum projections of wide-field images of HFG-Mto2-L133DL137D expressed from *nmt81* and *nmt41* promoters in the presence and absence of Atb2-GFP. Also see movie 3C. Scale bar = 10 µm. [B] Total extracts, including two isolates of nmt81:HFG-Mto2-L133DL137D [left isolate used in microscopy], were analysed by 10% SDS-PAGE and the western blot was probed with anti-Mto2 antibody. [C] Integrated intensity of IRDye800 signal was measured using Odyssey V3.0. nmt81:HFG-Mto2-L133DL137D signal represents the average signal of the two isolates. Image represents result from a single experiment. WCE = whole cell extract.

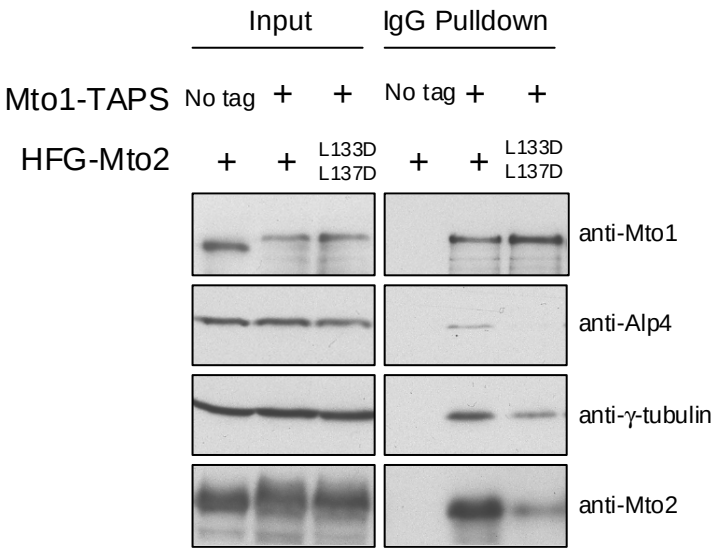

Figure 4.13 Analysis of Mto1 / γ-TuC interaction indicated that the interaction is perturbed in the Mto2-L133DL137D mutant. [Strains KS3915, KS4973 and KS4976]. The extracts were incubated with IgG-linked Dynabeads. The eluates were analysed by 10% SDS-PAGE and the western blot was probed anti-Mto2, anti-γ-tubulin [GTU-88], anti-Alp4 and anti-Mto1 antibodies. GT-34-HRP signal was detected with ECL. Image represents typical result obtained from two experiments.

4.3 SUMMARY OF RESULTS

The main objective of the research described in this chapter was to investigate the role of the Mto2-Mto2 interaction in Mto2 function and whether it contributes to the assembly of the Mto1/2 complex. Mto2 is required for multimerisation of the Mto1/2 complex containing full length Mto1, which is believed to consist of several copies of the Mto1/2 heterotetramer. I predicted that Mto2 multimerisation may drive this association.

Using purified recombinant protein and endogenous Mto2, I have shown that in the absence of Mto1, Mto2 forms a complex that is most likely to contain 4 molecules of Mto2.

I observed that the oligomerisation state of Mto2 changes during the cell cycle, with Mto2 forming a dimer during mitosis. This was interesting as it supported the prediction that the Mto1/2 heterotetramers may be multimerising through the association of Mto2 dimers, and this interaction is then disrupted during mitosis. However, this idea was contradicted by the phenotypic analysis of HFG-Mto2, which forms a dimer in the absence of Mto1 but does not affect MT nucleation from non-SPB iMTOCs. Additionally, as the Mto1-YFP foci present at iMTOCs in the presence of either CFP-Mto2 or untagged Mto2 were essentially the same, this suggests that tetramerisation of Mto2 does not contribute to the assembly of Mto1/2 complexes at iMTOCs (Samejima *et al.* 2005). Based on these results I believe that tetrameric Mto2 is most likely to be the default form of Mto2 dimers when not present in complex with Mto1. For example, if the Mto1 interaction domains of the Mto2 dimers are strongly hydrophobic, then dimeric Mto2 may be unstable. This

interpretation also suggests that the Mto2 dimer-dimer interface overlaps with the Mto1 interaction interface [fig 4.14, Panel A].

In summary, these results suggest that higher-order multimerisation of the Mto2 dimer is unlikely to facilitate the association of Mto1/2 heterotetramers. Alternatively, it is possible that Mto2 may promote Mto1/2 multimerisation through other mechanisms, e.g. inducing a conformational change in Mto1 that promotes Mto1 self-association. It is possible that recruitment of monomeric Mto2 may be sufficient to induce a conformation change in Mto1, but through Mto2 dimerisation the cell is able make this process more efficient.

To test whether Mto2 dimerisation is required for Mto2 activity, I attempted to make a monomeric version of Mto2, which required identification and disruption of both the Mto2 dimeric interaction domain, and the Mto2 dimer association interface. Thus, I identified a coiled-coil domain in the N-terminal region of Mto2 [114 – 147 aa]. Removal of a large section of Mto2 that contained the coiled-coil domain disrupted the interaction with full length Mto2 *in vitro*. Regions at the C-terminus of Mto2 were also shown to be required for the Mto2-Mto2 interaction. It is likely that these two domains represent the Mto2 dimeric and Mto2 dimer association interaction domains. However, removal of either of these proposed interaction domains did not preserve the Mto2-mto2 interaction, possibly due to a decrease in stability from exposure of hydrophobic domains that would usually be internalised within the Mto2 tetramer.

In addition, this interpretation assumes that MBP-Mto2 is tetrameric. The oligomeric state of MBP-Mto2 was not determined in this analysis, as hydrodynamic analysis of purified MBP-Mto2 was found to assemble into large aggregates [data

not shown]. Given that a tag of a similar size [HFG] has been shown to disrupt the Mto2 tetramer, it is possible that MBP-Mto2 is also dimeric. Unfortunately, further analysis of the truncation mutants *in vivo* was hindered by a decrease in protein stability.

Targeted mutagenesis of the coiled-coil domain resulted in a disruption of the Mto2-Mto2 interaction *in vitro* but not *in vivo*. I subsequently demonstrated by hydrodynamic analysis of yeast extract that the Mto2-L133DL137D coiled-coil mutant was dimeric in the absence of Mto1. The lost of Mto2 dimerisation *in vitro* may be a consequence of sub-optimal buffer conditions, particulary if the resulting dimer contains sensitive hydrophobic regions that would not normally be exposed through Mto2 tetramerisation/interaction with Mto1. However, it is unclear why this would not also be observed in yeast extract.

Previous analysis has demonstrated that dimeric protein does not affect MT nucleation, however, phenotypic analysis of the coiled-coil mutant revealed an *mto2Δ*-like phenotype; a reduction in the number of cytoplasmic MTs, and MT nucleation was restricted to the SPB. As HFG-Mto2-L133DL137D did not efficiently localise to non-SPB iMTOCs, the *mto2Δ*-like phenotype was predicted to result from a disruption of the Mto1-Mto2 interaction. This was confirmed biochemically, where it was also shown that mutation of the coiled-coil caused a reduction in the efficiency of the Mto1 / γ-TuSC interaction.

The hydrodynamic analysis of HFG-tagged Mto2 has indicated that it is dimeric. However, it is not clear whether the Mto2 dimeric interaction or the Mto2 dimer association interaction domain has been disrupted. Depending on which interaction has been disrupted, the resultant Mto1 / HFG-Mto2 complex would be

very different. Figure 4.14, Panel B and C, describe possible conformations of the Mto1 / HFG-Mto2 complex. The conformation described in Panel B is supported by the 50% reduction in HFG-Mto2 co-precipitated by Mto1-TAPS compared with untagged Mto2. This may have resulted from the disruption of dimeric interaction. This would result in an active complex that contained monomeric Mto2 and thus supports the theory that Mto2 induces a structural change in Mto1 that in turn, promotes Mto1 multimerisation.

Alternatively, the 50% reduction in HFG-Mto2 pulled down by Mto1 may represent a reduction in the affinity of Mto1-Mto2 interaction as a consequence of the HFG tag. This would support the model described in Panel C. The conformation described in Panel C is also supported by the hydrodynamic analysis of the Mto2 coiled-coil mutant. Both HFG-Mto2 and Mto2-L133DL137D are dimeric, suggesting that the dimer association domain and not the dimerisation domain has been disrupted. As HFG-Mto2-L133DL137D is dimeric this indicates that the same interaction interface has been disrupted in both cases. As the coiled-coil mutations also disrupt the Mto1-Mto2 interaction, this suggests that the Mto2 dimer association domain overlaps with the Mto1 interaction domain. Interestingly, it was shown also that Mto2-L133DL137D does not form monomers in mitosis, this indicates that the same Mto2 dimer association/Mto1-Mto2 interaction domain is disrupted by the coiled-coil mutation that is targeted in mitosis [fig 4.14, Panel D]. To definitively show that the Mto1 / HFG-Mto2 complex contains dimeric Mto2 the stoichiometry of the Mto1 / HFG-Mto2 complex would need to be determined.

Unfortunately, I was not able to construct monomeric Mto2 in this analysis. This form of Mto2 is required to assess the contribution of the Mto2-Mto2

interaction to the formation of an active Mto1/2 complex, with relation to Mto1/2 heterotetramer multimerisation and the proposed activation of the γ-TuSC. However, I did identify the Mto1 interaction domain, which may be useful to the subsequently structural studies of the protein complex that are required to fully understand the consequence of the Mto2 self-interaction.

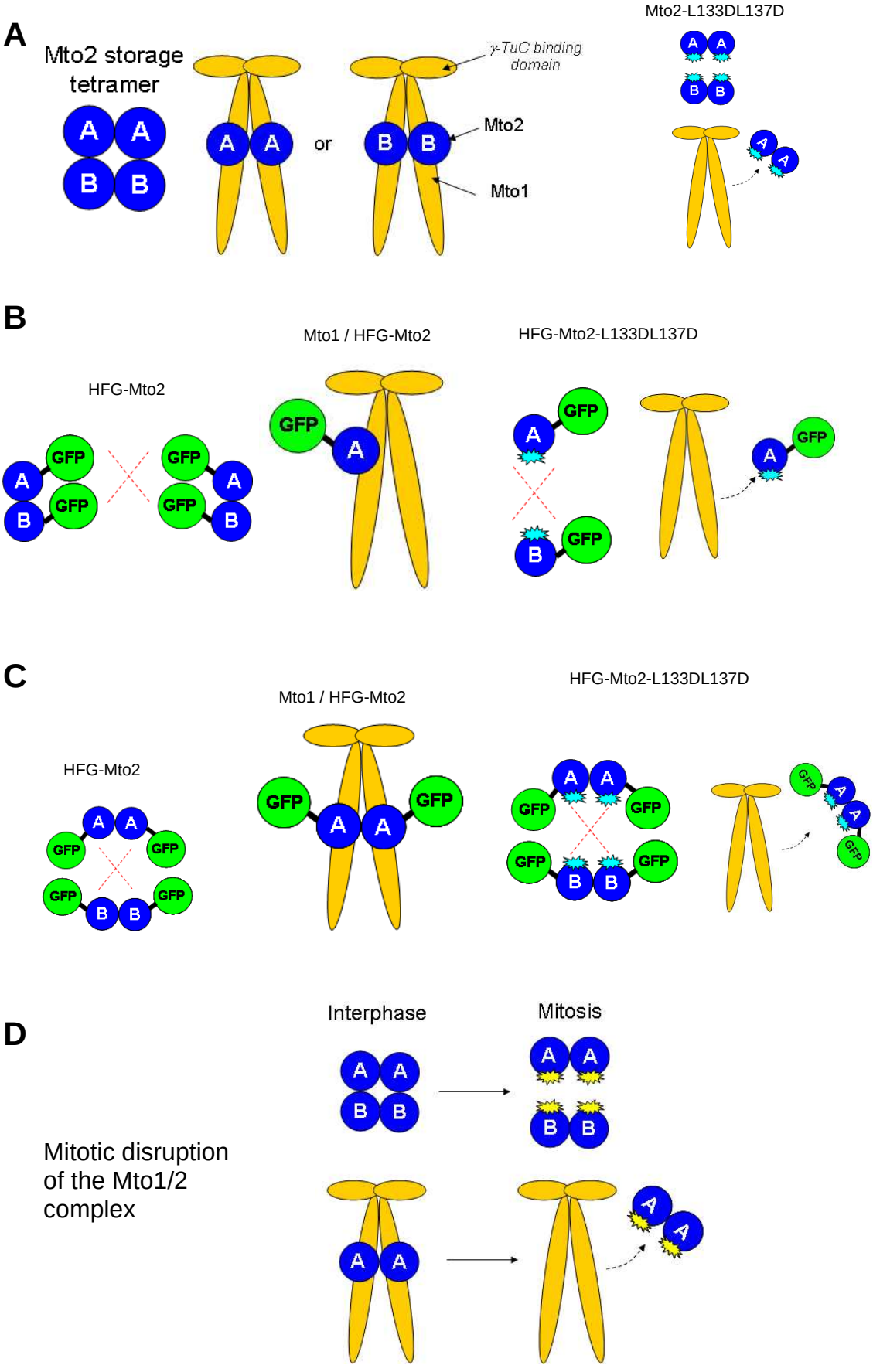
A
Mto2 storage tetramer
A
A
B
B
or
γ-TuC binding domain
Mto2
Mto1
Mto2-L133DL137D
B
HFG-Mto2
GFP
Mto1 / HFG-Mto2
HFG-Mto2-L133DL137D
C
HFG-Mto2
Mto1 / HFG-Mto2
HFG-Mto2-L133DL137D
D
Interphase
Mitosis
Mitotic disruption of the Mto1/2 complex

Figure 4.14 Schematic representation of Mto2 multimerisation. [A] In the absence of Mto1, Mto2 forms a tetramer. The A-B dimer-dimer interface forms the same region required to interact with Mto1. This interface is disrupted by the L133DL137D coiled-coil mutant. [B and C] HFG tagged Mto2 cannot form tetramers due to steric inhibition, however it can still interact with Mto1 to a level sufficient to promote the Mto1 / γ-TuSC interaction. The HFG tag can disrupt either Mto2 dimer interaction [B] or the Mto2 dimer association [C]. If B were true, the introduction of the coiled-coil mutation would result in monomeric protein, if C were true, the HFG-tagged coiled-coil mutant would be dimeric. [D] During mitosis the same Mto2 dimer-dimer interaction is disrupted as is perturbed by both the HFG tag and the coiled-coil mutant. This is predicted to cause the disruption of the Mto1-Mto2 interaction.

CHAPTER FIVE

ANALYSIS OF MTO2 PHOSPHORYLATION

5.1. INTRODUCTION

The *mto2Δ* phenotype demonstrates that the Mto1/2 complex is specifically required for MT nucleation from non-SPB iMTOCs. Nucleation does not occur from non-SPB sites during mitosis [e.g. on the nucleation envelope], indicating that the nucleation complexes containing Mto1/2 are either not assembled or not active during mitosis. This suggests that the Mto1/2 complex may be subject to some level of cell cycle-dependent regulation. Although phosphorylation of Mto1 has yet to be shown, phosphorylation of Mto1 homologs in other species has been documented. Dobbelaere and colleagues demonstrated that phosphorylation of *Cnn* in *D. melanogaster* during mitosis is dependent on Polo kinase (Dobbelaere *et al.* 2008). More recently it has been shown that SpPcp1, a paralogous protein required for nucleation from the nucleoplasmic face of the SPB, is also phosphorylated by PLK-1 (Fong, C. S. *et al.* 2009a). When analysed by SDS-PAGE and western blot, Mto2 is present as several isoforms, which indicates that Mto2 may also be phosphorylated.

In chapter four I have demonstrated that the oligomerisation state of Mto2 is altered in mitosis. I predict, based on evidence from this study, that this change in oligomerisation state may reflect the mitotic disruption of the Mto1-Mto2 interaction. It is possible that disruption of the Mto1-Mto2 interaction during mitosis may occur to allow a re-modelling of the Mto1/2-γ-TuC complex and subsequently re-

localisation of the γ-TuC to the SPB. Alternatively, the Mto1/2 complex may be disrupted to allow a different Mto1 complex, which does not require Mto2, to assemble at the SPBs.

5.1.2 Aims and Objectives

In this chapter I will attempt to confirm that Mto2 is phosphorylated, and investigate whether this correlates with a cell cycle-dependent regulation of Mto2. I will also examine the significance of Mto2 phosphorylation on the Mto1-Mto2 interaction. To do this I will take the following approaches:

- Confirm that Mto2 is phosphorylated using phosphatase treatment.
- Follow Mto2 phosphorylation over the cell cycle.
- Analyse the effect of Mto2 phosphorylation on the Mto1-Mto2 interaction.
- Use bioinformatic and biochemical phosphorylation mapping techniques to identify phosphorylated residues.
- Create phospho-mutants to confirm the significance of Mto2 phosphorylation for Mto2 function.

5.2 RESULTS

5.2.1 Identification and Characterisation of Mto2 phosphorylation

5.2.1.1 Mto2 is phosphorylated

Previous analysis of Mto2 by western blotting has demonstrated that it migrates as several isoforms by SDS-PAGE (Samejima *et al.* 2005). These isoforms could result from a number of post-translational modifications such as phosphorylation, ubiquitination, SUMOylation, acetylation, and biotinylation. To confirm phosphorylation of Mto2, fission yeast extract was treated with purified phosphatase, heat-inactivated λ-PPase and/or the phosphatase inhibitors. Figure 4.1 shows that when extract was treated with λ-PPase, the Mto2 isoforms collapse into a single, fast migrating form. This did not occur when heat-inactivated phosphatase was added, and the de-phosphorylation was incomplete when phosphatase inhibitors were also added. This result indicates that the isoforms of Mto2 are due to phosphorylation.

5.2.1.2 Mto2 phosphorylation is cell cycle-dependent

Mto2-dependent MT nucleation from non-SPB iMTOCs is specific to interphase and MT nucleation during mitosis is restricted to the SPB, a process that does not require Mto2. This suggests that the Mto1/2 complex may be subject to cell cycle regulation.

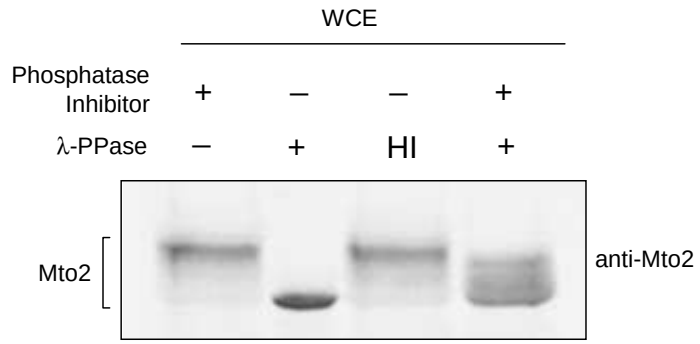

Figure 5.1 λ-protein phosphatase treatment of fission yeast confirms that Mto2 is phosphorylated. Total extracts from KS516 were treated with λ-PPase/heat-inactivated λ-PPase [HI] and/or phosphatase inhibitors. The extracts were analysed by 10% SDS-PAGE and the western blot was probed with anti-Mto2 antibody. The IRDye800 signal was detected using Odyssey V3.0. WCE = whole cell extract. Image represents a typical result from three experiments.

It is likely that this regulation is instigated through phosphorylation therefore Mto2 phosphorylation was examined over the cell cycle. Phosphorylation of Mto2 was analysed in a strain containing a temperature sensitive allele of the cell cycle regulator Cdc25 [*cdc25-22ts*], which at restrictive temperature blocks the cells in G_2 (Russell *et al.* 1986; Gould, K. L. *et al.* 1989). Following incubation at the restrictive temperature between 50 – 80 % of the culture was arrested in G_2 [indicated by the appearance of highly elongated cells [data not shown]. Upon return to the permissive temperature and release into mitosis, cells were harvested at 20 min intervals. Figure 5.2, Panel A shows the septation assay, which measures the proportion of cells in the culture that have formed septa. The septation index peaked at 60 min, at which point the synchrony of the culture was approximately 78% [n = 200]. Following the first septation peak, the cells entered a second mitosis at 140 min. Figure 5.2, Panel B shows that there was a distinct mobility shift as the cells proceeded though the cell cycle, which I interpret to be phosphorylation based on the results in section 5.2.1. Notably, there was an increase in hyperphosphorylated Mto2 20 min after G_2 release, corresponding to the time of entry into mitosis. These slower migrating isoforms are replaced by faster migrating de-phosphorylated isoforms of Mto2 as the septation index drops and cells enter interphase.

The uniformity of the non-specific band [*] suggests that the increase in Mto2 signal at 140 min is not due to loading error. Alternatively, it may have resulted from an enrichment of two or more phosphorylation states at this point, which then disperse into a range of phosphorylated forms as the cells pass through mitosis. At t = 160 the hyperphosphorylated isoforms of Mto2 observed at entry into the first mitosis returned, however, the signal from the slowest migrating bands was

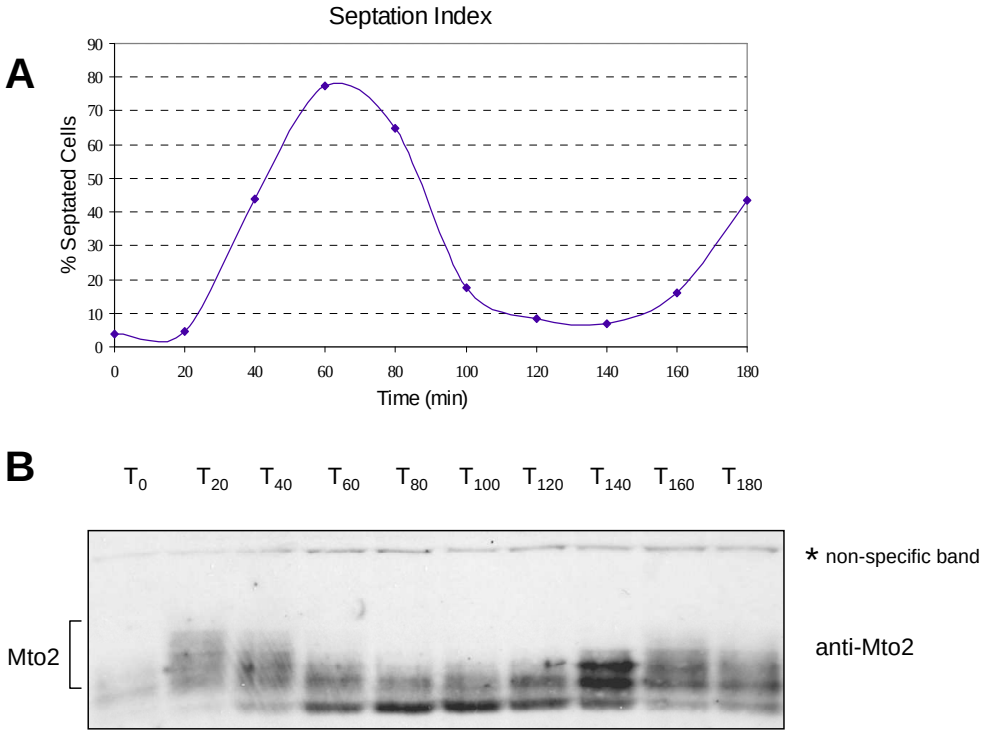

Figure 5.2 Analysis of Mto2 phosphorylation over the cell cycle indicates that Mto2 is hyperphosphorylated in mitosis. [A] Septation index of cell samples taken every 20 min after release from *cdc25-22*^{ts} G_2 arrest based on fluorescent brightener staining. [KS1280]. [B] Extracts made from samples taken from synchronous culture were analysed by 10% SDS-PAGE and the western blot was probed with anti-Mto2 antibody. Signal from GT-34-HRP secondary antibody was detected by ECL. Non-specific band indicates loading [*]. Time is indicated in minutes. Image represents a typical result from two experiments.

significantly weaker than the first mitosis. This likely to be caused by a reduction in cell synchrony by the time cells pass through the second mitosis.
This result indicates that Mto2 phosphorylation is regulated in a cell cycle specific manner.

5.2.1.3 The Mto1-Mto2 interaction is disrupted in a metaphase arrest

The most likely mechanism by which Mto2 phosphorylation down-regulates the activity of the Mto1/2 complex during mitosis, is through the disruption of the Mto1-Mto2 interaction. To test this idea, Mto2 co-precipitation by Mto1-TAPS was compared between asynchronous cell culture and cells arrested in metaphase using *nda3-KM311*. Figure 5.3 shows that the amount of Mto2 pulled down by Mto1-TAPS in mitotic extract is significantly reduced compared to Mto2 from asynchronous extract. The small amount of Mto2 present in the eluate of the mitotic pulldown is likely to be comparatively dephosphorylated Mto2 that has escaped the arrest. Examination of the supernatants from the pulldown demonstrated that the hyperphosphorylated Mto2 observed in the input of the *nda3-KM311* extract did not bind to Mto1-TAPS [data not shown].

Figure 5.3 shows a clear difference in the ability of dephosphorylated and phosphorylated Mto2 to interact with Mto1, where hyperphosphorylation of Mto2 appears to disrupt the Mto1-Mto2 interaction. This result confirms the prediction that the Mto1-Mto2 interaction is disrupted in mitosis. However, this result does not correlate with observations *in vivo*, as fluorescence microscopy has shown that Mto1-YFP and Mto2-CFP co-localise throughout the cell cycle (Samejima *et al.*

2005). It is possible that Mto2 associates with the γ-TuSC independently of Mto1, although, this interaction is very weak (Samejima *et al.* 2008). Further investigation is required to determine the mechanism by which Mto2 localises to the SPB during mitosis.

5.2.1.4 Analysis of the mitotic disruption of the Mto1-Mto2 interaction using *cdc25-22^{ts}* G_2 block and release

In addition to an *nda3-KM311* arrest, the Mto1-Mto2 interaction was examined over a *cdc25-22^{ts}* G_2 block and release, where the interaction could be followed over the entire cell cycle. A *cdc25-22^{ts}* strain containing Mto1-TAPS [KS5795] was arrested in G_2. On return to permissive temperature, samples were harvested at 20 min intervals. Figure 5.4, Panel A shows the septation index of cell samples taken at 20 min time points, indicating that septation peaked at 60 min [70% synchrony].

Western blot analysis of the Mto2 inputs showed a similar pattern to that observed in Figure 5.2, Panel B, in which Mto2 hyper-phosphorylation occurred as cells entered mitosis, in both the first and second mitoses after G_2 release. Examination of the eluates from the Mto1-TAPS precipitation showed that despite a uniform level of Mto1-TAPS, the Mto2 signal was lost at t =20 and t = 140 / t = 160, which corresponds to the G_2 / M transition of the first and second cell cycles, respectively [fig 5.4, Panel B]. Samples have been under-loaded at t = 60, resulting in a weaker signal than expected. These results confirm previous observations and show that the Mto1-Mto2 interaction is disrupted during mitosis, which correlates

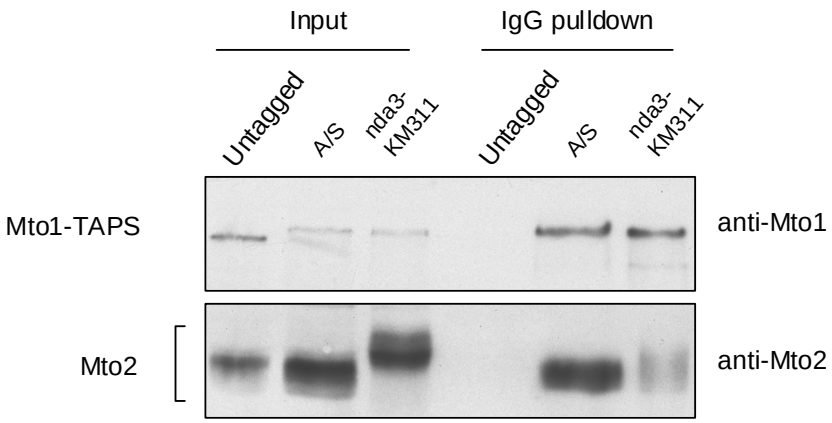

Figure 5.3 The Mto1-Mto2 interaction is disrupted during *nda3-KM311* metaphase arrest. Extracts from asynchronous and metaphase-arrested cells were incubated with IgG-Dynabeads [Strains KS516, KS3524 and KS3575]. The eluates were analysed by 10% SDS-PAGE and the western blot was probed with anti-Mto1 and anti-Mto2 antibodies. The signal from GT-34-HRP secondary antibody was detected by ECL. A / S – asynchronous extract. Image represents a typical result from three experiments.

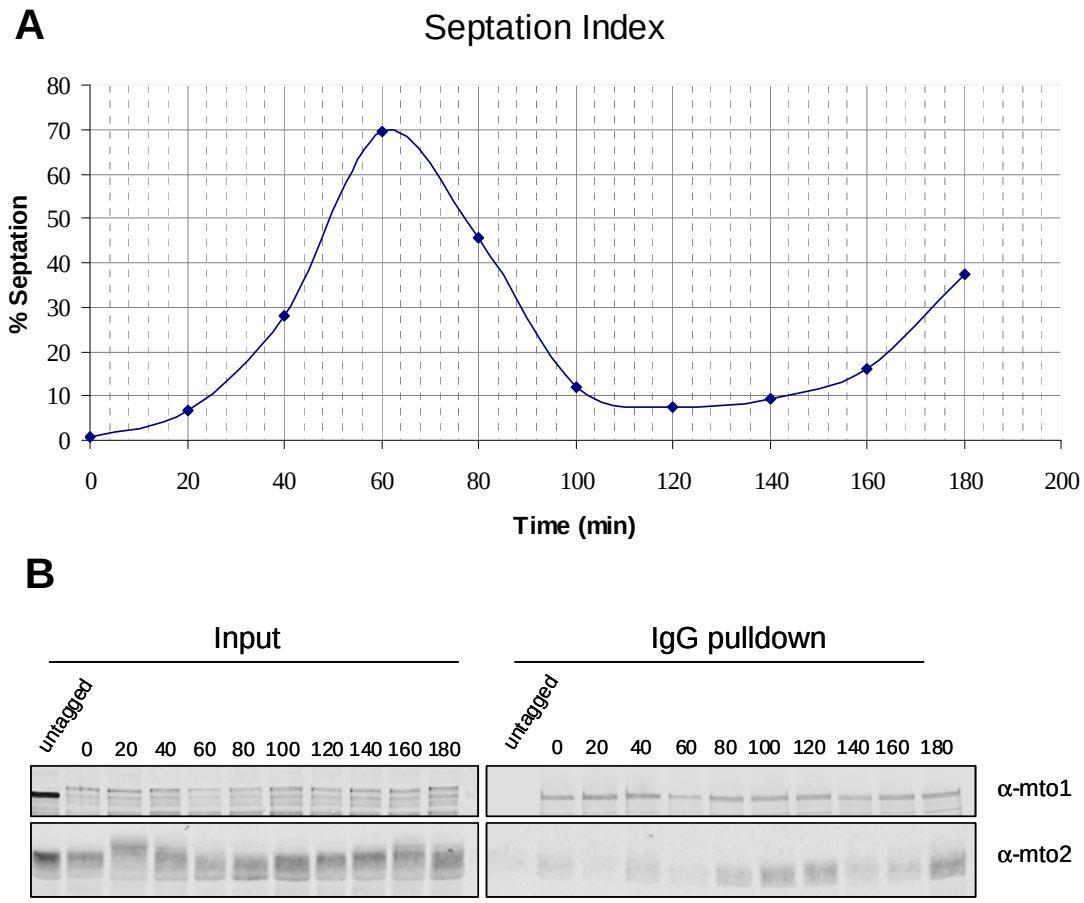

Figure 5.4 Analysis of the Mto1-Mto2 interaction in synchronised culture shows that it is disrupted in mitosis. [A] The septation index of cell samples taken every 20 min after release from *cdc25-22*^{ts} G_2 arrest based on fluorescent brightener staining. [B] Extracts made from sample of synchronous culture were incubated with IgG-Dynabeads. The eluates were analysed by 10% SDS-PAGE and the western blot was probed with anti-Mto1 and anti-Mto2 antibodies. Signal from IRDye800 was detected using Odyssey V3.0. Image represents the result from a single experiment.

with Mto2 hyper-phosphorylation. However, it remains unclear whether Mto2 phosphorylation directly causes the disruption of the Mto1/2 complex or whether phosphorylation is responsible for upstream events that lead to Mto1/2 disruption, e.g. recruitment of proteins that compete for Mto1 binding. It is also possible that Mto2 phosphorylation is purely coincidental and does not affect Mto1/2 complex formation.

5.2.1.5 The Mto1/2 complex is disrupted following CDK1-Cyclin B treatment

In order to test whether phosphorylation of the Mto1/2 complex is directly responsible for its mitotic disruption, purified Mto1/2 complex was incubated with purified recombinant human CDK1-Cyclin B. Mto1 [1-800]-TAPS was used in this experiment as a higher yield of protein can be recovered compared to full length Mto1-TAPS (K. Sawin, personal communication). Figure 5.5 shows that when the complex is treated with CDK1-Cyclin B, Mto2 becomes phosphorylated, as demonstrated by the appearance of slower migrating isoforms similar to those observed during an *nda3-KM311* metaphase arrest. Compared with untreated Mto1/2 complex, where the bulk of Mto2 remained associated with Mto1, the majority of phosphorylated Mto2 was present in the supernatant, having dissociated from Mto1 [1-800]-TAPS.

This result confirms that phosphorylation of the Mto1/2 complex directly causes the dissociation of Mto2 from Mto1. This analysis does not indicate whether phosphorylation of Mto1 or Mto2 [or both] causes the Mto1/2 complex to dissociate. In order to determine if phosphorylation of Mto1 contributes to the disruption of the

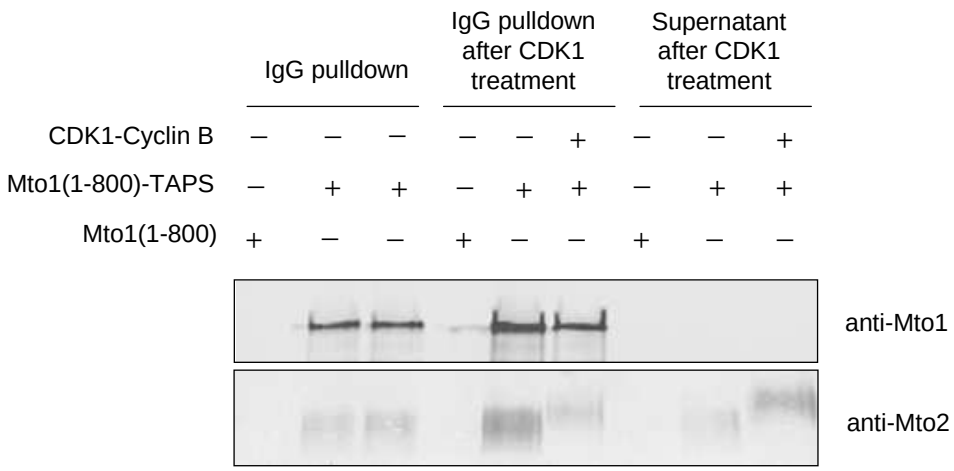

Figure 5.5 Treatment of purified Mto1/2 complex with CDK1-Cyclin B causes Mto2 to dissociate. [Strains KS3476 and KS1956]. Mto1/2 complex that had been purified on IgG-Dynabeads was incubated 100 U of CDK1-Cyclin B. Eluates and supernatants were analysed by 10% SDS-PAGE and the western blot was probed with anti-Mto1 and anti-Mto2 antibodies. IRDye800 signal was detected using Odyssey V3.0. Image represents a typical result from three experiments.

complex, individually purified Mto1 could be treated with CDK1-Cyclin B before the interaction with Mto2 is assayed. Due to the nature of this experiment it is also possible that incubation with CDK1-Cyclin B may phosphorylate the Mto1/2 complex in a non-physiological manner. This may artificially disrupt the Mto1-Mto2 interaction. The co-localisation of Mto1 and Mto2 during mitosis means that it is not possible to test whether the disruption of the Mto1-Mto2 complex occurs *in vivo* through methods such as fluorescence resonance energy transfer [FRET]. However, if one can isolate specific Mto2-dependent processes that are interrupted in mitosis, one can infer that the Mto1-Mto2 interaction may have been disrupted.

5.2.1.6 Mto2-dependent localisation Mto1 [1-549]-GFP at the nuclear envelope

Removal of Mto1 C-terminal targeting domains [1051 – 1115 aa] prevents Mto1 from localising to the SPB and eMTOC, and therefore Mto1 [1-1051] is only found at iMTOCs along the nuclear envelope and along pre-existing MTs (Samejima *et al.,* manuscript in preparation). Further truncation generates Mto1 [1-800], which only localises to iMTOCs on the nuclear envelope and to a small number of MT minus ends that are ejected from the surface of the nucleus and become bundled into adjacent MTs (Sawin *et al.,* data unpublished). Ongoing work by E. Lynch in our laboratory has shown that the nuclear envelope localisation is maintained upon further truncation of the C-terminus to Mto1 [1-549], however, this localisation is lost in Mto1 [1-500]. This correlates with disruption of the Mto2 interaction domain [461 – 549 aa] (Samejima *et al.* 2005).

To confirm that Mto1 [1-549]-GFP localisation at the nuclear envelope is dependent on Mto2, I created strains that contained Mto1 [1-549]-GFP expressed from both endogenous promoter and over-expressed from the *nmt81* promoter, in combination with *mto2*$^{+}$ [KS5349/KS5609], *nmt81:mto2* [KS5647/KS5801] and *mto2Δ* [KS5802/KS5803]. Figure 5.6 shows that Mto1 [1-549]-GFP failed to localise to the nuclear envelope in *mto2Δ* cells whether over-expressed or expressed from the endogenous promoter [fig 5.6 Panel B, I and II]. In the presence of endogenous Mto2 the level of Mto1 [1-549]-GFP present on the nuclear envelope did not increase when Mto1 expression level was up-regulated [fig 5.6 Panel B, III and IV]. Only when Mto2 was also up-regulated did over-expressed Mto1 [1-549]-GFP localise to the nuclear envelope [fig 5.6 Panel B, V and VI].

These results suggest that Mto1 [1-549]-GFP localisation to the nuclear envelope is dependent on Mto2, most likely as a consequence of assembly into the Mto1/2 complex, and that the quantitative levels of Mto2 protein limit the amount of Mto1 [1-549]-GFP that is able to localise. It is not known what the Mto1/2 complex binds to at the nuclear envelope. A screen was performed in the laboratory of P. Nurse to identify proteins involved in the establishment of the MT cytoskeleton. They identified the nucleoporin-like protein Amo1 (Pardo *et al.* 2005). Due to its punctate localisation at the nuclear envelope, Amo1 is a potential Mto1 targeting factor. This interaction could be tested by co-immunoprecipitation by Mto1 [1-549]-TAPS.

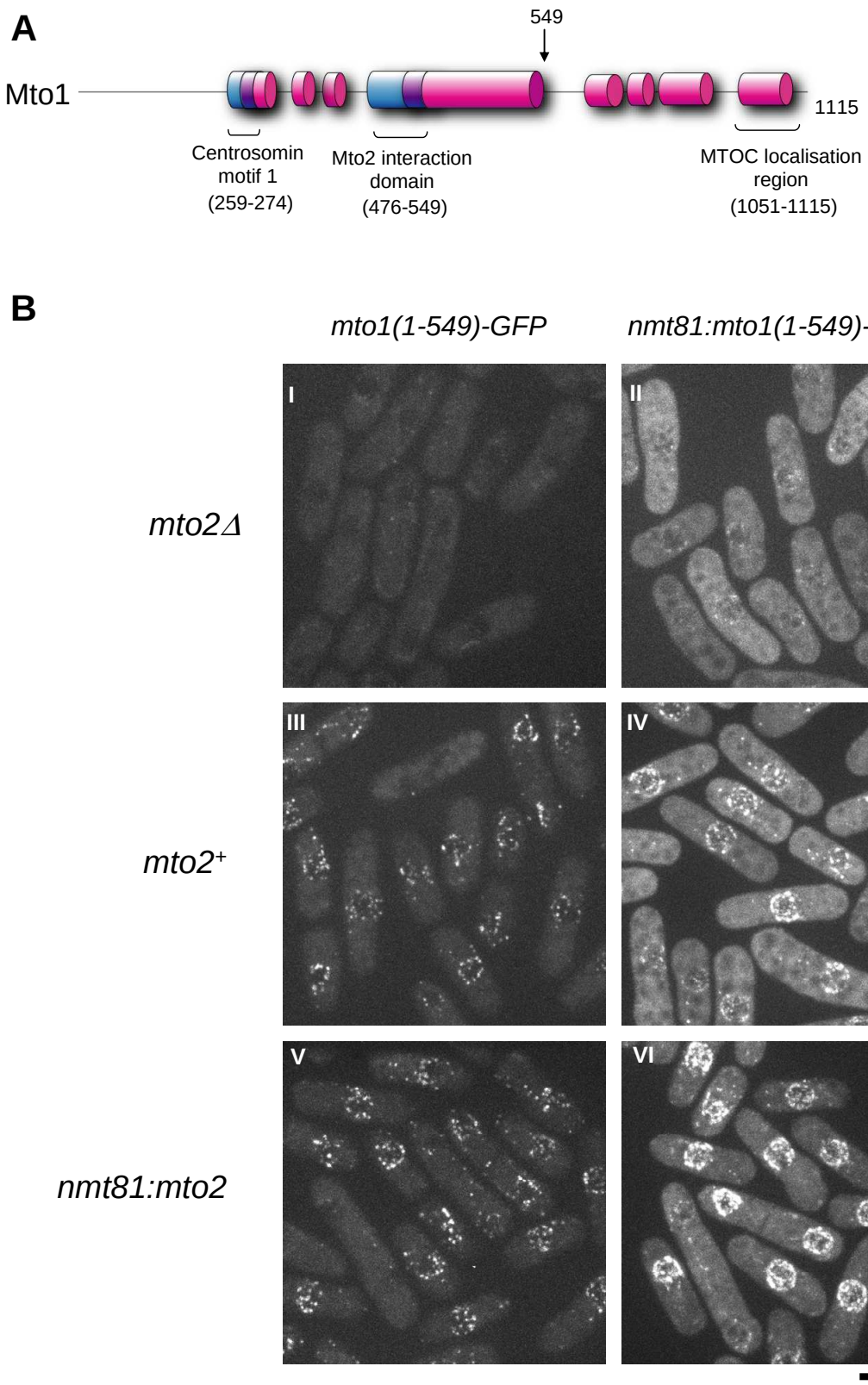
A
549
Mto1
1115
Centrosomin motif 1 (259-274)
Mto2 interaction domain (476-549)
MTOC localisation region (1051-1115)
B
mto1(1-549)-GFP
nmt81:mto1(1-549)-GFP
mto2Δ
mto2+
nmt81:mto2
I
II
III
IV
V
VI

Figure 5.6 Mto1 [1-549]-GFP localisation to the NE requires Mto2. [A] Schematic map of Mto1 depicting PAIRCOIL2 predicted coiled-coil domains [pink] and regions of overlap [purple] with protein interaction domains [blue]. Amino acid residue numbers are indicated including the Mto1 [1-549] truncation. [B, I-VI] Maximum projection of confocal images of Mto1 [1-549]-GFP expressed under *nmt81* and *nmt41* promoters in the presence and absence of Mto2. Scale bar = 10 µm.

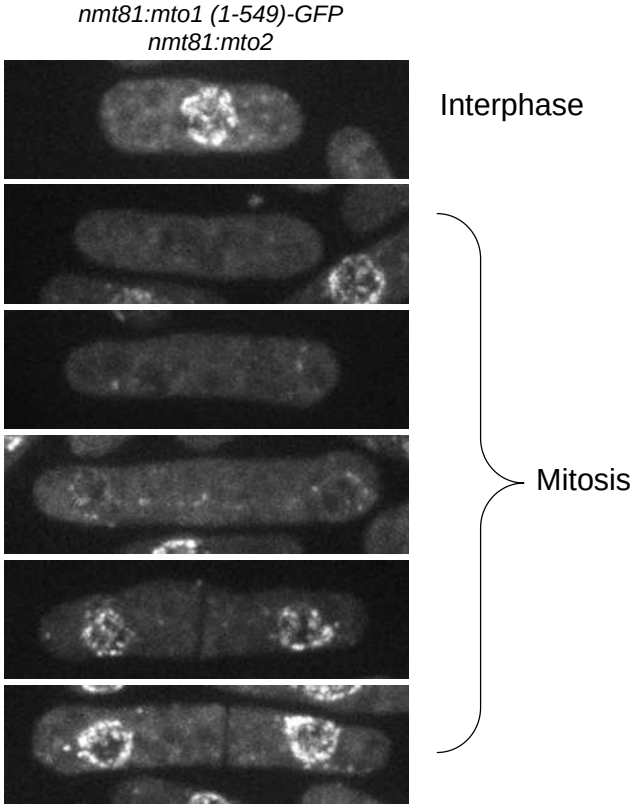

Figure 5.7 Mto1 1-549-GFP localisation at the NE is disrupted in mitosis. Maximum projection of confocal images taken of Mto1 [1-549]-GFP expressed under an *nmt41* promoter. Images were taken from different cells representing cell cycle localisation of Mto1 [1-549]-GFP. Scale bar = 10 µm.

5.2.1.7 Localisation of Mto1 [1-549]-GFP at the nuclear envelope is disrupted in mitosis

Mto1 [1-549]-GFP localisation at the nuclear envelope requires Mto2. Biochemical analysis has demonstrated that the Mto1-Mto2 interaction is disrupted during mitosis, therefore I predict that the nuclear envelope localisation of Mto1 [1-549]-GFP is also cell-cycle dependent. Figure 5.7 shows a montage of confocal images, each panel representing different stages of interphase and mitosis. Compared to the interphase cell [top], signal of Mto1 [1-549]-GFP is depleted at the NE during all stages of mitosis. The weak signal at the start of mitosis disappears until the end of anaphase. This result provides *in vivo* evidence to support the conclusion that the Mto1-Mto2 interaction is disrupted in mitosis.

5.2.1.8 Mto2 is not required for the Mto1 / γ-TuC interaction at the SPB or during mitosis

Mto2 is required for Mto1 to efficiently interact with the γ-TuSC (Samejima *et al.* 2008). In addition, my work has demonstrated that the Mto1-Mto2 interaction is disrupted during mitosis. Therefore, I investigated whether the requirement of Mto2 for an efficient Mto1 / γ-TuSC interaction is specific for the nucleation complex formed in interphase. As Mto2 is not required for nucleation from the SPB during mitosis, I predict that Mto1 / γ-TuSC interaction is not affected by the loss of Mto2. This was tested using a co-immunoprecipitation of Mto1-TAPS in

asynchronous culture and *nda3-KM311* metaphase-arrested cells in both *mto2*$^{+}$ and *mto2Δ* backgrounds.

The interaction of the γ-TuSC with a C-terminal truncation of Mto1 [1-1051] was also examined. As Mto1 [1-1051] is unable to localise to the SPB/eMTOC this would indicate whether the predicted requirement of Mto2 for the Mto1 / γ-TuSC interaction during interphase is specific to the localisation of the complex to the SPB. Figure 5.8, Panel A-F shows the integrated intensities of eluates from the Mto1-TAPS co-precipitation normalised against Mto1-TAPS in the pulldown and signal from the untagged control. The corresponding western blot is shown in figure 5.8, Panel F. Comparison of Mto1-TAPS eluates from both asynchronous culture showed that, in *mto2Δ*, the interaction efficiency of γ-TuSC with full length Mto1 was reduced by approximately five-fold compared to *mto2*$^{+}$. However, this reduction was not reflected in the metaphase arrest, which showed that the level of γ-TuSC is not affected by the loss of Mto2. This indicates that Mto2 does not contribute to the interaction between Mto1 and the γ-TuC during metaphase.

Interestingly, in asynchronous extract both Mto2 and the γ-TuSC interacted more efficiently with Mto1 [1-1051] than with full length Mto1. This may be a consequence of a redistribution of Mto1 [1-1051] molecules away from the protein dense SPB into the smaller iMTOCs where it may be more accessible to Mto2 and the γ-TuC.

In metaphase arrested extract only dephosphorylated Mto2 that has escaped the arrest interacted with Mto1-TAPS and Mto1 [1-1051]-TAPS. The level of dephosphorylated Mto2 was particularly high in the Mto1 [1-1051]-TAPS pull down. This is likely to have caused the efficiency of the γ-TuSC / Mto1 [1-1051]-TAPS

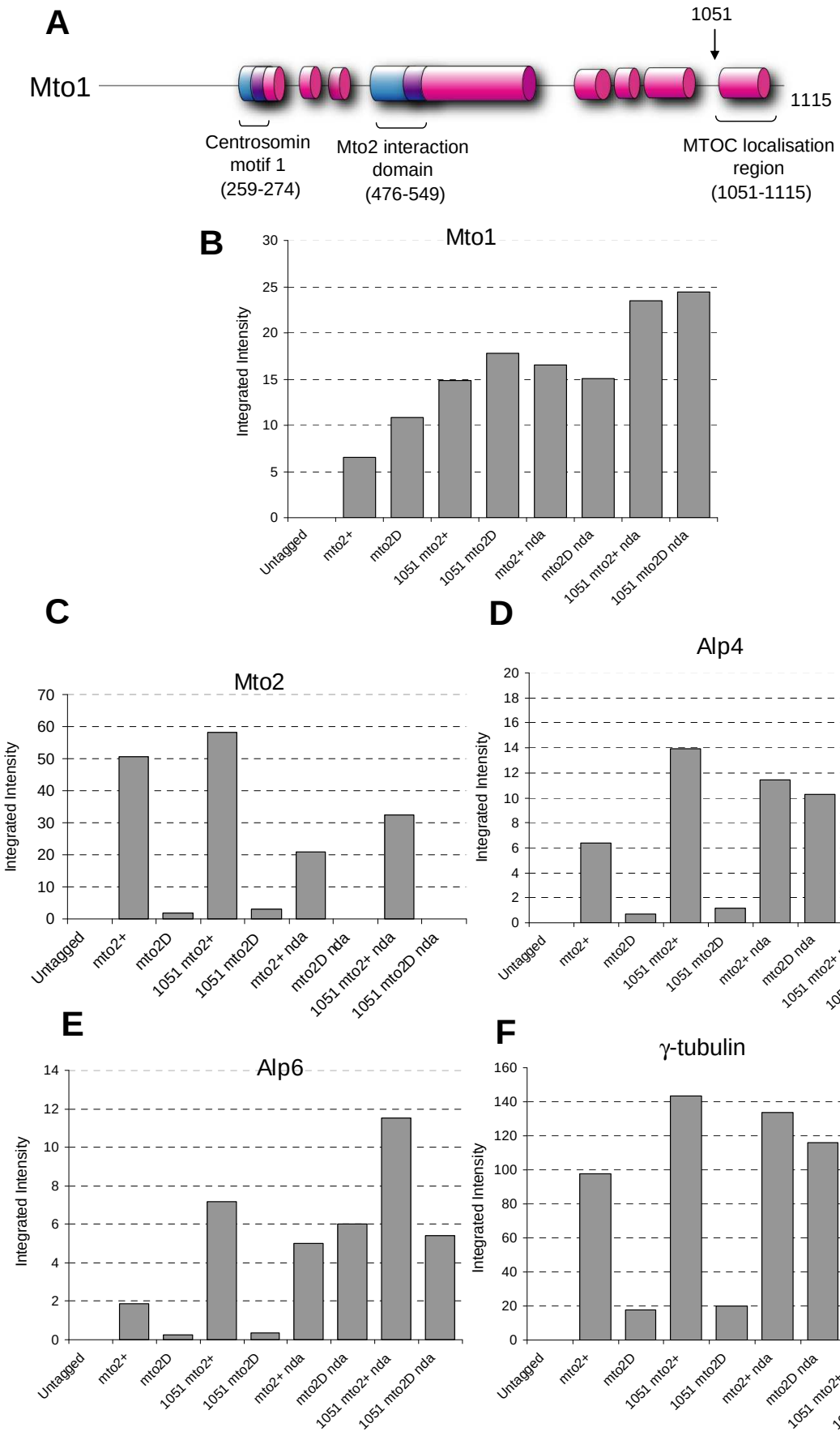
A
Mto1
1051
1115
Centrosomin motif 1 (259-274)
Mto2 interaction domain (476-549)
MTOC localisation region (1051-1115)
B
Mto1
Integrated Intensity
Untagged
mto2+
mto2D
1051 mto2+
1051 mto2D
mto2+ nda
mto2D nda
1051 mto2+ nda
1051 mto2D nda
C
Mto2
D
Alp4
E
Alp6
F
γ-tubulin

G

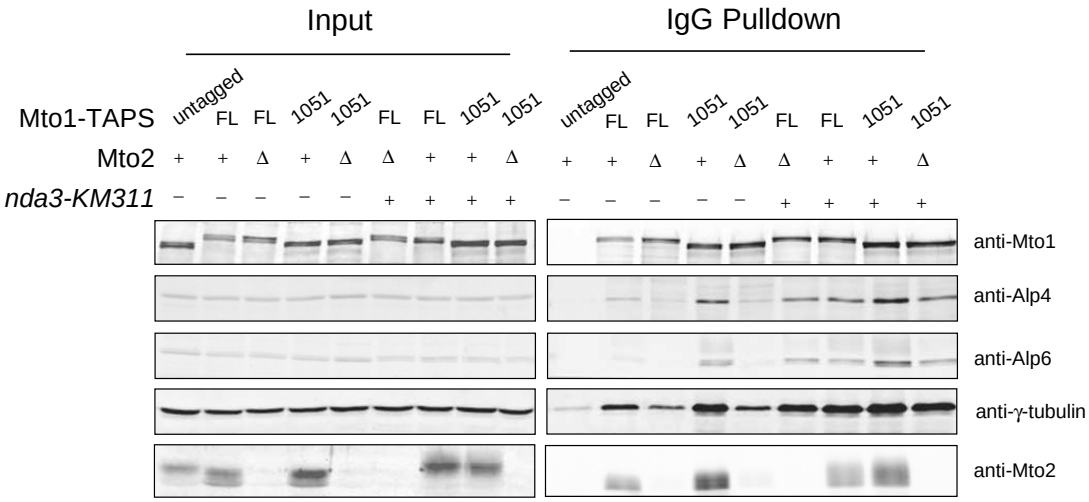

Figure 5.8 The Mto1 / γ-TuSC interaction during mitosis does not require Mto2 and is not effected by SPB localisation. [A] Schematic map of Mto1 depicting PAIRCOIL2 predicted coiled-coil domains [pink] and regions of overlap [purple] with protein interaction domains [blue]. Amino acid residue numbers are indicated including the Mto1 [1-1051] truncation. The Mto1-TAPS purifications were performed using the following strains: KS516, KS3475, KS3524, KS3575, KS3577, KS4323, KS5578, KS5579, KS5580. [G] The eluates were analysed by 10% SDS-PAGE and the western blot was probed with anti-Mto1, anti-Mto2, anti-Alp6 and anti-γ-tubulin [GTU-88] antibodies. [B-F] Integrated intensities of the IRDye800 signal were measured using Odyssey V3.0. Values were normalised relative to levels of protein in the untagged negative control and levels of Mto1-TAPS in the eluates. Mto2D = *mto2Δ*. Image represents a typical result from two experiments.

interaction to be artificially high compared to full length Mto1. This result suggests that the effect of redistributing Mto1 away from the SPB is not likely to change the indispensability of Mto2 for the Mto1/γ-TuSC interaction during mitosis.

This result indicates that the Mto1 / γ-TuC complex formed at the SPB in metaphase is different to the nucleation complex active at non-SPB iMTOCs during interphase. There is no evidence to suggest that the metaphase complex is a functional nucleator as MTs are not nucleated from the cytoplasmic face of the SPB during metaphase, however, as *mto2Δ* cells are still able to nucleate astral MTs, this would suggest that the Mto2 is also not required for Mto1 to form an active nucleation complex during anaphase.

5.2.2 Identification of Mto2 phosphorylation sites

Evidence collected in this chapter indicates that Mto2 phosphorylation [and potentially Mto1 phosphorylation] during mitosis causes Mto2 to dissociate from the Mto1/2 complex. In order to determine whether Mto2 phosphorylation is the primary cause of this disruption, the phosphorylation sites of Mto2 were identified using a number of different biochemical and bioinformatics based methods. This analysis may also provide insight to the identity of the Mto2 kinase.

5.2.2.1 Identification of phosphorylation sites through alignment with homologous sequence from *Schizosaccharomyces japonicus*

Sequence conservation is a powerful tool to identify areas of a gene that are important for function, as these regions are less tolerant to changes in nucleotide and amino acid sequence. The *S. japonicus* genome was used to identify conserved regions of Mto2 as it was the closest relative to *S. pombe* whose genome sequence was publically available at the time this analysis was performed. The *S. japonicus* homolog of *S. pombe* Mto2 was identified as SJAG_03264.2 by performing a PSI-BLAST search (Altschul *et al.* 1997) of the *S. japonicus* genome. The alignment of the sequences is shown in Figure 5.9. Five conserved S/T-P putative phosphorylation sites were identified [T35, S179, S220, S366 and T394] and are highlighted in red. These sites are closely related to the CDK1 kinase consensus sequence of [S/T]–P–X–[R/K] (Endicott *et al.* 1999).

5.2.2.2 Phosphorylation site prediction by NetPhos 2.0

The NetPhos 2.0 server is a phosphorylation prediction software developed at the Centre for Biological Sequence Analysis, University of Denmark (Blom *et al.* 1999). NetPhos 2.0 gives each S/T/Y residue a score describing the likelihood that it is phosphorylated, as well as identifying the presence of that residue within kinase consensus sites. 45 out of 106 S/T/Y residues of Mto2 had a NetPhos score greater than 0.75. The scores for each S/T/Y residues are listed in Appendix IX.

CLUSTAL 2.0.10 multiple sequence alignment

```
Spombe          MSEHNYQSDREVAEDPFLNYEASANQLSSNSRES-----------------TPRGSPWRA 43
Sjaponicus      MSRLSFSPKKQLDADPFLDYEASTGLSERSHRTVGSFLHDSVSENVNEEPRTPFFGPNSS 60
                **. .:...:::  ****:****:.  . . *                  **  .*  :

Spombe          GMRSASLMTEPLEDSMYSDNNYLDNG-------VSFTKDENPLYSPSWPSLADANVNSMK 96
Sjaponicus      SFQAQSIFSPNSTFQGKSQQNLRPSSQRRGKFLFQHARSETTNVYGRFASSSPTRPRQLD 120
                .::: *:::     .  *::*   ..       ...::.*..     :.* : :. ..:.

Spombe          SNNAIQEHKAAKFVSEKSLEKVSTADN-NLVLQELENLRERLNQVELQLSERPSSYLGYH 155
Sjaponicus      LALTMNDNNSDTALERATQQLSLTSPQPQVRSRELEHTVPNPATNEFIFRELRSLRERLG 180
                   ::::::: . :.. : :   *: : ::  :***:   .    *: : *  *

Spombe          NNLSPYRSPNSYPSLLPSTHSPHSPAPLSTMQTALMRLRTYHPSPIILKPVEQAVNHAIT 215
Sjaponicus      QVEAELARTRMEATTTLTRASLSSPVPAQKLQLALQRLASHHPPDDVLKPLERAARNALL 240
                :  :    ..  .:   :  *  **.* ..:* ** ** ::**.  :***:*:*..:*:

Spombe          LVNTSPSSVVDALCRSLAELCLGLVQEAIDASILSQQESSNSLDLVRHTPPLN-YTSSVD 274
Sjaponicus      LTQTSPGPTVDALCRSLTETCLGLVQECLNARMLADESQTPRLPGPNGEEEMSGYATITA 300
                *.:***...********:* *******.::* :*::::.:  *   .    :. *:: .

Spombe          SSPQRMASDSYGRPSLHLNDPFPSVDLQSNELSHHNVRTTLFSDDSRFHSKIHTHSTPPS 334
Sjaponicus      ASTGESGRNSYSFPVPTTAFTAPTLTNTNNNNNSNNEGLGRFSNAHTIMTTPRSQRIIPP 360
                :*. . . :**. *      . *::   .*: . :*     **:   : :. :::   *.

Spombe          QMYSAASHFR---YRSDPSTRHVSNSTNKSSLHPSPTSLRVAHPIIPQRASPASQSFP-- 389
Sjaponicus      TSSPLSDRVKTPVLRDRDGDQMPASSRFQSKISLSPNRELRASPVSPRSPPFHRKRFSKT 420
                   . :.:.:    *.  . :  :.*  :*.:  **.    * *: *: ..   : *.

Spombe          ------------------SLQDTPSP---------------- 397
Sjaponicus      ASSNVLVTPANAYAQPPTHSAQSSPTRFSLIDKVLSGHRDSLS 463
                                  * *.:*:
```

Figure 5.9 Sequence alignment of Mto2 homologs from *S. pombe* and *S. japonicus*. BLAST search against the *S. japonicus* sequence database identified SJAG_03264.2 as a homologue of Mto2. The alignment was generated by Clustal W2 (Larkin, 2007 #561) where SJAG_03264.2 and Mto2 have a sequence identity score of 16.1%. The five identified conserved S / T - P putative phosphorylation sites are labelled in red.

5.2.2.3 Identification of Mto2 residues within kinase consensus sites

An additional method for predicting Mto2 phosphorylation sites was to identify residues within consensus sites of mitotic kinases. Three CDK1 kinase consensus sites [S/T]–P–X–[R/K] (Endicott *et al.* 1999) were identified. 17 sites were identified that contained degenerate Aurora A consensus sites following [S/T]-X[1,2]-[R/K] or [R/K]-X[1,2]-[S/T], where the strict consensus would contain the basic residues on both side of the phospho-serine/threonine (Dephoure *et al.* 2008). 28 sites were identified that contained degenerate POLO consensus sequence following [S/T]-X[1,2]-[D/E] or [D/E]-X[1,2]-[S/T], where the strict PLK1 consensus sequence would contain acidic amino acids on both sides of the phospho-serine/threonine (Nakajima *et al.* 2003; Dephoure *et al.* 2008). These are labelled in Appendix IX. Interestingly, upon further examination of the sequence, 3 polo-box domain [PDB] interaction sites were identified based upon the following consensus S-[S/T]-P-[X/R] (Elia *et al.* 2003b). These were T35, S267, and T331. These domains are the sites of Polo kinase binding, and are primed by phosphorylation [often by CDK1] prior to Polo association (Elia *et al.* 2003b).

5.2.2.4 Identification of fungal homologs of Mto2

Following the release of the *S. japonicus* genome, the genome sequences of several other fungal species, including *Schizosaccharomyces octosporus* were also released. PSI-BLAST was performed using the Mto2 sequence as bait to identify a number of additional Mto2 homologs. The sequences listed in table 5.3 are a

selection of fungal genes which gave HSPs with an e-score < $1e^{-02}$. As the annotation of these sequences has been generated automatically through sequence similarity to known proteins, the majority of Mto2 homologs have been assigned as putative LPXTG-cell wall anchor domain proteins. The LPXTG motif is found in bacterial cell wall proteins therefore it has no relevance to Mto2 function in yeast. The sequences from the fungal homologs were used to generate a phylogenetic tree to demonstrate the relative sequence divergence between Mto2 homologs [fig 5.10]. The *S. octosporus* sequence SOCG_01774.2, was the closest sequence with fewer amino acid substitutions. Amino acid sequences were entered into the MegAlign software program [Lasergene 8, DNAstar] and the alignment report is shown in Appendix V. This alignment was used to assess whether S/T/Y residues were conserved i.e. if present in 8/15 of the homologs. 41 out of 106 S/T/Y residues were conserved in the fungal alignment and 11 of these residues were S/T-P sites. 3 out of 5 of the S/T–P residues conserved in the alignment with SJAG_03264.2 were also conserved in the large scale fungal alignment.

5.2.2.5 Identification of 25 phosphorylation sites using two-step denaturing purification of Mto2-HTB and mass spectrometry analysis

A tandem affinity tag that contained 6 x histidine residues and a biotinylation site was developed in the laboratory of Peter Kaiser (Tagwerker *et al.* 2006). This permits consecutive purification on Ni^{2+}-bound and streptavidin-linked resins under strong denaturing conditions. These conditions are expected to preserve phosphorylation, as a result of inactivation of phosphatases.

Species	Genomic Locus	Description	Mto2 alignment score
Magnaporthe grisea	XP_359559	hypothetical protein MGG_05218	$5e^{-05}$
Neurospora crassa	XP_962857	hypothetical protein NCU06253	$4e^{-05}$
Gibberella zeae	XP_387151	hypothetical protein FG06975.1	$4e^{-05}$
Penicillium marneffei	XP_002144160	LPXTG-motif cell wall anchor domain protein, putative	$2e^{-07}$
Coccidioides immitis	XP_001248197	hypothetical protein CIMG_01968	$8e^{-06}$
Ajellomyces capsulatus	XP_001538699	predicted protein	$1e^{-04}$
Penicillium chrysogenum Wisconsin	XP_002562312	Pc18g04810	$5e^{-08}$
Aspergillus nidulans	XP_662149	hypothetical protein AN4545.2	$6e^{-05}$
Aspergillus clavatus	XP_001272930	LPXTG-motif cell wall anchor domain protein, putative	$2e^{-05}$
Neosartorya fischeri	XP_001265845	LPXTG-motif cell wall anchor domain protein, putative	$2e^{-05}$
Aspergillus fumigatus	XP_749412	LPXTG-motif cell wall anchor domain protein	$3e^{-06}$
Aspergillus niger	XP_001391788	hypothetical protein An07g07140	$8e^{-05}$
Schizosaccharomyces octosporus	SOCG_01774.2	MT organizer Mto2	$9.2e^{-43}$
Aspergillus terreus	XP_001218235	conserved hypothetical protein	$3e^{-06}$
Aspergillus flavus	XP_002379344	conserved hypothetical protein	$1e^{-04}$

Table 5.1 Fugal homologs of Mto2. Genes were identified by BLASTP searches. The sequence hits which gave HSP e-scores < $1e^{-2}$ are included. Full alignment is available in Appendix V.

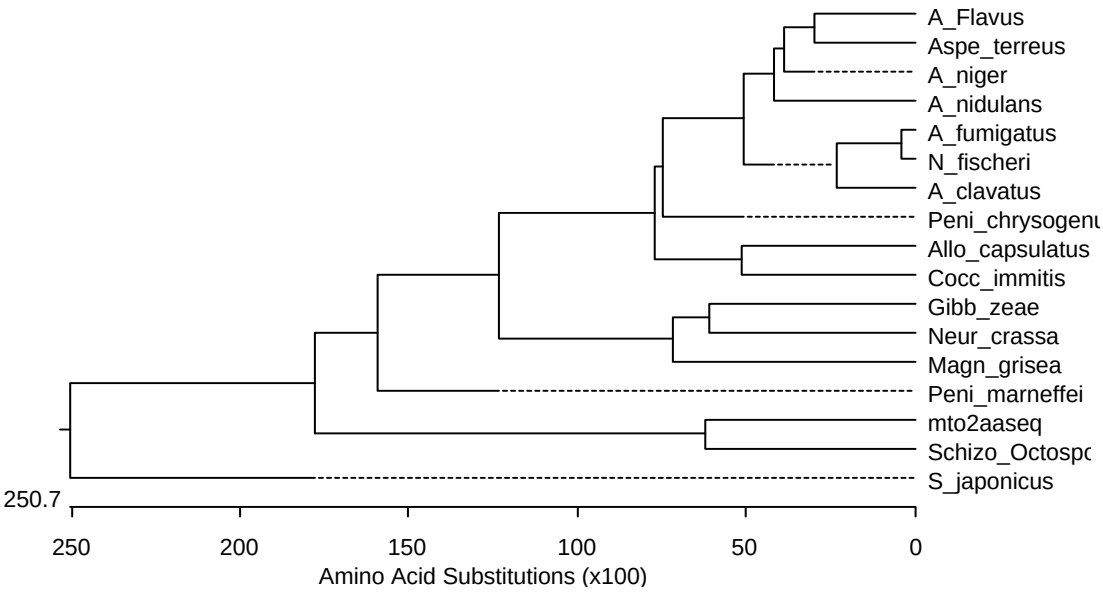

Figure 5.10 Phylogenetic tree generated from ClustalW alignment of Mto2 homologs. The sequences from homologs listed in table 5.1 were used to generate a phylogenetic tree that represents the divergence of the Mto2 sequence.

A two-step purification was performed as described in section 2.4.5.2.1. Two bands of a size corresponding to Mto2-HTB were excised from the gel, digested with trypsin, and analysed by the LTQ-Orbitrap Mass Spectrometer [fig 5.11, Panel A].

88 peptides from Mto2 were identified, and from these peptides 33 amino acid residues were shown to be phosphorylated. 25 of the predicted sites had an Identity score > 20 and were considered for further analysis. These sites included 19 serines, 4 threonines, and 2 tyrosines. The peptide assignments and identity scores for each residue are listed in table 5.1. If residues were identified in more than one peptide the highest identity score is given. Two of the serine residues had been previously identified as potential phosphorylation sites based on sequence alignment with *S. japonicus* SJAG_03264.2 [S179 and S366], and 10 residues were identified in the large-scale fungal alignment.

5.2.2.6 Identification of two mitosis specific phosphorylation sites using SILAC

I have previously shown by western blot that different isoforms of Mto2 exist during interphase [fig 5.2], indicating that Mto2 phosphorylation is not specifically a mitotic event. In order to identify mitotic phosphorylation sites, Stable Isotope Labelling of Amino acids in Cell culture [SILAC] was used to distinguish between phospho-peptides from mitotic and asynchronous Mto2. SILAC is a method used for quantitative proteomics developed in the laboratory of M. Mann (Ong *et al.* 2002). SILAC has been used for many proteomic applications e.g. mapping of protein-protein interactions and phosphorylation sites, and quantitation of translation and

protein degradation (Gruhler *et al.* 2005; Guerrero *et al.* 2006; Neher *et al.* 2006; Schwanhausser *et al.* 2009). SILAC is an accurate method for quantitative mass spectrometry as the isotopes are introduced at an early stage of sample preparation and have negligible effects on cell growth. Research performed by C. Bicho in our laboratory has developed a methodology that has enabled SILAC to be applied to fission yeast (Bicho *et al.*, manuscript in preparation).

A second mapping was performed on Mto2 isolated from both heavy labelled [$^{13}C6^{15}N4$-arginine and $^{13}C6^{15}N2$-lysine] asynchronous culture and 'light' non-labelled culture arrested in metaphase using an *nda3-KM311* arrest. Following the arrest, normalised numbers of cells from the two cultures were mixed and the resultant extract was used in a single step purification using an Mto2-TAPS binding to IgG-Dynabeads. Figure 5.12, Panel A shows the Coomassie stained SDS-PAGE gel containing a band representing purified Mto2-TAPS. The band was excised from the gel, digested with trypsin and analysed by the LTQ-Orbitrap Mass Spectrometer.

16 unique phosphorylation sites were found in 18 peptides [fig 5.12, Panel B; table 5.2]. The ratio of H/L is the quantitative amount of heavy labelled peptide to unlabelled peptide and reflects the ratio of interphase phosphorylation to mitotic phosphorylation. Therefore, ratios < 1 represent residues phosphorylated during mitosis, and ratios > 1 represent sites phosphorylated during interphase. Ratios were normalised relative to the ratio of total heavy to light protein present in the sample. The significance score was given to each phosphorylated residue based on comparison with a target-decoy database (Elias *et al.* 2007). Three significant residues [S2, S199 and S307] were identified [$p < 0.05$]. S2 was significantly enriched in the asynchronous extract, and S199 and S307 were significantly enriched

in the mitotic extract. None of these sites had been identified in the previous mapping, and only S307 was conserved in the large-scale fungal alignment. The identity scores of the 13 remaining sites were not significant [$p > 0.05$], and therefore were not assigned to mitotic or asynchronous extracts.

This phosphorylation site mapping has identified fewer phosphorylated residues compared to the previous analysis in section 5.2.2.5. I predict that this is due to a decrease in the amount of Mto2 analysed as a result of a two-fold reduction in the starting material used in the second mapping [30 g of cells vs. 15 g of cells]. 13 out of the 16 peptides identified in the second mapping were not statistically significant. This is likely to have been exacerbated by a ten-fold enrichment of peptides from metaphase arrested culture. It is possible that the over-representation of non-labelled protein is due to inefficient incorporation of the isotopes. To test this, random proteins were isolated from boiled extracts of cells grown in labelled isotopes. Analysis of the proteins by mass spectrometry demonstrated that isotope labels were being efficiently incorporated [data not shown]. Alternatively, it is possible that there was inaccurate mixing of the cultures prior to harvesting, therefore in future experiments extracts should be normalised after cell harvesting and extract preparation in order to minimise potential differences in protein levels.

A

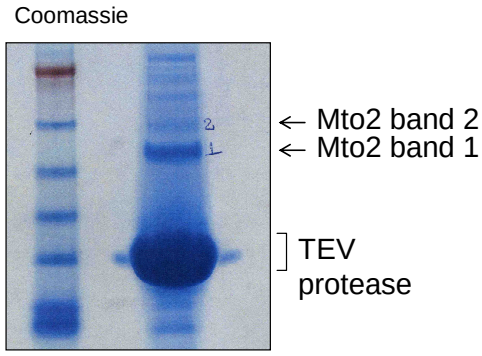

B

```
1    MSEHNYQSDR EVAEDPFLNY EASANQLSSN SRESTPRGSP WRAGMRSASL MTEPLEDSMY

61   SDNNYLDNGV SFTKDENPLY SPSWPSLADA NVNSMKSNNA IQEHKAAKFV SEKSLEKVST

121  ADNNLVLQEL ENLRERLNQV ELQLSERPSS YLGYHNNLSP YRSPNSYPSL LPSTHSPHSP

181  APLSTMQTAL MRLRTYHPSP IILKPVEQAV NHAITLVNTS PSSVVDALCR SLAELCLGLV

241  QEAIDASILS QQESSNSLDL VRHTPPLNYT SSVDSSPQRM ASDSYGRPSL HLNDPFPSVD

301  LQSNELSHHN VRTTLFSDDS RFHSKIHTHS TPPSQMYSAA SHFRYRSDPS TRHVSNSTNK

361  SSLHPSPTSL RVAHPIIPQR ASPASQSFPS LQDTPSP
```

Figure 5.11 Mto2 phosphorylation sites identified by mass spectrometry analysis of protein purified under denaturing conditions. [A] Purified Mto2 was analysed by 10% SDS-PAGE and the gel was stained with Coomassie [Strain KS3953]. Mto2 [right lane] was identified relative to molecular weight standards [left lane]. Mto2 bands 1 and 2 were analysed and the majority of Mto2 peptides were found in band 1. [B] The Mto2 amino acid sequence with the 25 identified phosphorylation sites indicated in red. Amino acid residue numbers indication on the left.

Residue number	Sequence	Residue	Top Mass Spec Identity Score
81	NPLY**S**PSWP	S	94
111	AKFV**S**EKSL	S	16
150	ERPS**S**YLGY	S	86
159	HNNL**S**PYRS	S	68
167	SPNS**Y**PSLL	Y	24
169	NSYP**S**LLPS	S	31
174	LLPS**T**HSPH	T	58
176	PSTH**S**PHSP	S	66
179	HSPH**S**PAPL	S	76
185	APLS**T**MQTA	T	58
264	LVRH**T**PPLN	T	71
269	PPLN**Y**TSSV	Y	69
271	LNYT**S**SVDS	S	85
272	NYTS**S**VDSS	S	52
275	SSVD**S**SPQR	S	52
276	SVDS**S**PQRM	S	76
282	QRMA**S**DSYG	S	36
284	MASD**S**YGRP	S	45
330	IHTH**S**TPPS	S	70
331	HTHS**T**PPSQ	T	77
334	STPP**S**QMYS	S	35
361	STNK**S**SLHP	S	42
362	TNKS**S**LHPS	S	42
366	SLHP**S**PTSL	S	29
369	PSPT**S**LRVA	S	30

Table 5.2 25 high-scoring phosphorylation sites identified by mass spectrometry analysis. 25/33 of the identified resides had an identity score > 20 and were considered for further analysis. These included 19 serines, 4 threonines, and 2 tyrosines. Peptide assignments and identity scores for the 25 residues are listed, where residues were identified in more than one peptide, the highest scores are listed above.

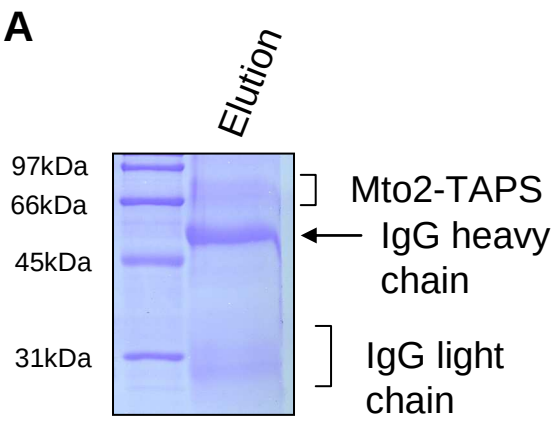

B

1 MSEHNYQSDR EVAEDPFLNY EASANQLSSN SRESTPRGSP WRAGMRSASL MTEPLEDSMY

61 SDNNYLDNGV SFTKDENPLY SPSWPSLADA NVNSMKSNNA IQEHKAAKFV SEKSLEKVST

121 ADNNLVLQEL ENLRERLNQV ELQLSERPSS YLGYHNNLSP YRSPNSYPSL LPSTHSPHSP

181 APLSTMQTAL MRLRTYHPSP IILKPVEQAV NHAITLVNTS PSSVVDALCR SLAELCLGLV

241 QEAIDASILS QQESSNSLDL VRHTPPLNYT SSVDSSPQRM ASDSYGRPSL HLNDPFPSVD

301 LQSNELSHHN VRTTLFSDDS RFHSKIHTHS TPPSQMYSAA SHFRYRSDPS TRHVSNSTNK

361 SSLHPSPTSL RVAHPIIPQR ASPASQSFPS LQDTPSP

Figure 5.12 Phosphorylation mapping of mitotic phosphorylation sites using SILAC identified two residues that were significantly enriched in metaphase arrested sample. [A] Mto2-TAPS was purified using IgG-linked Dynabeads [Strains KS5479 and KS5477]. Eluate was analysed by 10% SDS-PAGE and the gel was stained with Coomassie. [B] 16 phosphorylation sites were identified. 3 sites were found to be significantly enriched in either interphase or mitosis. Green = mitotic sites; blue = interphase sites; red = unassigned.

Residue number	Amino acid	Sequence window	Best Motif	Ratio H/L Normalized by Proteins	Significance
2	S	_____M**S**EHNYQS		7.6023	0.0002
81	S	DENPLY**S**PSWPSL		0.6439	0.2576
159	S	GYHNNL**S**PYRSPN	CDK2	0.523	0.1441
163	S	NLSPYR**S**PNSYPS	CK1	1.6237	0.1587
169	S	SPNSYP**S**LLPSTH	CK1	1.6237	0.1587
174	T	PSLLPS**T**HSPHSP	NEK6	1.6237	0.1587
176	S	LLPSTH**S**PHSPAP	CK1	0.6973	0.311
179	S	STHSPH**S**PAPLST		1.5083	0.1905
185	T	SPAPLS**T**MQTALM		1.6237	0.1587
199	S	LRTYHP**S**PIILKP	CK1	0.0983	6.28E-06
282	S	SPQRMA**S**DSYGRP	CAMK2	0.6894	0.3031
289	S	DSYGRP**S**LHLNDP	AURORA	0.8245	0.4358
303	S	PSVDLQ**S**NELSHH	GSK3	0.6894	0.3031
307	S	LQSNEL**S**HHNVRT	CK1	0.1531	0.0002
331	T	KIHTHS**T**PPSQMY	Polo box	0.5396	0.1587
366	S	KSSLHP**S**PTSLRV	NEK6	1.1906	0.3159

Table 5.3 Phosphorylation sites identified by mass spectrometry analysis of purified Mto2 using SILAC. 16 phosphorylation sites were identified. The ratio of H [heavy] / L [light] was normalised relative to total protein levels, and represents quantitative interphase/mitotic levels. The significance of each score was plotted and those residues with $p < 0.05$ were considered for further analysis.

5.2.3 Generation of phosphorylation mutants and analysis of phenotypes

Having identified a number of candidate phosphorylation sites on the Mto2 protein, a series of mutants were generated based on different criteria. For historical reasons, the phenotypic analyses of the preliminary mutants described in this section were based on cellular localisation of HFG-Mto2. The results described in the first part of this chapter show that phosphorylation by CDK1-Cyclin B disrupts the Mto1/2 complex, therefore, I predict that the Mto1-Mto2 interaction would be maintained by the introduction of non-phosphorylatable mutations. As wild-type Mto2 co-localises with Mto1 throughout the cell cycle, the subsequent maintenance of the Mto1-Mto2 interaction would not change Mto2 localisation. Alternatively, phospho-mimetic mutants could cause a constitutive disruption of the Mto1-Mto2 interaction and subsequently all HFG-Mto2 localisation would be lost, however, it would difficult to distinguish between loss of function due to the disruption of the Mto1-Mto2 interaction and loss of function due to perturbation of Mto2 protein folding.

Consequently, the phenotype of phospho-mutants constructed in the latter part of this section were assayed based on the nuclear envelope localisation of Mto1 [1-549]-GFP. In section 5.2.1.6 and 5.2.1.7, I showed that Mto1 [1-549]-GFP localisation at the nuclear envelope is dependent on Mto2 [most likely through the formation of the Mto1/2 complex] and that this localisation is lost during mitosis. This suggests that disruption of the Mto1/2 complex during mitosis is sufficient to dissociate the complex from the nuclear envelope. Therefore the nuclear envelope

localisation was used to indirectly assay the disruption of the Mto1/2 complex containing non-phosphorylatable Mto2 mutants. I predicted that as Mto2 is not phosphorylated, the Mto1 [1-549]-GFP / Mto2 complex, and subsequently the nuclear envelope localisation of Mto1 [1-549]-GFP would be maintained in mitosis.

However, this prediction is based on the assumption that maintenance of the Mto1/2 complex is sufficient to sustain nuclear envelope localisation during mitosis. It is possible that other factors may be involved, e.g. disruption of the interaction between Mto1 and the unidentified nuclear envelope protein. Consequently, biochemical methods are required to directly determine whether the Mto1-Mto2 interaction has been maintained during mitosis in the Mto2 non-phosphorylatable mutant background.

5.2.3.1 Phenotypic analysis of Mto2 phospho-mutants derived from conservation with *S. japonicus*

Five S/T-P residues conserved within the alignment of *S. japonicus* SJAG_03264.2 were mutated to alanine using site-directed mutagenesis. A sixth mutant was constructed that contained S/T → A mutations for all five sites. Each mutant was recombined into an *nmt81*:HFG-tagging vector (Matsuyama *et al.* 2004) and transformed into *mto2Δ* [KS976]. Control images were taken of both endogenous Mto2-GFP and *nmt81*:HFG-Mto2. Figure 5.13 demonstrates that the localisation of Mto2 at the eMTOC, iSPB, mSPB and MT-associated satellites in all six mutants was comparable to both wild-type controls. Examination of the mitotic cells demonstrates that there are no residual iMTOCs, and the level of Mto2 at the

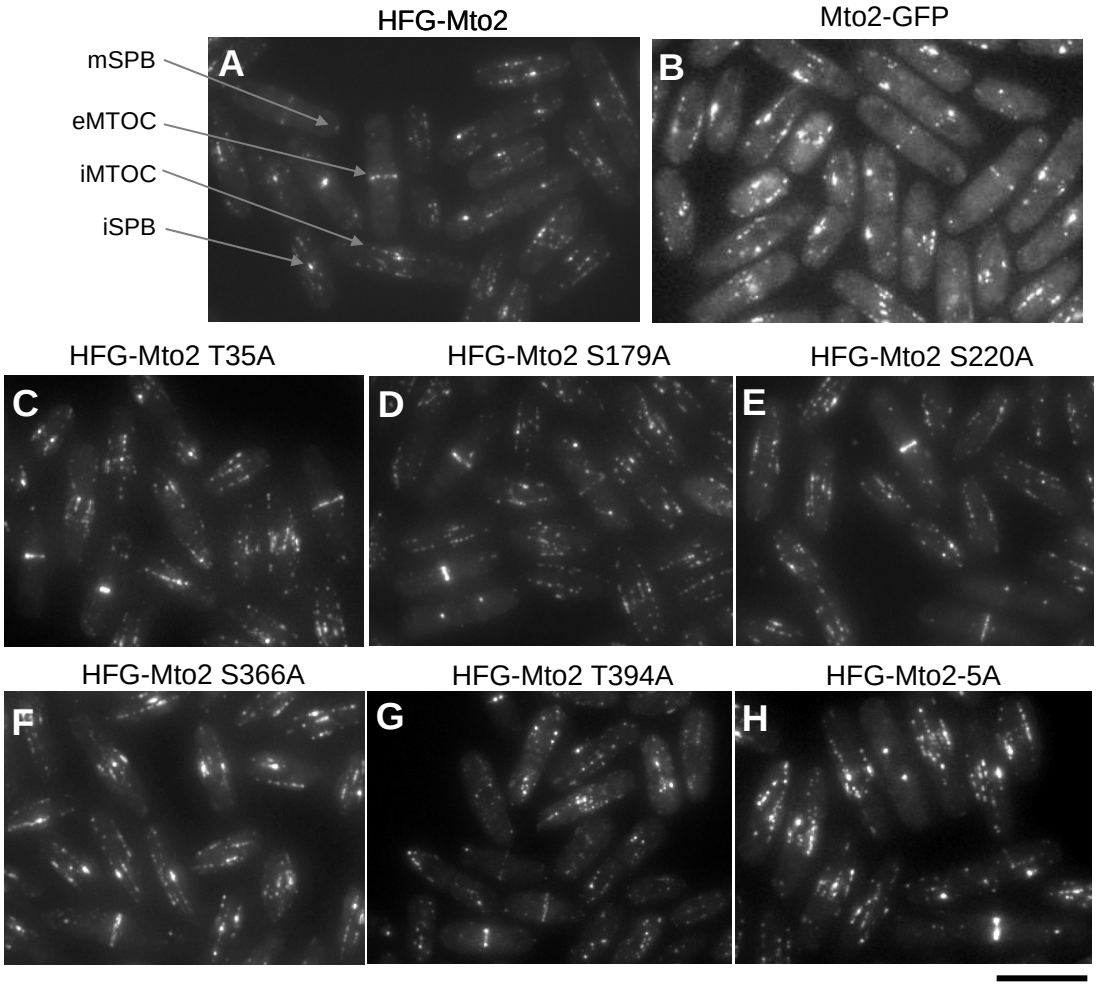

Figure 5.13 Phenotypic analysis of alanine mutants identified by conservation of Mto2 S/T-P sites with *S. japonicus* demonstrated that there were no defects in cellular localisation compared to WT. [Strains KS1460, KS3915, KS3923, KS3925, KS3927, KS3929, KS3931 and KS3933]. Maximum projections of wide-field images taken of HFG-Mto2. WT MTOCs indicated [grey arrows]. Scale bar = 10 µm.

SPB and eMTOC appears to be normal. Following this analysis, several other fungal homologs of Mto2 were identified, including the *S. octosporus* homolog SOCG_01774.2. This sequence was found to be significantly more closely related to Mto2 than *S. japonicus* SJAG_03264.2. The alignment with all fungal homologs showed that only two of the five S/T-P sites that were mutagenised in this analysis were conserved in other fungi [Appendix V]. Based on this observation, it is unlikely that further analysis would demonstrate that these non-phosphorylatable mutants could prevent the Mto1/2 complex dissociating in mitosis.

5.2.3.2 Phenotypic analysis of Mto2 phospho-mutants derived from mass spectrometry mapping

The 25 phosphorylation sites identified by the initial mass spectrometry analysis can be roughly divided into three clustered groups as shown in Figure 5.14, Panel A. These groups were separately targeted for mutagenesis. For all three groups, sequences that contained both non-phosphorylatable S/T→A and phospho-mimetic S/T→D substitutions were constructed. HFG-tagged mutants were constructed through recombination into an *nmt81:HFG* N-terminal tagging vector (Matsuyama *et al.* 2004). The sequences were transformed into *mto2Δ Atb2-GFP* [KS1409], where Mto2 was expressed from an *nmt81* promoter at the *leu1* locus. Figure 5.14, Panel B, shows the MT distribution in the HFG-Mto2 block mutant background. This was quantified in Figure 5.14, Panel C [summarised in table 5.4]. Mto2 localisation and MT length/number were compared for the six phosphorylation site mutants. The most striking difference in MT bundle number and length was observed for the

Mto2-1D mutant. HFG-Mto2-1D had fewer MT bundles [2.525 ± 0.733] than wild-type [3.737 ± 0.943], and the distribution of short to long MT bundles resembled the profile observed for *mto2Δ* strain [in *mto2Δ*, 80% of the MT bundles were longer than half the length of the cell]. Mto2-1A and Mto2-2A had the same number of MT bundles as wild-type but a higher proportion of short MT bundles. The significance of this observation is unclear.

These results suggest that the function of Mto2 has been compromised in HFG-Mto2 1D, particularly in relation to MT nucleation during interphase. The nature of this analysis meant that maintenance of the Mto1/2 complex in HFG-Mto2 1A could not be detected. However, due to the stronger phenotype, the properties of HFG-Mto2 1D were analysed further. This mutant is particularly interesting, as the mutated sites are close to the coiled-coil domain which is predicted to facilitate the Mto1-Mto2 interaction as described in chapter four.

5.2.3.3 MBP-Mto2 1D is able to interact with wild-type Mto2 and Mto1

In vivo characterisation of HFG-Mto2 1D suggests that the function of Mto2 has been compromised. In order to test this further both the Mto2-Mto2 and Mto1-Mto2 interaction of Mto2 1D were analysed *in vitro*. Figure 5.15, Panel A and B show amylose pulldown assays using MBP-Mto2 1D as bait. In fig 5.15, Panel A NusA-Mto2 protein was pulled down by both MBP-Mto2 and MBP-Mto2 1D at comparable levels, indicating that the phosphorylation site mutants did not affect the ability of Mto2 to self-interact. Figure 5.15, Panel B shows that Mto1-13myc was co-precipitated in the presence of MBP-Mto2 at similar levels for both wild-type and

A

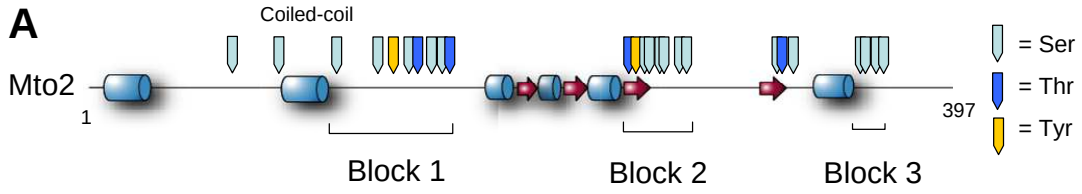

Block 1A	S159A, S169A, T174A, S176A, S179A, T185A
Block 2A	S275A, S276A, S282A, S284A
Block 3A	S361A, S362A, S366A, S369A
Block 1D	S169D, T174D, S176D, S179D
Block 2D	S282D, S284D
Block 3D	S366D, S369D

B

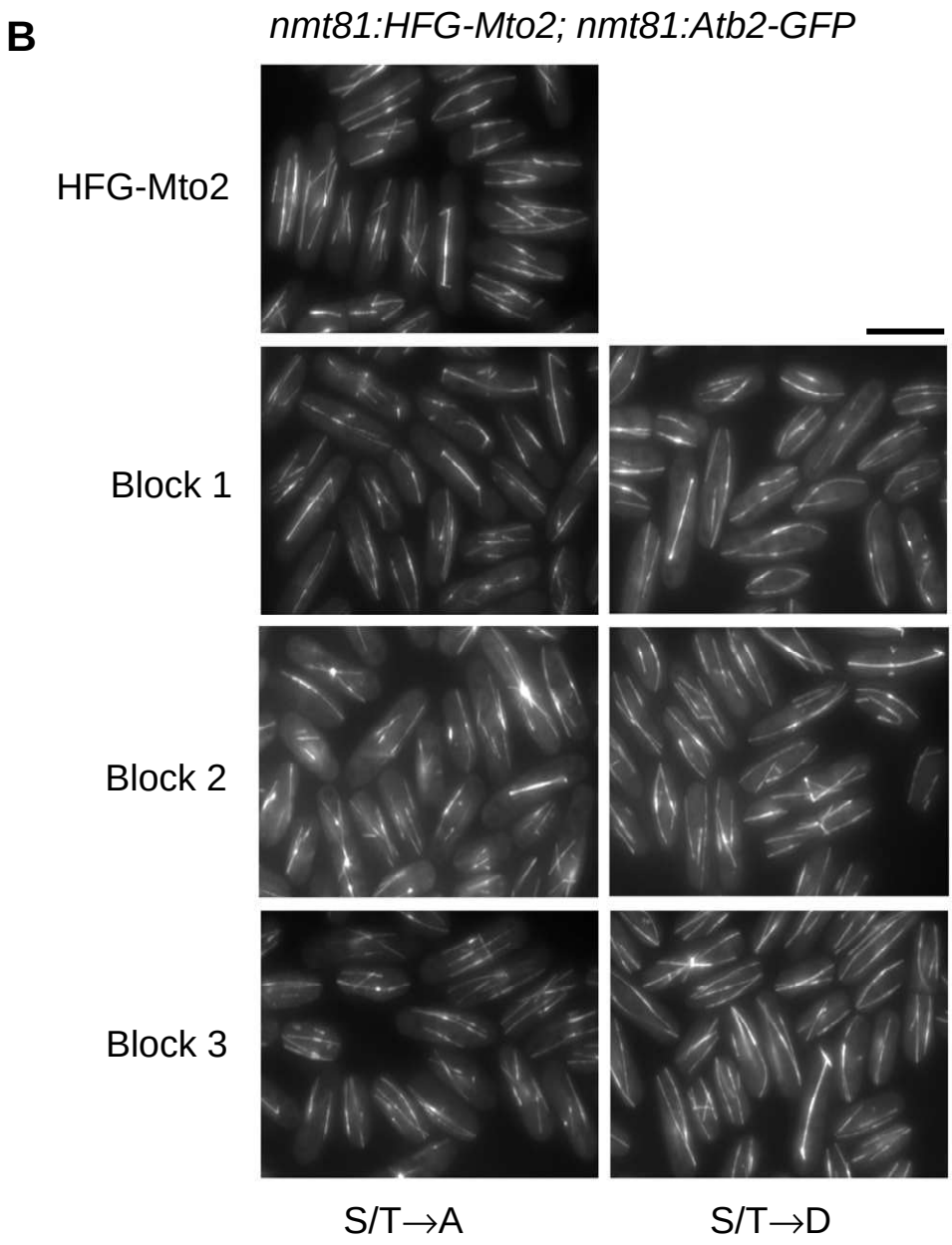

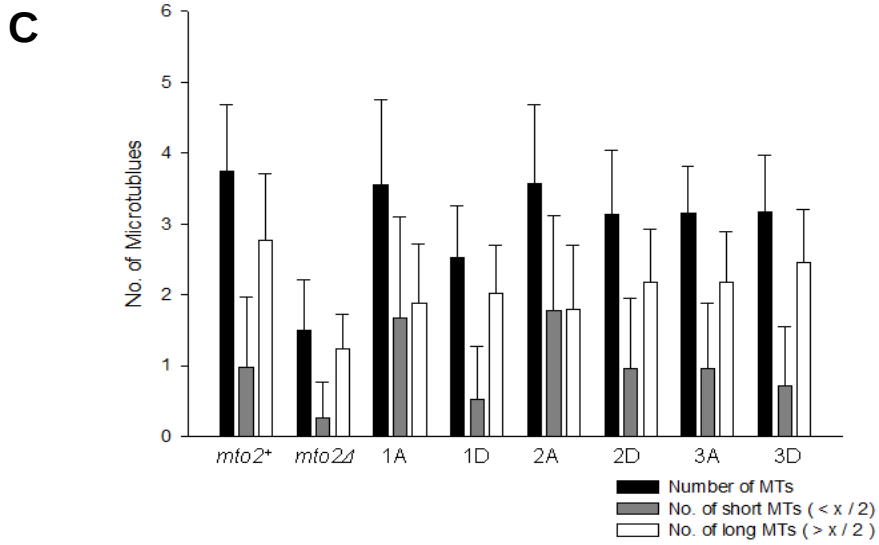

Figure 5.14 Analysis of MT dimensions in Mto2 large scale phospho-mutant demonstrates that Mto2 1D has a weak *mto2Δ*-like phenotype. [Strains KS1409, KS3915, KS4466, KS4469, KS4472, KS4475, KS4478 and KS4481] [A] Schematic diagram of 25 phosphorylation sites of Mto2 identified by mass spectrometry superimposed on predicted secondary structure. α-helix [blue cylinders], β-sheet [red arrows]. S/T/Y residues as indicated were divided into 3 Blocks. [B] Maximum projections of widefield images of HFG-tagged block mutants. Scale bar = 10 µm. [C] Quantitation of MT bundle number and length. X = length of the cell. Error bars are calculated from standard deviation.

Mutant	Mean No. of MT bundles (n = 100)	Significance compared with WT	% Short MT	% long MT	Mean No. of short MT bundles (n = 100)	Mean No. of long MT bundles (n = 100)
WT	3.737 ± 0.943		25.9	74	0.97 ± 0.989	2.768 ± 0.941
Mto2D	1.505 ± 0.705	p < 0.001	17.5	82.5	0.263 ± 0.504	1.242 ± 0.473
1A	3.364 ± 1.331	p = 0.235	50.7	49.3	1.705 ± 1.368	1.879 ± 0.832
1D	2.525 ± 0.733	p < 0.001	20.4	79.6	0.515 ± 0.747	2.010 ± 0.692
2A	3.566 ± 1.117	p = 0.244	49.6	50.42	1.768 ± 1.347	1.798 ± 0.899
2D	3.131 ± 0.900	p < 0.001	30.3	69.7	0.949 ± 0.989	2.182 ± 0.730
3A	3.141 ± 0.670	p < 0.001	30.6	69.4	0.960 ± 0.920	2.182 ± 0.702
3D	3.162 ± 0.804	p < 0.001	22.4	77.64	0.707 ± 0.832	2.455 ± 0.742

Table 5.4 Quantitative analysis of MT length and number in large scale phospho-mutants. Statistical analysis was performed using Students unpaired t test for comparison between two data sets. Mean values ± SD [Standard Deviation]. P values < 0.05 indicate a significance when compared to WT control. Mto2D = *mto2Δ*.

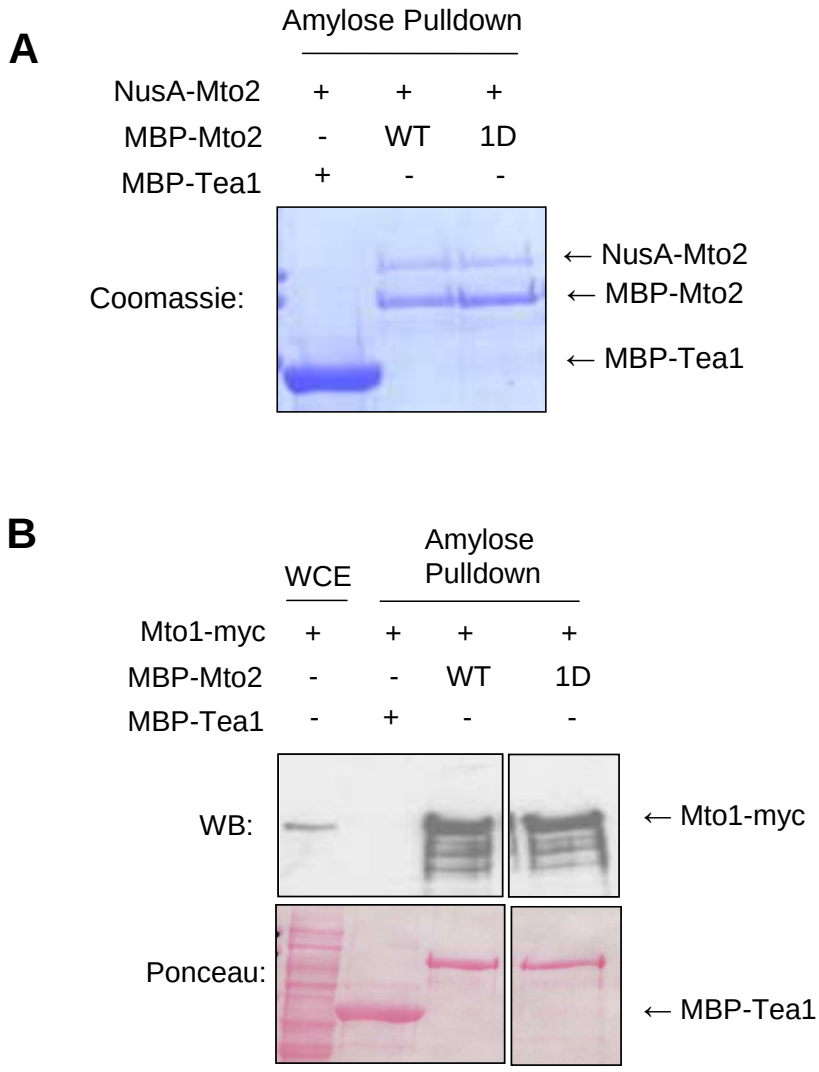

Figure 5.15 Biochemical analysis of Mto2-1D demonstrated that it is able to interact with recombinant Mto2 and Mto1 from yeast extract. Bacterial extract containing either MBP-Mto2 or MBP-Mto2 1D was incubated with either [A] bacterial NusA-Mto2 or [B] yeast extract containing Mto1-13Myc [KS1507]. Eluates were analysed by 10% SDS-PAGE and the gel was stained with Coomassie or the western blot was probed with anti-myc [9E10] antibody. Signal from anti-mouse-HRP secondary antibody was detected with ECL. WCE = whole cell extract. Images represent the result of a single experiment.

Mto2 1D mutant. This indicates that the phospho-mimetic mutations of the Block 1 residues do not affect the Mto1-Mto2 interaction. This contradicts the *in vivo* evidence which suggests that the Mto1-Mto2 interaction may have been disrupted in these mutants. One possible explanation is that *in vitro,* Mto2 1D lacks additional phosphorylated residues required to fully disrupt the Mto1-Mto2 interaction. Alternatively, as suggested by the analysis of the Mto2 coiled-coil mutant in chapter four, it is possible that small changes in the efficiency of the Mto1-Mto2 interaction that may not be detectable *in vitro*, may be sufficient to alter the function of the Mto1/2 complex. More direct methods should be used to assay the Mto1-Mto2 interaction in the Mto1-1D/1A mutant background such as those described in section 5.2.1.3.

5.2.3.4 Phenotypic analysis of tyrosine phosphorylation mutants

The mass spectrometry analysis of Mto2 purified under denaturing conditions identified two potential tyrosine phosphorylation sites [Y167, Y269]. To test whether phosphorylation of these residues is important for Mto2 function, Y168 and Y269 were mutated to non-phosphorylatable phenylalanine using site directed mutagenesis. Mutated sequences were then recombined into an N-terminal *nmt81:HFG* tagging vector (Matsuyama *et al.* 2004) and integrated into an *mto2Δ* strain under the *nmt81* promoter at the *leu1* locus. Figure 5.15, Panel A shows that for both mutants there were no observable defects in protein localisation at iMTOC, eMTOC, iSPB and mSPB, compared to wild-type HFG-Mto2. The large-scale fungal alignment showed that neither of the tyrosine residues were conserved [Appendix V]. Based on this

observation, it is unlikely that phosphorylation of these residues contributes to the disruption of the Mto1/2 complex during mitosis.

5.2.3.5 Biochemical analysis of purified Mto2 demonstrates that there is no tyrosine phosphorylation

To confirm that Mto2 is not phosphorylated on tyrosine residues, Mto2 was purified by performing an anti-Mto2 immunoprecipitation from extracts taken during a *cdc25-22ts* cell cycle block and release. These extracts were then probed with an antibody raised against phospho-tyrosine. Figure 5.16, Panel B shows that when compared with the positive control there was no detectable signal from purified Mto2. This indicates that, despite the obvious phosphorylation shift in Mto2 [shown when the western blot is probed with anti-Mto2], the tyrosine residues in Mto2 are not phosphorylated. This suggests that tyrosine residues identified by the mass spectrometry analysis in section 5.2.2.5 [Y168, Y269] may be false-positive identifications or the stoichiometry of this phosphorylation is below detectable levels, possibly having been lost during the preparation of native extract.

5.2.3.6 Design of Mto2 combinatorial phosphomutants

Six phospho-variants containing non-phosphorylatable S/T→ A mutations were designed based on combined evidence from bioinformatic and biochemical identification methods. Variant 1 [table 5.5] contained 17 mutations which were targeted if they had a NetPhos score greater than 0.9, and were either conserved in

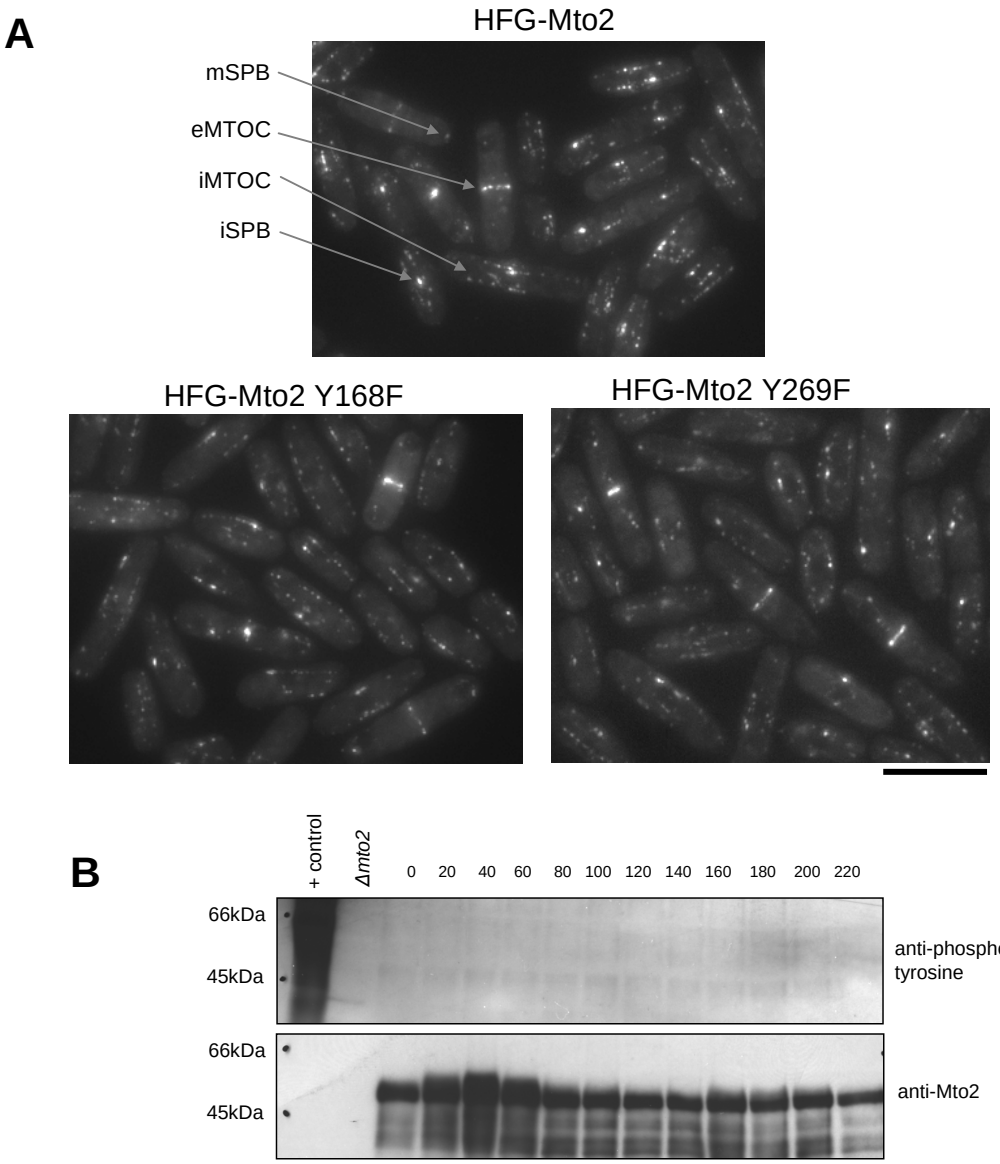

Figure 5.16 Lack of phospho-tyrosine signal and WT phenotype of Mto2-Y168F and Mto2-Y269F mutants suggests that Mto2 is not phosphorylated at tyrosine resides. [A] Maximum projections of wide-field images taken of HFG-Mto2-Y168F and HFG-Mto2-Y269F. [Strains KS3915, KS4185 and KS4186] WT MTOCs indicated [grey arrows]. Scale bar = 10 µm. [B] Mto2 was purified by anti-Mto2 immunoprecipitation from extracts made from samples taken every 20 min following release from a *cdc25-22ts* G_2 arrest [KS1280]. Eluates were analysed by SDS-PAGE and the western blot was probed with an anti-phospho-tyrosine antibody and anti-Mto2. EGF-stimulated mouse embryo extract was used as a positive control. Image represents the result of a single experiment.

8/14 species within the fungal alignment or identified in either of the two mass spectrometry based mappings. Variant 1 also contained all three residues that were identified within a PBD interaction site consensus sequence [S-S/T-P-X-R] (Elia *et al.* 2003b). Variant 2 contained 10 S/T-P sites identified by an *in vitro* CDK1 kinase assay performed in the laboratory of K. Gould, Vanderbuilt U.S.A. (Rosenburg, J. 2007) [table 5.6]. Variant 3 contained 14 mutations of sites that were found within a degenerate Aurora A consensus sequence following [S/T]-X[1,2]-[R/K] or [R/K]-X[1,2]-[S/T] [table 5.7] (Dephoure *et al.* 2008). Variant 4 contained 10 mutations in sites that were found within a degenerate PLK-1 consensus sequence following [S/T]-X[1,2]-[D/E] or [D/E]-X[1,2]-[S/T] [table 5.8] (Nakajima *et al.* 2003; Dephoure *et al.* 2008).

5.2.3.7 Mto2 phosphorylation does not affect the Mto1 [1-549]-GFP nuclear envelope localisation during mitosis

Four Mto2 phospho-variants were synthesised by GeneART [Germany]. Mutagenised Mto2 sequences containing 2 X STOP codons were recombined into a C-terminal *nmt81:GFH*-tagging vector and integrated into the genome where it was expressed from an *nmt81* promoter at the *leu1* locus. Transformed strains contained Cut12-tdTomato in order to identify mitotic cells [indicated by duplicated SPBs] and Mto1 [1-549]-GFP to detect the persistence of the Mto1-Mto2 interaction in mitosis through the localisation of Mto1 [1-549]-GFP at the nuclear envelope.

Figure 5.17 shows that all four of the Mto2 phospho-variants displayed Mto1 [1-549]-GFP nuclear envelope localisation during interphase, indicating that the folding and stabilisation of the Mto2 protein has not been affected by the mutations. Examination of the signal from Cut12-tdTomato in all four of the mutants demonstrated that Mto1 [1-549]-GFP did not localise to the nuclear envelope in mitosis. To examine the phosphorylation state of the Mto2 phospho-variants, extracts from each strain were analysed by western blot. Figure 5.18 shows that the level of hyperphosphorylation in Variant 3 and 4 is comparable with wild-type *nmt81:Mto2*, indicating that it is unlikely that Polo or Aurora kinases contribute to Mto2 phosphorylation. However, the hyperphosphorylation of Variant 1, and to a lesser extent Variant 2, was significantly reduced compared to wild-type. This suggests that the majority of the sites that have been targeted for mutagenesis in Variant 1 are genuine phosphorylation sites. Interestingly, this mutant contains three out of six of the Block 1 sites identified by both mass spectrometry mappings, which gave an *mto2Δ*-like phenotype when mutated to aspartate. This confirms that these sites appear to be significant in Mto2 function. The western blot also indicates that the C-terminal GFH tag is not expressed [expectant molecular weight of Mto2-GFH is 74 kDa].

As this assay does not examine the Mto1-Mto2 interaction directly, I cannot say conclusively whether the Mto1/2 complex remains intact during mitosis in the Variant 1 background. However, if the Mto1/2 complex has been maintained, this result suggests that although disruption of the Mto1/2 complex may be sufficient to dissociate Mto1 [1-549]-GFP from the nuclear envelope, maintenance of the complex is not sufficient to keep it at the nuclear envelope during mitosis. This

would indicate that there may be other mechanisms in place to ensure that Mto1 is removed from the nuclear envelope.

Alternatively, if the Mto1/2 complex has not been disrupted, this indicates that Mto2 phosphorylation does not contribute to the dissociation of the Mto1/2 complex. To confirm the Mto1-Mto2 interaction in the phospho-Variant 1 background in mitosis, co-precipitation of Mto2 in an Mto1-TAPS pull down assay could be compared between asynchronous and metaphase arrested extract, as described in section 5.2.1.3.

Residue Number	Sequence	Residue	NetPhos Score	S/T/Y-P site	Consensus	Conserved in Eukaryote Alignment	Identified in Rosenburg Kinase Assay	Identified by Mass Spec	Identified by Mitotic Mass Spec
35	SRES**T**PRGS	T	0.996	yes	AURORA	yes	yes		
39	TPRG**S**PWRA	S	0.994	yes	AURORA/CDK	yes	yes		
81	NPLY**S**PSWP	S	0.926	yes		yes		yes	yes
159	HNNL**S**PYRS	S	0.979	yes	CDK		yes	yes	yes
176	PSTH**S**PHSP	S	0.93	yes		yes		yes	yes
179	HSPH**S**PAPL	S	0.994	yes		yes		yes	yes
220	LVNT**S**PSSV	S	0.964	yes		yes			
264	LVRH**T**PPLN	T	0.169	yes	AURORA	yes	yes	yes	
271	LNYT**S**SVDS	S	0.955			yes		yes	
276	SVDS**S**PQRM	S	0.985	yes	CDK	yes	yes	yes	
282	QRMA**S**DSYG	S	0.982		AURORA	yes		yes	yes
314	NVRT**T**LFSD	T	0.89		AURORA	yes			
331	HTHS**T**PPSQ	T	0.578	yes			yes	yes	yes
341	YSAA**S**HFRY	S	0.978			yes			
366	SLHP**S**PTSL	S	0.964	yes			yes	yes	yes
394	SLQD**T**PSP-	T	0.772	yes		yes	yes		
396	QDTP**S**P---	S	0.325	yes		yes	yes		

Table 5.5 Mutated residues in Mto2 phospho-variant 1. Mutant contained S/T→A substitution at sites that had a NetPhos prediction score greater than 0.9 in addition to either being identified in the mass spectrometry mapping or conserved in 8/15 species in the fungal alignment. Residues were also included if present within a PBD recognition site consensus [17 sites].

Residue Number	Sequence	Residue	NetPhos Score	S/T/Y-P site	Consensus	Conserved in Eukaryote Alignment	Identified in Rosenburg Kinase Assay	Identified by Mass Spec	Identified by Mitotic Mass Spec
35	SRES**T**PRGS	T	0.996	yes	AURORA	yes	yes		
39	TPRG**S**PWRA	S	0.994	yes	AURORA/CDK	yes	yes		
159	HNNL**S**PYRS	S	0.979	yes	CDK		yes	yes	yes
264	LVRH**T**PPLN	T	0.169	yes	AURORA	yes	yes	yes	
276	SVDS**S**PQRM	S	0.985	yes	CDK	yes	yes	yes	
331	HTHS**T**PPSQ	T	0.578	yes			yes	yes	yes
366	SLHP**S**PTSL	S	0.964	yes			yes	yes	yes
382	PQRA**S**PASQ	S	0.992	yes	AURORA		yes		
394	SLQD**T**PSP-	T	0.772	yes		yes	yes		
396	QDTP**S**P---	S	0.325	yes		yes	yes		

Table 5.6 Mutated residues in Mto2 phospho-variant 2. Mutant contained S/T→A substitution of sites identified in CDK-1-Cyclin B *in vitro* kinase assay [10 sites] [Rosenburg, J. 2007].

Residue Number	Sequence	Residue	NetPhos Score	S/T/Y-P site	Consensus	Conserved in Eukaryote Alignment	Identified in Rosenburg Kinase Assay	Identified by Mass Spec	Identified by Mitotic Mass Spec
35	SRES**T**PRGS	T	0.996	yes	AURORA	yes	yes		
39	TPRG**S**PWRA	S	0.994	yes	AURORA/CDK	yes	yes		
49	MRSA**S**LMTE	S	0.888		AURORA				
111	AKFV**S**EKSL	S	0.965		AURORA			yes	
150	ERPS**S**YLGY	S	0.982		AURORA	yes		yes	
195	MRLR**T**YHPS	T	0.279		AURORA	yes			
264	LVRH**T**PPLN	T	0.169	yes	AURORA	yes	yes	yes	
282	QRMA**S**DSYG	S	0.982		AURORA	yes		yes	yes
289	YGRP**S**LHLN	S	0.981		AURORA				yes
314	NVRT**T**LFSD	T	0.89		AURORA	yes			
324	SRFH**S**KIHT	S	0.988		AURORA				
355	TRHV**S**NSTN	S	0.916		AURORA	yes			
362	TNKS**S**LHPS	S	0.782		AURORA			yes	
382	PQRA**S**PASQ	S	0.992	yes	AURORA		yes		

Table 5.7 Mutated residues in Mto2 phospho-variant 3. Mutant contained S/T→A substitution of sites found within Aurora kinase consensus sequence [14 sites].

Residue Number	Sequence	Residue	NetPhos Score	S/T/Y-P site	Consensus	Conserved in Eukaryote Alignment	Identified in Rosenburg Kinase Assay	Identified by Mass Spec	Identified by Mitotic Mass Spec
31	LSSN**S**REST	S	0.988			yes			
35	SRES**T**PRGS	T	0.996	yes	AURORA	yes	yes		
114	VSEK**S**LEKV	S	0.902		POLO	yes			
119	LEKV**S**TADN	S	0.955		POLO				
149	SERP**S**SYLG	S	0.938			yes			
223	TSPS**S**VVDA	S	0.995			yes			
271	LNYT**S**SVDS	S	0.955					yes	
276	SVDS**S**PQRM	S	0.985	yes	CDK	yes	yes	yes	
303	VDLQ**S**NELS	S	0.221		POLO				yes
390	QSFP**S**LQDT	S	0.992						

Table 5.8 Mutated residues in Mto2 phospho-variant 4. Mutant contained S/T→A substitution of sites found within Polo kinase consensus sequence [10 sites].

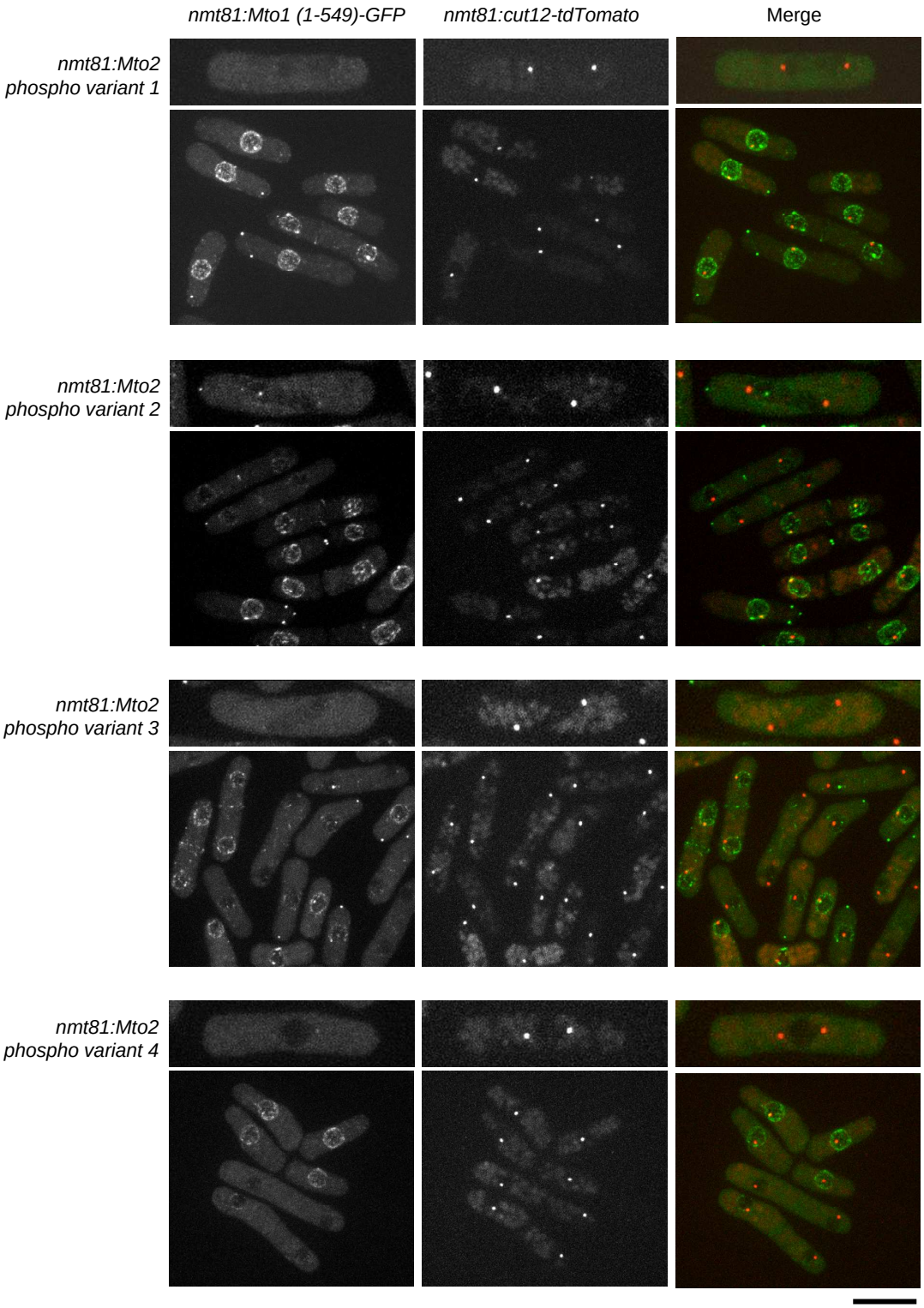
nmt81:Mto1 (1-549)-GFP
nmt81:cut12-tdTomato
Merge
nmt81:Mto2 phospho variant 1
nmt81:Mto2 phospho variant 2
nmt81:Mto2 phospho variant 3
nmt81:Mto2 phospho variant 4

Figure 5.17 NE localisation of Mto1 [1-549]-GFP in Mto2 phospho-mutant variants is comparable to WT Mto2. Maximum projections of confocal images taken of *nmt81*:Mto1 [1-549]-GFP and Cut12-tdTomato. Mitotic cell is shown in the top frame for each mutant [Strains KS5972, KS5973, KS5974, KS5975]. Mto2 was expressed under an *nmt81* promoter at the *leu1* locus. Scale bar = 10 µm.

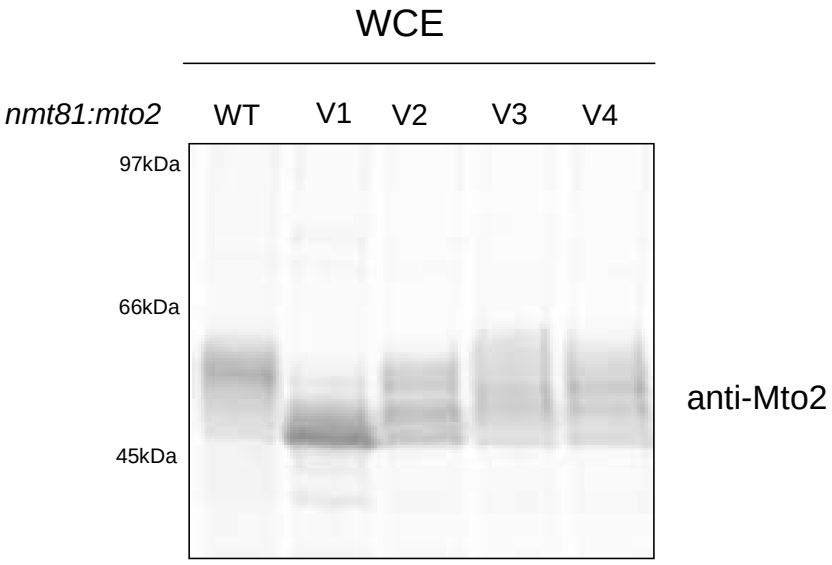

Figure 5.18 Western blot analysis of Mto2 phospho-variants. Extracts from WT Mto2 and Mto2 phospho-variants 1-4 were analysed by SDS-PAGE and the western blot was probed with anti-Mto2 antibody. The signal from IRDye800 was detected using Odyssey V3.0. [Strains KS5972, KS5973, KS5974, KS5975]. Molecular weight standards are indicated. Image represents the result of a single experiment.

5.3 SUMMARY OF RESULTS

In this chapter I demonstrated that Mto2 is phosphorylated. Mto2 phosphorylation was found to be regulated in a cell cycle-dependent manner, increasing as cells entered mitosis. Co-immunoprecipitation experiments demonstrated that when cells were arrested in metaphase, Mto2 was unable to interact with Mto1. The mitotic disruption was confirmed when the Mto1-Mto2 interaction was followed over the whole cell cycle.

In the process of analysing the localisation of the Mto1 truncation, Mto1 [1-549], I discovered that Mto1 [1-549]-GFP localisation at the nuclear envelope was dependent on Mto2. Upon further examination, I found that Mto1 [1-549]-GFP localisation at the nuclear envelope was disrupted as cells entered mitosis and returned during telophase. Based on this result, I conclude that the dissociation of Mto1 [1-549]-GFP from the nuclear envelope results from the disruption of the Mto1/2 complex most likely as a consequence of Mto2 phosphorylation.

Analysis of the Mto1 / γ-TuSC interaction revealed that Mto2 is not required for Mto1 to efficiently interact with the γ-TuSC during mitosis. This is not surprising given that astral MTs are nucleated in *mto2Δ* strains. This result suggests that a different Mto2-independent Mto1 complex is assembled at mSPBs [and probably iSPBs] compared with the Mto2-dependent Mto1 complex assembled at non-SPB iMTOCs. It is possible that Mto2 may not be required for nucleation from the SPB [and eMTOC to a lesser extent] as the high local concentration of low affinity γ-TuSC / Mto1 interactions may be sufficient to support MT nucleation. However, this result is contradicted by the localisation of Mto2 to the mSPB *in vivo* (Samejima *et al.*

2005). If the Mto1-Mto2 interaction is disrupted, how is Mto2 being targeted to the mSPB? It is possible that the weak interaction with the γ-TuSC is sufficient to recruit Mto2 to the SPBs (Samejima *et al.* 2008). An in depth analysis of the timing of Mto2-GFP recruitment [in addition to other fluorescent tags] in the absence of Mto1, may help to resolve this issue.

Multiple bioinformatic and biochemical based methods were used to identify potential phosphorylation sites on Mto2. These phosphorylation sites are listed in Appendix IX. Initial attempts to characterise the phenotype of several phospho-mutants was based on the cellular localisation of HFG-Mto2. This assay was subsequently discovered to be inappropriate, as I showed that the primary effect of Mto2 phosphorylation is likely to be through the disruption of the Mto1-Mto2 complex, therefore maintenance of the interaction via generation of non-phosphorylatable mutants would result in wild-type Mto2 localisation. Further analyses of these mutants should examine the Mto1-Mto2 interaction by co-immunoprecipitation.

The phospho-mutants that had been designed based on mass spectrometry mapping of Mto2 purified under denaturing conditions were also characterised based on MT length and number. This analysis demonstrated that the phosphorylation sites near to the predicted coiled-coil Mto1 interaction domain [Block 1] may contribute to disruption of the Mto1-Mto2 interaction, as phospho-mimetic mutations resulted in an *mto2Δ*-like phenotype [expected if the Mto2 was unable to interact with Mto1]. *In vitro* analysis of the Block 1 phospho-mimetic mutants demonstrated that both the Mto2-Mto2 interaction and the Mto1-Mto2 interaction had not been disrupted. It is

possible that the *in vitro* assay used to test the interactions was not sensitive enough to detect small changes in the efficiency of the Mto1-Mto2 interaction that may have large effects Mto1 function *in vivo*.

Overall this mutagenic analysis suggests that some or all of the phosphorylation sites in the Block 1 mutant are likely to be phosphorylated. It is possible that phosphorylation of these residues occurs in addition to several other sites, and only when all of these residues have been modified will this be sufficient to disrupt the Mto1-Mto2 interaction to a level that can be detected *in vitro*.

A method of SILAC labelling has been developed for fission yeast in our laboratory by C. Bicho (Bicho *et al.*, manuscript in preparation). The quantitative nature of this method made it possible to identify by mass spectrometry those residues that were specifically phosphorylated during mitosis. Unfortunately, the results from this mass spectrometry analysis only identified 15 unique phosphorylation sites, compared with 25 sites that were identified in the first mapping attempt. It is possible that this may be due to a reduction in the amount of purified material analysed. For future analysis, more Mto2 protein needs to be analysed in order to increase the likelihood of identifying more phosphorylation sites, particularly sites that are phosphorylated with a low stoichiometry.

Four additional non-phosphorylatable mutants were designed using evidence from a combination of biochemical and bioinformatic analyses. The sites in each mutant were selected based on the several criteria. Variant 1 sites were targeted if they had a high NetPhos score and were either highly conserved or identified in one of the two mass spectrometry mappings. Variant 1 also included the three residues

that were found within the PDB binding consensus sequence. Variant 2 sites were targeted for mutagenesis as they had previously been identified as *in vitro* CDK1-Cyclin B phosphorylation sites (Rosenberg *et al.,* 2007). Residues were mutated in Variants 3 and 4 if they were found within Aurora A and Polo kinase consensus sites, respectively. Unlike the first set of mutants, the Mto1-Mto2 interaction was assayed in these phospho-variants. This was based on the nuclear envelope localisation of Mto1 [1-549]-GFP during mitosis, where it was assumed that if the complex was maintained in a non-phosphorylatable mutant Mto2 background, the nuclear envelope localisation will also be maintained.

Microscopic analysis demonstrated that the mitotic nuclear envelope localisation of Mto1 [1-549]-GFP was disrupted in all four mutants. Interestingly, when the Mto2 phospho-variant proteins were examined by western blot, Variant 1 showed a significant reduction in Mto2 hyperphosphorylation. This result indicates that a proportion of the residues targeted in Variant 1, are phosphorylated *in vivo*.

This demonstrates that the inability to phosphorylate Mto2, and potentially the presence of an intact Mto1/2 complex, is not sufficient to maintain the Mto1 [1-549]-GFP at the nuclear envelope during mitosis. Other factors may be involved to ensure that nucleation complexes are re-localised in mitosis. For example, the nuclear envelope protein that binds Mto1, along with Mto1 itself, may also be phosphorylated. Mto1/2 complexes may be re-localised from iMTOCs other than the nuclear envelope in a similar manner, however, it is likely that in all cases other mechanisms are also in place to ensure that Mto1 is re-localised efficiently e.g. de-polymerisation of cytoplasmic MTs through the action of plus-end binding proteins and other MAPs (Grallert *et al.* 2006).

In order to conclusively examine the role of Mto2 phosphorylation in the formation of the Mto1/2 complex I need to directly demonstrate that the Mto1-Mto2 interaction has been maintained in the Variant 1 background in mitosis.

Alternatively, it is possible that Mto2 phosphorylation in mitosis is merely correlated with the disruption of the Mto1-Mto2 interaction and not causally linked i.e. Mto2 phosphorylation may play a role in a different aspect of Mto1/2 function. The phenotype of Mto2 Variant 1 needs to be examined in the full length Mto1 background, to determine the consequences of Mto2 phosphorylation to the MT nucleation efficiency of the subsequent Mto1/2 complex.

CHAPTER 6

DISCUSSION

One of the aims of this project was to determine the mechanism that underlies Mto1/2-mediated activation of the γ-TuSC in facilitating the nucleation of non-centrosomal linear MT arrays of *S. pombe*. Specifically, it was hoped that my research may be able to provide evidence to support a template model for γ-TuRC assembly by the Mto1/2 complex. Through calculation of the size of Mto1/2 complex I aimed to confirm whether multimerisation of several copies of the Mto1/2 complex is required to drive γ-TuRC assembly.

Determination of the copy number of Mto1 and Mto2 in the Mto1/2 complex has been challenging due to the formation of the Mto1/2 60 – 80 S complex. I was unable to determine whether the Mto1 60 – 80 S complex resulted from Mto1 association with large cellular particles, or whether it was caused by protein aggregation. Assembly of this large complex was promoted by association with the SPB, however, this was only true for a fraction of the 60 – 80 S complex and it remains possible that SPB-association may promote protein aggregation by increasing the local concentration.

Inclusion into a 60 - 80 S complex was also observed for members of the γ-TuSC, independently of Mto1. The hydrodynamic analyses of purified γ-TuSC proteins in other organisms has not revealed the presence of large complexes [> 35 S], suggesting that the complex formed in *S. pombe* may not represent the equivalent complex in higher eukaryotes (Kellogg *et al.* 1992; Raff *et al.* 1993; Stearns *et al.*

1994; Zheng *et al.* 1995; Oegema *et al.* 1999). Unlike the extraction buffers using in this study, these analyses have included 100 μM GTP, which has been shown to reduce γ-TuSC aggregation (Oegema *et al.* 1999). Therefore all future analysis of the γ-TuSC in *S. pombe* should be performed in the presence of GTP. It is possible that this may also help prevent aggregation of the Mto1/2 complex.

Hydrodynamic analysis of both Mto1 and Mto2 has been difficult due to the unusually large distribution of protein over both the sucrose density gradient and gel filtration fractions. The large spread of Mto1 and Mto2 following fractionation means that all molecular weight calculations are likely to represent an average value.

I hypothesised that the spreading may arise from the inclusion of protein within detergent micelles, however, use of a different detergent [0.5% v/v CHAPS] with a smaller micelle size had very little effect on protein distribution [data not shown]. When purified recombinant Mto2 was analysed by gel filtration following pre-fractionation by sucrose gradient, there was less spreading [fig 4.1]. This indicates that the spreading is likely to result from the presence of other cellular proteins; therefore future hydrodynamic analyses should be performed using purified yeast protein, as I predict that this will produce a more homogenous mixture of protein that would distribute among fewer fractions.

Using protein quantification methods derived from protocols performed in the laboratory of T. Pollard (Wu *et al.* 2005), I was able to determine that there are equivalent numbers of Mto1 and Mto2 molecules within the cell [Appendices VII and VIII]. Additionally, in chapter five I have shown that the nuclear envelope localisation of over-expressed Mto1 [1-549]-GFP requires simultaneous over-expression of Mto2. Therefore, although I was not able to demonstrate the copy

numbers of Mto1 and Mto2 within an active nucleation complex, these additional results suggest that the Mto1/2 complex is likely to contain comparable levels of Mto1 and Mto2.

In chapter three I demonstrated that removal of the C-terminal 315 aa of Mto1 prevents it from associating with or assembling into the 60 – 80 S complex. This allowed me to determine that the Mto1 [1-800] / Mto2 complex is likely to be a heterotetramer composed of two molecules of Mto1 and two molecules of Mto2. *In vivo* evidence suggests that multiple Mto1/2 heterotetramers are present at non-SPB iMTOCs. However, as only single heterotetramers are detected by hydrodynamic analysis, it has not been possible to determine the copy number of Mto1 [1-800] and Mto2 within the active complex. It would be interesting to investigate using purified proteins *in vitro*, whether single heterotetramers are able to promote MT nucleation. Although this is unlikely to reflect the situation *in vivo*, the activity of single Mto1/2 heterotetramers would at least suggest that the γ-TuSC has the potential to nucleate MT without further assembly into the γ-TuRC. The nature of this association would reinforce the Protofilament model of MT nucleation (Erickson *et al.* 1996a). Arguments against γ-TuSC-mediated nucleation from higher eukaryotes propose that the efficiency of nucleation from this complex would not be high enough to support a dynamic MT array. However, as *S. pombe* does not have as many MT bundles it is possible that a high concentration of low efficiency complexes may be sufficient. Alternatively, single Mto1/2 heterotetramers may not induce nucleation from single γ-TuSCs e.g. possible that each heterotetramer, which contain two γ-TuSC binding domains, can induce γ-TuRC formation by an increase in local concentration of γ-TuSC, sufficient to promote γ-TuRC self-assembly.

In summary, I have shown that it will not be possible to analyse the Mto1/2 complex containing full length Mto1. The inconsistencies between the *in vitro* and *in vivo* data highlight the difficulties of studies of this nature. Subsequent purification and structural analysis should therefore be performed using the Mto1/2 complex containing truncated forms of Mto1, such as Mto1 [1-800] or Mto1 [1-549], in order to determine the level of Mto1/2 complex multimerisation. This line of research is currently being pursued in the Sawin lab. This should be accompanied by *in vivo* methods such as Fluorescence Correlation Spectroscopy (FCS) that may be able to measure the concentration of molecules at iMTOCs.

My research has also addressed the role of Mto2 within the Mto1/2 complex. I proposed that Mto2 binding has two functions: firstly, Mto2 may facilitate Mto1 multimerisation either through forming higher-order complexes or through inducing structural changes in Mto1 that promotes Mto1 self association, and secondly, Mto2 binding may activate Mto1 which promotes the Mto1 / γ-TuSC interaction. This hypothesis was supported by observations in this study, whereby *in vivo*, the signal from Mto1-tdRFP satellite foci was reduced in the absence of Mto2 and I have shown *in vitro* that there is approximately a 4-fold reduction in the amount of γ-TuSC that interacted with Mto1-TAPS in *mto2Δ*.

The observation that Mto2 is present in dimeric form within an active nucleation complex [Mto1 [1-800] / Mto2] suggested that the Mto2-Mto2 interaction may play an important role in one or both of these functions. In chapter four, I described attempts to determine the contribution of Mto2 multimerisation to Mto1/2 complex function. This analysis was encumbered by the fact that Mto2 was found to

be tetrameric, therefore there are a number of interaction sites that needed to be identified and disrupted in order to generate the monomeric form of Mto2 required to conclusively test the contribution of the Mto2 multimerisation to the function of the Mto1/2 complex.

Mapping of the Mto2-Mto2 interaction and subsequent identification and mutagenesis of Mto2 coiled-coil, suggested that this region is required for the Mto2-Mto2 interaction. Hydrodynamic analysis of the coiled-coil mutant demonstrated that it was dimeric, consequently there are other regions near the C-terminus that also facilitate the Mto2-Mto2 interaction. Further analysis of the Mto2 coiled-coil mutant has shown that this region is required for the efficient interaction with Mto1. Despite being sufficient to disrupt the Mto2-Mto2 interaction, mutation of hydrophobic residues within the Mto2 coiled-coil domain to aspartic acid was not sufficient to completely interrupt the Mto1-Mto2 interaction. However, phenotypic analysis of this mutant revealed an *mto2Δ* phenotype whereby MT nucleation from non-SPB iMTOCs was abolished. This result suggests that the system is highly sensitive to changes in interaction efficiencies e.g. a 50% drop in the efficiency of the Mto1-Mto2 interaction [in a HFG-Mto2 background] does not affect the function of the nucleation complex, however, further a reduction [coiled-coil mutant] causes loss of all non-SPB iMTOC nucleation.

In chapter four I demonstrated that dimeric HFG-Mto2 is sufficient to promote wild-type MT nucleation, which in addition to previous analysis of Mto1-YFP satellite foci in the presence of Mto2-CFP and untagged Mto2 (Samejima *et al.* 2005) suggest that Mto2 tetramerisation is not required for Mto1/2 complex

assembly or function. Rather, tetrameric Mto2 may arise from the association of un-complexed Mto2 dimers, acting as a storage form of protein.

This analysis does not support my prediction that large-scale multimerisation of Mto2 is able to drive Mto1/2 assembly. Alternatively, it is possible that Mto2 binding induces a structural change in Mto1 that promotes multimerisation of Mto1.

Weak Mto1-tdRFP satellite foci were observed in *mto2Δ*. This suggests that Mto1 has a limited capacity to self-assemble, which is likely to be promoted by increasing the local concentration of Mto1 through targeting the protein to MTOCs. When the localisation signals in the C-terminus of Mto1 are removed, assembly of the complex appears to be facilitated solely by the presence of Mto2, as large Mto1 [1-549]-GFP foci at the nuclear envelope were not present in the absence of Mto2. Although no obvious differences can be observed between the Mto1 satellites in the full length and Mto1 [1-549] backgrounds, it would be interesting to investigate whether they are structurally different, the former having been assembled primarily through the Mto1 coiled-coil, and the latter having been assembled though the action of Mto2.

In addition to inducing Mto1 multimerisation it was proposed that Mto2 may also function by promoting the Mto1 / γ-TuC interaction. For example, Mto2 binding may cause a structural change in the conformation of Mto1 that increases the affinity for γ-TuC [and also potentially promote Mto1 multimerisation]. It is also possible that Mto2 may provide part of the γ-TuC interaction interface as suggested by the observation that Mto2 can interact with the γ-TuSC independently of Mto1 (Samejima *et al.* 2008). Further work is required to determine whether this aspect of Mto2 function occurs independently of Mto1/2 complex multimerisation, or whether

the increase in Mto1-γ-TuC interaction efficiency occurs as a result of Mto2-dependent association of γ-TuC-binding sites. In addition, further mutagenesis is required to obtain monomeric Mto2, which would allow one to assess the significance of the Mto2-Mto2 interaction to the function of Mto2.

The research presented in chapter five examined the role of Mto2 phosphorylation in the regulation of Mto1/2 complex activity. The regulation of this complex is proposed to be a key mechanism to allow the cell to specify when and where MT nucleation occurs. Spatial and temporal mis-regulation of MT nucleation may have drastic effects on cellular organisation, particularly in mitosis when nucleation of an interphase array may restrict the level of αβ-tubulin available to polymerise the MT spindle.

Thus, I demonstrated that hyperphosphorylation of Mto2 during mitosis corresponds to the disruption of the Mto1/2 complex. The Mto1/2 complex may be disrupted during mitosis to facilitate re-modelling of the Mto1 / γ-TuC complex i.e. allowing Mto1 and the γ-TuC to relocate to the SPB where they are required to nucleate the spindle and astral MTs. Simultaneously, by preventing Mto2 from interacting with Mto1, this may be part of a number of redundant mechanisms that discourage iMTOCs being assembled during mitosis.

In this analysis I used several bioinformatic and biochemical based techniques to identify Mto2 phosphorylation sites. These include identification of conserved S/T residues and analysis of purified Mto2 by mass spectrometry. Purification of Mto2-HTB under denaturing conditions successfully identified 25 phosphorylation sites, however, attempts to enrich for mitotic sites using SILAC did

not generate convincing results. It is thought that the reduction in identifications may be due to the relative amounts of purified protein; this should be considered when performing Mto2 purifications in future analyses.

Initial attempts to assess the contribution of the identified potential phosphorylation sites to Mto2 function were not successful, with the exception of the analysis of the Block 1 mutant, constructed based on the results of the mass spectrometry analysis. This mutant included four residues that were within 30 aa of the Mto2 coiled-coil domain / Mto1 interaction domain. This result correlates with the conclusions drawn from previous data which state that the Mto1-Mto2 interaction is disrupted as a result of Mto2 phosphorylation.

Phenotypic analysis of the mutants constructed in the latter stages of my study involved examination of the Mto2-dependent localisation of Mto1 [1-549]-GFP at the nuclear envelope. These mutants were constructed based on several lines of evidence gathered over the course of my project. Unfortunately, none of the four non-phosphorylatable Mto2 variants displayed the retention of Mto1 [1-549]-GFP on the nuclear envelope that was predicted based on a sustained Mto1-Mto2 interaction. However, Mto2 Variant 1 did show a significant reduction in phosphorylation when the protein was analysed by SDS-PAGE and western blot. This result is interesting as several of the phosphorylation sites uniquely targeted in Variant 1 overlap with sites identified by both mass spectrometry based mappings and a number of these sites were mutated in the Mto2 Block 1 mutant. Again, supporting previous evidence that phosphorylation of the Mto1 interaction domain of Mto2 may contribute to the disruption of the Mto1/2 complex. Unfortunately, the local environment of the residues that had been uniquely targeted in Variant 1 was not indicative of a specific

kinase consensus. However, as the phosphorylation state of Mto2 was partially reduced in the Variant 2 background, this suggests that Cdc2 is the most likely candidate. This is supported by my *in vitro* kinase assay, and the observation that Cdc2 interacts with Mto1 during mitosis *in vivo* [data not shown].

Further investigation of Mto2 Variant 1 should first determine biochemically whether the Mto1-Mto2 interaction is maintained during mitosis. Without showing that the complex has been disrupted it is not possible to conclude that Mto2 phosphorylation plays a role in Mto1/2 complex formation. My *in vitro* CDK kinase assay did not distinguish whether Mto1/2 disruption was caused by Mto1 phosphorylation or Mto2 phosphorylation. This is important as previous evidence have indicated that Mto1 homologs are phosphorylated during mitosis in other organisms (Dobbelaere *et al.* 2008).

One key question regarding the function of Mto2 that was not directly addressed in this study is why Mto2 is specifically required for nucleation from iMTOCs and not the SPB. The research presented in this report may provide information that can help to answer this question. I hypothesise that Mto2 may not be required at the SPB because Mto1 dimers [and probably higher order complexes] are present at a high enough concentration that their weak affinity for the γ-TuSC is able to compensate for the lack of high efficiency Mto1/2 complexes, and is sufficient to support MT nucleation. For example, if 1 out of every 10 Mto1 dimers were able to initiate MT nucleation, but 9 out of every 10 Mto1/2 complexes were able to nucleate MTs, then 9 Mto1 complexes would be required to nucleate that same amount of MTs for every single Mto1/2 complex. As relatively few MTs are nucleated from the

SPB, particularly during mitosis, it is likely that the cell can tolerate this low efficiency of MT nucleation.

This theory partially applies to nucleation from the eMTOC. The high number of Mto1 binding sites increases the number of low efficiency Mto1 / γ-TuSC nucleation events, therefore a low level of MT nucleation can be achieved in the absence of Mto1/2 complex. However, based on the weak PAA formed in *mto2Δ*, it appears that it is not sufficient to nucleate a wild-type array.

The formation of high efficiency Mto1/2 nucleation complexes may also explain why the Mto1/2 complex is disrupted in mitosis. For example, in addition to highly efficient MT nucleation not being required at this point, it would probably be detrimental to have highly efficient nucleation complexes at the SPB as retention or depletion of cytoplasmic free-tubulin may prevent sufficient levels from entering the nucleus. In summary, the Mto1/2 complex may be disrupted during mitosis as it is too efficient at nucleating MTs, and the cell needs to limit the level of nucleation from the SPB.

This idea can be related to the nature of the γ-TuC formed in the presence of different types of Mto1 complex. The Mto1/2-linked nucleation complexes are efficient MT nucleators because they may be able to efficiently facilitate γ-TuRC assembly as a result of Mto2-induced multimerisation of Mto1 γ-TuSC interaction domains and/or the presence of a form of Mto1 that can interact with the γ-TuSC more efficiently. This is compared with a slow Mto1-mediated γ-TuRC assembly at the SPB, which, due to the concentration of Mto1 is able to undergo some level of multimerisation, but due to the absence of Mto2, interacts with the γ-TuRC less efficiently.

The presence of both high and low efficiency MT nucleation complexes would be advantageous to the cells as in addition to regulating the time and place of MT nucleation, it also allows it to regulate the efficiency of the nucleation. This level of regulation may be instigated in part by Mto2. This may be why there are no known homologs Mto2 in higher eukaryotes, as in these cells the majority of cytoplasmic MT nucleation is restricted to the centrosome, where there may be less requirement to regulate the efficiency or location of the nucleation complexes.

APPENDIX I

Sucrose Gradient calibration for recombinant protein

A 2 ml 5-20% sucrose gradient was calibrated using gel filtration molecular weight markers [Sigma]. Lyophilised protein was made up to 50 X stock solution [10 $mgml^{-1}$] in 1 X TBS. This contained carbonic anhydrase [2.8 S, $_{MW}$ = 29 kDa], bovine serum albumin [4.3 S, $_{MW}$ = 66 kDa], alcohol dehydrogenase [7.4 S, $_{MW}$ = 37 kDa], β-amylase [9 S, $_{MW}$ = 50 kDa] and thyroglobulin [19 S, $_{MW}$ = 110 kDa]. Prior to use markers were diluted in 1 X TBS and 100 µl was loaded onto the gradient. After centrifugation, 50 µl fractions were collected diluted in 2 X SB. 50µl of each sample was analysed by SDS-PAGE and gel was stained with Coomassie. Signal was quantified using Odyssey V3.0 software.

Intensities were plotted and graph was used to visually estimate the peak fraction for each marker [Figure AI, Panel A and B]. The peak was then plotted against the known S-values for each protein [Figure AI, Panel C]. This curve was used for estimation of S-values for purified protein.

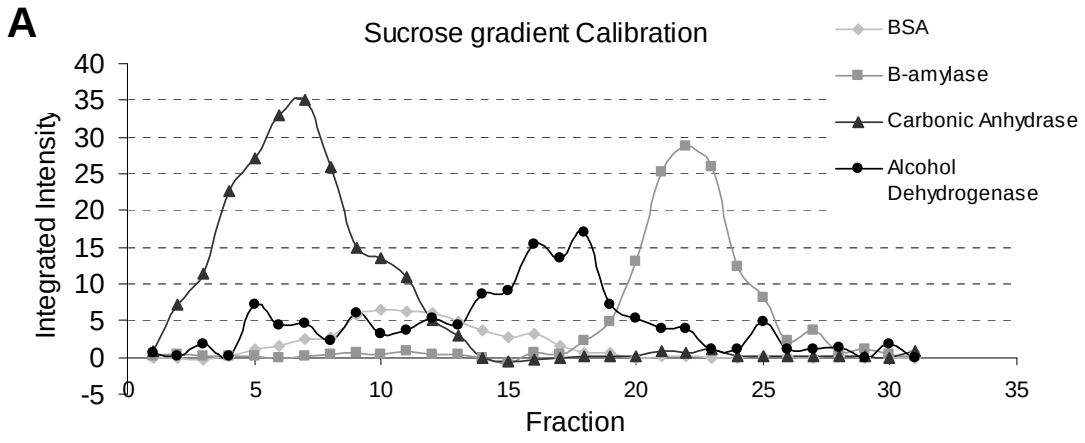

B

	S-value	Peak Fraction
Carbonic Anhydrase	2.8	6.7
BSA	4.3	10.2
Alcohol Dehydrogenase	7.4	17.5
B-amylase	9	22

C

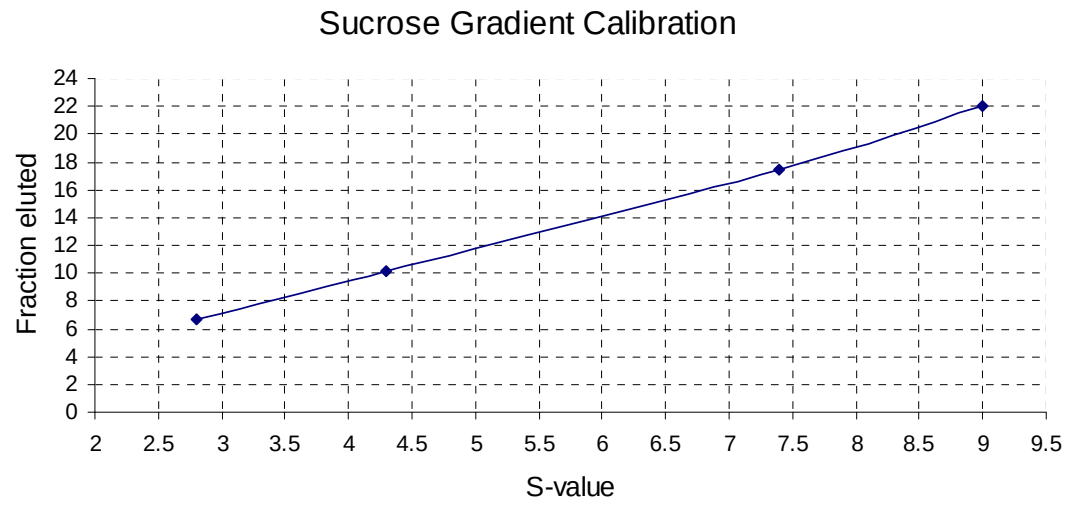

Figure I.a Calibration of the 5-20 % sucrose gradient for purified protein. [A] Graph plotting the integrated intensities for four molecular weight standards listed in table AI. Intensities were measured using Odyssey V3.0 [Licor Biosciences, U.S.A.]. Peak fractions listed in [B] were used to construct a calibration curve against known S-values [C).

APPENDIX II

Sucrose Gradient calibration for yeast extract analyses.

A 2 ml 5-20% sucrose gradient was calibrated using gel filtration molecular weight markers. Lyophilised protein was made up to 50 X stock solution [10 $mgml^{-1}$] in 1 X TBS. This contained carbonic anhydrase [2.8 S, $_{MW}$ = 29 kDa], bovine serum albumin [4.3 S, $_{MW}$ = 66 kDa], alcohol dehydrogenase [7.4 S, $_{MW}$ = 37 kDa], β-amylase [9 S, $_{MW}$ = 50 kDa] and thyroglobulin [19 S, $_{MW}$ = 110 kDa]. Prior to use markers were diluted in 1 X TBS and 100 µl was loaded onto the gradient. After centrifugation, 100 µl fractions were collected diluted in 2 X SB. 50 µl of each sample was analysed by SDS-PAGE and gel was stained with Coomassie. Signal was quantified using Odyssey V3.0 software.

Intensities were plotted on a graph which was used to visually estimate the peak fraction for each marker. The peak was then plotted against the known S-values for each protein. This curve was used for estimation of S-values for purified protein.

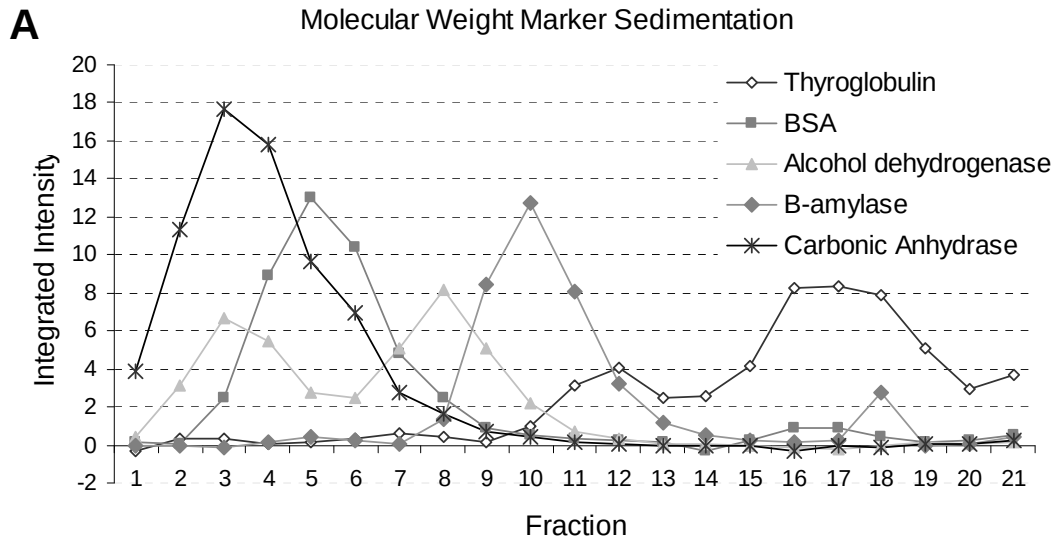

B

	S-value	Peak Fraction
Thyroglobulin	19	17
BSA	4.3	5
Alcohol dehydrogenase	7.4	8
B-amylase	9	10
Carbonic Anhydrase	2.8	3

C

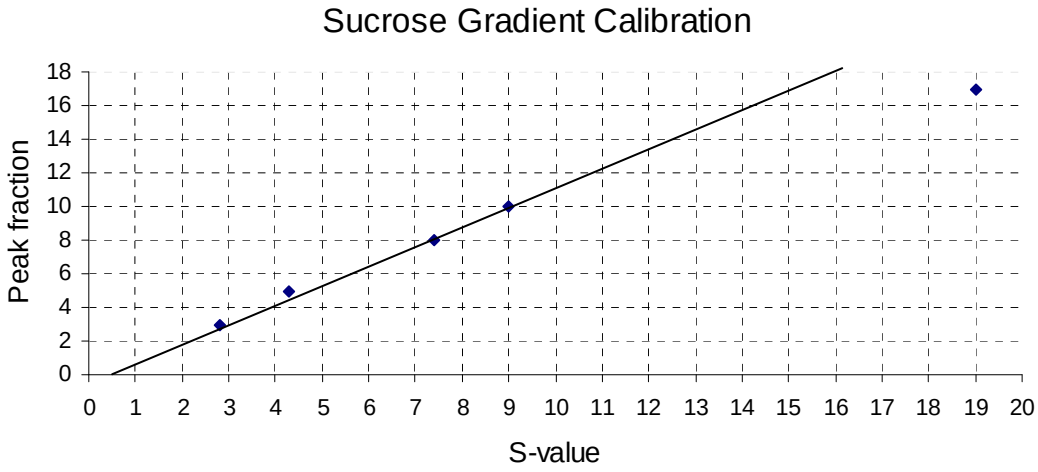

Figure II.a Calibration of the 5-20% sucrose gradient for purified protein. [A] Graph plotting the integrated intensities for four molecular weight standards. Intensities were measured using Odyssey V3.0 [Licor Biosciences, U.S.A.]. Peak fractions listed in [B] were used to construct a calibration curve against known S-values [C].

APPENDIX III

Superose-6 calibration for KS1

KS1 Superose 6 10/300GL high performance column [GE healthcare, U.S.A] was used for analysis of yeast lysate. Calibration was performed using markers from a Gel Filtration Calibration Kit [GE healthcare, U.S.A] [thyroglobulin, β-amylase and ferretin], in combination with molecular weight markers from Sigma, U.S.A. [BSA and carbonic anhydrase]. A 10 X stock solution of molecular weight markers were made in 1 X TBS as follows: thyroglobulin = 5 $mgml^{-1}$, β-amylase = 4 $mgml^{-1}$, ferritin = 0.3 $mgml^{-1}$, BSA = 4 $mgml^{-1}$, carbonic anhydrase = 3 $mgml^{-1}$ [stock made up in dH_2O]. Prior to use stock solution was diluted with 1 X TBS, and 100µl was loaded onto the column. AU 600 nm was measured for 30 ml at a flow rate of 0.4 $mlmin^{-1}$. **Ve** was used to calculate $\mathbf{K_{av}}$ for each marker as follows:

$$K_{av} = \frac{Ve - V_0}{Vt - V_0}$$

Ve = elution volume
V_0 = void volume of the column
Vt = total volume of the gel bed

Column volume [$\mathbf{V_t}$] = 24 ml. Void volume of the column [$\mathbf{V_o}$] = 7 ml.

KS1	Rm	Ve	Kav	√-log (Kav)
Thyroglobulin	8.5	11.8	0.28	0.74
Ferretin	6.1	13.7	0.39	0.64
β-amylase	5.4	14.8	0.46	0.58
BSA	3.5	16.1	0.54	0.52
Carbonic Anhydrase	2	17.7	0.63	0.45

Table III.a Molecular weight markers used for calibration of KS1. Rm = Stokes Radius, Ve = elution volume.

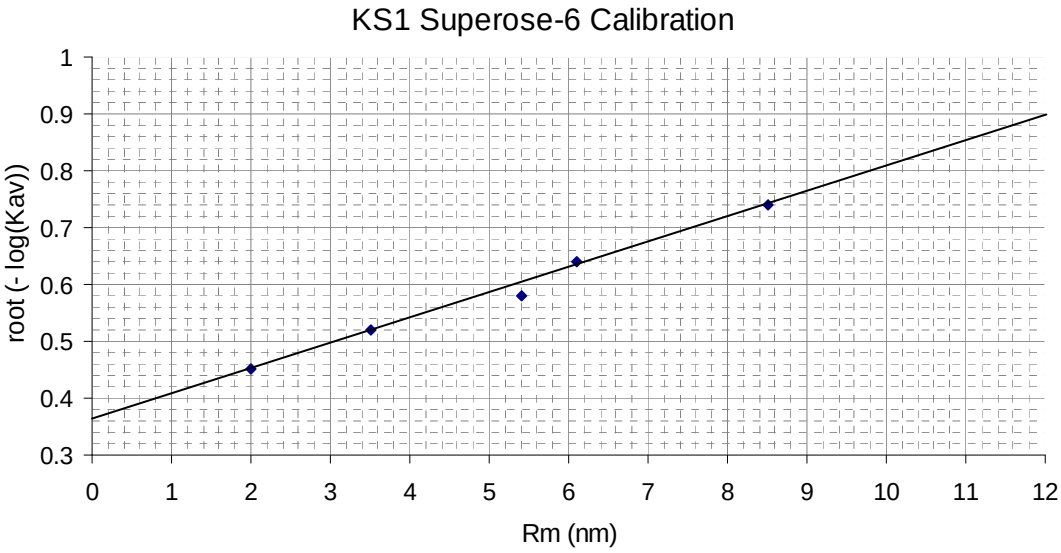

Figure III.a Calibration plot for KS1. Stokes radii of known molecular weight markers, were plotted against $\sqrt{-\log[K_{av}]}$.

APPENDIX IV

Superose-6 calibration for KS2

KS2 Superose 6 10/300GL high performance column [GE healthcare, U.S.A] was used for analysis of purified protein. Calibration was performed using molecular weight standards from a Gel Filtration Calibration Kit [GE healthcare, U.S.A] [thyroglobulin, ferretin, aldolase, ovalbumin, ribonuclease A], in combination with molecular weight markers from Sigma, U.S.A [carbonic anhydrase]. A 10 X stock solution of molecular weight markers were made in 1 X TBS as follows: thyroglobulin = 5 $mgml^{-1}$, ferritin = 0.3 $mgml^{-1}$, aldolase = 4 $mgml^{-1}$, ovalbumin 4 $mgml^{-1}$, ribonuclease A = 3$mgml^{-1}$, carbonic anhydrase = 3 $mgml^{-1}$ [stock made up in dH_2O]. Prior to use stock solution was diluted with 1 X TBS, and 100µl was loaded onto the column. AU 600 nm was measured for 30 ml at a flow rate of 0.3 $mlmin^{-1}$.

Ve was used to calculate $\mathbf{K_{av}}$ for each marker as follows:

$$K_{av} = \frac{Ve - V_0}{Vt - V_0}$$

Ve = elution volume
V_0 = void volume of the column
Vt = total volume of the gel bed

Column volume [$\mathbf{V_t}$] = 24 ml. Void volume of the column [$\mathbf{V_o}$] = 8 ml.

KS2	Rm	Ve	Kav	√-log (Kav)
Thyroglobulin	8.5	13.1	0.32	0.7
Ferretin	6.1	15	0.44	0.6
Aldolase	4.8	16.5	0.53	0.53
Ovalbumin	3	17.7	0.61	0.46
Carbonic Anhydrase	2	18.6	0.66	0.43
Ribonuclease A	1.6	19.5	0.72	0.38

Table 1V.a Molecular weight markers used for calibration of KS2. Rm = Stokes Radius, Ve = elution volume.

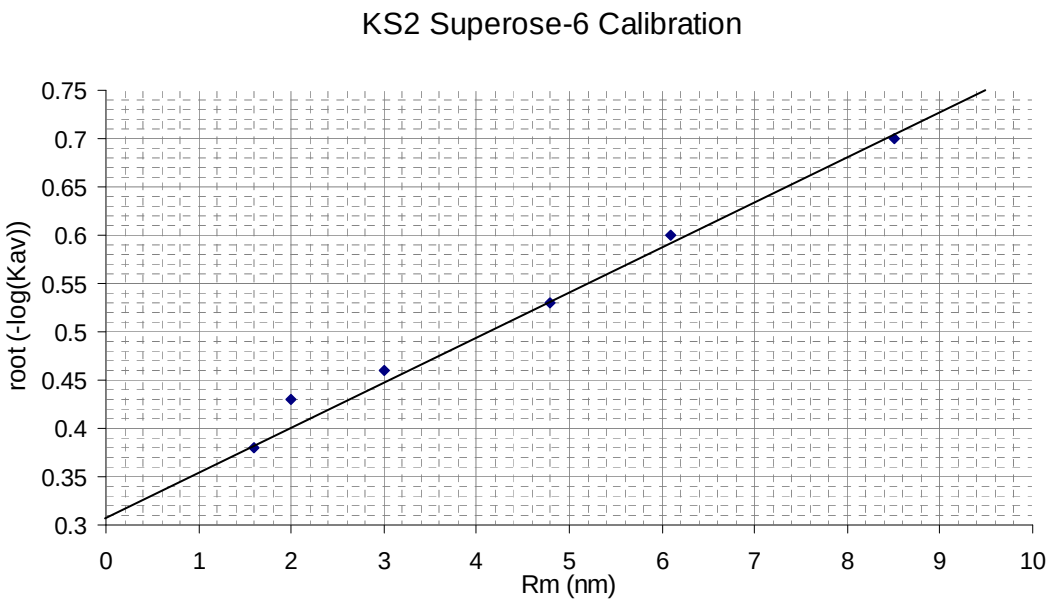

Figure 1V.a Calibration plot for KS2. Stokes radii of known molecular weight markers, were plotted against √-log[K_{av}].

APPENDIX V

Fungal alignment of Mto2 homologs

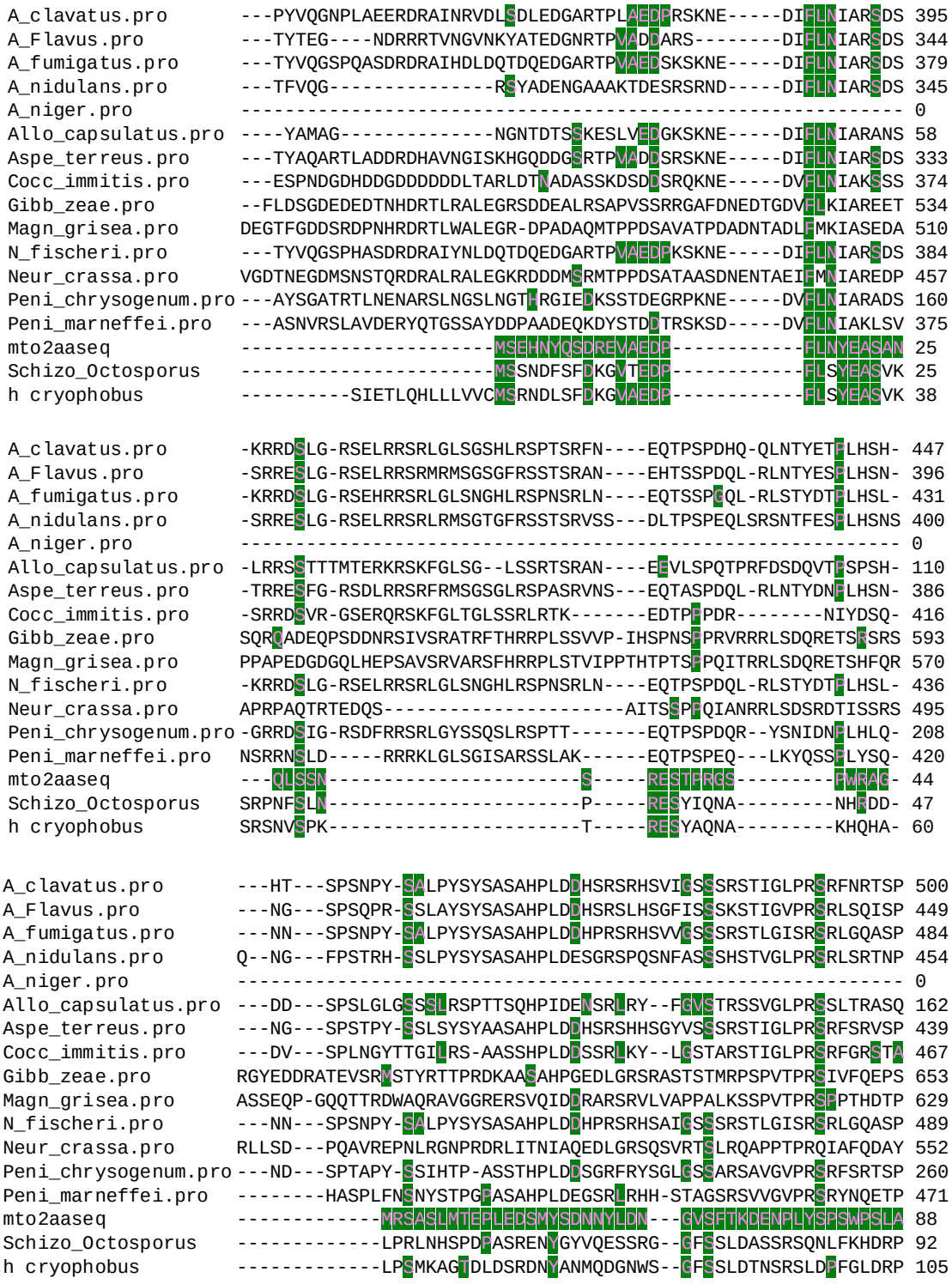

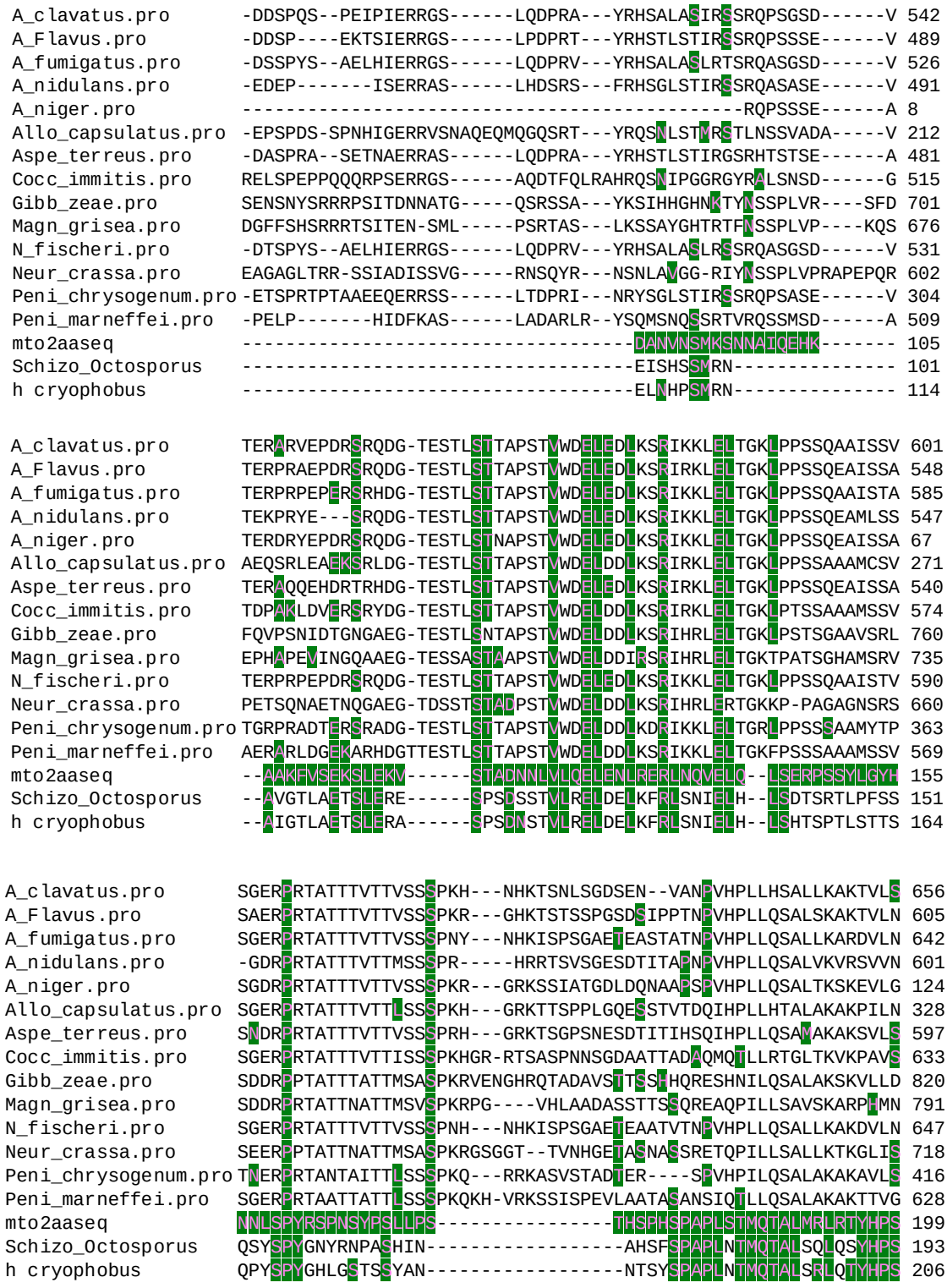
A_clavatus.pro -DDSPQS--PEIPIERRGS------LQDPRA---YRHSALASIRSSRQPSGSD------V 542
A_Flavus.pro -DDSP----EKTSIERRGS------LPDPRT---YRHSTLSTIRSSRQPSSSE------V 489
A_fumigatus.pro -DSSPYS--AELHIERRGS------LQDPRV---YRHSALASLRTSRQASGSD------V 526
A_nidulans.pro -EDEP-------ISERRAS------LHDSRS---FRHSGLSTIRSSRQASASE------V 491
A_niger.pro ----------RQPSSSE------A 8
Allo_capsulatus.pro -EPSPDS-SPNHIGERRVSNAQEQMQGQSRT---YRQSNLSTMRSTLNSSVADA-----V 212
Aspe_terreus.pro -DASPRA--SETNAERRAS------LQDPRA---YRHSTLSTIRGSRHTSTSE------A 481
Cocc_immitis.pro RELSPEPPQQQRPSERRGS------AQDTFQLRAHRQSNIPGGRGYRALSNSD------G 515
Gibb_zeae.pro SENSNYSRRRPSITDNNATG-----QSRSSA---YKSIHHGHNKTYNSSPLVR----SFD 701
Magn_grisea.pro DGFFSHSRRRTSITEN-SML-----PSRTAS---LKSSAYGHTRTFNSSPLVP----KQS 676
N_fischeri.pro -DTSPYS--AELHIERRGS------LQDPRV---YRHSALASLRSSRQASGSD------V 531
Neur_crassa.pro EAGAGLTRR-SSIADISSVG-----RNSQYR---NSNLAVGG-RIYNSSPLVPRAPEPQR 602
Peni_chrysogenum.pro -ETSPRTPTAAEEQERRSS------LTDPRI---NRYSGLSTIRSSRQPSASE------V 304
Peni_marneffei.pro -PELP-------HIDFKAS------LADARLR--YSQMSNQSSRTVRQSSMSD------A 509
mto2aaseq ----------DANVNSMKSNNAIQEHK------- 105
Schizo_Octosporus ----------EISHSSMRN---------- 101
h cryophobus ----------ELNHPSMRN---------- 114
A_clavatus.pro TERARVEPDRSRQDG-TESTLSTTAPSTVWDELEDLKSRIKKLELTGKLPPSSQAAISSV 601
A_Flavus.pro TERPRAEPDRSRQDG-TESTLSTTAPSTVWDELEDLKSRIRKLELTGKLPPSSQEAISSA 548
A_fumigatus.pro TERPRPEPERSRHDG-TESTLSTTAPSTVWDELEDLKSRIKKLELTGKLPPSSQAAISTA 585
A_nidulans.pro TEKPRYE---SRQDG-TESTLSTTAPSTVWDELEDLKSRIKKLELTGKLPPSSQEAMLSS 547
A_niger.pro TERDRYEPDRSRQDG-TESTLSTNAPSTVWDELEDLKSRIKKLELTGKLPPSSQEAISSA 67
Allo_capsulatus.pro AEQSRLEAEKSRLDG-TESTLSTTAPSTVWDELDDLKSRIRKLELTGKLPPSSAAAMCSV 271
Aspe_terreus.pro TERAQQEHDRTRHDG-TESTLSTTAPSTVWDELEDLKSRIRKLELTGKLPPSSQEAISSA 540
Cocc_immitis.pro TDPAKLDVERSRYDG-TESTLSTTAPSTVWDELDDLKSRIRKLELTGKLPTSSAAAMSSV 574
Gibb_zeae.pro FQVPSNIDTGNGAEG-TESTLSNTAPSTVWDELDDLKSRIHRLELTGKLPSTSGAAVSRL 760
Magn_grisea.pro EPHAPEVINGQAAEG-TESSASTAAPSTVWDELDDIRSRIHRLELTGKTPATSGHAMSRV 735
N_fischeri.pro TERPRPEPDRSRQDG-TESTLSTTAPSTVWDELEDLKSRIKKLELTGKLPPSSQAAISTV 590
Neur_crassa.pro PETSQNAETNQGAEG-TDSSTSTADPSTVWDELDDLKSRIHRLERTGKKP-PAGAGNSRS 660
Peni_chrysogenum.pro TGRPRADTERSRADG-TESTLSTTAPSTVWDELDDLKDRIKKLELTGRLPPSSSAAMYTP 363
Peni_marneffei.pro AERARLDGEKARHDGTTESTLSTTAPSTVWDELDDLKSRIKKLELTGKFPSSSAAAMSSV 569
mto2aaseq --AAKFVSEKSLEKV------STADNNLVLQELENLRERLNQVELQ--LSERPSSYLGYH 155
Schizo_Octosporus --AVGTLAETSLERE------SPSDSSTVLRELDELKFRLSNIELH--LSDTSRTLPFSS 151
h cryophobus --AIGTLAETSLERA------SPSDNSTVLRELDELKFRLSNIELH--LSHTSPTLSTTS 164
A_clavatus.pro SGERPRTATTTVTTVSSSPKH---NHKTSNLSGDSEN--VANPVHPLLHSALLKAKTVLS 656
A_Flavus.pro SAERPRTATTTVTTVSSSPKR---GHKTSTSSPGSDSIPPTNPVHPLLQSALSKAKTVLN 605
A_fumigatus.pro SGERPRTATTTVTTVSSSPNY---NHKISPSGAETEASTATNPVHPLLQSALLKARDVLN 642
A_nidulans.pro -GDRPRTATTTVTTMSSSPR-----HRRTSVSGESDTITAPNPVHPLLQSALVKVRSVVN 601
A_niger.pro SGDRPRTATTTVTTVSSSPKR---GRKSSIATGDLDQNAAPSPVHPLLQSALTKSKEVLG 124
Allo_capsulatus.pro SGERPRTATTTVTTLSSSPKH---GRKTTSPPLGQESSTVTDQIHPLLHTALAKAKPILN 328
Aspe_terreus.pro SNDRPRTATTTVTTVSSSPRH---GRKTSGPSNESDTITIHSQIHPLLQSAMAKAKSVLS 597
Cocc_immitis.pro SGERPRTATTTVTTISSSPKHGR-RTSASPNNSGDAATTADAQMQILLRTGLTKVKPAVS 633
Gibb_zeae.pro SDDRPPTATTTATTMSASPKRVENGHRQTADAVSITTSSPHQRESHNILQSALAKSKVLLD 820
Magn_grisea.pro SDDRPRTATTNATTMSVSPKRPG----VHLAADASSTTSSQREAQPILLSAVSKARPPMN 791
N_fischeri.pro SGERPRTATTTVTTVSSSPNH---NHKISPSGAETEAATVTNPVHPLLQSALLKAKDVLN 647
Neur_crassa.pro SEERPPTATTNATTMSASPKRGSGGT--TVNHGETASNASSRETQPILLSALLKTKGLIS 718
Peni_chrysogenum.pro TNERPRTANTAITTLSSSPKQ---RRKASVSTADTER----SPVHPILQSALAKAKAVLS 416
Peni_marneffei.pro SGERPRTAATTATTLSSSPKQKH-VRKSSISPEVLAATASANSIQTLLQSALAKAKTTVG 628
mto2aaseq NNLSPYRSPNSVPSLLPS----------THSPHSPAPLSTMQTALMRLRTYHPS 199
Schizo_Octosporus QSYSPYGNYRNPASHIN----------AHSFSPAPLNTMQTALSQLQSYHPS 193
h cryophobus QPYSPYGHLGSTSSYAN----------NTSYSPAPLNTMQTALSRLQTYHPS 206

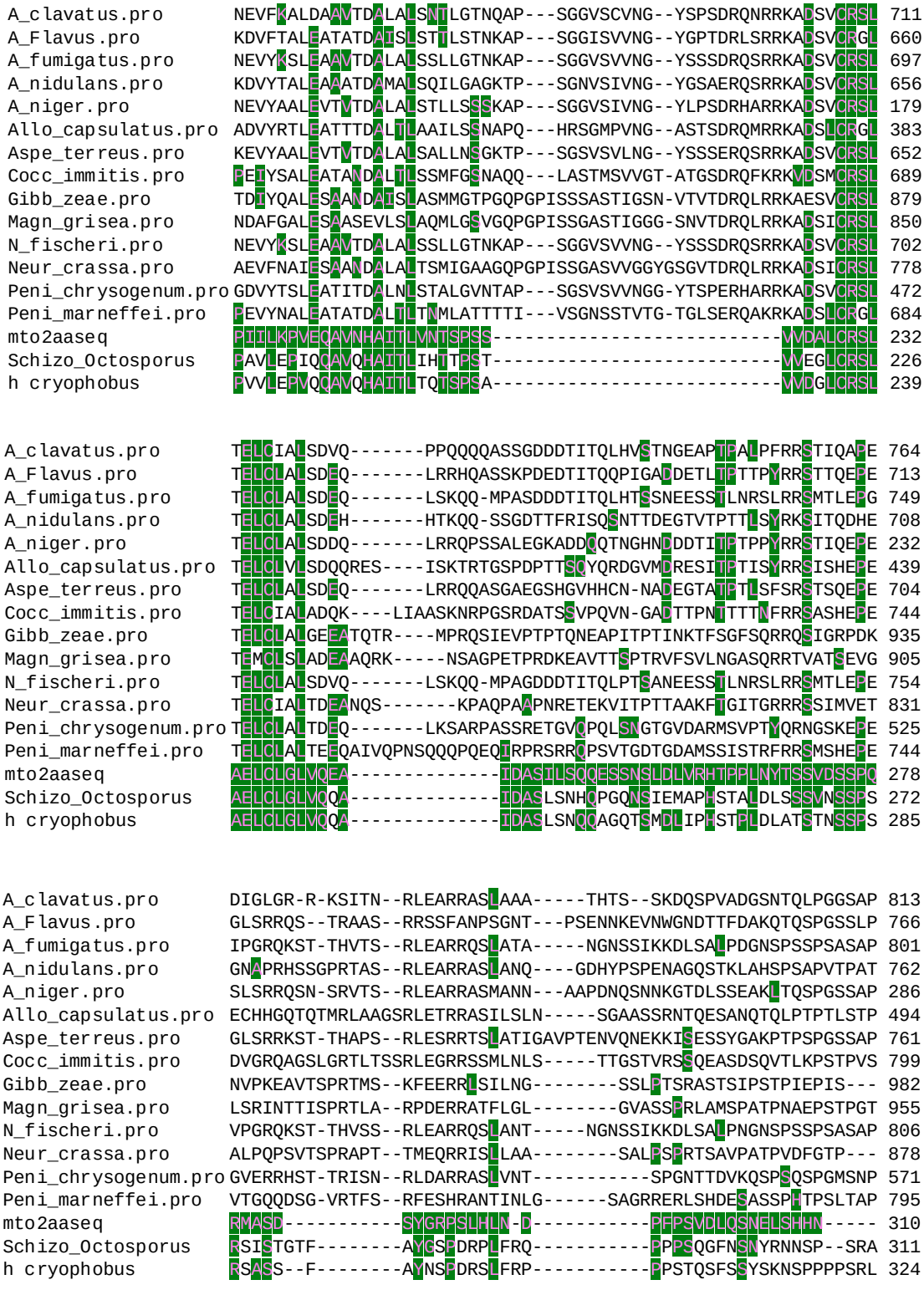
A_clavatus.pro NEVFKALDAAVTDALALSNILGTNQAP---SGGVSCVNG--YSPSDRQNRRKADSVCRSL 711
A_Flavus.pro KDVFTALEATATDAISLSTILSTNKAP---SGGISVVNG--YGPTDRLSRRKADSVCRGL 660
A_fumigatus.pro NEVYKSLEAAVTDALALSSLLGTNKAP---SGGVSVVNG--YSSSDRQSRRKADSVCRSL 697
A_nidulans.pro KDVYTALEAAATDAMALSQILGAGKTP---SGNVSIVNG--YGSAERQSRRKADSVCRSL 656
A_niger.pro NEVYAALEVTVTDALALSTLLSSSKAP---SGGVSIVNG--YLPSDRHARRKADSVCRSL 179
Allo_capsulatus.pro ADVYRTLEATTTDALTLAAILSSNAPQ---HRSGMPVNG--ASTSDRQMRRKADSLCRGL 383
Aspe_terreus.pro KEVYAALEVTVTDALALSALLNSGKTP---SGSVSVLNG--YSSSERQSRRKADSVCRSL 652
Cocc_immitis.pro PEIYSALEATANDALTLSSMFGSNAQQ---LASTMSVVGT-ATGSDRQFKRKVDSMCRSL 689
Gibb_zeae.pro TDIYQALESAANDAISLASMMGTPGQPGPISSSASTIGSN-VTVTDRQLRRKAESVCRSL 879
Magn_grisea.pro NDAFGALESAASEVLSLAQMLGSVGQPGPISSGASTIGGG-SNVTDRQLRRKADSICRSL 850
N_fischeri.pro NEVYKSLEAAVTDALALSSLLGTNKAP---SGGVSVVNG--YSSSDRQSRRKADSVCRSL 702
Neur_crassa.pro AEVFNAIESAANDALALTSMIGAAGQPGPISSGASVVGGYGSGVTDRQLRRKADSICRSL 778
Peni_chrysogenum.pro GDVYTSLEATITDALNLSTALGVNTAP---SGSVSVVNGG-YTSPERHARRKADSVCRSL 472
Peni_marneffei.pro PEVYNALEATATDALTLTNMLATTTTI---VSGNSSTVTG-TGLSERQAKRKADSLCRGL 684
mto2aaseq PIILKPVEQAVNHAITLVNTSPSS---------- VVDALCRSL 232
Schizo_Octosporus PAVLEPIQQAVQHAITLIHTTPST---------- VVEGLCRSL 226
h cryophobus PVVLEPVQQAVQHAITLTQTSPSA---------- VVDGLCRSL 239
A_clavatus.pro TELCIALSDVQ-------PPQQQQASSGDDDTITQLHVSTNGEAPTPALPFRRSTIQAPE 764
A_Flavus.pro TELCLALSDEQ-------LRRHQASSKPDEDTITQQPIGADDETLTPTTPYRRSTTQEPE 713
A_fumigatus.pro TELCLALSDEQ-------LSKQQ-MPASDDDTITQLHTSSNEESSTLNRSLRRSMTLEPG 749
A_nidulans.pro TELCLALSDEH-------HTKQQ-SSGDTTFRISQSNTTDEGTVTPTTLSYRKSITQDHE 708
A_niger.pro TELCLALSDDQ-------LRRQPSSALEGKADDQQTNGHNDDDTITPTPPYRRSTIQEPE 232
Allo_capsulatus.pro TELCLVLSDQQRES----ISKTRTGSPDPTTSQYQRDGVMDRESITPTISYRRSISHEPE 439
Aspe_terreus.pro TELCLALSDEQ-------LRRQQASGAEGSHGVHHCN-NADEGTATPTLSFSRSTSQEPE 704
Cocc_immitis.pro TELCIALADQK----LIAASKNRPGSRDATSSVPQVN-GADTTPNTTTTNFRRSASHEPE 744
Gibb_zeae.pro TELCLALGEEATQTR----MPRQSIEVPTPTQNEAPITPTINKTFSGFSQRRQSIGRPDK 935
Magn_grisea.pro TEMCLSLADEAAQRK-----NSAGPETPRDKEAVTTSPTRVFSVLNGASQRRTVATSEVG 905
N_fischeri.pro TELCLALSDVQ-------LSKQQ-MPAGDDDTITQLPTSANEESSTLNRSLRRSMTLEPE 754
Neur_crassa.pro TELCIALTDEANQS-------KPAQPAAPNRETEKVITPTTAAKFTGITGRRRSSIMVET 831
Peni_chrysogenum.pro TELCLALTDEQ-------LKSARPASSRETGVQPQLSNGTGVDARMSVPTYQRNGSKEPE 525
Peni_marneffei.pro TELCLALTEEQAIVQPNSQQQPQEQIRPRSRRQPSVTGDTGDAMSSISTRFRRSMSHEPE 744
mto2aaseq AELCLGLVQEA--------------IDASILSQQESSNSLDLVRHTPPLNYTSSVDSSPQ 278
Schizo_Octosporus AELCLGLVQQA--------------IDASLSNHQPGQNSIEMAPHSTALDLSSSVNSSPS 272
h cryophobus AELCLGLVQQA--------------IDASLSNQQAGQTSMDLIPHSTPLDLATSTNSSPS 285
A_clavatus.pro DIGLGR-R-KSITN--RLEARRASLAAA-----THTS--SKDQSPVADGSNTQLPGGSAP 813
A_Flavus.pro GLSRRQS--TRAAS--RRSSFANPSGNT---PSENNKEVNWGNDTTFDAKQTQSPGSSLP 766
A_fumigatus.pro IPGRQKST-THVTS--RLEARRQSLATA-----NGNSSIKKDLSALPDGNSPSSPSASAP 801
A_nidulans.pro GNAPRHSSGPRTAS--RLEARRASLANQ----GDHYPSPENAGQSTKLAHSPSAPVTPAT 762
A_niger.pro SLSRRQSN-SRVTS--RLEARRASMANN---AAPDNQSNNKGTDLSSEAKLTQSPGSSAP 286
Allo_capsulatus.pro ECHHGQTQTMRLAAGSRLETRRASILSLN-----SGAASSRNTQESANQTQLPTPTLSTP 494
Aspe_terreus.pro GLSRRKST-THAPS--RLESRRTSLATIGAVPTENVQNEKKISESSYGAKPTPSPGSSAP 761
Cocc_immitis.pro DVGRQAGSLGRTLTSSRLEGRRSSMLNLS-----TTGSTVRSSQEASDSQVTLKPSTPVS 799
Gibb_zeae.pro NVPKEAVTSPRTMS--KFEERRLSILNG--------SSLPTSRASTSIPSTPIEPIS--- 982
Magn_grisea.pro LSRINTTISPRTLA--RPDERRATFLGL--------GVASSPRLAMSPATPNAEPSTPGT 955
N_fischeri.pro VPGRQKST-THVSS--RLEARRQSLANT-----NGNSSIKKDLSALPNGNSPSSPSASAP 806
Neur_crassa.pro ALPQPSVTSPRAPT--TMEQRRISLLAA--------SALPSPRTSAVPATPVDFGTP--- 878
Peni_chrysogenum.pro GVERRHST-TRISN--RLDARRASLVNT----------SPGNTTDVKQSPSQSPGMSNP 571
Peni_marneffei.pro VTGQQDSG-VRTFS--RFESHRANTINLG------SAGRRERLSHDESASSPHTPSLTAP 795
mto2aaseq RMASD----------SYGRPSLHLN-D----------PFPSVDLQSNELSHHN----- 310
Schizo_Octosporus RSISTGTF--------AYGSPDRPLFRQ----------PPPSQGFNSNYRNNSP--SRA 311
h cryophobus RSASS--F--------AYNSPDRSLFRP----------PPSTQSFSSYSKNSPPPPSRL 324

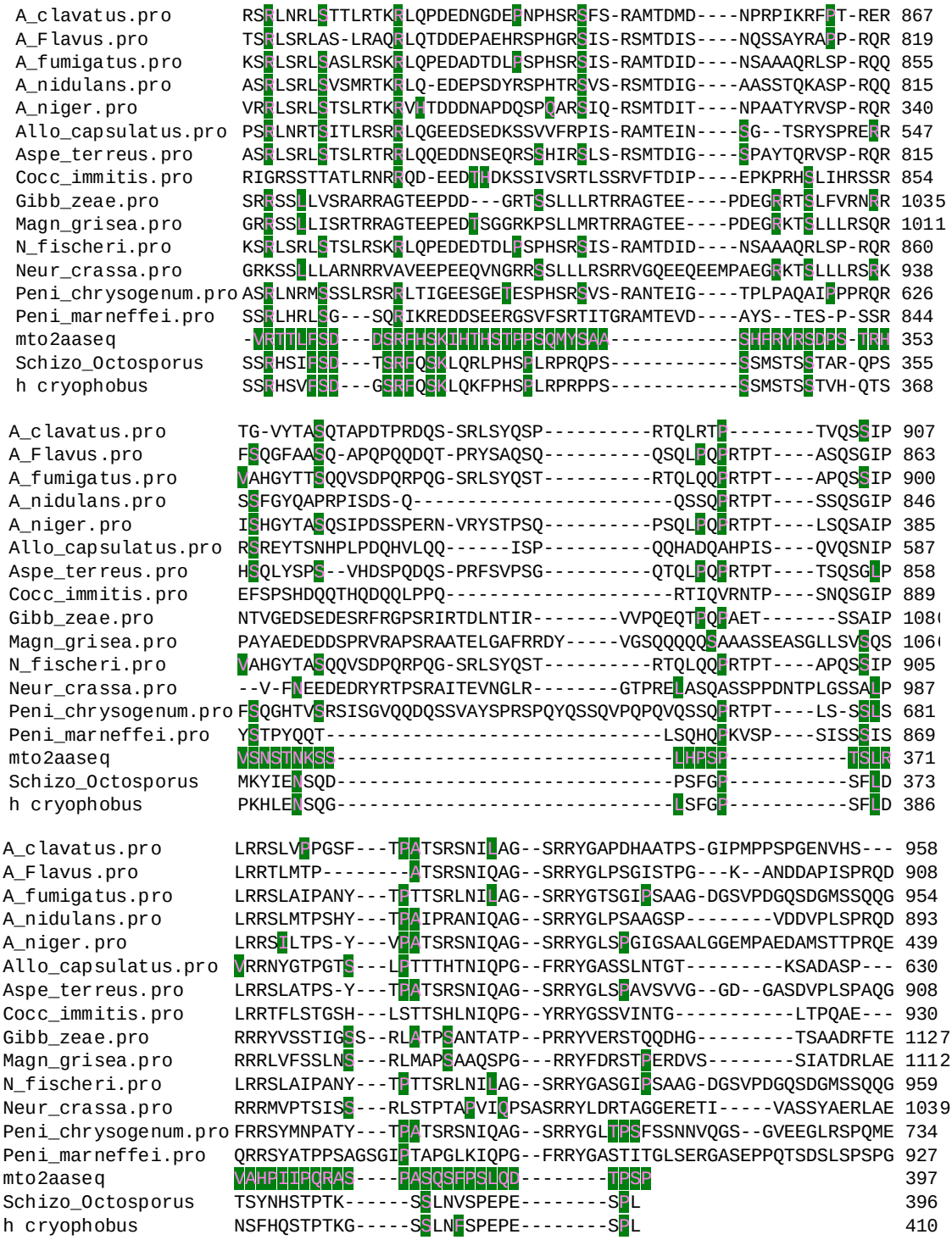

Alignment was performed using the MegAlign software program [Lasergene 8, DNAstar]. Residues highlighted in green indicate conservation of amino acid similarity with the Mto2 sequence in 8 or more homologs. *H. cryophobus* sequence was identified by D. Bitton and provided by IM. Hagan.

APPENDIX VI

PAIRCOIL2 prediction scores for Mto2 [104 – 152aa]

Residue Number	Amino Acid	Score	P-value		Residue Number	Amino Acid	Score	P-value
104	H	0.45	0.16722		129	E	10.8	0.01407
105	K	0.45	0.16722		130	L	10.8	0.01407
106	A	1.65	0.13399		131	E	10.8	0.01407
107	A	2.47	0.11409		132	N	10.8	0.01407
108	K	3.07	0.10071		133	L	10.8	0.01407
109	F	3.07	0.10071		134	R	10.8	0.01407
110	V	3.07	0.10071		135	E	10.8	0.01407
111	S	4.08	0.08114		136	R	10.8	0.01407
112	E	5.4	0.06007		137	L	10.8	0.01407
113	K	5.4	0.06007		138	N	10.8	0.01407
114	S	6.23	0.04931		139	Q	10.8	0.01407
115	L	7.24	0.03824		140	V	10.8	0.01407
116	E	7.5	0.03574		141	E	10.8	0.01407
117	K	10.8	0.01407		142	L	10.8	0.01407
118	V	10.8	0.01407		143	Q	10.8	0.01407
119	S	10.8	0.01407		144	L	10.8	0.01407
120	T	10.8	0.01407		145	S	10.8	0.01407
121	A	10.8	0.01407		146	E	10.8	0.01407
122	D	10.8	0.01407		147	R	8.37	0.02827
123	N	10.8	0.01407		148	P	2.16	0.12111
124	N	10.8	0.01407		149	S	2.16	0.12111
125	L	10.8	0.01407		150	S	1.58	0.1358
126	V	10.8	0.01407		151	Y	0.58	0.16338
127	L	10.8	0.01407		152	L	-0.81	0.20737
128	Q	10.8	0.01407					

Table VI.a PAIRCOIL2 probability scores for amino acids surrounding predicted coiled-coil. PAIRCOIL2 scores for amino acid sequence 104 - 152 are listed, where those residues found to have a significant score are highlighted in grey [114 – 147 aa]. The cut-off score used for prediction was 6.0 where significance was indicated by p-values < 0.05.

APPENDIX VII

Quantification of Cellular levels of Mto2

Quantification of MBP-Mto2

The concentration of purified MBP-Mto2 was calculated through comparison with a calibration curve created from purified BSA of known concentration [NEB, U.S.A.]. A dilution series of extract made from *E. coli* expressing MBP-Mto2 was analysed by SDS-PAGE. The integrated intensity of the Coomassie stain gel, scanned using the 600 channel, was quantified by Odyssey V3.0 [fig 5.10, Panel A]. This was compared to a standard curve from a Coomassie stained gel of known amounts of BSA [fig 5.10, Panel B]. On comparison with the calibration curve, the concentration of MBP-Mto2 was calculated as 0.15 µgµl^{-1}.

For example, 6 µl of MBP-Mto2 has an intensity of 1.82 which corresponds to 0.98 µg BSA, 0.98 / 6 = 0.153 µgµl^{1}

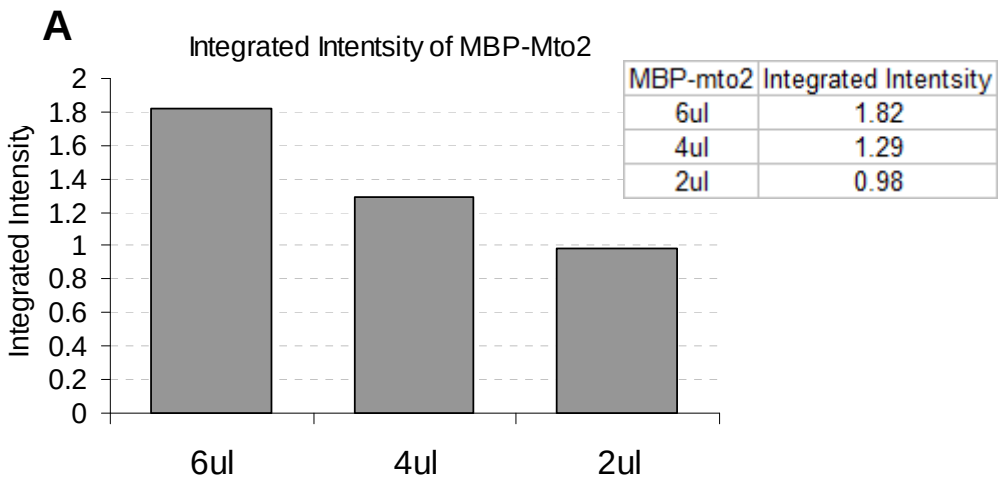

MBP-mto2	Integrated Intentsity
6ul	1.82
4ul	1.29
2ul	0.98

B

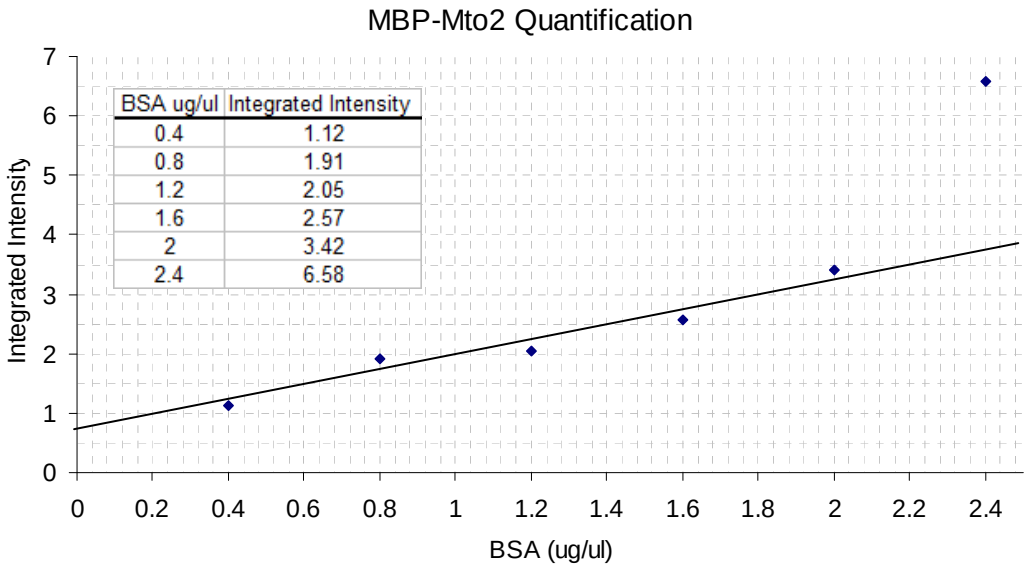

Figure VII.a Quantification of MBP-Mto2. [A] Integrated intensities of a range of volumes of the MBP-Mto2 sample were measured using Odyssey V3.0 software. Average intensity was compared with a BSA standard curve [B] and the concentration was calculated as 0.153 µgµl^{1}

In vivo Quantification of Mto2

Known amounts of MBP-Mto2 were then added to yeast extract made from 3 x10^{6} cells [KS516], as determined using a haemocytometer. Extracts were then analysed by western blot and probed with anti-Mto2. IRDye800 signal from both endogenous Mto2 and MBP-Mto2 was quantified using Odyssey V3.0 [Licor Biosciences, U.S.A.]. Average intensity of endogenous Mto2 from 3 x 10^{6} cells was calculated as 19.1, which when compared with the MBP-Mto2 calibration curve [fig 5.11] equates to 0.61 ng of MBP-Mto2.

The molecular weight of endogenous Mto2 is 44 kDa, therefore there are 44,017.5 g in 1 mole. Avogadro's constant states that there are 6.022×10^{23} molecules of Mto2 in 1 mole, therefore:

$6.022 \times 10^{23} / 44017.5 \times 10^{12}$ pg = 1.368×10^{7} molecules of Mto2 in 1 pg.

0.61 ng of Mto2 in 3×10^{6} cells

2.03×10^{-10}pg of Mto2 in 1 cell

2.03×10^{-10}pg X 1.368×10^{7} molecules per pg = 2777 ± 277 molecules of Mto2 per cell.

The quantification of MBP-Mto2 used Coomassie stain to identify the protein. The stain binds to both MBP and Mto2 portions of the protein. The molecular weight of MBP is equal to Mto2 therefore the contribution of Mto2 to the concentration of the MBP-Mto2 is exactly half. Therefore, the *in vivo* quantification of Mto2 is an underestimate by a factor of two. Consequently, the molecules per cell can be reduced by a factor of two resulting in 1388 ± 139 molecules of Mto2 per cell.

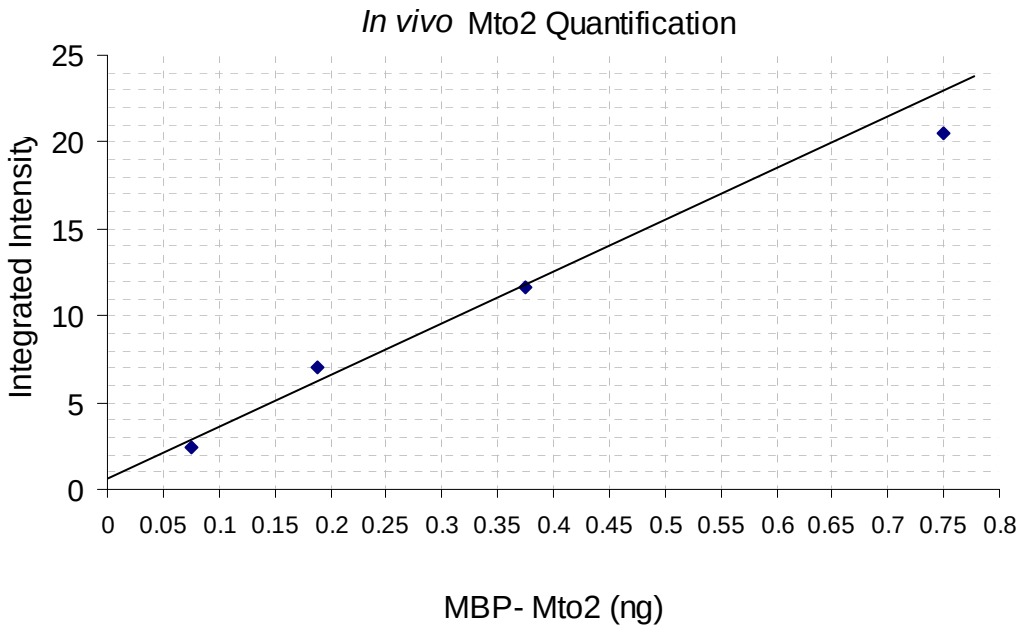

Figure VII.b Calibration curve for MBP-Mto2. Known amount of MBP-Mto2 were used to spike cell extracts. Extracts were then analysed by SDS-PAGE and the western blot was probed with α-Mto2. The integrated intensity of the signal from both endogenous and MBP-Mto2 was quantified by Odyssey V3.0. The average intensity for endogenous Mto2 was 19.1, which when compared to the MBP-Mto2 calibration curve was estimated to represent 0.61 ng of protein.

APPENDIX VIII

Quantification of Cellular levels of Mto1

Mto1-6His Quantification

A dilution series of extract made for *E. coli* expressing Mto1-His6 was analysed by SDS-PAGE. The integrated intensity of the Coomassie stain gel scanned using the 600 channel, was quantified by Odyssey V3.0 [fig 5.12, Panel A]. This was compared to a standard curve from a Coomassie stained gel of known amounts of BSA [fig 5.12, Panel B]. On comparison with the calibration curve, the concentration of Mto1-6His was calculated as 0.18 $\mu g \mu l^{-1}$.

For example, 5 µl of Mto1-6His has an intensity of 3.99 which corresponds to 0.9 µg BSA, 0.9 / 5 = 0.18 $\mu g \mu l^{1}$

A

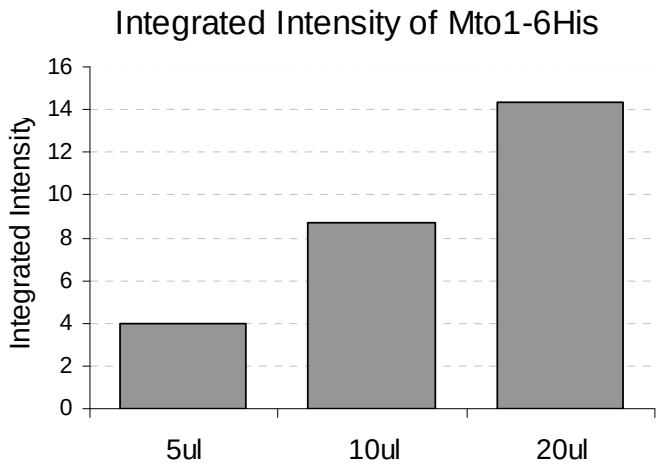

Mto1-6His	Integrated Intensity
5ul	3.99
10ul	8.71
20ul	14.31

B

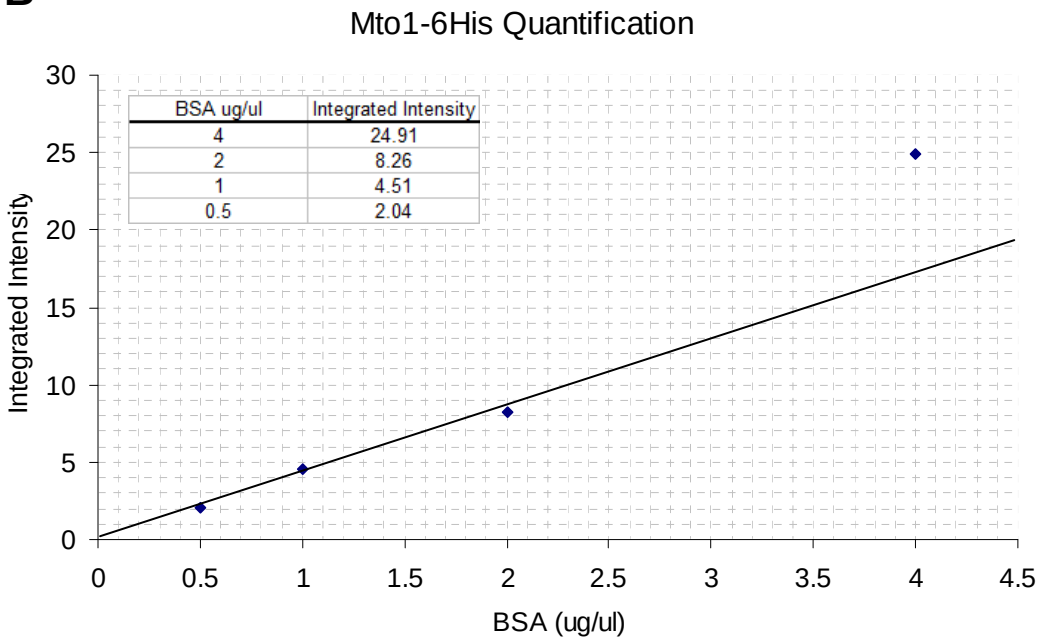

Figure VIII.a Quantification of Mto1-His6. (A) Integrated intensities of a range of volumes of the Mto1-6His sample was measured using Odyssey V3.0 software. Average intensity was compared with a BSA standard curve (B) and the concentration was calculated as 0.18 µgµl^{1}

In vivo Quantification of Mto1

Yeast extract was made from 6 x10^5 and 1.2 x 10^6 cells from strains expressing endogenous *mto1*$^+$ and *mto1Δ* [KS516 and KS1017]. The *mto1Δ* extract was spiked with serial dilutions of bacterial lysate containing known amounts of Mto1-6His. Extracts were then analysed by SDS-PAGE and the western blot was probed α-Mto1 [fig 5.13, Panel A]. The integrated intensity of the IRDye800 signal was quantified using Odyssey V3.0 [fig 5.13, Panel B]. Average intensity of

endogenous Mto1 from 1.2 x 10^6 cells was calculated as 24.22, when compared with the Mto1-6His calibration curve equates to 0.34 ng of Mto1.

The molecular weight of endogenous Mto1 is 128,469.08 Da, therefore there are 128,469.08 g in 1 mole. Avogadro's constant states that there are 6.022x10^{23} molecules of Mto1 in 1 mole, therefore:

6.022x10^{23} / 128,469.08 x 10^{12} pg = 4.69 x10^6 molecules of Mto1 in 1 pg.

0.34 ng of Mto1 in 1.2 x 10^6 cells

2.83 x 10^{-4} pg of Mto1 in 1 cell

2.83 x 10^{-4} pg X 4.69 x 10^7 molecules per pg = 1327 ± 133 molecules of Mto1 per cell

Quantification has shown that the number of protein molecules of both Mto2 and Mto1 present within the cell are approximately equal. This does not give any indication as to the relative levels of Mto1 and Mto2 present within a functional nucleation complex, as at any one time as not all of the expressed protein is incorporated at the MTOC.

When compared with quantification performed following a similar methods on other molecules, ~1,300 molecules per cell of both Mto1 and Mto2 fall within a similar range to proteins involved in the fission yeast cytoskeleton and cytokinesis (Wu *et al.* 2005). For example Sad1, a SPB protein, has 3,300 ± 1,100 molecules per cell, and Mid1 anillin-like protein has 2,100 ± 500.

A

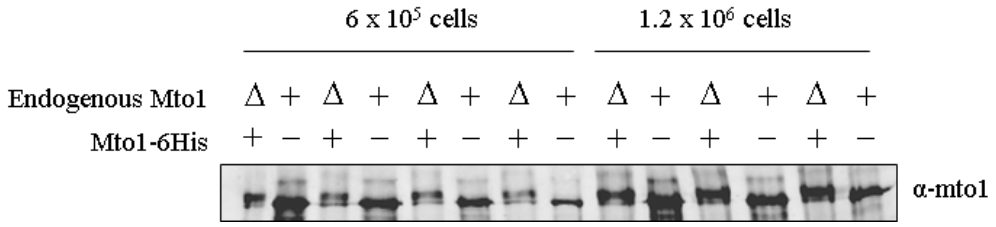

B

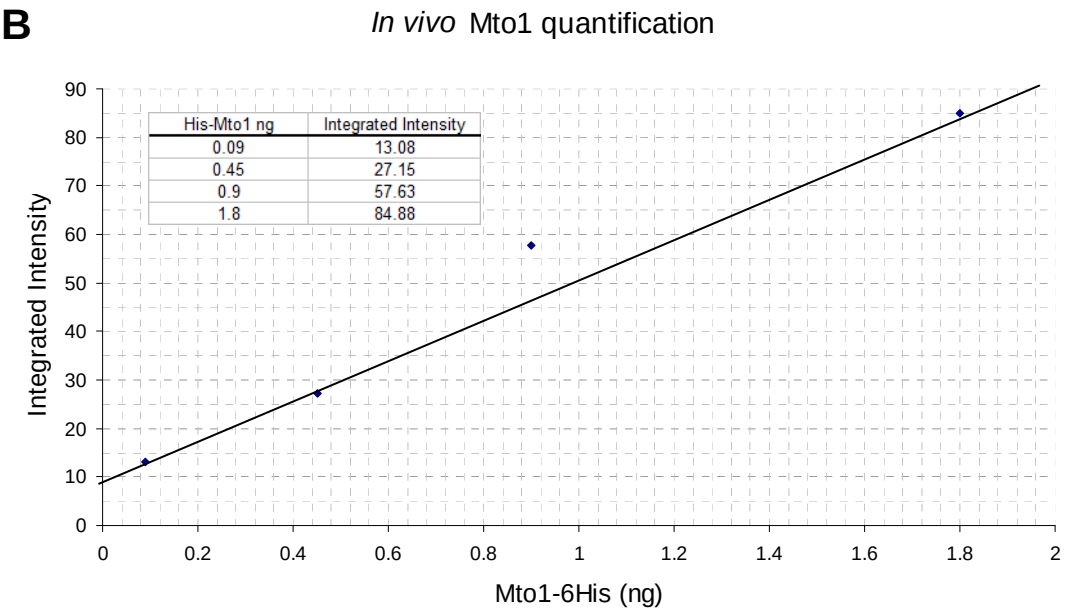

Figure VIII.b Quantification of cellular levels of Mto1. [A] Western blot analysis of endogenous Mto1, where Mto1-6His was added to extract from *mto1Δ* strain. Average signal intensity for endogenous Mto1 was compared with a calibration curve created from known amounts of Mto1-6His [B]. The amount of Mto1 expressed from 1.2 x 10^6 cells was estimated as 0.34 ng of protein.

APPENDIX IX

List of putative Mto2 phosphorylation sites

Residue Number	Sequence	S/T /Y	NetPhos Score	S/T-P	Consensus	Conserved in Eukaryote Alignment	Identified in Rosenburg Kinase Assay	Identified by Mass Spec	Identified by Mitotic Mass Spec
2	M**S**EHNY	S	0.004						yes [I]
6	SEHN**Y**QSDR	Y	0.913						
8	HNYQ**S**DREV	S	0.792						
20	PFLN**Y**EASA	Y	0.311						
23	NYEA**S**ANQL	S	0.003						
28	ANQL**S**SNSR	S	0.046						
29	NQLS**S**NSRE	S	0.997			yes			
31	LSSN**S**REST	S	0.988			yes			
34	NSRE**S**TPRG	S	0.997						
35	SRES**T**PRGS	T	0.996	yes	AURORA/ PDB	yes	yes		
39	TPRG**S**PWRA	S	0.994	yes	AURORA/ CDK	yes	yes		
47	AGMR**S**ASLM	S	0.038			yes			
49	MRSA**S**LMTE	S	0.888		AURORA				
52	ASLM**T**EPLE	T	0.04			yes			
58	PLED**S**MYSD	S	0.151						
60	EDSM**Y**SDNN	Y	0.98						
61	DSMY**S**DNNY	S	0.074						
65	SDNN**Y**LDNG	Y	0.985						
71	DNGV**S**FTKD	S	0.063						
73	GVSF**T**KDEN	T	0.294						
80	ENPL**Y**SPSW	Y	0.798						
81	NPLY**S**PSWP	S	0.926	yes		yes		yes	yes
83	LYSP**S**WPSL	S	0.017						
86	PSWP**S**LADA	S	0.394			yes			
94	ANVN**S**MKSN	S	0.461						
97	NSMK**S**NNAI	S	0.019			yes			
111	AKFV**S**EKSL	S	0.965		AURORA			yes	
114	VSEK**S**LEKV	S	0.902		POLO	yes			

119	LEKV**S**TADN	S	0.955		POLO				
120	EKVS**T**ADNN	T	0.109		AURORA	yes			
145	ELQL**S**ERPS	S	0.871						
149	SERP**S**SYLG	S	0.938			yes			
150	ERPS**S**YLGY	S	0.982		AURORA	yes		yes	
151	RPSS**Y**LGYH	Y	0.094						
154	SYLG**Y**HNNL	Y	0.767						
159	HNNL**S**PYRS	S	0.979	yes	CDK		yes	yes	yes
161	NLSP**Y**RSPN	Y	0.242						
163	SPYR**S**PNSY	S	0.732	yes					yes
166	RSPN**S**YPSL	S	0.597						
167	SPNS**Y**PSLL	Y	0.523	yes		yes		yes	
169	NSYP**S**LLPS	S	0.313					yes	yes
173	SLLP**S**THSP	S	0.331			yes			
174	LLPS**T**HSPH	T	0.029			yes		yes	yes
176	PSTH**S**PHSP	S	0.93	yes		yes		yes	yes
179	HSPH**S**PAPL	S	0.994	yes		yes		yes	yes
184	PAPL**S**TMQT	S	0.797						
185	APLS**T**MQTA	T	0.014					yes	yes
188	STMQ**T**ALMR	T	0.12			yes			
195	MRLR**T**YHPS	T	0.279		AURORA	yes			
196	RLRT**Y**HPSP	Y	0.037						
199	TYHP**S**PIIL	S	0.091	yes					yes [M]
215	NHAI**T**LVNT	T	0.363			yes			
219	TLVN**T**SPSS	T	0.058			yes			
220	LVNT**S**PSSV	S	0.964	yes		yes			
222	NTSP**S**SVVD	S	0.087			yes			
223	TSPS**S**VVDA	S	0.995			yes			
231	ALCR**S**LAEL	S	0.11			yes			
247	AIDA**S**ILSQ	S	0.014						
250	ASIL**S**QQES	S	0.877						
254	SQQE**S**SNSL	S	0.164			yes			
255	QQES**S**NSLD	S	0.098			yes			
257	ESSN**S**LDLV	S	0.027						
264	LVRH**T**PPLN	T	0.169	yes	AURORA	yes	yes	yes	

269	PPLN**Y**TSSV	Y	0.171					yes	
270	PLNY**T**SSVD	T	0.064			yes			
271	LNYT**S**SVDS	S	0.955					yes	
272	NYTS**S**VDSS	S	0.051					yes	
275	SSVD**S**SPQR	S	0.643			yes		yes	
276	SVDS**S**PQRM	S	0.985	yes	CDK/PDB	yes	yes	yes	
282	QRMA**S**DSYG	S	0.982		AURORA	yes		yes	yes
284	MASD**S**YGRP	S	0.988					yes	
285	ASDS**Y**GRPS	Y	0.9						
289	YGRP**S**LHLN	S	0.981		AURORA				yes
298	DPFP**S**VDLQ	S	0.013			yes			
303	VDLQ**S**NELS	S	0.221		POLO				yes
307	SNEL**S**HHNV	S	0.158			yes			yes [M]
313	HNVR**T**TLFS	T	0.015			yes			
314	NVRT**T**LFSD	T	0.89		AURORA	yes			
317	TTLF**S**DDSR	S	0.337						
320	FSDD**S**RFHS	S	0.268						
324	SRFH**S**KIHT	S	0.988		AURORA				
328	SKIH**T**HSTP	T	0.029		AURORA				
330	IHTH**S**TPPS	S	0.381					yes	
331	HTHS**T**PPSQ	T	0.578	yes	PDB		yes	yes	yes
334	STPP**S**QMYS	S	0.104					yes	
337	PSQM**Y**SAAS	Y	0.081						
338	SQMY**S**AASH	S	0.034						
341	YSAA**S**HFRY	S	0.978						
345	SHFR**Y**RSDP	Y	0.263						
347	FRYR**S**DPST	S	0.846		AURORA				
350	RSDP**S**TRHV	S	0.785						
351	SDPS**T**RHVS	T	0.112						
355	TRHV**S**NSTN	S	0.916		AURORA	yes			
357	HVSN**S**TNKS	S	0.8						
358	VSNS**T**NKSS	T	0.167						
361	STNK**S**SLHP	S	0.048					yes	
362	TNKS**S**LHPS	S	0.782		AURORA			yes	
366	SLHP**S**PTSL	S	0.964	yes			yes	yes	yes

368	HPSP**T**SLRV	T	0.26						
369	PSPT**S**LRVA	S	0.479					yes	
382	PQRA**S**PASQ	S	0.992	yes	AURORA		yes		
385	ASPA**S**QSFP	S	0.974						
387	PASQ**S**FPSL	S	0.013			yes			
390	QSFP**S**LQDT	S	0.992						
394	SLQD**T**PSP-	T	0.772	yes		yes	yes		
396	QDTP**S**P---	S	0.325	yes		yes	yes		

REFERENCES

Addinall, S. G. and J. Lutkenhaus (1996). "FtsZ-spirals and -arcs determine the shape of the invaginating septa in some mutants of Escherichia coli." Mol Microbiol 22(**2**): 231-7.

Ahringer, J. (2003). "Control of cell polarity and mitotic spindle positioning in animal cells." Curr Opin Cell Biol 15(**1**): 73-81.

Alberts, B., Johnson, A., Lewis, J., *et al.* (2002). 'The Cytoskeleton'. In: Molecular Biology of the Cell. 4th ed. New York. Garland Sciences. pp. 907-982.

Alderton, G. K., L. Galbiati, E. Griffith, *et al.* (2006). "Regulation of mitotic entry by microcephalin and its overlap with ATR signalling." Nat Cell Biol 8(**7**): 725-33.

Altschul, S. F., T. L. Madden, A. A. Schaffer, *et al.* (1997). "Gapped BLAST and PSI-BLAST: a new generation of protein database search programs." Nucleic Acids Res 25(**17**): 3389-402.

Ambrose, J. C. and R. Cyr (2008). "Mitotic spindle organization by the preprophase band." Mol Plant 1(**6**): 950-60.

Anders, A., P. C. Lourenco and K. E. Sawin (2006). "Noncore components of the fission yeast gamma-tubulin complex." Mol Biol Cell 17(**12**): 5075-93.

Archambault, V. and D. M. Glover (2009). "Polo-like kinases: conservation and divergence in their functions and regulation." Nat Rev Mol Cell Biol 10(**4**): 265-75.

Ayscough, K., N. M. Hajibagheri, R. Watson and G. Warren (1993). "Stacking of Golgi cisternae in Schizosaccharomyces pombe requires intact microtubules." J Cell Sci 106 (Pt 4): 1227-37.

Bahler, J., J. Q. Wu, M. S. Longtine, *et al.* (1998). "Heterologous modules for efficient and versatile PCR-based gene targeting in Schizosaccharomyces pombe." Yeast 14(**10**): 943-51.

Balasubramanian, M. K., D. M. Helfman and S. M. Hemmingsen (1992). "A new tropomyosin essential for cytokinesis in the fission yeast S. pombe." Nature 360(**6399**): 84-7.

Ballestrem, C., B. Wehrle-Haller, B. Hinz and B. A. Imhof (2000). "Actin-dependent lamellipodia formation and microtubule-dependent tail retraction control-directed cell migration." Mol Biol Cell 11(**9**): 2999-3012.

Barr, F. A., H. H. Sillje and E. A. Nigg (2004). "Polo-like kinases and the orchestration of cell division." Nat Rev Mol Cell Biol 5(**6**): 429-40.

Bartolini, F. and G. G. Gundersen (2006). "Generation of noncentrosomal microtubule arrays." J Cell Sci 119(**Pt 20**): 4155-63.

Berg, H. C. and R. A. Anderson (1973). "Bacteria swim by rotating their flagellar filaments." Nature 245(**5425**): 380-2.

Berger, B., D. B. Wilson, E. Wolf, T. Tonchev, M. Milla and P. S. Kim (1995). "Predicting coiled coils by use of pairwise residue correlations." Proc Natl Acad Sci U S A 92(**18**): 8259-63.

Bertolini, B., G. Monaco and A. Rossi (1970). "Ultrastructure of a regular arrangement of microtubules and neurofilaments." J Ultrastruct Res 33(**1**): 173-86.

Bezanilla, M., S. L. Forsburg and T. D. Pollard (1997). "Identification of a second myosin-II in Schizosaccharomyces pombe: Myp2p is conditionally required for cytokinesis." Mol Biol Cell 8(**12**): 2693-705.

Blom, N., S. Gammeltoft and S. Brunak (1999). "Sequence and structure-based prediction of eukaryotic protein phosphorylation sites." J Mol Biol 294(**5**): 1351-62.

Bloom, K. (2003). "Microtubule cytoskeleton: navigating the intracellular landscape." Curr Biol 13(**11**): R430-2.

Bradford, M. M. (1976). "A rapid and sensitive method for the quantitation of microgram quantities of protein utilizing the principle of protein-dye binding." Anal Biochem 72: 248-54.

Brennan, I. M., U. Peters, T. M. Kapoor and A. F. Straight (2007). "Polo-like kinase controls vertebrate spindle elongation and cytokinesis." PLoS One 2(**5**): e409.

Bringmann, H. and A. A. Hyman (2005). "A cytokinesis furrow is positioned by two consecutive signals." Nature 436(**7051**): 731-4.

Brune, C., S. E. Munchel, N. Fischer, A. V. Podtelejnikov and K. Weis (2005). "Yeast poly(A)-binding protein Pab1 shuttles between the nucleus and the cytoplasm and functions in mRNA export." Rna 11(**4**): 517-31.

Bugnard, E., K. J. Zaal and E. Ralston (2005). "Reorganization of microtubule nucleation during muscle differentiation." Cell Motil Cytoskeleton 60(**1**): 1-13.

Burnett, G. and E. P. Kennedy (1954). "The enzymatic phosphorylation of proteins." J Biol Chem 211(**2**): 969-80.

Burton, P. R. (1966). "Substructure of certain cytoplasmic microtubules: an electron microscopic study." Science 154(**751**): 903-5.

Busch, K. E. and D. Brunner (2004). "The microtubule plus end-tracking proteins mal3p and tip1p cooperate for cell-end targeting of interphase microtubules." Curr Biol 14(**7**): 548-59.

Busso, D., B. Delagoutte-Busso and D. Moras (2005). "Construction of a set Gateway-based destination vectors for high-throughput cloning and expression screening in Escherichia coli." Anal Biochem 343(**2**): 313-21.

Carazo-Salas, R. and P. Nurse (2007). "Sorting out interphase microtubules." Mol Syst Biol 3: 95.

Carmena, M., M. G. Riparbelli, G. Minestrini, *et al.* (1998). "Drosophila polo kinase is required for cytokinesis." J Cell Biol 143(**3**): 659-71.

Casenghi, M., P. Meraldi, U. Weinhart, P. I. Duncan, R. Korner and E. A. Nigg (2003). "Polo-like kinase 1 regulates Nlp, a centrosome protein involved in microtubule nucleation." Dev Cell 5(**1**): 113-25.

Caviston, J. P. and E. L. Holzbaur (2006). "Microtubule motors at the intersection of trafficking and transport." Trends Cell Biol 16(**10**): 530-7.

Chalfie, M. and J. N. Thomson (1982). "Structural and functional diversity in the neuronal microtubules of Caenorhabditis elegans." J Cell Biol 93(**1**): 15-23.

Chang, F., D. Drubin and P. Nurse (1997). "cdc12p, a protein required for cytokinesis in fission yeast, is a component of the cell division ring and interacts with profilin." J Cell Biol 137(**1**): 169-82.

Chang, F., A. Woollard and P. Nurse (1996). "Isolation and characterization of fission yeast mutants defective in the assembly and placement of the contractile actin ring." J Cell Sci 109 (Pt 1): 131-42.

Cheeseman, I. M., C. Brew, M. Wolyniak, *et al.* (2001). "Implication of a novel multiprotein Dam1p complex in outer kinetochore function." J Cell Biol 155(**7**): 1137-45.

Chen, H. R., M. T. Hsu and S. C. Cheng (1995). "Spheroplast preparation facilitates PCR screening of yeast sequence." Biotechniques 19(**5**): 744-6, 748.

Ching, Y. P., Z. Qi and J. H. Wang (2000). "Cloning of three novel neuronal Cdk5 activator binding proteins." Gene 242(**1-2**): 285-94.

Ciosk, R., W. Zachariae, C. Michaelis, A. Shevchenko, M. Mann and K. Nasmyth (1998). "An ESP1/PDS1 complex regulates loss of sister chromatid cohesion at the metaphase to anaphase transition in yeast." Cell 93(**6**): 1067-76.

Cole, C., J. D. Barber and G. J. Barton (2008). "The Jpred 3 secondary structure prediction server." Nucleic Acids Res 36(**Web Server issue**): W197-201.

Cuschieri, L., R. Miller and J. Vogel (2006). "Gamma-tubulin is required for proper recruitment and assembly of Kar9-Bim1 complexes in budding yeast." Mol Biol Cell 17(**10**): 4420-34.

Dephoure, N., C. Zhou, J. Villen, *et al.* (2008). "A quantitative atlas of mitotic phosphorylation." Proc Natl Acad Sci U S A 105(**31**): 10762-7.

Desai, A. and T. J. Mitchison (1997). "Microtubule polymerization dynamics." Annu Rev Cell Dev Biol 13: 83-117.

Dictenberg, J. B., W. Zimmerman, C. A. Sparks, *et al.* (1998). "Pericentrin and gamma-tubulin form a protein complex and are organized into a novel lattice at the centrosome." J Cell Biol 141(**1**): 163-74.

Ding, R., R. R. West, D. M. Morphew, B. R. Oakley and J. R. McIntosh (1997). "The spindle pole body of Schizosaccharomyces pombe enters and leaves the nuclear envelope as the cell cycle proceeds." Mol Biol Cell 8(**8**): 1461-79.

Dobbelaere, J., F. Josue, S. Suijkerbuijk, B. Baum, N. Tapon and J. Raff (2008). "A genome-wide RNAi screen to dissect centriole duplication and centrosome maturation in Drosophila." PLoS Biol 6(**9**): e224.

Doxsey, S., D. McCollum and W. Theurkauf (2005). "Centrosomes in cellular regulation." Annu Rev Cell Dev Biol 21: 411-34.

Drubin, D. G. and W. J. Nelson (1996). "Origins of cell polarity." Cell 84(**3**): 335-44.

Drummond, D. R. and R. A. Cross (2000). "Dynamics of interphase microtubules in Schizosaccharomyces pombe." Curr Biol 10(**13**): 766-75.

Ehrhardt, D. W. (2008). "Straighten up and fly right: microtubule dynamics and organization of non-centrosomal arrays in higher plants." Curr Opin Cell Biol 20(**1**): 107-16.

Elia, A. E., L. C. Cantley and M. B. Yaffe (2003a). "Proteomic screen finds pSer/pThr-binding domain localizing Plk1 to mitotic substrates." Science 299(**5610**): 1228-31.

Elia, A. E., P. Rellos, L. F. Haire*, et al.* (2003b). "The molecular basis for phosphodependent substrate targeting and regulation of Plks by the Polo-box domain." Cell 115(**1**): 83-95.

Elias, J. E. and S. P. Gygi (2007). "Target-decoy search strategy for increased confidence in large-scale protein identifications by mass spectrometry." Nat Methods 4(**3**): 207-14.

Endicott, J. A., M. E. Noble and J. A. Tucker (1999). "Cyclin-dependent kinases: inhibition and substrate recognition." Curr Opin Struct Biol 9(**6**): 738-44.

Eng, K., N. I. Naqvi, K. C. Wong and M. K. Balasubramanian (1998). "Rng2p, a protein required for cytokinesis in fission yeast, is a component of the actomyosin ring and the spindle pole body." Curr Biol 8(**11**): 611-21.

Erickson, H. P. (2000). "Gamma-tubulin nucleation: template or protofilament?" Nat Cell Biol 2(**6**): E93-6.

Erickson, H. P. and D. Stoffler (1996a). "Protofilaments and rings, two conformations of the tubulin family conserved from bacterial FtsZ to alpha/beta and gamma tubulin." J Cell Biol 135(**1**): 5-8.

Erickson, H. P., D. W. Taylor, K. A. Taylor and D. Bramhill (1996b). "Bacterial cell division protein FtsZ assembles into protofilament sheets and minirings, structural homologs of tubulin polymers." Proc Natl Acad Sci U S A 93(**1**): 519-23.

Evans, L., T. Mitchison and M. Kirschner (1985). "Influence of the centrosome on the structure of nucleated microtubules." J Cell Biol 100(**4**): 1185-91.

Fan, J., A. D. Griffiths, A. Lockhart, R. A. Cross and L. A. Amos (1996). "Microtubule minus ends can be labelled with a phage display antibody specific to alpha-tubulin." J Mol Biol 259(**3**): 325-30.

Fankhauser, C., A. Reymond, L. Cerutti, S. Utzig, K. Hofmann and V. Simanis (1995). "The S. pombe cdc15 gene is a key element in the reorganization of F-actin at mitosis." Cell 82(**3**): 435-44.

Fawcett, D.W. and Porter, K.R. [1954] A study of the fine structure of ciliated epithelia. *J. Morphol.* (**94**): 221–281.

Flory, M. R., M. Morphew, J. D. Joseph, A. R. Means and T. N. Davis (2002). "Pcp1p, an Spc110p-related calmodulin target at the centrosome of the fission yeast Schizosaccharomyces pombe." Cell Growth Differ 13(**2**): 47-58.

Fong, C. S., M. Sato and T. Toda (2009a). "Fission yeast Pcp1 links polo kinase-mediated mitotic entry to gamma-tubulin-dependent spindle formation." Embo J.

Fong, K. W., Y. K. Choi, J. B. Rattner and R. Z. Qi (2008). "CDK5RAP2 is a pericentriolar protein that functions in centrosomal attachment of the gamma-tubulin ring complex." Mol Biol Cell 19(**1**): 115-25.

Fong, K. W., S. Y. Hau, Y. S. Kho, Y. Jia, L. He and R. Z. Qi (2009b). "Interaction of CDK5RAP2 with EB1 to track growing microtubule tips and to regulate microtubule dynamics." Mol Biol Cell 20(**16**): 3660-70.

Fujita, A., L. Vardy, M. A. Garcia and T. Toda (2002). "A fourth component of the fission yeast gamma-tubulin complex, Alp16, is required for cytoplasmic microtubule integrity and becomes indispensable when gamma-tubulin function is compromised." Mol Biol Cell 13(**7**): 2360-73.

Geissler, S., G. Pereira, A. Spang, *et al.* (1996). "The spindle pole body component Spc98p interacts with the gamma-tubulin-like Tub4p of Saccharomyces cerevisiae at the sites of microtubule attachment." Embo J 15(**15**): 3899-911.

Gibbons, I. R. (1961). "The relationship between the fine structure and direction of beat in gill cilia of a lamellibranch mollusc." J Biophys Biochem Cytol 11: 179-205.

Gibney, J. and J. Q. Zheng (2003). "Cytoskeletal dynamics underlying collateral membrane protrusions induced by neurotrophins in cultured Xenopus embryonic neurons." J Neurobiol 54(**2**): 393-405.

Glotzer, M. (2009). "The 3Ms of central spindle assembly: microtubules, motors and MAPs." Nat Rev Mol Cell Biol 10(**1**): 9-20.

Gould, K. L. and P. Nurse (1989). "Tyrosine phosphorylation of the fission yeast cdc2+ protein kinase regulates entry into mitosis." Nature 342(**6245**): 39-45.

Gould, R. R. and G. G. Borisy (1977). "The pericentriolar material in Chinese hamster ovary cells nucleates microtubule formation." J Cell Biol 73(**3**): 601-15.

Grallert, A., C. Beuter, R. A. Craven, *et al.* (2006). "S. pombe CLASP needs dynein, not EB1 or CLIP170, to induce microtubule instability and slows polymerization rates at cell tips in a dynein-dependent manner." Genes Dev 20(**17**): 2421-36.

Gruber, S., P. Arumugam, Y. Katou, *et al.* (2006). "Evidence that loading of cohesin onto chromosomes involves opening of its SMC hinge." Cell 127(**3**): 523-37.

Gruhler, A., J. V. Olsen, S. Mohammed, *et al.* (2005). "Quantitative phosphoproteomics applied to the yeast pheromone signaling pathway." Mol Cell Proteomics 4(**3**): 310-27.

Guerrero, C., C. Tagwerker, P. Kaiser and L. Huang (2006). "An integrated mass spectrometry-based proteomic approach: quantitative analysis of tandem affinity-purified in vivo cross-linked protein complexes (QTAX) to decipher the 26 S proteasome-interacting network." Mol Cell Proteomics 5(**2**): 366-78.

Gunawardane, R. N., S. B. Lizarraga, C. Wiese, A. Wilde and Y. Zheng (2000a). "gamma-Tubulin complexes and their role in microtubule nucleation." Curr Top Dev Biol 49: 55-73.

Gunawardane, R. N., O. C. Martin, K. Cao, *et al.* (2000b). "Characterization and reconstitution of Drosophila gamma-tubulin ring complex subunits." J Cell Biol 151(**7**): 1513-24.

Gunawardane, R. N., O. C. Martin and Y. Zheng (2003). "Characterization of a new gammaTuRC subunit with WD repeats." Mol Biol Cell 14(**3**): 1017-26.

Hagan, I. and M. Yanagida (1995). "The product of the spindle formation gene sad1+ associates with the fission yeast spindle pole body and is essential for viability." J Cell Biol 129(**4**): 1033-47.

Hagan, I. and M. Yanagida (1997). "Evidence for cell cycle-specific, spindle pole body-mediated, nuclear positioning in the fission yeast Schizosaccharomyces pombe." J Cell Sci 110 (Pt 16): 1851-66.

Hagan, I. M. (1998). "The fission yeast microtubule cytoskeleton." J Cell Sci 111 (Pt 12): 1603-12.

Hagan, I. M. (2008). "The spindle pole body plays a key role in controlling mitotic commitment in the fission yeast Schizosaccharomyces pombe." Biochem Soc Trans 36(**Pt 5**): 1097-101.

Hagan, I. M. and J. S. Hyams (1988). "The use of cell division cycle mutants to investigate the control of microtubule distribution in the fission yeast Schizosaccharomyces pombe." J Cell Sci 89 (Pt 3): 343-57.

Haren, L., M. H. Remy, I. Bazin, I. Callebaut, M. Wright and A. Merdes (2006). "NEDD1-dependent recruitment of the gamma-tubulin ring complex to the centrosome is necessary for centriole duplication and spindle assembly." J Cell Biol 172(**4**): 505-15.

Harlow, E and Lane, D. (1988). Antibodies: A Laboratory Manual. Cold Spring Harbor Laboratory Press. New York.

Hartley, J. L., G. F. Temple and M. A. Brasch (2000). "DNA cloning using in vitro site-specific recombination." Genome Res 10(**11**): 1788-95.

Heitz, M. J., J. Petersen, S. Valovin and I. M. Hagan (2001). "MTOC formation during mitotic exit in fission yeast." J Cell Sci 114(**Pt 24**): 4521-32.

Hiraoka, Y., T. Toda and M. Yanagida (1984). "The NDA3 gene of fission yeast encodes beta-tubulin: a cold-sensitive nda3 mutation reversibly blocks spindle formation and chromosome movement in mitosis." Cell 39(**2 Pt 1**): 349-58.

Horio, T., S. Uzawa, M. K. Jung, B. R. Oakley, K. Tanaka and M. Yanagida (1991). "The fission yeast gamma-tubulin is essential for mitosis and is localized at microtubule organizing centers." J Cell Sci 99 (Pt 4): 693-700.

Hunter, T. (1995). "Protein kinases and phosphatases: the yin and yang of protein phosphorylation and signaling." Cell 80(**2**): 225-36.

Inoue, Y. H., M. S. Savoian, T. Suzuki, E. Mathe, M. T. Yamamoto and D. M. Glover (2004). "Mutations in orbit/mast reveal that the central spindle is comprised of two microtubule populations, those that initiate cleavage and those that propagate furrow ingression." J Cell Biol 166(**1**): 49-60.

Jackson, A. P., H. Eastwood, S. M. Bell, *et al.* (2002). "Identification of microcephalin, a protein implicated in determining the size of the human brain." Am J Hum Genet 71(**1**): 136-42.

Janson, M. E., T. G. Setty, A. Paoletti and P. T. Tran (2005). "Efficient formation of bipolar microtubule bundles requires microtubule-bound gamma-tubulin complexes." J Cell Biol 169(**2**): 297-308.

Joshi, H. C., M. J. Palacios, L. McNamara and D. W. Cleveland (1992). "Gamma-tubulin is a centrosomal protein required for cell cycle-dependent microtubule nucleation." Nature 356(**6364**): 80-3.

Jurgens, G. (2005). "Plant cytokinesis: fission by fusion." Trends Cell Biol 15(**5**): 277-83.

Karsenti, E., S. Kobayashi, T. Mitchison and M. Kirschner (1984). "Role of the centrosome in organizing the interphase microtubule array: properties of cytoplasts containing or lacking centrosomes." J Cell Biol 98(**5**): 1763-76.

Keating, T. J. and G. G. Borisy (1999). "Centrosomal and non-centrosomal microtubules." Biol Cell 91(**4-5**): 321-9.

Keating, T. J. and G. G. Borisy (2000). "Immunostructural evidence for the template mechanism of microtubule nucleation." Nat Cell Biol 2(**6**): 352-7.

Kellogg, D. R. and B. M. Alberts (1992). "Purification of a multiprotein complex containing centrosomal proteins from the Drosophila embryo by chromatography with low-affinity polyclonal antibodies." Mol Biol Cell 3(**1**): 1-11.

Khodjakov, A., R. W. Cole, B. R. Oakley and C. L. Rieder (2000). "Centrosome-independent mitotic spindle formation in vertebrates." Curr Biol 10(**2**): 59-67.

Khodjakov, A. and C. L. Rieder (2001). "Centrosomes enhance the fidelity of cytokinesis in vertebrates and are required for cell cycle progression." J Cell Biol 153(**1**): 237-42.

Kitayama, C., A. Sugimoto and M. Yamamoto (1997). "Type II myosin heavy chain encoded by the myo2 gene composes the contractile ring during cytokinesis in Schizosaccharomyces pombe." J Cell Biol 137(**6**): 1309-19.

Kofron, M., E. Nadezdina, A. Vassilev, *et al.* (1998). "Interaction of an Overexpressed gamma-Tubulin with Microtubules In Vivo and In Vitro." Zoolog Sci 15(**4**): 477-87.

Kollman, J. M., A. Zelter, E. G. Muller, *et al.* (2008). "The Structure of the {gamma}-Tubulin Small Complex: Implications of Its Architecture and Flexibility for Microtubule Nucleation." Mol Biol Cell 19(**1**): 207-15.

Kramer, A., N. Mailand, C. Lukas, *et al.* (2004). "Centrosome-associated Chk1 prevents premature activation of cyclin-B-Cdk1 kinase." Nat Cell Biol 6(**9**): 884-91.

Krapp, A., M. P. Gulli and V. Simanis (2004). "SIN and the art of splitting the fission yeast cell." Curr Biol 14(**17**): R722-30.

Krapp, A. and V. Simanis (2008). "An overview of the fission yeast septation initiation network (SIN)." Biochem Soc Trans 36(**Pt 3**): 411-5.

Laemmli, U. K. (1970). "Cleavage of structural proteins during the assembly of the head of bacteriophage T4." Nature 227(**5259**): 680-5.

Lander, E. S., L. M. Linton, B. Birren, *et al.* (2001). "Initial sequencing and analysis of the human genome." Nature 409(**6822**): 860-921.

Landy, A. (1989). "Dynamic, structural, and regulatory aspects of lambda site-specific recombination." Annu Rev Biochem 58: 913-49.

Langford, G. M. (1980). "Arrangement of subunits in microtubules with 14 profilaments." J Cell Biol 87(**2 Pt 1**): 521-6.

Larkin, M. A., G. Blackshields, N. P. Brown, *et al.* (2007). "Clustal W and Clustal X version 2.0." Bioinformatics 23(**21**): 2947-8.

Ledbetter, M. C. and K. R. Porter (1963). "A "Microtubule" in Plant Cell Fine Structure." J Cell Biol 19(**1**): 239-250.

Lee, J. C. and S. N. Timasheff (1975). "The reconstitution of microtubules from purified calf brain tubulin." Biochemistry 14(**23**): 5183-7.

Leguy, R., R. Melki, D. Pantaloni and M. F. Carlier (2000). "Monomeric gamma - tubulin nucleates microtubules." J Biol Chem 275(**29**): 21975-80.

Lowe, J., H. Li, K. H. Downing and E. Nogales (2001). "Refined structure of alpha beta-tubulin at 3.5 A resolution." J Mol Biol 313(**5**): 1045-57.

Luders, J., U. K. Patel and T. Stearns (2006). "GCP-WD is a gamma-tubulin targeting factor required for centrosomal and chromatin-mediated microtubule nucleation." Nat Cell Biol 8(**2**): 137-47.

Lutkenhaus, J. and S. G. Addinall (1997). "Bacterial cell division and the Z ring." Annu Rev Biochem 66: 93-116.

Lutkenhaus, J. F., H. Wolf-Watz and W. D. Donachie (1980). "Organization of genes in the ftsA-envA region of the Escherichia coli genetic map and identification of a new fts locus (ftsZ)." J Bacteriol 142(**2**): 615-20.
Manton, I. and Clarke, R. [1952]. An electron microscopy study of the spermatozoid of sphagnum. *J. Exp. Bot.* (**3**): 265–275.
Margolis, R. L. and L. Wilson (1978). "Opposite end assembly and disassembly of microtubules at steady state in vitro." Cell 13(**1**): 1-8.
Marshall, W. F. (2009). "Centriole evolution." Curr Opin Cell Biol 21(**1**): 14-9.
Martin, O. C., R. N. Gunawardane, A. Iwamatsu and Y. Zheng (1998). "Xgrip109: a gamma tubulin-associated protein with an essential role in gamma tubulin ring complex (gammaTuRC) assembly and centrosome function." J Cell Biol 141(**3**): 675-87.
Mata, J. and P. Nurse (1997). "tea1 and the microtubular cytoskeleton are important for generating global spatial order within the fission yeast cell." Cell 89(**6**): 939-49.
Matsumura, S., F. Toyoshima and E. Nishida (2007). "Polo-like kinase 1 facilitates chromosome alignment during prometaphase through BubR1." J Biol Chem 282(**20**): 15217-27.
Matsuyama, A., A. Shirai, Y. Yashiroda, A. Kamata, S. Horinouchi and M. Yoshida (2004). "pDUAL, a multipurpose, multicopy vector capable of chromosomal integration in fission yeast." Yeast 21(**15**): 1289-305.
Maundrell, K. (1990). "nmt1 of fission yeast. A highly transcribed gene completely repressed by thiamine." J Biol Chem 265(**19**): 10857-64.
McDonnell, A. V., T. Jiang, A. E. Keating and B. Berger (2006). "Paircoil2: improved prediction of coiled coils from sequence." Bioinformatics 22(**3**): 356-8.
McEwen, B. and S. J. Edelstein (1980). "Evidence for a mixed lattice in microtubules reassembled in vitro." J Mol Biol 139(**2**): 123-45.
Mejillano, M. R., J. S. Barton and R. H. Himes (1990). "Stabilization of microtubules by GTP analogues." Biochem Biophys Res Commun 166(**2**): 653-60.
Melki, R., I. E. Vainberg, R. L. Chow and N. J. Cowan (1993). "Chaperonin-mediated folding of vertebrate actin-related protein and gamma-tubulin." J Cell Biol 122(**6**): 1301-10.
Miller, J. (1972). Experiments in Molecular Genetics. Cold Spring Harbor Laboratory Press. New York.
Mishima, M., V. Pavicic, U. Gruneberg, E. A. Nigg and M. Glotzer (2004). "Cell cycle regulation of central spindle assembly." Nature 430(**7002**): 908-13.
Mitchison, T. and M. Kirschner (1984a). "Dynamic instability of microtubule growth." Nature 312(**5991**): 237-42.
Mitchison, T. and M. Kirschner (1984b). "Microtubule assembly nucleated by isolated centrosomes." Nature 312(**5991**): 232-7.
Mitchison, T. J. (1993). "Localization of an exchangeable GTP binding site at the plus end of microtubules." Science 261(**5124**): 1044-7.
Mogensen, M. M. (1999). "Microtubule release and capture in epithelial cells." Biol Cell 91(**4-5**): 331-41.

Mogensen, M. M., A. Malik, M. Piel, V. Bouckson-Castaing and M. Bornens (2000). "Microtubule minus-end anchorage at centrosomal and non-centrosomal sites: the role of ninein." J Cell Sci 113 (Pt 17): 3013-23.

Moreno, S., A. Klar and P. Nurse (1991). "Molecular genetic analysis of fission yeast Schizosaccharomyces pombe." Methods Enzymol 194: 795-823.

Moritz, M. and D. A. Agard (2001). "Gamma-tubulin complexes and microtubule nucleation." Curr Opin Struct Biol 11(**2**): 174-81.

Moritz, M., M. B. Braunfeld, J. C. Fung, J. W. Sedat, B. M. Alberts and D. A. Agard (1995a). "Three-dimensional structural characterization of centrosomes from early Drosophila embryos." J Cell Biol 130(**5**): 1149-59.

Moritz, M., M. B. Braunfeld, V. Guenebaut, J. Heuser and D. A. Agard (2000). "Structure of the gamma-tubulin ring complex: a template for microtubule nucleation." Nat Cell Biol 2(**6**): 365-70.

Moritz, M., M. B. Braunfeld, J. W. Sedat, B. Alberts and D. A. Agard (1995b). "Microtubule nucleation by gamma-tubulin-containing rings in the centrosome." Nature 378(**6557**): 638-40.

Moritz, M., Y. Zheng, B. M. Alberts and K. Oegema (1998). "Recruitment of the gamma-tubulin ring complex to Drosophila salt-stripped centrosome scaffolds." J Cell Biol 142(**3**): 775-86.

Murphy, S. M., A. M. Preble, U. K. Patel, *et al.* (2001). "GCP5 and GCP6: two new members of the human gamma-tubulin complex." Mol Biol Cell 12(**11**): 3340-52.

Murphy, S. M., L. Urbani and T. Stearns (1998). "The mammalian gamma-tubulin complex contains homologues of the yeast spindle pole body components spc97p and spc98p." J Cell Biol 141(**3**): 663-74.

Nakajima, H., F. Toyoshima-Morimoto, E. Taniguchi and E. Nishida (2003). "Identification of a consensus motif for Plk (Polo-like kinase) phosphorylation reveals Myt1 as a Plk1 substrate." J Biol Chem 278(**28**): 25277-80.

Neher, S. B., J. Villen, E. C. Oakes, *et al.* (2006). "Proteomic profiling of ClpXP substrates after DNA damage reveals extensive instability within SOS regulon." Mol Cell 22(**2**): 193-204.

Nogales, E., M. Whittaker, R. A. Milligan and K. H. Downing (1999). "High-resolution model of the microtubule." Cell 96(**1**): 79-88.

Nogales, E., S. G. Wolf and K. H. Downing (1998). "Structure of the alpha beta tubulin dimer by electron crystallography." Nature 391(**6663**): 199-203.

Oakley, B. R., C. E. Oakley, Y. Yoon and M. K. Jung (1990). "Gamma-tubulin is a component of the spindle pole body that is essential for microtubule function in Aspergillus nidulans." Cell 61(**7**): 1289-301.

Oakley, C. E. and B. R. Oakley (1989). "Identification of gamma-tubulin, a new member of the tubulin superfamily encoded by mipA gene of Aspergillus nidulans." Nature 338(**6217**): 662-4.

Oegema, K., C. Wiese, O. C. Martin, *et al.* (1999). "Characterization of two related Drosophila gamma-tubulin complexes that differ in their ability to nucleate microtubules." J Cell Biol 144(**4**): 721-33.

Ong, S. E., B. Blagoev, I. Kratchmarova, *et al.* (2002). "Stable isotope labeling by amino acids in cell culture, SILAC, as a simple and accurate approach to expression proteomics." Mol Cell Proteomics 1(**5**): 376-86.

Ou, Y. Y., G. J. Mack, M. Zhang and J. B. Rattner (2002). "CEP110 and ninein are located in a specific domain of the centrosome associated with centrosome maturation." J Cell Sci 115(**Pt 9**): 1825-35.

Paluh, J. L., E. Nogales, B. R. Oakley, K. McDonald, A. L. Pidoux and W. Z. Cande (2000). "A mutation in gamma-tubulin alters microtubule dynamics and organization and is synthetically lethal with the kinesin-like protein pkl1p." Mol Biol Cell 11(**4**): 1225-39.

Pardo, M. and P. Nurse (2003). "Equatorial retention of the contractile actin ring by microtubules during cytokinesis." Science 300(**5625**): 1569-74.

Pardo, M. and P. Nurse (2005). "The nuclear rim protein Amo1 is required for proper microtubule cytoskeleton organisation in fission yeast." J Cell Sci 118(**Pt 8**): 1705-14.

Pavletich, N. P. (1999). "Mechanisms of cyclin-dependent kinase regulation: structures of Cdks, their cyclin activators, and Cip and INK4 inhibitors." J Mol Biol 287(**5**): 821-8.

Penningroth, S. M. and M. W. Kirschner (1978). "Nucleotide specificity in microtubule assembly in vitro." Biochemistry 17(**4**): 734-40.

Petronczki, M., P. Lenart and J. M. Peters (2008). "Polo on the Rise-from Mitotic Entry to Cytokinesis with Plk1." Dev Cell 14(**5**): 646-59.

Pfaff, K. L., C. T. Straub, K. Chiang, D. M. Bear, Y. Zhou and L. I. Zon (2007). "The zebra fish cassiopeia mutant reveals that SIL is required for mitotic spindle organization." Mol Cell Biol 27(**16**): 5887-97.

Pickett-Heaps, J.D. [1969]. The evolution of the mitotic apparatus: An attempt at comparative ultrastructural cytology in dividing plant cells. *Cytobios* (**3**), 257-280.

Pidoux, A. L., E. S. Choi, J. K. Abbott, *et al.* (2009). "Fission yeast Scm3: A CENP-A receptor required for integrity of subkinetochore chromatin." Mol Cell 33(**3**): 299-311.

Radcliffe, P., D. Hirata, D. Childs, L. Vardy and T. Toda (1998). "Identification of novel temperature-sensitive lethal alleles in essential beta-tubulin and nonessential alpha 2-tubulin genes as fission yeast polarity mutants." Mol Biol Cell 9(**7**): 1757-71.

Raff, J. W., D. R. Kellogg and B. M. Alberts (1993). "Drosophila gamma-tubulin is part of a complex containing two previously identified centrosomal MAPs." J Cell Biol 121(**4**): 823-35.

Rappsilber, J., Y. Ishihama and M. Mann (2003). "Stop and go extraction tips for matrix-assisted laser desorption/ionization, nanoelectrospray, and LC/MS sample pretreatment in proteomics." Anal Chem 75(**3**): 663-70.

Rauch, A., C. T. Thiel, D. Schindler, *et al.* (2008). "Mutations in the pericentrin (PCNT) gene cause primordial dwarfism." Science 319(**5864**): 816-9.

Ravelli, R. B., B. Gigant, P. A. Curmi, *et al.* (2004). "Insight into tubulin regulation from a complex with colchicine and a stathmin-like domain." Nature 428(**6979**): 198-202.

Rosenburg, J.A. [2007]. Assembly and regulation of signalling proteins at fission yeast microtubule organising centres. Thesis [PhD]. Vanderbilt University.

Russell, P. and P. Nurse (1986). "cdc25+ functions as an inducer in the mitotic control of fission yeast." Cell 45(**1**): 145-53.

Russell, P. and P. Nurse (1987). "Negative regulation of mitosis by wee1+, a gene encoding a protein kinase homolog." Cell 49(**4**): 559-67.
Sagolla, M. J., S. Uzawa and W. Z. Cande (2003). "Individual microtubule dynamics contribute to the function of mitotic and cytoplasmic arrays in fission yeast." J Cell Sci 116(**Pt 24**): 4891-903.
Sambrook, J. and Russell, D. (2001). Molecular Cloning: A Laboratory Manual. 3rd ed. Cold Spring Harbor Laboratory Press. New York.
Samejima, I., P. C. Lourenco, H. A. Snaith and K. E. Sawin (2005). "Fission yeast mto2p regulates microtubule nucleation by the centrosomin-related protein mto1p." Mol Biol Cell 16(**6**): 3040-51.
Samejima, I., V. J. Miller, L. M. Groocock and K. E. Sawin (2008). "Two distinct regions of Mto1 are required for normal microtubule nucleation and efficient association with the gamma-tubulin complex in vivo." J Cell Sci 121(**Pt 23**): 3971-80.
Santamaria, A., R. Neef, U. Eberspacher, *et al.* (2007). "Use of the novel Plk1 inhibitor ZK-thiazolidinone to elucidate functions of Plk1 in early and late stages of mitosis." Mol Biol Cell 18(**10**): 4024-36.
Sawin, K. E., P. C. Lourenco and H. A. Snaith (2004). "Microtubule nucleation at non-spindle pole body microtubule-organizing centers requires fission yeast centrosomin-related protein mod20p." Curr Biol 14(**9**): 763-75.
Sawin, K. E. and P. Nurse (1998). "Regulation of cell polarity by microtubules in fission yeast." J Cell Biol 142(**2**): 457-71.
Schimmang, T., D. Tollervey, H. Kern, R. Frank and E. C. Hurt (1989). "A yeast nucleolar protein related to mammalian fibrillarin is associated with small nucleolar RNA and is essential for viability." Embo J 8(**13**): 4015-24.
Schwanhausser, B., M. Gossen, G. Dittmar and M. Selbach (2009). "Global analysis of cellular protein translation by pulsed SILAC." Proteomics 9(**1**): 205-9.
Shevchenko, A., M. Wilm, O. Vorm and M. Mann (1996). "Mass spectrometric sequencing of proteins silver-stained polyacrylamide gels." Anal Chem 68(**5**): 850-8.
Siegel, L. M. and K. J. Monty (1966). "Determination of molecular weights and frictional ratios of proteins in impure systems by use of gel filtration and density gradient centrifugation. Application to crude preparations of sulfite and hydroxylamine reductases." Biochim Biophys Acta 112(**2**): 346-62.
Singla, V. and J. F. Reiter (2006). "The primary cilium as the cell's antenna: signaling at a sensory organelle." Science 313(**5787**): 629-33.
Slautterback, D. B. (1963). "Cytoplasmic Microtubules. I. Hydra." J Cell Biol 18: 367-88.
Small, J. V. and I. Kaverina (2003). "Microtubules meet substrate adhesions to arrange cell polarity." Curr Opin Cell Biol 15(**1**): 40-7.
Smith, P. K., R. I. Krohn, G. T. Hermanson, *et al.* (1985). "Measurement of protein using bicinchoninic acid." Anal Biochem 150(**1**): 76-85.
Snaith, H. A., I. Samejima and K. E. Sawin (2005a). "Multistep and multimode cortical anchoring of tea1p at cell tips in fission yeast." Embo J 24(**21**): 3690-9.
Snaith, H. A. and K. E. Sawin (2005b). "Tea for three: control of fission yeast polarity." Nat Cell Biol 7(**5**): 450-1.

Sohrmann, M., C. Fankhauser, C. Brodbeck and V. Simanis (1996). "The dmf1/mid1 gene is essential for correct positioning of the division septum in fission yeast." Genes Dev 10(**21**): 2707-19.

Soldati, T. and M. Schliwa (2006). "Powering membrane traffic in endocytosis and recycling." Nat Rev Mol Cell Biol 7(**12**): 897-908.

Spang, A., S. Geissler, K. Grein and E. Schiebel (1996). "gamma-Tubulin-like Tub4p of Saccharomyces cerevisiae is associated with the spindle pole body substructures that organize microtubules and is required for mitotic spindle formation." J Cell Biol 134(**2**): 429-41.

Stearns, T., L. Evans and M. Kirschner (1991). "Gamma-tubulin is a highly conserved component of the centrosome." Cell 65(**5**): 825-36.

Stearns, T. and M. Kirschner (1994). "In vitro reconstitution of centrosome assembly and function: the central role of gamma-tubulin." Cell 76(**4**): 623-37.

Stoppin, V., M. Vantard, A. C. Schmit and A. M. Lambert (1994). "Isolated Plant Nuclei Nucleate Microtubule Assembly: The Nuclear Surface in Higher Plants Has Centrosome-like Activity." Plant Cell 6(**8**): 1099-1106.

Sumara, I., J. F. Gimenez-Abian, D. Gerlich, *et al.* (2004). "Roles of polo-like kinase 1 in the assembly of functional mitotic spindles." Curr Biol 14(**19**): 1712-22.

Tagwerker, C., H. Zhang, X. Wang, *et al.* (2006). "HB tag modules for PCR-based gene tagging and tandem affinity purification in Saccharomyces cerevisiae." Yeast 23(**8**): 623-32.

Terada, Y., Y. Uetake and R. Kuriyama (2003). "Interaction of Aurora-A and centrosomin at the microtubule-nucleating site in Drosophila and mammalian cells." J Cell Biol 162(**5**): 757-63.

Tibelius, A., J. Marhold, H. Zentgraf, *et al.* (2009). "Microcephalin and pericentrin regulate mitotic entry via centrosome-associated Chk1." J Cell Biol 185(**7**): 1149-57.

Tilney, L. G., J. Bryan, D. J. Bush, *et al.* (1973). "Microtubules: evidence for 13 protofilaments." J Cell Biol 59(**2 Pt 1**): 267-75.

Tolic-Norrelykke, I. M., L. Sacconi, G. Thon and F. S. Pavone (2004). "Positioning and elongation of the fission yeast spindle by microtubule-based pushing." Curr Biol 14(**13**): 1181-6.

Toyoshima, F. and E. Nishida (2007). "Spindle orientation in animal cell mitosis: roles of integrin in the control of spindle axis." J Cell Physiol 213(**2**): 407-11.

Tran, P. T., V. Doye, F. Chang and S. Inoue (2000). "Microtubule-dependent nuclear positioning and nuclear-dependent septum positioning in the fission yeast Schizosaccharomyces [correction of Saccharomyces] pombe." Biol Bull 199(**2**): 205-6.

Tran, P. T., P. Joshi and E. D. Salmon (1997). "How tubulin subunits are lost from the shortening ends of microtubules." J Struct Biol 118(**2**): 107-18.

Tran, P. T., L. Marsh, V. Doye, S. Inoue and F. Chang (2001). "A mechanism for nuclear positioning in fission yeast based on microtubule pushing." J Cell Biol 153(**2**): 397-411.

Trimborn, M., S. M. Bell, C. Felix, *et al.* (2004). "Mutations in microcephalin cause aberrant regulation of chromosome condensation." Am J Hum Genet 75(**2**): 261-6.

Uhlmann, F., F. Lottspeich and K. Nasmyth (1999). "Sister-chromatid separation at anaphase onset is promoted by cleavage of the cohesin subunit Scc1." Nature 400(**6739**): 37-42.

Uzawa, S., F. Li, Y. Jin, *et al.* (2004). "Spindle pole body duplication in fission yeast occurs at the G1/S boundary but maturation is blocked until exit from S by an event downstream of cdc10+." Mol Biol Cell 15(**12**): 5219-30.

Vardy, L. and T. Toda (2000). "The fission yeast gamma-tubulin complex is required in G(1) phase and is a component of the spindle assembly checkpoint." Embo J 19(**22**): 6098-111.

Venkatram, S., J. L. Jennings, A. Link and K. L. Gould (2005). "Mto2p, a novel fission yeast protein required for cytoplasmic microtubule organization and anchoring of the cytokinetic actin ring." Mol Biol Cell 16(**6**): 3052-63.

Venkatram, S., J. J. Tasto, A. Feoktistova, J. L. Jennings, A. J. Link and K. L. Gould (2004). "Identification and characterization of two novel proteins affecting fission yeast gamma-tubulin complex function." Mol Biol Cell 15(**5**): 2287-301.

Venter, J. C., M. D. Adams, E. W. Myers, *et al.* (2001). "The sequence of the human genome." Science 291(**5507**): 1304-51.

Verollet, C., N. Colombie, T. Daubon, H. M. Bourbon, M. Wright and B. Raynaud-Messina (2006). "Drosophila melanogaster gamma-TuRC is dispensable for targeting gamma-tubulin to the centrosome and microtubule nucleation." J Cell Biol 172(**4**): 517-28.

Wakefield, J. G., S. Bonaccorsi and M. Gatti (2001). "The drosophila protein asp is involved in microtubule organization during spindle formation and cytokinesis." J Cell Biol 153(**4**): 637-48.

Wang, H. W. and E. Nogales (2005). "Nucleotide-dependent bending flexibility of tubulin regulates microtubule assembly." Nature 435(**7044**): 911-5.

Weisenberg, R. C., G. G. Borisy and E. W. Taylor (1968). "The colchicine-binding protein of mammalian brain and its relation to microtubules." Biochemistry 7(**12**): 4466-79.

Weisenberg, R. C. and A. C. Rosenfeld (1975). "In vitro polymerization of microtubules into asters and spindles in homogenates of surf clam eggs." J Cell Biol 64(**1**): 146-58.

Wiese, C. and Y. Zheng (2000). "A new function for the gamma-tubulin ring complex as a microtubule minus-end cap." Nat Cell Biol 2(**6**): 358-64.

Willems, M., D. Genevieve, G. Borck, *et al.* (2009). "Molecular analysis of Pericentrin gene (PCNT) in a series of 24 Seckel/ MOPD II families." J Med Genet.

Williams, R. S., G. Moncalian, J. S. Williams, *et al.* (2008). "Mre11 dimers coordinate DNA end bridging and nuclease processing in double-strand-break repair." Cell 135(**1**): 97-109.

Wu, J. Q., J. Bahler and J. R. Pringle (2001). "Roles of a fimbrin and an alpha-actinin-like protein in fission yeast cell polarization and cytokinesis." Mol Biol Cell 12(**4**): 1061-77.

Wu, J. Q. and T. D. Pollard (2005). "Counting cytokinesis proteins globally and locally in fission yeast." Science 310(**5746**): 310-4.

Yaffe, M. P., D. Harata, F. Verde, M. Eddison, T. Toda and P. Nurse (1996). "Microtubules mediate mitochondrial distribution in fission yeast." Proc Natl Acad Sci U S A 93(**21**): 11664-8.

Yoshida, S., K. Kono, D. M. Lowery, *et al.* (2006). "Polo-like kinase Cdc5 controls the local activation of Rho1 to promote cytokinesis." Science 313(**5783**): 108-11.

Zhang, J. and T. L. Megraw (2007). "Proper recruitment of gamma-tubulin and D-TACC/Msps to embryonic Drosophila centrosomes requires Centrosomin Motif 1." Mol Biol Cell 18(**10**): 4037-49.

Zhang, X., Q. Chen, J. Feng, *et al.* (2009). "Sequential phosphorylation of Nedd1 by Cdk1 and Plk1 is required for targeting of the gammaTuRC to the centrosome." J Cell Sci 122(**Pt 13**): 2240-51.

Zheng, Y., M. K. Jung and B. R. Oakley (1991). "Gamma-tubulin is present in Drosophila melanogaster and Homo sapiens and is associated with the centrosome." Cell 65(**5**): 817-23.

Zheng, Y., M. L. Wong, B. Alberts and T. Mitchison (1995). "Nucleation of microtubule assembly by a gamma-tubulin-containing ring complex." Nature 378(**6557**): 578-83.

Zheng, Y., M. L. Wong, B. Alberts and T. Mitchison (1998). "Purification and assay of gamma tubulin ring complex." Methods Enzymol 298: 218-28.

Zimmerman, S. and F. Chang (2005). "Effects of {gamma}-tubulin complex proteins on microtubule nucleation and catastrophe in fission yeast." Mol Biol Cell 16(**6**): 2719-33.

Zimmerman, S., R. R. Daga and F. Chang (2004a). "Intra-nuclear microtubules and a mitotic spindle orientation checkpoint." Nat Cell Biol 6(**12**): 1245-6.

Zimmerman, W. C., J. Sillibourne, J. Rosa and S. J. Doxsey (2004b). "Mitosis-specific anchoring of gamma tubulin complexes by pericentrin controls spindle organization and mitotic entry." Mol Biol Cell 15(**8**): 3642-57.

Zolnierowicz, S. and M. Bollen (2000). "Protein phosphorylation and protein phosphatases. De Panne, Belgium, September 19-24, 1999." Embo J 19(**4**): 483-8.